Geology and Geochemistry of the West Ore Body and Associated Skarns, Copper Canyon Porphyry Copper Deposits, Lander County, Nevada

GEOLOGICAL SURVEY PROFESSIONAL PAPER 798-C

Geology and Geochemistry of the West Ore Body and Associated Skarns, Copper Canyon Porphyry Copper Deposits, Lander County, Nevada

By TED G. THEODORE *and* DAVID W. BLAKE

With a section on Electron Microprobe Analyses of Andradite and Diopside

By NORMAN G. BANKS

GEOCHEMISTRY OF THE PORPHYRY COPPER ENVIRONMENT IN THE BATTLE MOUNTAIN MINING DISTRICT, NEVADA

GEOLOGICAL SURVEY PROFESSIONAL PAPER 798–C

UNITED STATES GOVERNMENT PRINTING OFFICE, WASHINGTON: 1978

UNITED STATES DEPARTMENT OF THE INTERIOR

CECIL D. ANDRUS, *Secretary*

GEOLOGICAL SURVEY

V. E. McKelvey, ***Director***

Library of Congress catalog-card number 78-600003

For sale by the Superintendent of Documents, U.S. Government Printing Office
Washington, D.C. 20402
Stock Number 024-001-03041-1

CONTENTS

ILLUSTRATIONS

TABLES

But the unfinished edifice whose missing parts serve to suggest and direct further search for truth is of value, while the apparently completed structure may be entirely the "baseless fabric of a vision."

F.L. Ransome, 1904, p. 151

GEOCHEMISTRY OF THE PORPHYRY COPPER ENVIRONMENT IN THE BATTLE MOUNTAIN MINING DISTRICT, NEVADA

GEOLOGY AND GEOCHEMISTRY OF THE WEST ORE BODY AND ASSOCIATED SKARNS IN THE COPPER CANYON PORPHYRY COPPER DEPOSITS, LANDER COUNTY, NEVADA

By TED G. THEODORE and DAVID W. BLAKE[1]

ABSTRACT

The Copper Canyon porphyry copper deposits in north-central Nevada include a small, 4-million-tonne, copper-gold-silver skarn ore body, herein called the west ore body, that developed in favorable beds of calcareous argillite of the Pennsylvanian and Permian Pumpernickel Formation. Metallization occurred during late Eocene and early Oligocene time and is concentrated in a flat-lying tabular body of garnetite in which iron-rich garnet, containing up to 99 percent of the andradite molecular end member, is the predominant silicate. This tabular body is adjacent to a potassic-altered granodiorite, but the intrusion apparently postdates the skarn. Silicate mineral assemblages are symmetrically zoned in the skarn, and they vary from andradite-diopside in the most intensely metamorphosed and metasomatized rock, through diopside-sphene, diopside± tremolite, tremolite, and finally biotite-potassium feldspar±tremolite assemblages in the least metamorphosed rock. The zone boundaries are approximately horizontal, at right angles to the adjacent granodiorite. This relation and the absence of skarn in porous, calcareous, and hematitic conglomerate of the Middle Pennsylvanian Battle Formation that is in contact with the granodiorite strongly suggest the granodiorite did not provide the fluids involved in the skarn's generation.

In the skarn, andradite-rich rock was the site of most metallization. Chalcopyrite is the main ore mineral, and most ore includes pyrrhotite-pyrite-chalcopyrite, pyrrhotite-chalcopyrite, and pyrite-chalcopyrite mineral assemblages as fracture fillings and replacements of earlier silicates. There are also minor amounts of marcasite, covellite, and chalcocite. In places there is massive replacement of andradite by pyrrhotite with diopside remaining as an unaffected relict in the pyrrhotite. Locally close to the granodiorite and partly coincident with ore, andradite-pyrrhotite is replaced by epidote-pyrite that is in turn cut by a second generation of hydrothermal biotite. This second generation of hydrothermal biotite is thought to be related primarily to the potassic alteration, disseminated and in veins, throughout the granodiorite.

Fluid-inclusion studies suggest that early crystallization of andradite occurred at temperatures of about 500°±50°C from highly saline fluids. Temperatures were probably about 320°±40°C during crystallization of most of the pyrrhotite-chalcopyrite ores in the skarn, and the fluids by then were much more saline, possibly about 35–45 weight percent NaCl equivalent. Most important, fluid-inclusion relations suggest that the andradite-bearing assemblages of the skarn crystallized under lithostatic conditions (possibly about 380 bars), whereas most other assemblages may have formed under hydrostatic conditions (150 bars) with the fluid boiling. Indeed, there is some evidence in the granodiorite for a very late, low-density, high-temperature fluid that may reflect some additional opening of channels to the surface after they were sealed by silica. Sometime during the final hypogene stages of the skarn, less saline fluids at 160°–220°C circulated through the ore body concomitant with emplacement of minor chlorite-iron oxide-carbonate veinlets.

Geochemical data obtained from skarn and from bedrock and residual soil exposed above skarn show that concentrations of bismuth, manganese, and lead are higher in the skarn than in the east ore body, the other major copper deposit in the Copper Canyon area. Throughout the southern part of the area above the skarn, the primary zonations of nine elements (Ag, Au, Bi, Co, Cu, Hg, Fe, Pb, and Zn) are most evident in exposed parts of the Pumpernickel Formation, probably because these rocks are not so intensely fractured as rocks of the other formations, and the relative impermeability of chert and argillite of the Pumpernickel impeded supergene alteration. In the granodiorite, however, the primary zonation of all these metals is overwhelmed by secondary copper, which may have been derived from one of the topographically high ore bodies. Although concentrations of silver, arsenic, gold, bismuth, copper, and possibly nickel, lead, and mercury in soil above the skarn are generally anomalous, they show little, if any, specific spatial relation to underlying ore. Concentrations of arsenic, gold, copper, mercury, and lead do, however, decrease roughly with distance away from underlying ore. The concentrations of arsenic may reflect some downslope contamination from mineralized segments of the Virgin fault, one of the major faults in the area, which crops out topographically higher than the skarn in the same drainage basin as the skarn.

[1]Duval Corp., Battle Mountain, Nev. 89820.

INTRODUCTION

In 1975, twenty-four domestic porphyry copper deposits accounted for about 90 percent of the newly mined copper used by the copper industry in the United States. They made significant by-product contributions to our national production of molybdenum, gold, silver, rhenium, and platinum-group metals. In addition, this class of copper deposits contains about 85 percent of the known copper reserves in the conterminous United States (see Ageton and Greenspoon, 1970; Titley, 1972; Beall, 1973; Cox and others, 1973; Sutulov, 1974). In 1974, Nevada, with about 5 percent of the total copper production, was the fifth largest copper-producing state (U.S. Bureau of Mines, 1974). Copper production in 1974 from one of the two copper deposits in the Copper Canyon area, 18 km southwest of the town of Battle Mountain, ranked third behind the other two major copper deposits in production in Nevada at Ely and at Yerington. Production of copper by Duval Corporation began in 1967 from its two Battle Mountain mining district properties at Copper Canyon and Copper Basin by open-pit methods (fig. 1). Table 1 lists Duval Corporation reserve and production data from Battle Mountain obtained from World Mining (1971), and from a prospectus issued on May 10, 1973, by Pennzoil Company, of which Duval is a consolidated subsidiary. Through 1974, copper production amounted to about 92,800 tonnes from the two pits at Battle Mountain. Gold produced up to 1975 from these prophyry deposits is second in dollar value to copper. These deposits are among the smallest porphyry systems that have been exploited by industry in the United States.

Major economic concentrations of copper known in north-central Nevada are widespread and occur in diverse geologic environments. About 80 percent of the copper reserves discovered in the Battle Mountain mining district are in the Copper Canyon area, and the remainder is mostly at Copper Basin (Sayers and others, 1968; Noble, 1970). Both of these are Tertiary porphyry copper sulfide systems, with the economic concentrations of copper in Paleozoic wallrock. The Mountain City copper mine, a massive sulfide deposit in eugeosynclinal rocks of Paleozoic age about 170 km northeast of Copper Canyon, yielded approximately 91,000 tonnes of copper metal from 1932 to 1947 (Coats and Stephens, 1968). The Big Mike copper mine, another massive sulfide deposit in Paleozoic rocks about 65 km west of Copper Canyon (Johnson, 1977), yielded about 86,000 tonnes of high-grade ore with a gross value of $11.2 million during 1970 and 1971 (Engineering and Mining Journal, 1971).

Because of their economic importance, the deposits at Copper Canyon warranted comprehensive study of their geology to further understanding of their genesis and to help thereby the search for additional metal reserves. The study yielded genetic and exploration data with widespread implications because they are strikingly similar to many much larger porphyry deposits.

This report results from a series of cooperative studies between the U.S. Geological Survey and Duval Corporation dealing with the porphyry copper environment in the Battle Mountain mining district, Nevada. Theodore, Silberman, and Blake (1973) reported the potassium-argon ages of plutonism in the district, and Theodore and Blake (1975) described the geology of the east ore body, one of the major ore bodies at Copper Canyon in production in 1975. Three other reports (Nash and Theodore, 1971; Theodore and Nash, 1973; Batchelder and others, 1976) discuss the chemistry and distribution of the ore-forming fluids. Roberts (1964) and Roberts and Arnold (1965) previously had described the geology and ore deposits of the mining district. In this report we provide geologic, fluid-inclusion, and geochemical data from a 4-million-tonne copper-gold-silver skarn ore body at Copper Canyon. The geochemical data were obtained from (1) ore at depth in the calc-silicate metamorphic rocks, (2) altered rocks exposed above the ore, and (3) thin soil developed along the present erosion surface in the general area of the ore body. Because the ore body was not exposed during the main writing of this report in 1975, many of our data from ore have been assembled from drill core. Thus, many conclusions must be tentative until detailed observation of relations in the ore body

TABLE 1.—*Summary of the reserves and production of Duval Corporation in the Battle Mountain mining district*

[Modified from World Mining (1971); a prospectus, issued by Pennzoil Company on May 10, 1973; and T. Jancic, written commun., 1976]

Reserves

	Ore[1] (tons)	Average metal content		
		Cu[2]	Au[3]	Ag[3]
Copper Canyon	9,950,000	0.57	0.027	0.36
Copper Basin	948,000	1.49	.027	.39

Production[4]

Year	Milling operations	Leach-precipitation operations
	Tons copper produced	Tons copper produced
1967	4,731	1,145
1968	7,510	2,323
1969	9,752	3,008
1970	9,337	4,181
1971	9,581	6,214
1972	9,492	6,830
1973	7,239	6,681
1974	6,854	7,205

[1]Estimated as of December 31, 1972; 1.1 tons, short (2,000 lbs, English) = 1 tonne (SI).
[2]In weight percent.
[3]In ounces per ton.
[4]Includes both the Copper Canyon and Copper Basin mines. About 80 percent of the tonnage milled has come from the east ore body at the Copper Canyon mine.

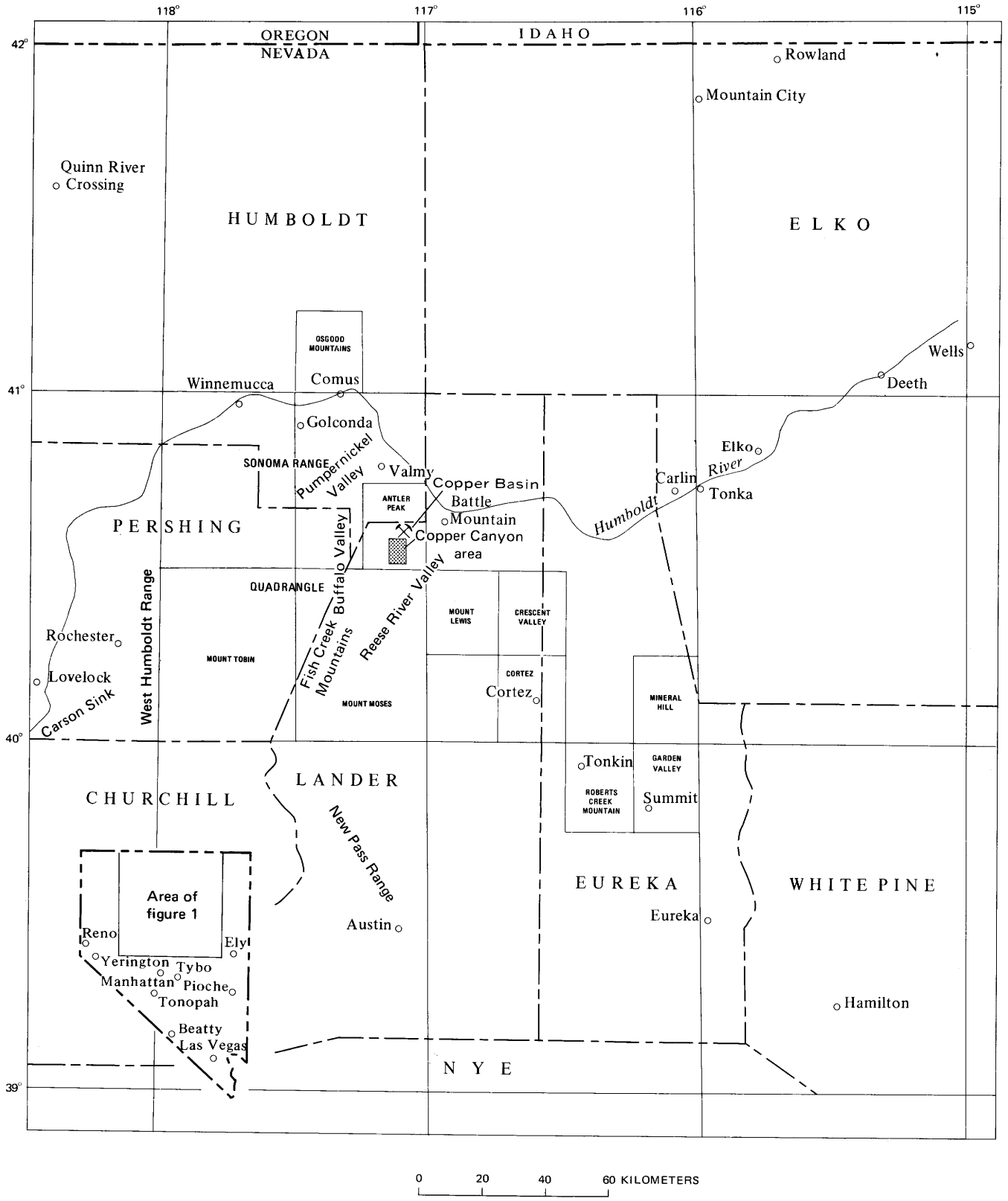

FIGURE 1.—Location of Battle Mountain mining district in north-central Nevada.

are made. In late 1977, Duval Corporation, after having mined about one-half of the west ore body, suspended the milling of ore from the west ore body because of an economically depressed copper market.

ACKNOWLEDGMENTS

This study of the geologic history of the Copper Canyon area would not have been possible without the continued cooperation of the management of Duval Corporation, in particular J. P. McCarty, A. E. Shiell, and F. H. Howell. The preceding investigations by Ralph J. Roberts, who first unraveled the complex geology of the Battle Mountain mining district, were an invaluable framework for our studies. Drill cores were analyzed for copper, gold, silver, lead and zinc in the analytical laboratory of Duval Corporation at Copper Canyon by J. R. Simmons, Jr.., using standard wet-chemical and atomic-absorption techniques. The concentrations of nine other elements in core were determined in the laboratories of the Duval Corporation at Sierrita, Ariz., by atomic-absorption techniques. Fluid-inclusion studies were carried out in the laboratory of Wayne E. Hall, and determinations of D/H and $\delta^{18}O$ compositions of tremolite and $\delta^{18}O$ of quartz were made by Stephen J. Grigg and Lanford Adami in the laboratory of James R. O'Neil of the U.S. Geological Survey, Menlo Park, Calif.

GENERAL GEOLOGY OF THE COPPER CANYON DEPOSITS

The Copper Canyon porphyry copper deposits are predominantly in fractured and altered sedimentary rocks of late Paleozoic age (fig. 2), in an area overridden in north-central Nevada by three successive thrust plates, two of which moved during middle Paleozoic time and one during late Paleozoic or early Mesozoic time. Between these intervals of major thrusting, an authochthonous block of rocks, the Antler sequence, was deposited. It overlies unconformably the two lowermost plates and is itself overridden by the uppermost thrust plate (table 2). The thrust plates include rocks floored by (1) the middle Paleozoic Roberts Mountains thrust, (2) the middle Paleozoic Dewitt thrust, and (3) the early Mesozoic Golconda thrust (Roberts, 1964).

During the Eocene and Oligocene Epochs two epigenetic ore deposits (the east and west ore bodies) formed at Copper Canyon, one chiefly in rocks belonging to the Antler sequence and the other chiefly in the upper thrust plate or Golconda plate that is structurally above the Antler sequence. These two deposits are within 300 m of a small altered granodiorite body (Nash and Theodore, 1971; Theodore and Blake, 1975), dated by the potassium-argon method as late Eocene or early Oligocene (38 m.y.) (Theodore and others, 1973). This granodiorite is generally ovoid in plan view, about 1,500 m across, and drilling has shown it to be a laccolith in its overall configuration (Blake, 1971). Our data will show that eventual emplacement of the granodiorite at its present level followed development of skarn and preceded the bulk of the mineralization in the east ore body. In the east ore body, most ore occurs as hypogene sulfides that replace former hematite- and calcite-bearing beds in the lower member of the Battle Formation of Middle Pennsylvanian age (Theodore and Blake, 1975). In the west ore body, a copper-gold-silver skarn, concentrations of sulfides occur as replacements and fracture fillings of skarn which formed previously in favorable calcareous argillite and limy shale beds, mostly of the Pennsylvanian and Permian (Erickson and Marsh, 1974) Pumpernickel Formation (fig. 2). Al-

TABLE 2.—*Stratigraphic units exposed in the immediate area of the west ore body, Copper Canyon*
[See Roberts (1964) for comprehensive discussion of regional changes in lithology and their tectonic implications]

Formation		Age	Thickness (m)	Lithology
Pumpernickel Formation[1]		Pennsylvanian and Permian	150+	Argillite, chert, and limy shale where unmetamorphosed; chief host for copper skarn deposit.
				Golconda thrust (early Mesozoic)
Battle Formation[2]	Upper member	Middle Pennsylvanian	60	Quartzite and chert-pebble conglomerate.
	Middle member		40	Calcareous shale and shaly hornfels.
	Lower member		130	Chert-pebble conglomerate, calcareous and hematitic.
				Major unconformity
Harmony Formation		Upper Cambrian	10+	Sandstone, arkose, feldspathic sandstone where unmetamorphosed; biotite hornfels where metamorphosed.
				(Base not exposed; not penetrated by drill holes)

[1]Lower member of Pumpernickel Formation exposed east of Copper Canyon fault (plate 1). Entire formation thickens rapidly to the west (Roberts, 1964; Theodore and Blake, 1975).

[2]Basal formation of the Antler sequence (Roberts, 1964).

tered sandstone and shale of the Upper Cambrian Harmony Formation, which underlies the Battle Formation unconformably, also are widely metallized in the east ore body, but at concentrations of copper generally less than in the Battle Formation. The hypogene minerals in both ore bodies include pyrite, chalcopyrite, pyrrhotite, and marcasite; there are also smaller concentrations of arsenopyrite, native gold, and silver, and traces of sphalerite, molybdenite, and galena. Wallrocks contain sulfide minerals from 600 to 3,600 m beyond the ore (fig. 2), and all known copper-gold-silver ore bodies are within an irregularly shaped sulfide-rich shell where the total sulfide content is greater than 2 percent (Blake and others, 1977). The economic boundaries of these ore bodies are also closely defined by rock that has more than 1 volume percent pyrrhotite.

GEOLOGY OF THE WEST ORE BODY

FORM AND SETTING OF THE ORE BODY

The west ore body is a replacement deposit in metasedimentary rocks near the granodiorite of Copper Canyon, predominantly in the upper plate of the Golconda thrust (pl. 1). The ore body comprises minable thicknesses of copper-, gold-, and silver-bearing rock containing more than 0.4 weight percent copper equivalent. Some rocks below the thrust and very close to the granodiorite also contain economic concentrations of copper, gold, and silver. The ore body is entirely between the north-trending West Ridge and Virgin faults, along which major normal displacements, west block down, occurred probably during Tertiary time. The West Ridge fault locally has abundant silicified breccia along its trace, and it is a major splay off the Copper Canyon fault (plate 1). The uneroded part of the upper thrust plate is about 60–90 m thick east of the West Ridge fault but thickens rapidly to the west (Roberts, 1964; Theodore and Blake, 1975). Although most of the ore in this plate is in a tectonic block that belongs structurally higher than the block in which the east ore body occurs, the elevation of the west ore body is now about 60 m lower than some of the lowest ore in the east ore body (Theodore and Blake, 1975). The west ore body occupies an irregular ovoid zone about 370 m long in an east-west direction along the northern contact of the granodiorite. On the east, it is bounded by a tongue of the granodiorite along the Virgin fault; its base is generally at the Golconda thrust, along which a sill was emplaced probably as a tongue from the main intrusive body. This sill underlies most of the ore body. Economic metallization extends about 180 m to the north roughly along strike in the metasedimentary rocks, at depths of 12–90 m below ground surface; the ore is generally about 45 m thick adjacent to the granodiorite and thins irregularly to about 30 m at the northern margins of the outlined ore body. Near the Virgin fault, the ore body is nearly horizontal. Some rocks also are enriched to minable grades and tonnages by secondary concentration of copper in shattered rocks near the Virgin fault where it intersects the granodiorite. Just to the east of the Virgin fault, however, the lower and middle units of the Battle Formation between the Virgin and Hayden faults contain relatively low concentrations of hypogene copper sulfides.

Drill holes reveal additional details of the form and setting of the ore body (fig. 3) along a north-south section. This section (*A–A'*, pl. 1) extends about 440 m from the granodiorite, through the west edge of the ore body, and then into outlying rock that is sulfidized also, but at subeconomic levels. Combined copper, gold, and silver concentrations center roughly on a tabular body of garnet-rich rock or garnetite outlined by drilling. The garnetite is generally encased sequentially outward by surrounding zones of diopside- and tremolite-bearing rock, and the garnetite has been found only in the subsurface and only between the West Ridge and Virgin faults. However, near the granodiorite, it is conspicuously absent from an irregularly shaped epidote-rich volume of rock that includes about one-third of the west ore body (fig. 4). Along section *A–A'* (fig. 3) the garnetite is about 11 m thick next to the granodiorite, and it thickens irregularly to about 21 to 37 m at distances of 260 to 410 m north of the granodiorite. We have no data from the subsurface farther north than DDH–1 (pl. 1). The garnetite has not been found west of the West Ridge fault, presumably because holes were not drilled deep enough.

The term skarn is used in this report to describe the garnetite and its closely associated metasedimentary rock. Skarn and tactite have been applied synonymously to contact metamorphosed rock by many authors (Bateman, 1965; Burt, 1972a). Others, however, applied skarn to both regionally and contact metamorphosed rock (Ramberg, 1952). Hess (1918) originally applied the term tactite to contact metasomatic rock "* * * of complex mineralogy formed by the contact metamorphism of limestone, dolomite, or other soluble rock into which foreign matter from the intruding magma has been introduced by hot solutions or gases." Gary, McAfee, and Wolf (1972, p. 663) define skarn as "* * * lime bearing silicates of any geologic age derived from nearly pure limestone and dolomite with the introduction of large amounts of Si, Al, Fe, and Mg." Titley (1973) suggested that the terms pyrometasomatic or skarn be used in a purely descriptive sense as a type of alteration commonly occurring in many prophyry copper deposits. Indeed, the term

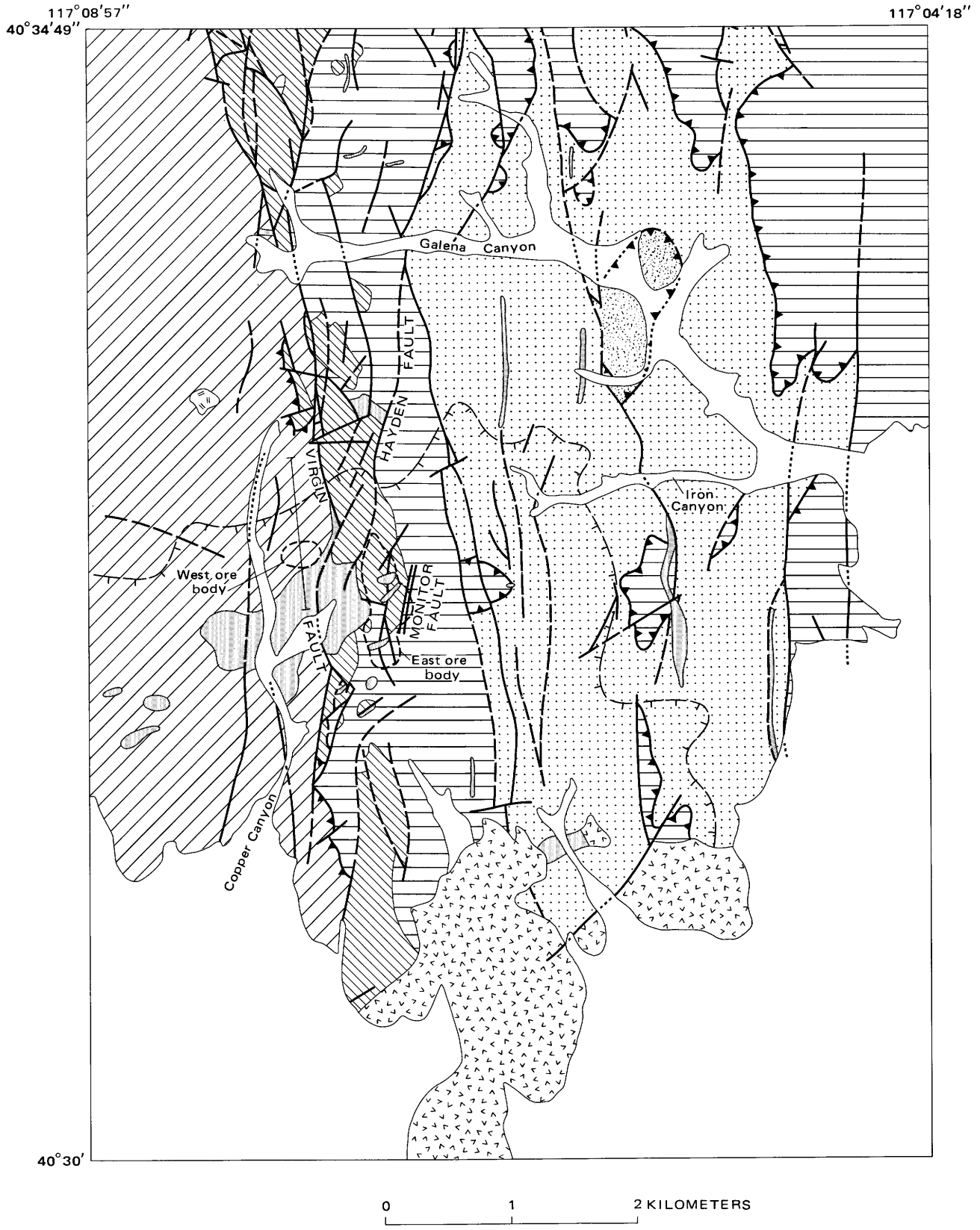

FIGURE 2.—(Above and right.) Generalized geology of southeastern part of Antler Peak quadrangle showing location of west and east ore bodies of Copper Canyon. Modified from Roberts and Arnold (1965).

skarn is well entrenched in the porphyry copper literature (Lowell and Guilbert, 1970), although in many deposits, including those at Copper Canyon, pure limestone and dolomite were not the reactive host rock. In addition, the skarn at Copper Canyon apparently did not form solely as a result of hot fluids emanating from a crystallizing magma (see below).

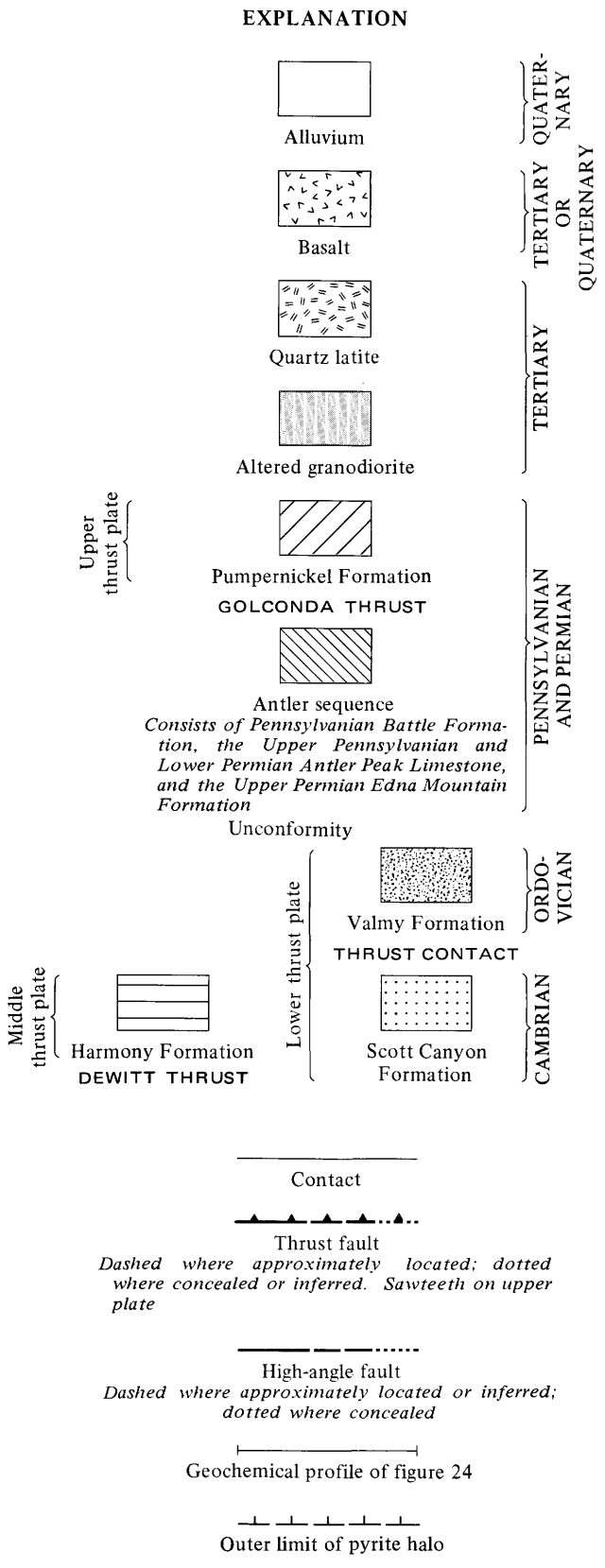

Elevation differences of the garnetite (fig. 3) may reflect (1) original chemical irregularities in the unmetamorphosed sedimentary rock, (2) minor offset along postgarnetization faults, (3) folding along generally east-trending fold axes, or a combination of these three. Most folds in the Golconda plate, however, are tightly overturned to the east along north-trending fold axes (Theodore and Blake, 1975). The apparent thinning of the garnetite for 150 m adjacent to the granodiorite may reflect volume losses from decarbonation reactions similar to those described by Cooper (1957).

Pyrite and pyrrhotite are the dominant iron sulfides in and around the ore body; minor marcasite is also present. Pyrrhotite is especially abundant in the garnetite relative to the surrounding rock (fig. 3). Pyrite and pyrrhotite near DDH–1 compose about 11 volume percent of the garnetite; the pyrrhotite:pyrite ratio is about 3:1. These iron-sulfide percentages and ratios remain fairly constant through the garnetite to about 90 m from the edge of the granodiorite, where pyrite plus pyrrhotite increases to about 50 percent, including a corresponding increase in the pyrrhotite:pyrite ratio to about 9:1. Near DDH–5, the rocks contain ore-grade concentrations of chalcopyrite, the predominant ore mineral, closely coincident with this massive increase of pyrrhotite near the granodiorite. Details at the contact of the granodiorite are sketchy, but from the data available, we infer that economic concentrations of copper, gold, and silver are present only in the metasedimentary rock.

STRATIGRAPHIC RELATIONS OF THE ORE

Most of the ore body is in the lower member of the Pumpernickel Formation in the upper plate of the Golconda thrust; some ore is in the upper member of the Battle Formation below the thrust. Interbedded argillite, chert, siltstone, and shale of the lower member of the Pumpernickel Formation are exposed around the west ore body and are typical of the formation throughout the Antler Peak quadrangle (Roberts, 1964). Sedimentary carbonates are somewhat uncommon in the Pumpernickel Formation. However, in this formation a prominent zone of garnetite, which must have formed from carbonate-rich beds, was the locus for abundant metallization in the west ore body. Epigenetic hypogene sulfides replace widespread garnet-bearing metamorphic assemblages there.

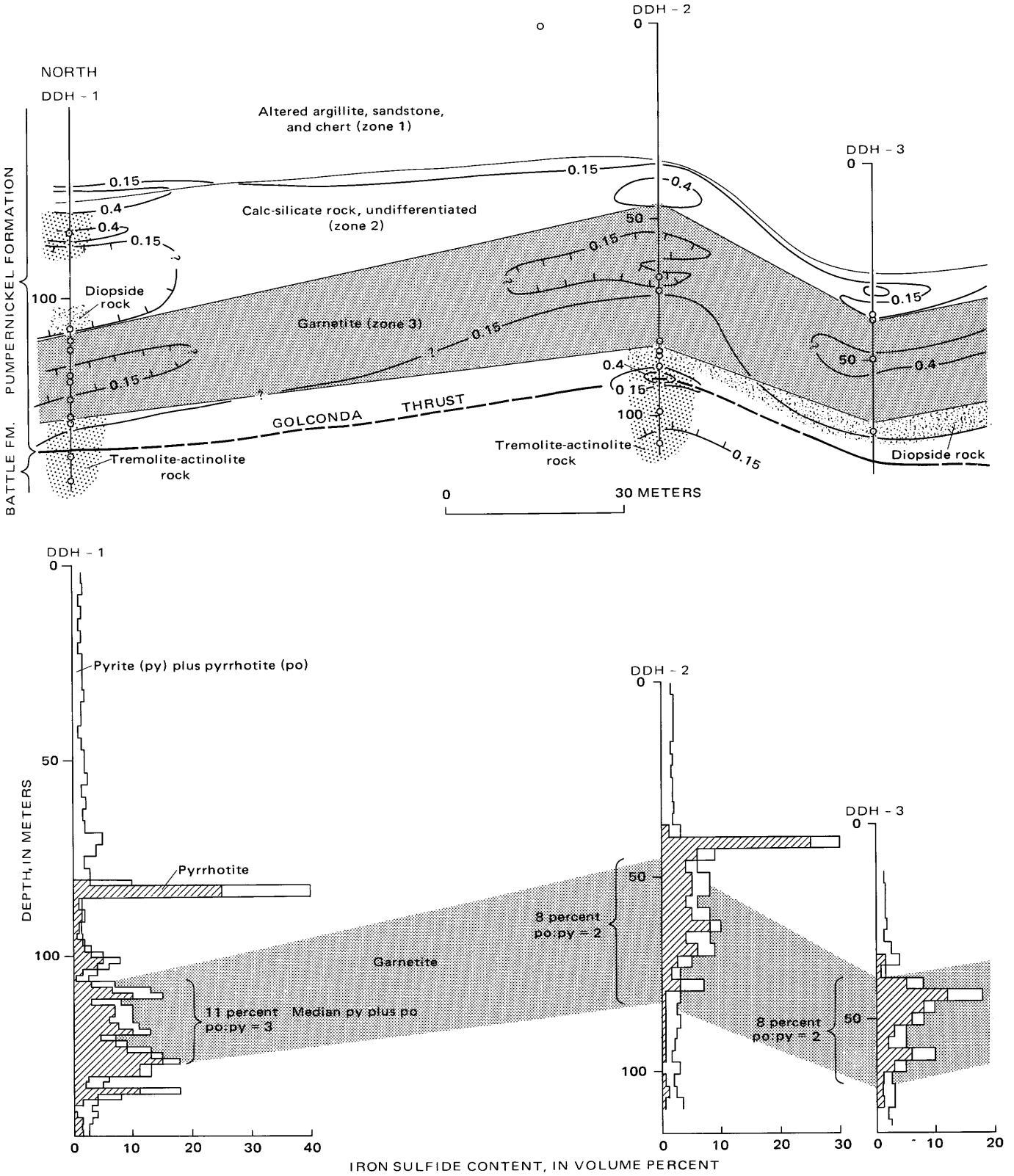

FIGURE 3.—Percentage of iron sulfides and weight percent copper equivalent in diamond drill core taken along section *A–A'* of plate 1. Iron-sulfide percentages visually estimated in drill core. Equivalent copper value calculated from concentrations of copper, gold, and silver

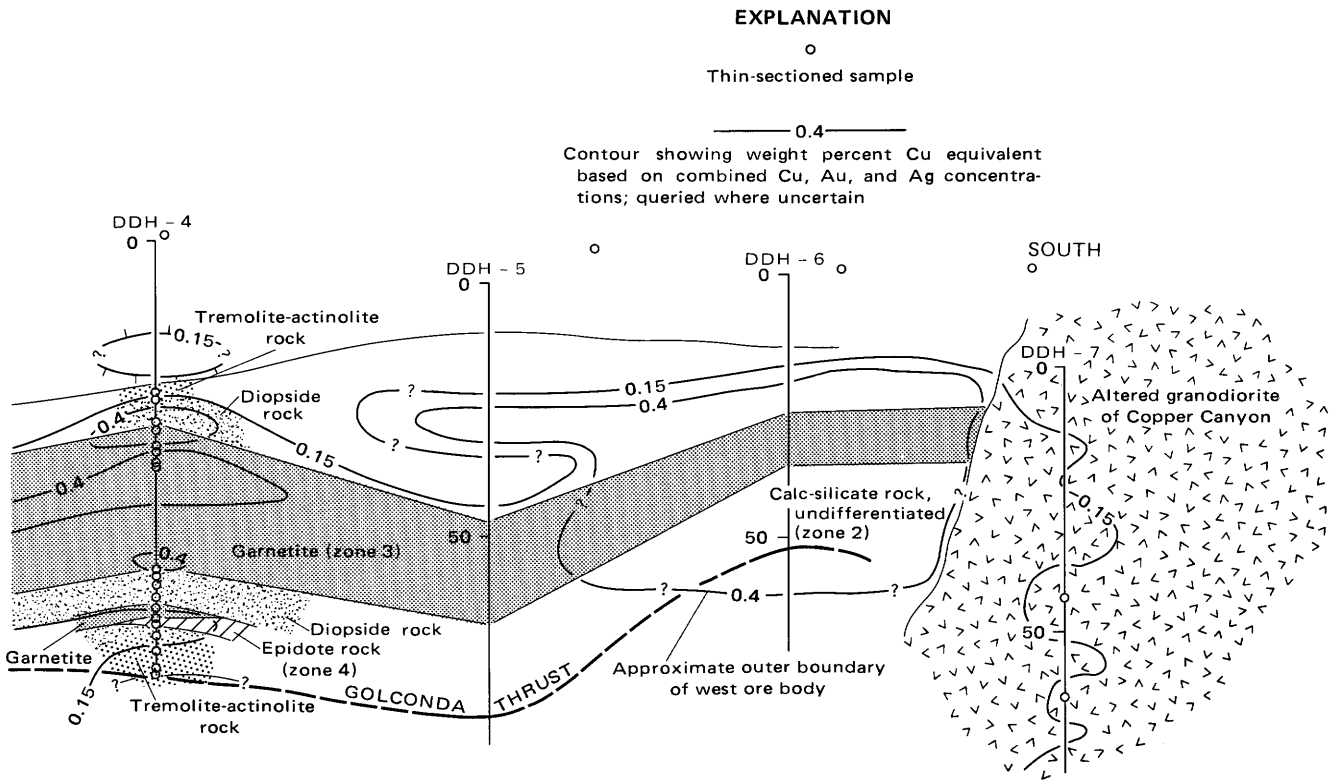

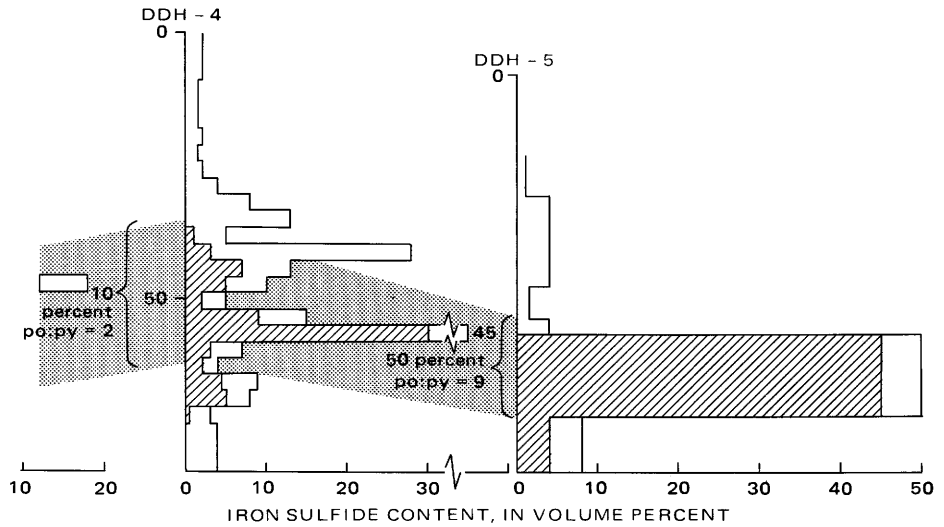

in channel samples of drill core. Domestic average price quoted in 1973 for copper, gold, and silver ($0.60 per pound, $75.00 per ounce, and $2.00 per ounce, respectively) was used.

ORE METALS IN THE SULFIDE ZONE

ANALYSIS AND SAMPLING

Quantitative and semiquantitative chemical analyses were made on splits from systematically collected channel samples of drill core and on sulfide-rich grab samples of core to establish elemental concentrations and associations in the sulfide zone in rocks of the Pumpernickel Formation. All intervals of drill core were analyzed for copper, gold, and silver. In addition, various parts of three holes were analyzed for 11 other elements (As, Bi, Co, Cr, Mn, Mo, Ni, Pb, Zn, Te, and W). About 87 percent of these supplemental determinations were made on cores from the general area of DDH–1, which was collared in some of the less intensely metallized ground, about 410 m from the granodiorite (fig. 3). All of these analyses form the basis for our statistical studies; the number of analyses vary from 40 for arsenic to 109 for copper, gold, and silver. Figures 5, 6, and 7 show the variations in the concentrations of ore metals in three representative holes along section *A–A′* (pl. 1).

In 15 grab samples of sulfide-rich rock, the concentrations of minor elements were determined in U.S. Geological Survey laboratories (table 3). These hand-sized samples of sulfide-rich skarn were obtained from six drill holes collared from 130 to 410 m from the granodiorite.

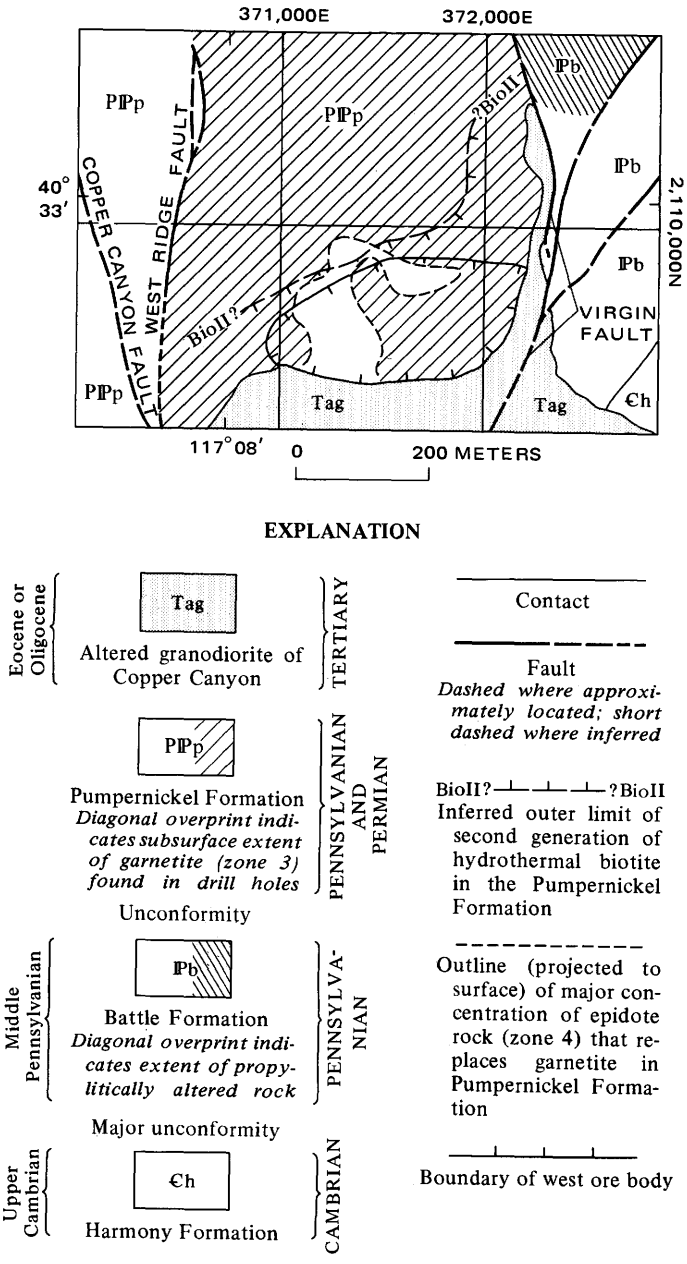

FIGURE 4.—Subsurface distribution of garnetite in Pumpernickel Formation and west ore body. Overall geometry of ore and garnetite was mapped from data obtained from drill holes, generally spaced about 60 m apart.

GEOGRAPHIC VARIATIONS OF COPPER, GOLD, SILVER, AND SOME OTHER METALS

Copper, gold, and silver concentrations vary significantly both vertically and laterally across the skarn. Drilling has revealed no enrichment of secondary copper above the skarn. There is only a very slight gain in the copper content of the rocks, measured in several hundred parts per million, near the base of the oxide zone (figs. 5 and 6). Below the oxide zone in DDH–1, the concentration of copper is 100 ppm or less for about 30 m in slightly recrystallized chert and argillite. In the next 30 m of chert and argillite, a few restricted zones with high concentrations of copper were penetrated. These zones contain chalcopyrite and pyrite assemblages in veins and as local replacements with copper concentrations as high as 8,000 ppm, and also with more than 1 ppm gold. The highest concentrations of silver, about 30 ppm, straddle the gradational boundary between the hornfels and chert and argillite. In this hole, copper is also distributed rather uniformly at concentrations of about 500 ppm through the main zone of garnetite. Distribution of gold is erratic through the garnetite; its concentrations fluctuate from less than 0.03 to 1.0 ppm. Gold probably averages, however, about 0.2 ppm in the garnetite, and the average ratio of silver:gold in it is close to 20:1, on the basis of calculations from analyses representing 70 percent of the garnetite penetrated.

Copper and gold are enriched strongly in garnetite toward the granodiorite. In garnetite from DDH–4, about 155 m from the granodiorite, the copper content is typically 1,000 ppm (fig. 6), about a twofold enrichment relative to its concentrations in DDH–1. Gold also increases from about 0.2 ppm in DDH–1 to about 1.0 ppm in DDH–4. Silver, on the other hand, seems to

TABLE 3.—*Analyses for minor metals in grab samples of drill core from the skarn*

[Semiquantitative spectrographic analyses by Chris Heropoulos. Results are reported to the nearest number in the series 1, 0.7, 0.5, 0.3, 0.2, 0.15, 0.1, 0.07, and so on, which represent approximate midpoints of interval data on a geometric scale. The precision of a reported value is approximately plus or minus one series interval at 68 percent confidence, or two intervals at 95 percent confidence. Looked for but not found: Cd, La, Nb, Pd, Pt, Sb, Te, U, Ce, Ga, Hf, In, Li, Re, Ta, Th, Tl, and Eu. Sample nos. 4 and 14 contain 30 and 20 ppm Ge, respectively. ____, not detected. Chemical analyses by J. Budinsky, C. Burton, H.N. Elsheimer, and R. Moore.]

	1	2	3	4	5	6	7	8	9	10	11	12	13	14	15
Drill hole (figs. 3, 4)	1	15	3	4	4	4	4	4	4	16	16	16	12	12	12
Depth (meters)	82	123	41	40	52	52	53	60	67	52	61	155	64	65	65
Semiquantitative spectrographic analyses (weight percent)															
Ag	0.05	0.0001	0.0001	0.007	0.0003	0.00015	0.0002	0.015	0.00015	0.0002	0.00015	0.007	0.0002	0.0005	0.0007
B	____	____	____	____	____	____	____	____	____	____	____	____	____	____	____
Ba	<.0002	.03	<.0002	.015	<.0002	<.0002	<.0002	.007	.07	.0003	.0015	.01	<.0002	<.0002	<.0002
Be	____	____	____	.0003	____	____	____	____	____	____	____	____	____	____	____
Bi	.003	____	.003	____	____	____	____	.01	____	____	____	.003	____	____	____
Co	.015	.001	.05	.002	.005	.007	.02	.003	.007	.015	.03	.005	____	____	.0005
Cr	____	.015	.0015	.007	.0015	.002	.002	.005	.03	.002	.007	.0015	.0005	.003	.0007
Mn	.01	.15	.07	.15	.1	.07	.07	.2	.02	.2	.07	.02	.03	.1	.07
Mo	____	____	____	____	____	____	____	____	.003	____	____	____	____	____	____
Ni	.2	.03	.007	.007	.007	.002	.005	.005	.02	.007	.005	.007	____	.001	.0002
Sc	____	.0005	____	____	____	____	____	____	.001	____	____	____	____	____	____
Sn	____	.005	.02	.05	____	____	____	.01	.007	____	.005	____	____	.003	____
Sr	____	.003	____	.001	____	____	____	____	.007	____	.0005	____	____	____	____
V	____	.007	____	.005	____	.0007	____	.003	.015	.001	.003	.007	____	.001	____
W	____	____	.015	.07	____	____	____	____	____	____	____	____	____	.005	____
Y	.001	.005	____	.005	____	____	____	.0015	.002	.001	.0015	____	.001	.0015	.001
Zr	____	.005	.002	.007	____	____	____	.01	.01	____	.002	.005	____	.007	____
Chemical analyses (parts per million)															
As	<10.0	<10.0	29.0	<10.0	<10.0	<10.0	<10.0	<10.0	18.0	295.	<10.0	1260.	<10.0	<10.0	<10.0
Au	1.7	.12	.1	170.	____	<.08	.19	2.7	.46	.07	.39	5.8	.24	.15	.51
Cu	55000.	620.	800.	5200.	780.	1100.	2500.	19000.	400.	1300.	980.	13000.	2100.	4400.	5200.
Hg	.086	.043	.008	.13	.014	.021	.019	.055	.023	.018	.03	.039	.017	.052	.015
Pb	39.	24.	31.	29.	32.	33.	27.	29.	27.	20.	38.	39.	24.	31.	30.
Sb	.7	2.3	2.6	1.	.4	1.1	.4	2.2	2.7	.7	1.4	.9	.6	.7	1.3
Zn	1140.	31.	1.	42.	15.	19.	24.	240.	10.	41.	11.	95.	18.	22.	35.

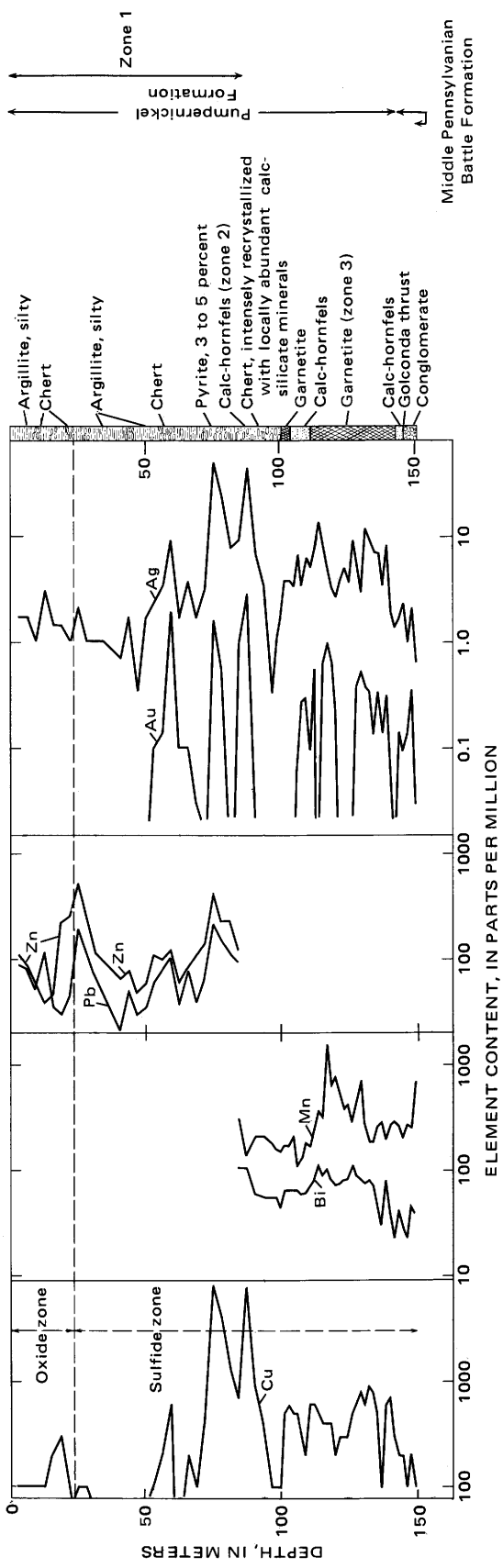

FIGURE 5.—Lithology and concentrations of seven elements in DDH–1, 410 m from the granodiorite of Copper Canyon. Analytical determinations plotted at depth of mid-point of channel samples taken from drill core.

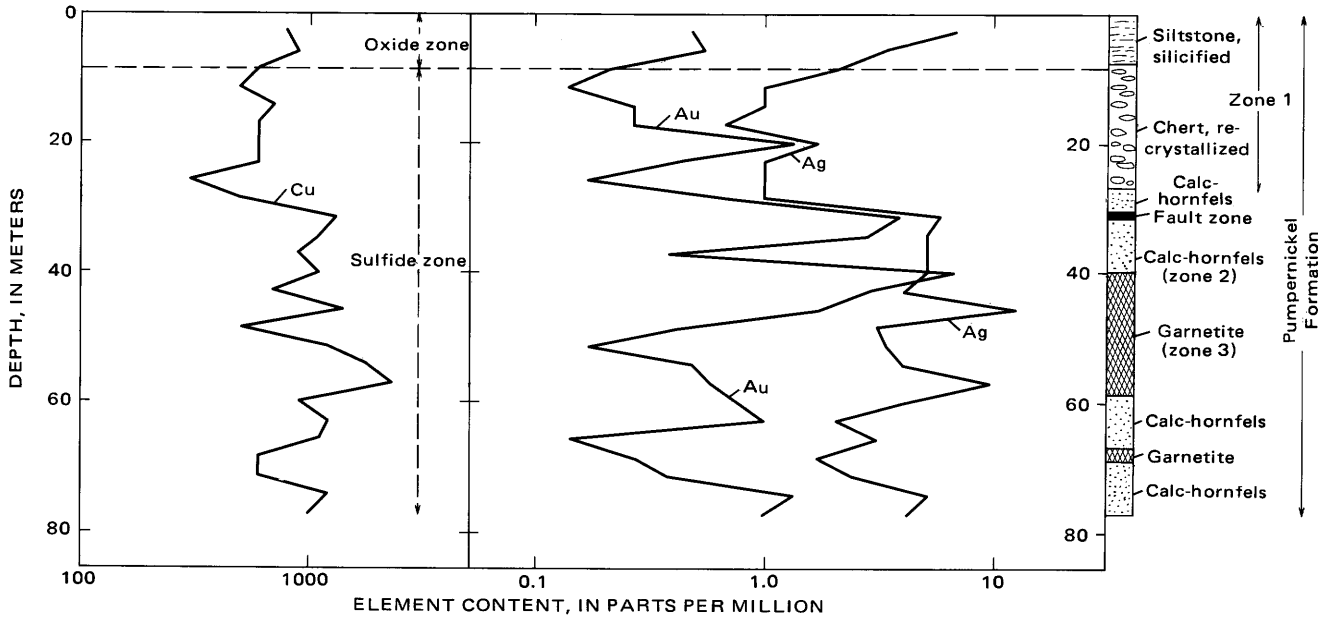

FIGURE 6.—Lithology and concentrations of copper, gold, and silver in DDH–4, 155 m from the granodiorite of Copper Canyon. Analytical determinations plotted at depth of midpoint of channel samples taken from drill core.

show no comparable increase along the garnetite from DDH–1 to DDH–4, although the silver:gold ratio in garnetite decreases from 20:1 to 10:1. This decrease in the silver:gold ratio primarily reflects an increase in the gold content of these rocks. Compared with its concentrations of about 1 ppm in hydrothermally altered chert and siltstone above the garnetite, silver is enriched roughly fivefold in the garnetite.

A significant thickness of ore (37 m) was penetrated by DDH–6 (fig. 7) about 40 m from the granodiorite on section *A–A'*. Ore-grade concentrations of copper, gold, and silver in this hole mostly include metasomatized rocks of the Pumpernickel Formation, and about 6 m of the upper member of the Battle Formation below the Golconda thrust. In addition, 2.5 m of altered granodiorite was penetrated near the base of the garnetite.

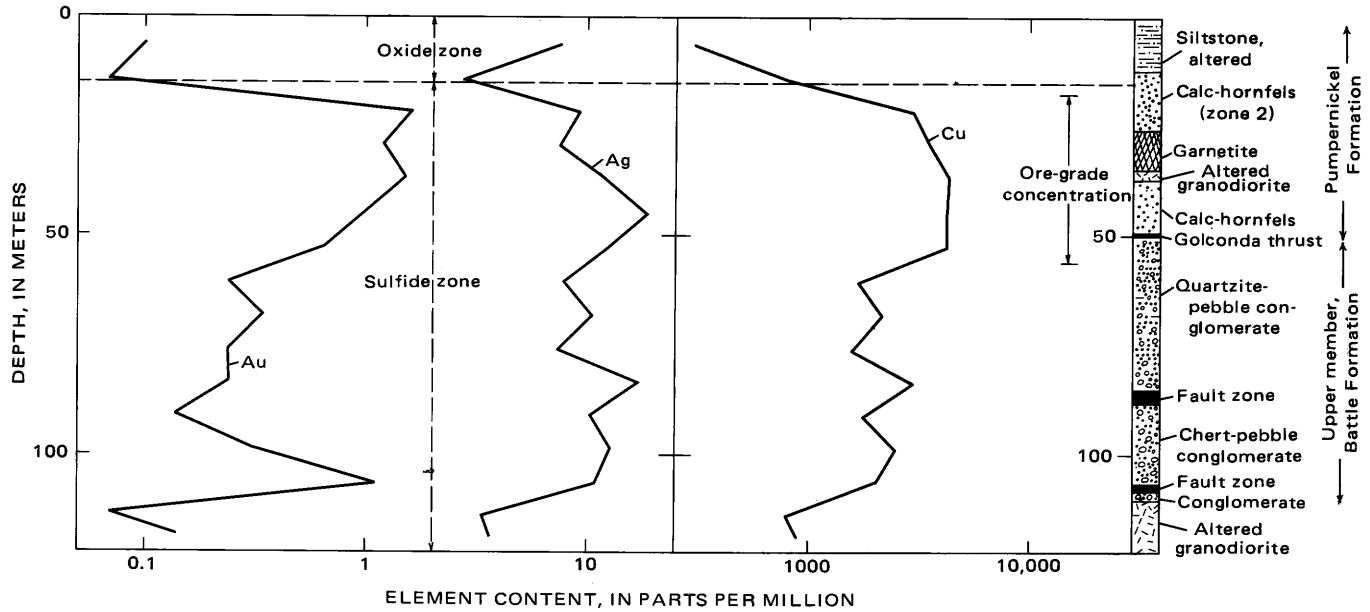

FIGURE 7.—Lithology and concentrations of gold, silver, and copper in DDH–6, 37 m from the granodiorite of Copper Canyon. Analytical determinations plotted at depth of midpoint of channel samples taken from drill core.

Copper concentrations here near the periphery of the ore body range from 3,000 to 4,300 ppm, gold from 0.65 to 1.6 ppm, and silver from 7.5 to 19 ppm. Five analyses of splits from 7.7-m (25-foot) channel samples of drill core through ore yield an average silver:gold ratio of 12:1. Heavily sulfidized ore-grade garnetite has a silver:gold ratio of 6:1. Thus, from north to south across the garnetite along section *A–A'* there is a consistent decrease of the silver:gold ratio from 20:1 to 6:1 in ore. About 45 percent of the 1973–74 dollar value of ore penetrated by DDH–6 was derived from the precious-metal content of the rocks. However, the dollar value of ore changed significantly in the intervening years so that by early 1976, just as the ore was being exposed, the precious-metal content of the west ore body made up more than 50 percent of the commercial metals.

Rocks below the ore body are also metallized but at subeconomic levels (fig. 7). For the most part, copper in the upper member of the Battle Formation has a fairly uniform concentration of about 2,000 ppm in this general area. The subeconomic concentration of copper, gold, and silver contained in most of the Battle Formation below the west ore body is a contrast to the strong concentrations in the east ore body (Theodore and Blake, 1975); this may reflect in part a premetallization lithology and chemistry unfavorable for the development of ore. We infer the absence in these rocks of significant calcite and hematite, which were important for metallization in the east ore body; this will be discussed in more detail below. Below the Battle Formation, however, concentrations of copper decrease sharply; copper concentrations in altered granodiorite near the bottom of DDH–6 are less than 1,000 ppm. This granodiorite is inferred to be contiguous with the main intrusive mass that crops out farther to the south. If this geometry is correct, the contact between the granodiorite and its wallrock must dip about 70° north here.

Grab samples several centimeters in size and consisting of 50–90 percent sulfides were taken from drill core of garnetite to determine the approximate content of minor metals in some of the most sulfide-rich skarn. Pyrrhotite is the dominant iron sulfide in all samples but one (sample 12, table 3), in which pyrite is the most abundant sulfide. Wispy intergrowths of marcasite and pyrite in pyrrhotite, and sporadic clots of pyrite also occur in all of the pyrrhotite-bearing rocks. Chalcopyrite is the main ore mineral in them; chalcocite, sphalerite, and arsenopyrite are minor constituents. Three samples (nos. 13–15, table 3) are from the west ore body.

Chemical analyses of grab samples demonstrate an extreme variation of minor metals and their generally low concentrations in small volumes of skarn. For example, the highest concentration of gold (170 ppm; no. 4, table 3) was detected in DDH–4, 40 m below the collar of the hole, in garnetite. However, analysis of a 3-m channel sample across the locality of this grab sample yielded a gold content of only 6.8 ppm. Thus, gold apparently is distributed very unevenly through these rocks. This sample with the highest concentration of gold also contains the most tungsten (700 ppm) and mercury (0.13 ppm) of the samples analyzed. Nonetheless, the overall content of mercury is low in both subeconomic and ore-grade sulfidized rocks around the west ore body compared to its concentration in the east ore body (Theodore and Blake, 1975). In addition, these analyses of grab samples also reveal generally low concentrations of molybdenum, lead, tungsten, and zinc in the garnetite. Analytical determinations of three samples from the ore body (nos. 13–15, table 3) yielded <5 ppm molybdenum, 24–31 ppm lead, <50 ppm tungsten, and 18–35 ppm zinc. In many copper-bearing skarn deposits elsewhere, these metals occur in significant concentrations (Gale, 1965; Hernon and Jones, 1968; Himes, 1972).

FREQUENCY DISTRIBUTIONS AND CONCENTRATIONS OF MINOR ELEMENTS

Histograms prepared from chemical analyses of the channel samples transformed to common logarithms form a graphic base to which we will later compare the distributions of elements in the oxide zone above the skarn (fig. 8). Our conclusions are preliminary because of the small number of analytical determinations available, and because of the relatively low sensitivity of the analytical methods used for many of the elements reported here. In addition, about 87 percent of the analytical determinations we used to construct figure 8 are based on rock from drill holes in the general area of DDH–1 (fig. 3), about 410 m from the granodiorite. Thus, the distribution, concentrations, and associations of the elements ascribed to the sulfide zone are strongly biased toward the subeconomic sulfidized rocks. Frequency distributions for some elements such as gold, molybdenum, and tungsten are indeterminate because of inadequate sensitivity of the analytical methods; from 43 to 65 percent of the analyzed samples have concentrations below the limits of detection. The median of the gold analyses is 0.1ppm; the histogram for gold probably reflects a multimodal distribution if we assume that analytical discrimination is good near the detection threshold. The histogram for silver is unimodal, with a 3-ppm median. Histograms of the other 10 elements show unimodal distributions. The distributions of nickel, zinc, and arsenic(?) are skewed positively, with a longer tail toward high values than toward low values (Miesch,

1967). Those for bismuth and tellurium are skewed negatively. Thus, most of the elements (particularly Ag, Bi, Co, Cr, Cu, Mn, Pb, and Te) in these rocks show distributions that approximate a lognormal distribution, mostly with a relatively small logarithmic standard deviation.

These data (fig.8) include the only analyses available for tellurium from the Copper Canyon area. Tellurium seems to be fairly well distributed through sulfide-bearing rock in and around the garnetite at 20 to 150 ppm. Tellurium has also been reported in the core of the Robinson mining district near Ely, Nev. (Gott and others, 1966; James, 1971, p. 139).

The minor-element content of sulfidized rocks

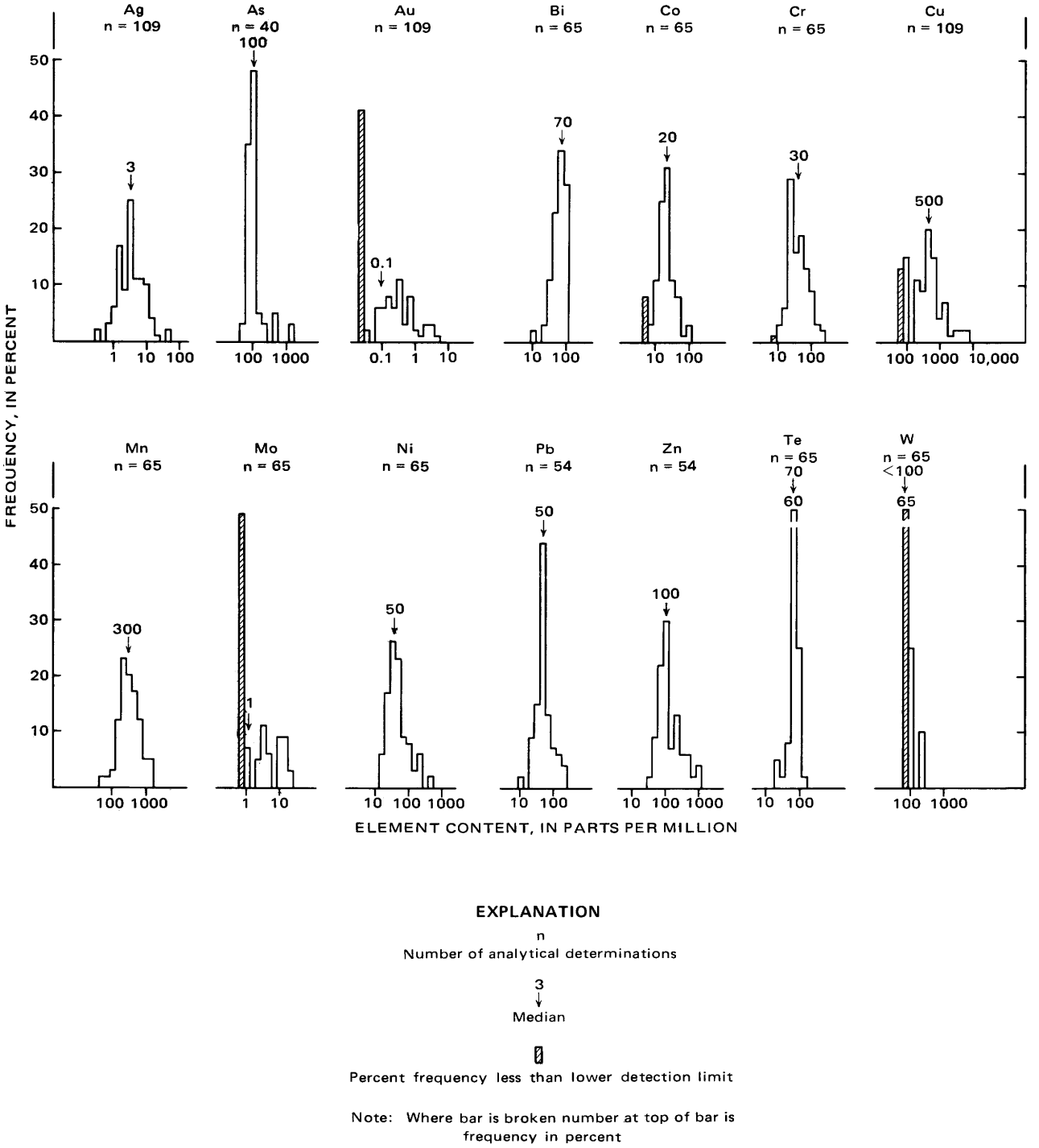

FIGURE 8.—Frequency distributions of 14 metals in drill core from sulfide zone, primarily in general area of DDH–1 (fig. 3).

TABLE 4.—*Ranges and median values for 13 metals from around the skarn and from the east ore body*
[In parts per million]

Element	Rocks around the skarn[1]		East ore body[2]	
	Range	Median	Range	Median
Ag	0.3 – 500	3.0	<0.5 – 70	3.0
As	<10 – 1,500	70	<200 –>10,000	<200
Au	<0.03– 170	.07	.02– 7	.2
Bi	<7 – 100	50	<10 – 1,000	<10
Co	<2 – 500	15	<5 – 700	30
Cr	<5 – 200	30	5 – 500	70
Cu	<100 –>20,000	500	150 –>20,000	3,000
Mn	50 – 2,000	200	<10 – 1,000	70
Mo	<1 – 30	1	<5 – 50	<5
Ni	<2 – 2,000	30	5 – 300	50
Pb	10 – 200	30	<10 – 2,000	<10
Zn	1 – 1,000	70	<200 –>10,000	300
W	<100 – 700	<100	<50 – 150	<50

[1]Data combined from figure 8 and table 3.
[2]Determined from analytical determinations of 45 1-kg rock samples from the 6,450 bench, east ore body (Theodore and Blake, 1975). Ten of these samples are of fault breccia and include iron oxides developed during supergene leaching.

around the west ore body differs somewhat from that previously reported in the east ore body. Table 4 lists ranges and medians for 13 metals in these two bodies of rock. Judging from their median values, bismuth, manganese, and lead appear to be more abundant in the sulfidized Pumpernickel Formation than in the east ore body, whereas the east ore body seems to contain more chromium, zinc, and gold(?). Significant concentrations of gold occur in the east ore body in quartz-arsenopyrite veins that cut disseminated replacement copper ore (Theodore and Blake, 1975).

STATISTICAL ANALYSIS OF ELEMENTAL ASSOCIATIONS

Associations among elements in the sulfide zone around the garnetite were calculated by statistical methods. A prerequisite for proper calculation of product moment correlation coefficients, one of the most commonly used methods for determining strength of association, is that the samples studied be representative of a normally (or here, lognormally) distributed population. This was not true of all the chemical data shown in figure 8. Thus, elemental associations in the garnetite and enclosing rocks were determined by Spearman rank correlation techniques, best employed where data are not normally distributed (Siegel, 1956; Lovering, 1963; Lovering and others, 1968). Table 5, prepared from the analytical data used to construct figure 8, shows correlation coefficients calculated for those pairs of elements that have at least 20 paired-element analyses. The relatively small number of analytical determinations available for these rocks (40–109) constrains us to determine statistical associations with an unusually small set of samples. All corre-

TABLE 5.—*Array of numbers of pairs of elements and Spearman correlation coefficients calculated from analytical determinations on channel samples of drill core from the sulfide zone of the Pumpernickel Formation*
[N.d., not determined, less than 20 paired-element analyses; *, significant at 99.5-percent confidence level]

	Ag	As	Au	Bi	Co	Cr	Cu	Mn	Mo	Ni	Pb	Zn	Te	W
Ag		0.09	0.50*	0.31	0.36*	−0.45*	0.79*	−0.25	−0.19	0.25	0.14	0.44*	−0.11	−0.17
As	40		.27	.39	.11	−.21	.14	.20	N.d.	.10	N.d.	N.d.	.34	−.28
Au	64	26		.29	.21	.00	.43*	−.03	.16	.13	−.19	.37	−.14	N.d.
Bi	65	40	50		.32	−.22	.34*	−.31	.52*	.48*	N.d.	N.d.	.24	.14
Co	60	35	46	60		−.18	.60*	−.16	.27	.29	N.d.	N.d.	.02	−.32
Cr	64	39	49	64	59		−.26	−.05	.22	.03	N.d.	N.d.	.25	−.13
Cu	95	40	63	65	60	64		−.16	−.11	.49*	−.08	.24	.14	−.26
Mn	65	40	50	65	60	64	65		.29	−.19	N.d.	N.d.	.09	.32
Mo	33	14	28	33	30	33	33	33		.12	N.d.	N.d.	−.23	N.d.
Ni	65	40	50	65	60	64	65	65	33		N.d.	N.d.	.46*	.13
Pb	24	0	24	10	10	10	40	10	9	10		.42*	N.d.	N.d.
Zn	54	0	24	10	10	10	40	10	9	10	54		N.d.	N.d.
Te	65	40	50	65	60	64	65	65	33	65	10	10		.21
W	23	20	17	23	21	22	23	23	10	23	1	1	23	

Numbers of pairs of elements

Correlation coefficients

lations, both negative and positive, that are statistically significant at the 99.5-percent confidence level (less than five chances in 1,000 that such a high correlation is invalid) are indicated by an asterisk (*) on table 5. In this data set from the sulfide zone, copper has statistically significant positive correlations with silver, gold, bismuth, cobalt, and nickel at the 99.5-percent confidence level; gold is similarly associated with silver, and silver with cobalt and zinc. In addition, silver and chromium tend to vary inversely, as indicated by a statistically significant negative correlation, which may reflect some removal of chromium from the Pumpernickel during hypogene metallization (see also Theodore and Nash, 1973; and below). The correlation of copper and chromium in this data set is also negative and significant at the 97.5-percent confidence level. Gold and chromium seem to vary independently.

Several other associations in the data set require further discussion. Positive correlations for molybdenum-bismuth, nickel-bismuth, lead-zinc, and nickel-tellurium pairs are significant at the 99.5-percent confidence level (table 5). Certainly, the strong lead-zinc association is not surprising near the northern parts of the garnetite, where most of the samples in the data set come from, and this relation may reflect in part the enrichment of a lead-zinc halo around the central copper-gold-silver zone described by Roberts and Arnold (1965). In addition, in this data set copper shows no variation with lead, and it shows a weak positive correlation with zinc that is statistically significant at the 90-percent confidence level. The absence of a strong positive association of copper with lead and zinc in the sulfide zone may partly reflect the fact that sparse galena and sphalerite were introduced after the deposition of most chalcopyrite (Nash and Theodore, 1971; Theodore and Blake, 1975). The very strong copper-nickel correlation (table 5) in this data set suggests a chalcopyrite-pyrrhotite association because in the east ore body preliminary studies of minor elements in concentrates of pyrrhotite showed them to contain some nickel. The absence of a direct variation of nickel with chromium in the sulfide zone, however, contrasts with the strong positive correlations of nickel with Ba, Cr, Ti, and Zr at the surface in sparsely mineralized areas of the Pumpernickel (Theodore and Nash, 1973; see section below "Geochemistry of Bedrock Exposed Around the Skarn"). Thus, in the most intensely sulfidized rocks, some nickel was probably mobilized and incorporated into the sulfides during metallization. The lack of significant correlation between copper and molybdenum is consistent, we believe, with the very few occurrences of coexisting chalcopyrite and molybdenite we observed in the east ore body (Theodore and Blake, 1975). There, sparse quartz-molybdenite veinlets with white mica selvages cut and therefore postdate the chalcopyrite-potassium silicate mineral assemblages in the Battle Formation. Lastly, manganese shows no significant correlation with copper, which suggests to us that manganese is probably a poor pathfinder element here for copper; however, in garnetite there is a suggestion of covariation between manganese and gold (fig. 5), but this association is not maintained in rock other than garnetite (-0.03 correlation coefficient for Au–Mn, table 5).

PETROLOGY OF ROCKS AROUND THE WEST ORE BODY

HARMONY FORMATION

The Upper Cambrian Harmony Formation crops out east of the Virgin fault in a small 100 by 300 m area adjacent to the granodiorite and near the southeast corner of the area of plate 1. Elsewhere in the district the Harmony Formation crops out widely, especially north and east of Copper Canyon (Roberts, 1964). The formation was also penetrated near the bottoms of three holes between the Virgin and Copper Canyon faults (DDH–2, –11, and –16; pl. 1), beginning at depths of about 250 m below ground surface. In these three holes, the Harmony unconformably underlies the Battle Formation, which is underneath the overthrust Pumpernickel Formation, host for most of the west ore body. The Harmony Formation has also been reached at a depth of 170 m by another hole collared east of the main trace of the Virgin fault (DDH–17, pl. 1). The hypogene, supergene, and detrital mineralogy of three rocks from the Harmony Formation are listed in table 6 (nos. 1–3).

The Harmony Formation includes mostly purplish-gray to pinkish-brown altered sandstone and silty sandstone with an overall hornfelsic texture. Total pyrite-pyrrhotite-chalcopyrite content of the Harmony Formation in the holes is about 1 to 2 percent, and the sulfides are concentrated in quartz-pyrite, quartz-pyrrhotite, pyrite-pyrrhotite-chalcopyrite-quartz, and chalcopyrite-pyrite veinlets with various amounts of marcasite and potassium feldspar. Marcasite formed as a secondary alteration product from pyrrhotite. The copper content typically ranges form 0.01 to 0.2 weight percent, and it reaches about 0.5 weight percent locally in rock directly below the unconformity with the overlying Battle formation. Similar increases in copper near the unconformity were found in the east ore body (Theodore and Blake, 1975).

Generally, the altered silty sandstone of the Harmony Formation consists of an assemblage of metamorphic plus detrital minerals. Subrounded to subangular detrital quartz grains 0.3 –0.5 mm across are the predominant mineral in the rocks. Generally these

TABLE 6.—*Mineralogy of altered sandstone of the Harmony Formation, and altered argillite and chert (zone 1) of the Pumpernickel Formation*

[X, mineral present; Tr, mineral present in trace amounts; ?, questionably present; ____, not found]

	1	2	3	4	5	6	7	8	9	10	11	12	13	14
	Harmony Formation			Pumpernickel Formation										
				Surface samples (locs. on fig. 3)					Drill core (loc. DDH–18, pl. 1)					DDH–12
Field No.	8–833	43–571	43–606	W–1	W–2	W–3	W–4	W–5	3–63	3–66	3–92	3–107	3–143	2–137
Hypogene constituents														
Quartz	X	X	Tr	X	X	X	X	X	X	?	X	X	X	X
Potassium feldspar	X	X	____	?	X	____	____	X	Tr	____	Tr	____	Tr	X
Biotite	X	Tr	X	Tr	____	X	____	X	____	____	X	X	____	X
White mica	X	Tr	X	X	____	Tr	X	X	Tr	____	____	X	Tr	____
Chlorite	X	X	____	Tr	____	Tr	____	Tr	X	____	X	Tr	____	____
Tremolite	____	____	____	____	X	X	____	____	____	X	____	____	X	X
Epidote	X	X	____	____	X	____	____	____	X	Tr	X	X	Tr	Tr
Sphene	X	X	Tr	Tr	X	X	Tr	Tr	Tr	X	X	X	X	X
Vesuvianite	____	____	____	____	____	____	____	____	____	____	____	____	X	____
Pyrite	X	Tr	X	____	X	X	X	X	X	X	X	X	X	X
Chalcopyrite	X	____	____	____	____	____	____	____	____	____	?	____	____	____
Carbonate	X	____	____	____	____	____	____	____	____	____	____	____	X	____
Supergene constituents														
Hematite	X	____	____	Tr	X	X	X	X	X	____	Tr	Tr	Tr	Tr
Carbonate	____	X	____	____	____	____	X	____	____	____	____	____	____	____
Detrital constituents														
Quartz	X	X	X	X	X	X	X	X	X	X	X	X	X	X
Potassium feldspar	____	X	X	X	X	____	Tr	Tr	____	Tr	Tr	____	Tr	?
Plagioclase	X	X	X	Tr	Tr	Tr	____	X	____	X	X	X	____	X
Biotite	____	____	X	Tr	____	____	____	Tr	____	____	____	____	____	____
White mica	____	____	X	X	____	____	____	____	____	____	____	____	____	____
Allanite	X	____	____	____	____	____	____	____	____	____	____	____	____	____
Apatite	X	X	X	Tr	Tr	Tr	____	____	Tr	X	Tr	Tr	____	Tr
Zircon	X	X	X	Tr	Tr	Tr	X	X	Tr	X	Tr	Tr	Tr	Tr
Tourmaline	____	____	Tr	Tr	____	____	____	____	____	____	____	Tr	____	____
Rock fragments	____	____	____	____	____	____	____	____	X	____	X	X	X	____

grains are set in a very fine, complexly sutured aggregate of quartz, potassium feldspar, white mica, and biotite (fig. 9). Secondary biotite is the major hypogene mineral in one of the rocks studied (no. 3, table 6). Crystals of reddish-brown biotite make up a dispersed felted aggregate between detrital quartz grains; much of the biotite apparently has grown from detrital micas and clays. Some hydrothermal biotite, however, is cream to pale tan under the microscope and includes sparse granules of sphene. None of these hydrothermal biotites show greenish hues under the microscope, as ascribed to the zones with weak copper mineralization and hydrothermal biotite described by Carson and Jambor (1974) in British Columbia. Hydrothermal potassium feldspar is apparently stable in two of the rocks, whereas detrital grains of potassium feldspar are sparsely altered to white mica, possibly reflecting slight differences in their orthoclase content. Some plagioclase is also altered locally to white mica and clouded, possibly reflecting very fine grained late-stage alteration products. The rocks of the Harmony locally are flooded by pervasive quartz veins, typically 2–3 mm wide, that are barren of sulfides but include traces of potassium feldspar and white mica. This barren quartz stage is crosscut by carbonate (siderite?)-chlorite veinlets with possibly supergene hematite along hairline fractures.

PUMPERNICKEL FORMATION

In the general area of the west ore body, the Pumpernickel Formation can best be classified into four metamorphic zones: (zone 1) altered argillite, silty sandstone, and chert with secondary biotite as the diagnostic zonal indicator; (zone 2) calc-silicate rock, which can be subdivided further into rock containing locally abundant diopside or tremolite; (zone 3) andradite-diopside-rich garnetite; and (zone 4) epidote-rich rock derived largely from garnetite. The rocks in zone 1 are farthest away from the ore, and they probably correspond to the biotite hornfels ascribed to thermal metamorphic effects at many other porphyry copper deposits. We believe that the alteration mineralogy of zone 1 reflects a prograde recrystallization contemporaneous with that shown by zones 2 and 3 (see below); the mineralogy of zone 4 has developed primarily as a retrograde alteration of garnetite (zone 3). Furthermore, combinations of mineral assemblages locally can occur in a single hand sample, largely as the result of superposed, incomplete metamorphic reactions. Cross sections show the zonal geometry of the first three assemblages and their relations to ore and to one another (pl. 1, fig. 3). Figure 10 illustrates additional mineralogic details, primarily in mineral assemblage zones 2 and 3 along DDH–4; this drill hole is the closest to ore along section line A–A′ for which we have observations with the microscope. Epidote-rich rock, the fourth type of metamorphosed rock, is best developed as a replacement of garnetite in an irregular volume of rock near the granodiorite, and it is largely coincident with ore (fig. 4) but less extensive. Note that the front of the mineral zones, as depicted on figure 3, in the skarn at Copper Canyon is oriented roughly at right angles to the edge of the granodiorite. Implications of this geometry for the overall petrogenesis of the skarn will be discussed fully below. In addition, all these mineral assemblages have been flooded by an even later suite of hydrous silicates, chiefly biotite, and sulfides in the immediate area of the west ore body.

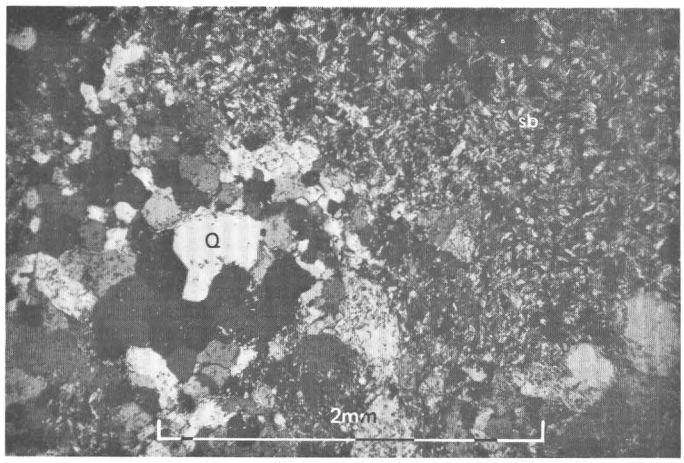

FIGURE 9.—Photomicrograph showing altered silty sandstone of the Harmony Formation from DDH–2, 253 m depth; Q, quartz, sb, secondary biotite. Crossed nicols.

ALTERED ARGILLITE AND SANDSTONE

Zone 1, the least recrystallized rock around the west ore body, includes argillite, fine-grained sandstone, and chert belonging to the lower member of the Pumpernickel Formation (fig. 3). The rocks of this metamorphic zone are the only ones of the Pumpernickel to crop out in the general area of the granodiorite, and they extend from the edge of the granodiorite to beyond the northern boundary of the area on plate 1. Thus, it is important from an exploration geologist's viewpoint to know whether detailed petrologic study of the exposed rocks during the early stages of exploration would have suggested the presence of the underlying and unexposed ore-bearing skarn. The rocks of zone 1 primarily are distinguished from the other zones by secondary biotite, and by the relict sedimentary fabric of their incompletely recrystallized detrital minerals. Altered argillite and a great variety of associated rock types, complexly interbedded with one another on the

meter and centimeter scale, all have highly variable thicknesses as revealed in many drill holes. Secondary biotite, characteristic of potassic alteration (Creasey, 1966), seems to extend to the edge of the sulfide en-

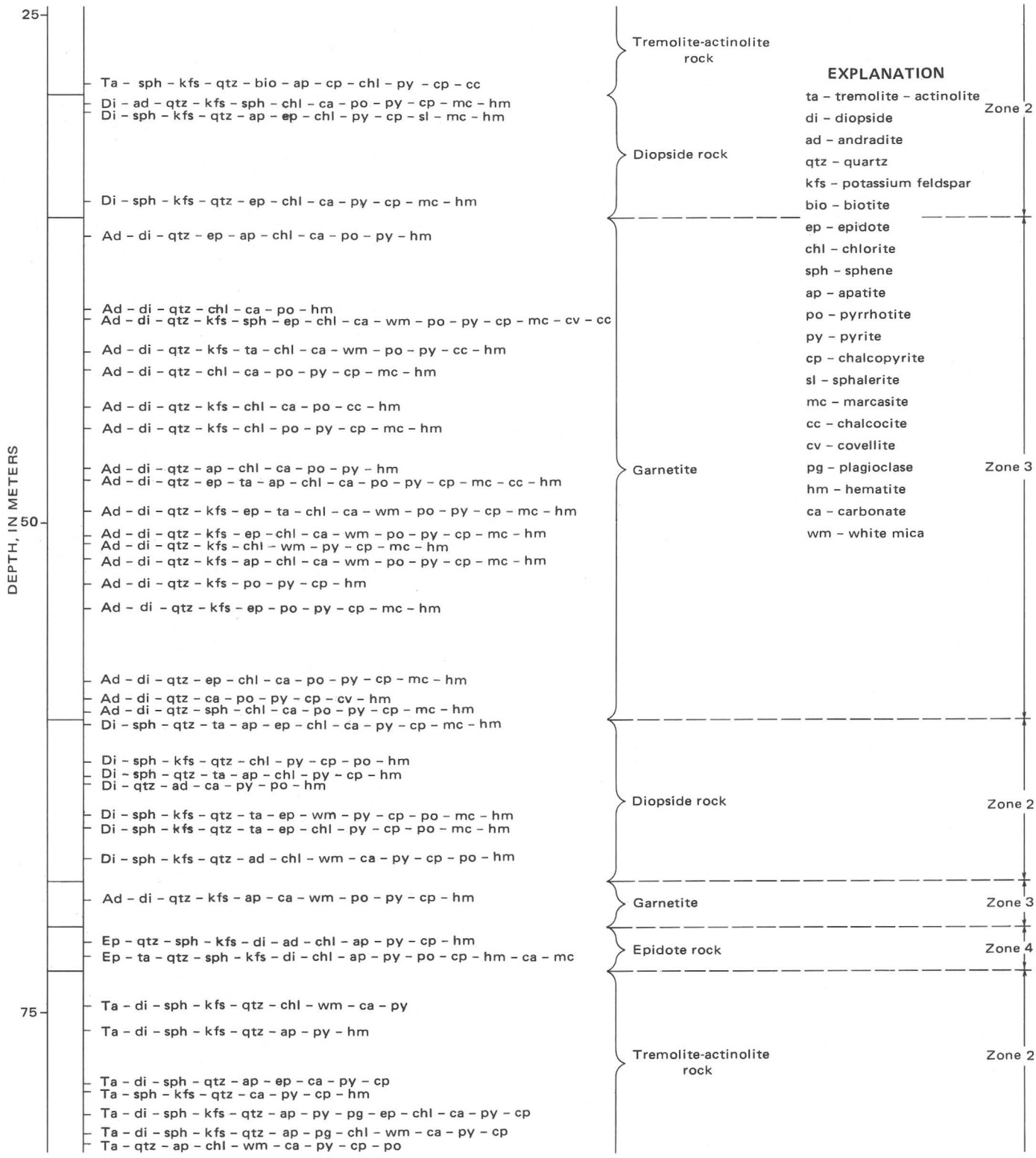

FIGURE 10.—Lithology of part of DDH–4 and its mineralogic details and zonations.

velope that surrounds the porphyry system (fig. 2). This mineralogical zone generally ranges from 10 to 45 m beyond the calc-silicate minerals in zone 2. The maximum distance that the mineral assemblages of zone 1 once extended cannot be determined because of postmineralization erosion, but the entire lower member of the formation is estimated to have had a stratigraphic thickness of 150 to 300 m (Roberts, 1964, p. A39; Theodore and Blake, 1975). The local variations in thickness of the rocks assigned to zone 1 (fig. 3) are largely due to encroachment of the underlying calc-silicate rock with its almost completely recrystallized fabric. The sulfide content of rocks in zone 1 typically is several volume percent, composed mostly of pyrite. In addition, copper content in the rocks of zone 1 within the sulfide zone ranges from 100 to about 700 ppm (figs. 5–7). Below zone 1, diopside- and tremolite-rich rock of zone 2 surrounds the garnetite that composes zone 3 (see also pl. 1, fig. 3). Table 6 lists the mineralogy of ten samples of altered argillite and silty sandstone; five are from the surface near section line *A–A′* (nos. 4–8), and five are from DDH–18 at 19 to 44 m below ground surface.

The intensity of alteration does not systematically increase from north to south in the rocks of the Pumpernickel Formation exposed north of the granodiorite. Furthermore, well within the sulfide alteration halo (fig. 2), hypogene effects are only very subtly displayed at the surface. For example, about 350 m from the granodiorite, in brown silty argillite that is slightly hornfelsic (no. 4, table 6), subangular detrital fragments of quartz (about 0.1 mm across) compose about 40–50 percent of the rocks, and they are set in a very fine grained white mica matrix that is recrystallized. The matrix has an average grain size of less than 0.01 mm, and only about 2–3 percent of the matrix is hydrothermal biotite; there is an undetermined amount of hydrothermal potassium feldspar in the matrix also. Under the microscope, some detrital grains (including quartz, sparse white mica, and sparse biotite) show incipient signs of recrystallization only along their margins. Nonetheless, the occurrence in this general area of some apparently stable hydrothermal potassium feldspar both in the groundmass and in sparse quartz veins, and hydrothermal biotite (although in limited amounts), reflects widespread potassic alteration related to a metamorphic event. Chlorite and sphene are hydrothermal minerals, formed from a subsequent alteration of early hydrothermal biotite; traces of detrital plagioclase, zircon, and tourmaline also occur through these rocks.

Closer to the intrusion, tremolite is an important hypogene silicate in quartz-potassium feldspar-pyrite-sphene±biotite±epidote±white mica-bearing rocks collected 75–155 m from the granodiorite (nos. 5–6, table 6). In these rocks, stubby 0.1- to 0.2-mm clusters of tremolite needles are sprinkled throughout some domains and may compose 20–30 volume percent of an entire rock. The tremolite apparently is coexisting stably with potassium feldspar. However, within some other millimeter- to centimeter-sized domains of one of the samples (no. 6), there is excellent textural evidence for antithetic relations between very early hydrothermal biotite plus potassium feldspar and later tremolite plus potassium feldspar. The biotite is only slightly pleochroic, and very pale tan under the microscope and thus probably phlogopitic. Wispy discontinuous veinlets of tremolite-sphene-pyrite that have a sparse tremolite selvage 1 mm wide cut a well-developed assemblage of biotite-potassium feldspar-quartz-pyrite that locally makes up most of the groundmass of these rocks (fig. 11). Thus, in some rocks crystallization of tremolite definitely postdates crystallization of some hydrothermal biotite; crystallization of some biotite and potassium feldspar continued along minor slip planes that offset the tremolite-bearing veinlets. The crystallization of secondary biotite along these slip planes suggests its prolonged stability and forms some of the textural evidence used to map the distribution of a second generation of biotite in the rocks (BIO II, fig. 4). These observations are significant because they establish for these rocks overlapping paragenetic relations for tremolite, one of the typical minerals of a calc-silicate contact metasomatic assemblage, and hydrothermal biotite and potassium feldspar. Introduction of copper-bearing hydrothermal solutions into preexisting contact metamorphic aureoles has been reported in the literature (Lindgren, 1905; Creasey,

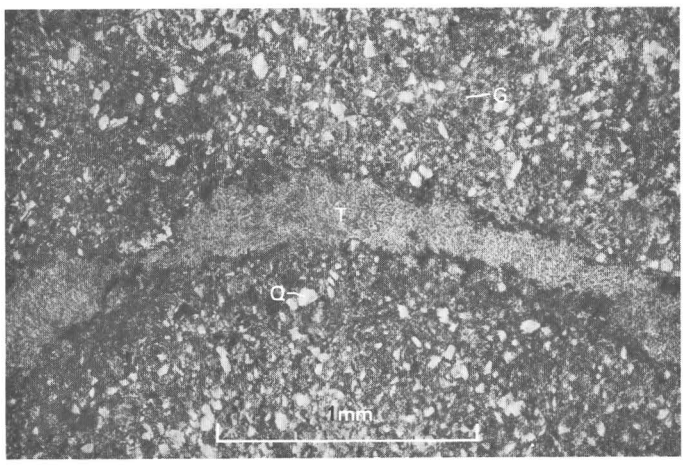

FIGURE 11.—Photomicrograph showing tremolite (T) in a veinlet cutting a very fine grained groundmass (G) of hydrothermal biotite, potassium feldspar, and quartz. Detrital quartz grains (Q) are largely unrecrystallized. Sample W3, from an exposure 75 m north of the granodiorite; plane-polarized light.

1966; Zharikov, 1968; Phan, 1969), but recent studies indicate that fluids altering calc-alkaline plutonic rocks to a potassic alteration assemblage may yield skarn-type assemblages if they come in contact with carbonates (James, 1971). Others suggest skarn in porphyry copper deposits may develop in any of the classic alteration zones (Sillitoe, 1973; Titley, 1973). Thus, textural suggestions of calcium-bearing minerals recrystallizing about the same time as hydrothermal biotite or potassium feldspar might form a basis for continued exploration for any unexposed skarn in the proper geologic setting. Such an exploration hypothesis would be based partly on the generally accepted phenomenon of successive migration of crystallization fronts away from centers of zoned skarn.

South of the tremolite-bearing zone (nos. 5–6, table 6), the rocks pass into a poorly defined but seemingly restricted area of white-bleached rock, where the hypogene assemblage is quartz-white mica-pyrite (no. 7; table 6). There are also in the rock trace amounts of hydrothermal(?) carbonate, possibly siderite, in hairline microveinlets. Detrital quartz grains, that average about 0.07 mm across, show abundant signs of recrystallization under the microscope. Although we have not established definitely the temporal relations between the white-mica alteration in these rocks and the widespread surrounding potassic alteration, elsewhere at Copper Canyon most of the alteration to white-mica-rich assemblages followed crystallization of secondary biotite or potassium feldspar. In addition the Hayden and the Monitor faults near the east ore body apparently controlled the distribution of white-mica. We should emphasize again that relative to all of the other hydrothermal silicates, the amount of white-mica in the prophyry system is small; however, some white-mica coincides with gold and silver mineralization, which contains sparse copper, just north of the east ore body and near the Tomboy mine, south of the east ore body (Blake and others, 1977).

Immediately adjacent to the granodiorite, weathered surface exposures of the lower member of the Pumpernickel Formation show abundant staining by yellow-brown and ochre iron oxides. These iron oxides principally are derived from pyrite that is both dispersed sparsely through the rock and concentrated along millimeter-sized quartz veinlets that flood the rocks. Fresh unweathered surfaces are pinkish brown. Study with the microscope reveals a well-developed potassium feldspar-quartz-white mica-biotite-pyrite mineral assemblage (no. 8, table 6); potassium feldspar is conspicuous both in the groundmass and in quartz-potassium feldspar-white mica (trace) veinlets. Detrital minerals are quartz, potassium feldspar (sparsely altered to white mica), plagioclase (strongly clouded), and zircon.

Study of the mineralogy of five samples from DDH–18 (table 6), which was collared about 150 m east of section line *A–A′* and 37 m north of the surface projection of ore (plate 1), reveals a seemingly irregular alternation between biotite- and tremolite-altered rock; epidote is a common accessory to both biotite- and tremolite-altered rock. These rocks span a 25-m interval from about 19 m (no. 9) to 44 m (no. 13) below ground surface. Furthermore, DDH–18 was put down only 10 m from the surface projection of the contact between garnetite (zone 3) and the replacement of garnetite by epidote-rich rock (zone 4). The epidote in these samples from DDH–18 probably reflects, then, some recrystallization during the development of zone 4 mineral assemblage. Sulfides are fairly abundant in DDH–18; pyrite makes up about 5 percent of the rocks about 19 m below the surface, and it is very closely associated spatially with chlorite, epidote, and sphene in clots sprinkled among detrital quartz grains (fig. 12).

Several other mineralogical relations in these rocks deserve comment. The association biotite-tremolite was not found in rock from zone 1 in DDH–18. In other porphyry systems, the intimate textural association of hydrothermal biotite and amphibole occurs both interior and exterior to cores of intense copper mineralization (Carson and Jambor, 1974; T. G. Theodore, unpub. data). Nonetheless, widespread crystallization of fine-grained shredded biotite at Copper Canyon apparently occurred early during the metamorphism of the area, and this early biotite is one of the outermost secondary minerals surrounding the skarn. This pale-tan to reddish-tan biotite locally is concentrated in what may have been shaly or argillitic sedimentary rock that

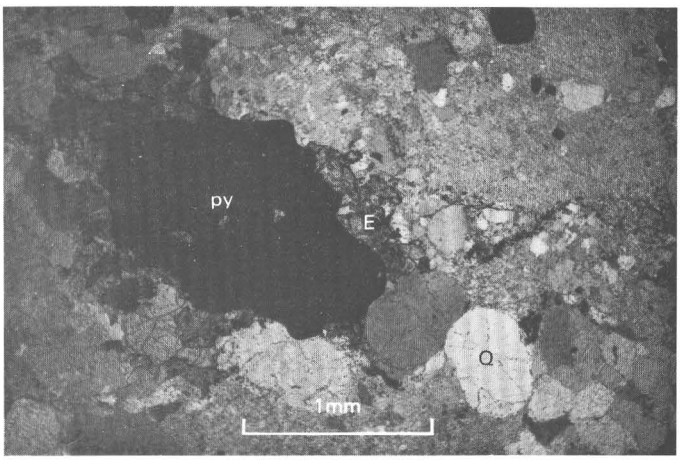

FIGURE 12.—Photomicrograph showing clot of epidote (E) and pyrite (py) in altered sandstone of the Pumpernickel Formation (no. 9, table 6). Many well-rounded detrital quartz grains (Q) have not recrystallized. Partially crossed nicols.

contains silt-sized angular fragments of detrital quartz. These biotitic domains, generally 0.5 to 1.0 cm thick, are interlayered with irregular and discontinuous layers of recrystallized chert. In places, biotitic rock is cut by epidote-chlorite-white mica-pyrite-quartz veins that are 0.2–0.3 mm wide and have 0.7- to 1.0-mm white mica-chlorite-pyrite-sphene selvages. These relations suggest early dispersed biotitization was followed by a local propylitic alteration that principally was restricted to narrow veinlets.

Finally, in altered sandstone beds about 10 m above rocks of zone 2, we find a mineral tentatively identified as vesuvianite (no. 13, table 6), which typically is found in many contact metamorphic rocks elsewhere but is sparse in the Copper Canyon area. This vesuvianite(?) has honey-brown pleochroic colors in zones and patches and has a very low birefringence (~0.001–0.002). It is partly replaced by tremolite, the dominant hypogene silicate in the immediate area; this relation suggests a decrease with time in the calcium:magnesium ratio of the hypogene fluids. Most tremolite is dispersed through the sandstone, whose detrital fraction includes rock fragments of quartzite and chert about 4–5 mm across. Tremolite is also concentrated in wispy, monomineralic, 0.1-mm-wide veinlets through fragments of chert. Textural relations under the microscope likewise suggest compatible associations of tremolite with epidote and potassium feldspar.

CALC-SILICATE ROCK

We use nongenetic terminology throughout our descriptions of calc-silicate rocks, because our hypotheses of their genesis differ somewhat from conventional ones. In this report, we apply the term calc-silicate rock to metamorphic rocks that show a complete recrystallization of their initial sedimentary fabrics into granoblastic, tight textures and that are made up predominantly of diopside or tremolite-actinolite.[2] We have clear textural evidence that much of the tremolite-actinolite at Copper Canyon formed from diopside. Where data are available, we further recognize and differentiate this metamorphic zone into two types of rock, diopside rock and tremolite-actinolite rock, largely on the basis of the presence or absence of amphibole (fig. 3). As mapped, diopside rock includes a few thin layers of garnetite, and the boundary shown between diopside rock and tremolite-actinolite rock is located where tremolite-actinolite first appears. The mineralogy of 35 calc-silicate rocks from zone 2 (see figs. 3 and 10) is listed in table 7.

The calc-siliiates of zone 2 occupy a roughly tabular zone that surrounds the garnetite. As summarized in figure 10, we documented, by petrographic study of closely spaced samples in a few critical localities, that the calc-silicate rock contains a symmetrical zonation of diopside rock and tremolite-actinolite rock about the enclosed large garnetite (fig. 3). Near the outermost parts of zone 2, gray to blue-gray rock of tremolite-actinolite gives way to rock with mixed tremolite-actinolite and diopside. This rock in turn grades into a pale-tan to buff, massive, diopside-bearing rock. There is a slight deviation in this mineral zoning in DDH–1. Here the basal contact of the garnetite marks a sharp transition into tremolite-actinolite rock that contains abundant medium-grained laths of relict diopside (fig. 3). These relict diopside grains indicate that diopside-bearing assemblages were stable prior to the crystallization of tremolite-actinolite. In most of the calc-silicates, pyrite is the dominant iron sulfide; it generally makes up about 3–5 percent of these rocks. Nonetheless, the total sulfide content in zone 2 reaches 30 to 40 volume percent in a few sections of rock approximately 3 m thick. In these sections, the pyrite:pyrrhotite ratio typically is less than 1:2 (fig. 3). A few isolated 1- to 2-cm clots of pyrrhotite in diopside have been altered to tightly intergrown marcasite plus pyrite (table 7) that is dark gray in hand samples. We found a similar paragenesis for marcasite plus pyrite in the east ore body (Nash and Theodore, 1971; Theodore and Blake, 1975). Finally, the content of copper of zone 2 generally is more than 1,500 ppm across most of the approximately 400-m length of these rocks studied; the zone reaches more than 0.4 percent copper near the granodiorite in and around the west ore body.

DIOPSIDE ROCK

Although we studied the mineralogy of only nine hand samples of diopside-bearing rock without tremolite-actinolite, we nevertheless were able to determine the mineralogy of very small diopside-rich patches (smaller than a standard thin section in size) that are relicts in tremolite-actinolite. In all, eight apparently stable specific mineral assemblages of the diopside-rich patches were observed under the microscope (abbreviations same as shown in table 8):

1. di-ep-q-s
2. di-s-kf-ap
3. di-ep-q-s-kf-py
4. di-q-s-kf-py
5. di-q-s-kf-po-cp
6. di-q-s-kf-po
7. di-s-py
8. di-s

Vesuvianite questionably is present in one of the diopside-bearing rocks (no. 33, table 7).

[2]Under the microscope, the amphibole in individual hand samples from zone 2 is either a colorless or a pale-green to blue-green, weakly to moderately pleochroic variety. Both types of amphibole occur in some hand samples. Limited study of these amphiboles with the electron microprobe by N. G. Banks (written commun., 1975) reveals that the colorless varieties contain 10–11 molecular percent of the ferrotremolite ($Ca_2Fe_2+{}^2Si_8O_{22}(OH,F)_2$) end member and should be termed tremolite (see Deer and others, 1963), whereas pleochroic varieties contain 41–45 molecular percent ferrotremolite and thus fall into the compositional range termed actinolite.

TABLE 7.—*Mineralogy of calc-silicate hornfels (zone 2) of the Pumpernickel Formation*

[X, mineral present; Tr, mineral present in trace amounts; ?, questionably present; ____, not found]

	1	2	3	4	5	6	7	8	9	10	11	12	13	14	15	16	17
					Loc. DDH–4, plate 1; fig. 3												
Field No.	1–353	0–412	1–459	2–227	6–93	6–97	6–112	6–197	6–203	6–206	6–207	6–212	6–214	6–219	6–243	6–247	6–256
Metamorphic																	
Diopside	X	X	____	X	____	X	X	X	X	X	X	X	X	X	X	X	X
Sphene	X	Tr	X	Tr	X	X	Tr	X	X	Tr	____	Tr	X	X	X	X	Tr
Potassium feldspar	X	Tr	X	____	X	X	X	____	X	____	____	X	X	X	X	Tr	____
Quartz	X	X	X	X	X	X	X	X	X	X	X	X	X	X	X	X	X
Garnet	____	____	____	____	____	____	____	____	____	____	X	____	____	Tr	____	____	____
Amphibole[a]	____	X	X	X	X	____	____	X	____	X	____	Tr	X	____	X	X	X
Biotite	____	____	Tr	____	X	____	____	____	____	____	____	____	____	____	____	____	____
Apatite	____	X	X	Tr	X	X	____	X	____	X	____	____	____	____	____	X	X
Plagioclase	____	____	____	____	____	____	____	____	____	____	____	____	____	____	____	____	____
Epidote	X	____	Tr	____	X	X	X	X	____	____	____	X	X	____	____	____	Tr
Chlorite	____	____	Tr	Tr	Tr	Tr	X	X	Tr	Tr	____	____	X	Tr	X	____	____
White mica	____	____	____	____	____	____	____	____	____	____	____	Tr	____	X	X	____	____
Carbonate	Tr	X	Tr	____	____	____	X	X	____	____	Tr	____	____	Tr	X	____	X
Pyrite	____	X	X	X	X	X	X	X	X	X	X	X	X	X	X	X	X
Chalcopyrite	Tr	____	____	____	X	Tr	Tr	X	Tr	Tr	____	X	X	Tr	____	____	X
Pyrrhotite	X	____	____	____	____	____	____	____	Tr	____	X	X	X	X	____	____	____
Sphalerite	____	____	____	____	____	Tr	____	____	____	____	____	____	____	____	____	____	____
Marcasite	____	____	____	____	____	X	X	X	____	____	?	X	X	____	____	____	____
Chalcocite	____	?	____	____	X	____	____	____	____	____	____	____	____	____	____	____	____
Hematite	Tr	Tr	X	____	____	Tr	X	X	Tr	Tr	X	Tr	X	Tr	____	Tr	____
Detrital																	
Rock fragments	____	____	X	____	X	____	____	____	____	____	____	____	____	____	____	____	____
Zircon	____	____	X	____	____	____	X	____	____	____	____	____	____	____	____	X	____
Allanite	____	____	____	____	X	____	____	____	____	____	____	____	____	____	____	____	____

TABLE 7.—*Mineralogy of calc-silicate hornfels (zone 2) of the Pumpernickel Formation*—Continued

	18	19	20	21	22	23	24	25	26	27	28	29	30	31	32	33	34	35
	Loc. DDH–4, plate 1; fig. 3																	
Field No.	6–257	6–261	6–264	6–265	2–191	2–247	[1]5–112	5–182	0–273	[2]45–113	45–199	1–431	8–276	8–279	8–287	[2]3–226	0–238	0–241
Metamorphic																		
Diopside	----	X	X	----	----	----	----	X	----	X	X	X	X	X	----	X	X	X
Sphene	X	X	X	----	X	----	X	X	X	X	Tr	X	----	Tr	----	Tr	Tr	Tr
Potassium feldspar	Tr	X	X	----	X	----	X	X	X	X	?	----	X	----	----	Tr	----	X
Quartz	X	X	X	X	X	----	X	X	X	X	X	X	X	X	X	X	X	X
Garnet	----	----	----	----	----	----	----	?	----	----	Tr	----	Tr	----	----	Tr	Tr	Tr
Amphibole[3]	X	X	X	X	X	X	X	X	X	X	----	X	----	X	X	----	X	?
Biotite	----	----	----	----	X	----	----	----	----	----	----	----	----	----	X	----	----	----
Apatite	----	X	X	X	X	----	----	X	X	----	----	----	Tr	----	----	Tr	----	----
Plagioclase	----	X	X	----	----	----	----	----	----	----	----	----	----	----	----	----	----	----
Epidote	----	Tr	----	----	----	----	Tr	X	X	X	----	----	X	----	----	X	X	X
Chlorite	----	Tr	Tr	X	----	----	----	----	----	Tr	Tr	Tr	Tr	----	X	----	----	----
White mica	----	----	Tr	Tr	Tr	----	X	Tr	----	----	----	----	----	----	----	----	----	----
Carbonate	Tr	[4]X	[4]X	[4]X	----	----	----	----	----	X	----	X	X	----	[5]X	Tr	----	----
Pyrite	X	X	X	X	X	X	X	X	X	X	X	X	X	X	X	X	X	X
Chalcopyrite	X	Tr	Tr	X	----	X	Tr	X	----	X	Tr	----	----	----	----	Tr	Tr	Tr
Pyrrhotite	----	----	----	Tr	----	----	----	----	X	Tr	X	X	----	----	----	----	X	X
Sphalerite	----	----	----	----	----	----	----	----	----	----	----	----	----	----	----	----	----	----
Marcasite	?	----	----	----	----	----	----	----	----	----	----	----	X	----	----	----	----	X
Chalcocite	----	----	----	----	----	----	----	----	----	----	----	----	----	----	----	----	----	----
Hematite	Tr	----	----	----	----	----	Tr	----	X	X	----	X	X	----	X	X	Tr	----
Detrital																		
Rock fragments	----	----	----	----	----	----	----	----	----	----	----	----	----	----	----	----	----	----
Zircon	----	----	----	X	----	----	X	----	----	----	----	----	----	----	----	----	----	----
Allanite	----	----	----	----	----	----	----	----	----	----	----	----	----	----	----	----	----	----

[1]Includes trace amounts of covellite in the central part of a pyrite veinlet.

[2]Vesuvianite questionably present in trace amounts.

[3]Most common type is colorless tremolite ($Ca_2Mg_5Si_8O_{22}(OH)_2$). Pleochroic, iron-bearing types notably confined to sulfide-rich veinlets and domains.

[4]Siderite along grain boundaries, and microfractures through diopside.

[5]Siderite fairly abundant in veins with hematite and some pyrolusite(?).

TABLE 8.—*Some minerals in diopside rock and tremolite-actinolite rock at Copper Canyon*

Mineral	Abbreviation	Formula (inferred)
Diopside	di	$CaMgSi_2O_6$
Tremolite-actinolite	ta	$Ca_2(Mg,Fe)_5Si_8O_{22}(OH,F)_2$
Sphene	s	$CaTiSiO_5$
Potassium feldspar	kf	$KAlSi_3O_8$
Epidote	ep	$Ca_2FeAl_2Si_3O_{12}(OH)$
Quartz	q	SiO_2
Biotite	bio	$K(Mg,Fe)_3AlSi_3O_{10}(OH)_2$
Apatite	ap	$Ca_5F(PO_4)_3$
Plagioclase	pg	Oligoclase-andesine
Siderite	sid	$FeCO_3$
Marcasite	mc	FeS_2
Pyrite	py	FeS_2
Pyrrhotite	po	$Fe_{1-x}S$
Chalcopyrite	cp	$CuFeS_2$
White mica	wm	$K_2(Al,Mg,Fe)_4[Si_6Al_2O_{20}](OH,F)_4$

Diopside rock locally shows small- and large-scale variability. Where measured directly in drill holes, diopside rock is about 5–12 m thick. Diopside, as either fine (0.01 mm) or medium (2–4 mm) crystals in a tightly intergrown mat, typically composes as much as 95 volume percent of much of this rock (fig. 13). Over the entire diopside zone, however, diopside content ranges widely, and at many localities there seems to be more than one generation of diopside. Some very fine grained domains of diopside are cut by randomly oriented veins of a later diopside, about 0.5 mm thick with 0.2- to 0.3-mm crystals in the veins. Minor accessory minerals most commonly are quartz, sphene, potassium feldspar, and pyrite. Most potassium feldspar usually occurs as an anhedral space filler in the diopside zones, some with swarms of included crystals of diopside. Salt-bearing fluid inclusions are common in some diopside crystals; most appear to have formed secondarily along microfractures. Additional data from fluid inclusions are included below in a separate section of this report. In addition, some minor pyrite, pyrrhotite, and chalcopyrite is dispersed through parts of the diopside rocks. These widely dispersed sulfides are notable in that they are not conspicuously related to any veins, and they seemingly form an integral part of the overall metamorphic fabric of the skarn. Thus, we infer that crystallization of some sulfides occurred during growth of the diopside zone, perhaps during its late stages. Indeed, we should emphasize that diopside in zone 3 seemingly remained stable during the massive replacement of andradite by pyrrhotite in the general area of the ore body. This is especially well documented in the vicinity of DDH–5 (fig. 3).

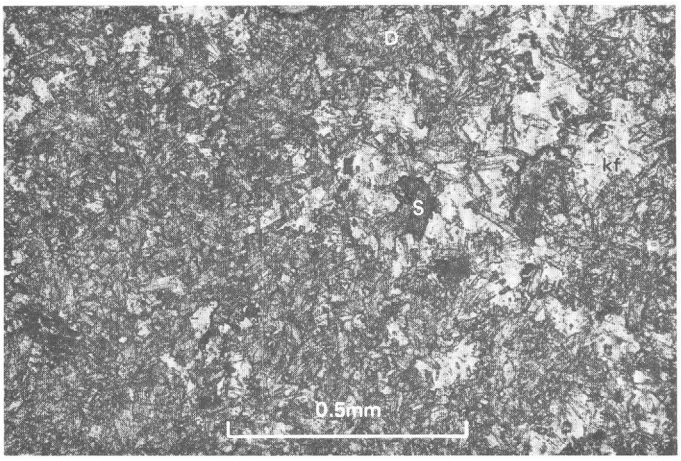

FIGURE 13.—Photomicrograph showing diopside rock with very tight, almost monomineralic mat of diopside (d) crystals, some intergrown with potassium feldspar (f). Sphene (S) is sparse. Plane-polarized light.

Siderite probably is younger than diopside, although textural relations are commonly unclear in the diopside rock. Very fine grained siderite, verified by X-ray diffraction, is concentrated for the most part along diopside grain boundaries and is resolvable in some samples only at magnifications of 1,000 X. It also occurs as patchy inclusions in other diopside grains. There are also some buff-colored diopside-siderite domains with either quartz or pyrite as finely dispersed minor accessories. Some unambiguous textural observations of this finely dispersed siderite suggest that its crystallization followed that of diopside. In addition, sparse siderite veins about 0.5 cm wide locally cut some of the diopside zones.

The overall mineralogy of veins that cut diopside rock is complex, and this mineralogy, together with that of the associated narrow alteration zones, suggests continuing physical and chemical changes during the later stages of skarn development (table 9). The diagnostic mineral is tremolite-actinolite, both in the veins themselves and as a reaction product in the wallrocks. Sparse amounts of apparently stable potassium feldspar also occur in many of the veins. The rocks also seem to show a general and marked increase in total sulfide content during the vein stage, including the introduction of additional chalcopyrite as the main ore mineral. Chalcopyrite was introduced during the initial stages of some veining as sparsely dispersed grains in closely packed diopside in the veins' wallrocks, and during the final stages of vein emplacement as hairline concentrations in the veins' cores. Where the veins contain fairly abundant sulfides with tremolite-actinolite, the tremolite-actinolite is notably more strongly pleochroic, and presumably richer in iron, than that in the

TABLE 9.—*Mineralogy of typical veins and their alteration zones that cut diopside rock*

[----, not found; Tr, trace; q, quartz; py, pyrite; ap, apatite; ta, tremolite-actinolite; di, diopside; cp, chalcopyrite; kf, potassium feldspar; chl, chlorite; po, pyrrhotite; c, carbonate; wm, white mica; hem, hematite; ep, epidote; s, sphene; sid, siderite]

	Vein		Reaction zone		Comments
	Mineralogy	Width	Mineralogy	Width	
			[1]Group 1		
1.	q-py-ap	1.5 mm	ta-py	0.5 mm	Dispersed concentration of py in di adjacent to ta.
2.	q-py	1–2 mm	----	----	Dispersed concentration of cp in di tactite generally within 1–2 mm of vein wall.
3.	q-kf(Tr)-chl(Tr)-po-cp-py	.6–0.7 cm	ta-po-cp	1.0 mm	Some po altered to marcasite-pyrite; cp concentrated along hairline core of vein; some exotic fragments of epidote torn from wallrock.
4.	po	<.5 mm	----	----	Painted along fracture surface.
5.	q-py-kf(Tr)-ta-c	5–6 mm	ta-q-py-chl-wm	1 cm	Ta strongly pleochroic in vein but colorless in wallrock reaction zone; wm concentrated in 5–6-mm clots; reaction zone has a knife edge outer boundary with di skarn.
6.	q-ta-ap-kf-py-hem	3 mm	ta	.5–1.0 cm	Ta more strongly pleochroic in vein than in reaction zone; hem, secondary.
7.	q-ta-py-ep(Tr)-c(Tr)	.5 cm	ta-s-q(Tr)	.1–1.0 mm	Ta colorless in vein; s most likely relict in reaction zone from replaced di-s assemblage.
8.	q-py-cp	1–2 mm	----	----	Some cp dispersed for distances of 1–2 mm from the veins.
			Group 2		
1.	hem-q	<1.0 mm	----	----	
2.	q-hem-py-c	do.	----	----	
3.	q-hem-chl	do.	----	----	
4.	sid	.5 cm	----	----	Possibly some sid along di grain boundaries.

[1]Group 1 veins older than group 2 veins.

surrounding reaction zones. After emplacement of these veins that generally have tremolite-actinolite in them or in their associated reaction zones (group 1, table 9), very minor microveinlets of group 2 (table 9) cut the rocks with no surrounding reaction zones. These microveinlets are quartz-hematite±chlorite±pyrite±carbonate-bearing; also some 0.5-cm-wide monomineralic veins of siderite cut the rocks, as mentioned above.

Magnetite is an extremely rare mineral around the west ore body. We can document only one locality with abundant occurrences. It apparently formed during the early paragenetic stages of skarn development. Elsewhere at Copper Canyon, Roberts and Arnold (1965) also report some local occurrences of magnetite that probably crystallized sometime during the early paragenesis of the skarn. It occurs in the Copper Canyon underground mine in copper-bearing skarn very close to the granodiorite. In addition to these two occurences of early magnetite, some magnetite may be associated with intermediate stage marcasite that locally replaces pyrrhotite throughout much of this part of the district. Because this early-stage magnetite appears to be so uncommon around the west ore body, its occurrence there merits some additional discussion. Within the ore body, a 1-m-thick section in DDH–19 of skarn of unknown horizontal extent contains about 30 volume percent magnetite as disseminated, 0.05-mm-sized grains in diopside and tremolite-actinolite (pl. 1). Under the microscope, the magnetite appears to be coexisting stably with both diopside and tremolite-actinolite, although it is partially replaced locally and also microviened by pyrite and quartz. There is also some white mica in the rock as well as sparse very late carbonate and chlorite along microveinlets. We suggest that this early magnetite in the west ore body crystallized together with diopside and tremolite-actinolite, but that the absence of early sulfides from these magnetite-rich rocks may reflect either a local pocket of anomalously low fugacity of sulfur during the skarn's development or a relict of a more widespread, presulfidation alkaline environment in the skarn (Barnes and Czamanske, 1967).

TREMOLITE-ACTINOLITE ROCK

Specific mineral assemblages that appear to be stable in tremolite-actinolite rock include the following (abbreviations same as in table 8):

1. ta-s-q-ap-py
2. ta-s-py-ap-pg
3. ta-kf-q-bio
4. ta-py-cp
5. ta-s-py-cp-q
6. ta-q-s
7. ta-s-po-kf
8. ta-s-q-ep-ap-py
9. ta-bio-py-q-s-kf-ap
10. ta-kf-q-s-ap

Some of these assemblages may result from a partial consumption of diopside rock as evidenced by apparently relict sphene. In addition, sulfides are relatively more abundant than in the diopside zone. Most of the amphibole in these rocks is colorless under the microscope and presumably rich in the tremolite molecular end member. Nonetheless, traces of slightly pleochroic amphibole occur in many of the rocks; it is usually concentrated in sulfide-rich veins and intensely silicated domains. Some of the most strongly pleochroic amphibole was found in tremolite-actinolite rock within the west ore body. There, this amphibole is very pale tan (X = Y) to light bluish green (Z) and is associated with pyrrhotite, sphene, and potassium feldspar. The potassium feldspar is slightly altered to white mica and partially replaced by epidote. Generally around the ore body, however, tremolite-actinolite is associated with pyrite. Although it is not a widespread association, in some rocks of zone 2, tremolite-actinolite is very tightly intergrown with pale-tan secondary biotite that presumably is rich in magnesium.

The tremolite-actinolite rocks apparently show some evidence of fluorine metasomatism during their development. Some of these rocks contain discontinuous 0.5-mm-thick veinlets composed of about 95 percent apatite and 5 percent quartz, pyrite, and tremolite-actinolite (listed in decreasing amounts). These apatite veins cut earlier tremolite-actinolite that is both in a dispersed mat of very fine crystals and that is also in some pre-apatite monomineralic veinlets. A very thin reaction rim around the apatite veins primarily shows a coarsening of the tremolite-actinolite grains in the wallrock. We studied the apatites by X-ray diffraction techniques (Silverman and others, 1952) and found that the difference between the d-spacings of the apatites 231 and 004 reflections coincided exactly with fluorapatite. Also in these rocks, sparse 2–3-cm tremolite-actinolite veins with pyrite, siderite, and quartz and secondary hematite include some mica whose d-spacings are remarkably similar to those for synthetic fluorphlogopite published by Borg and Smith (1969). This mica forms an alteration halo 2–3 cm wide on both sides of the veins. We previously found biotite in the altered granodiorite of Copper Canyon to contain

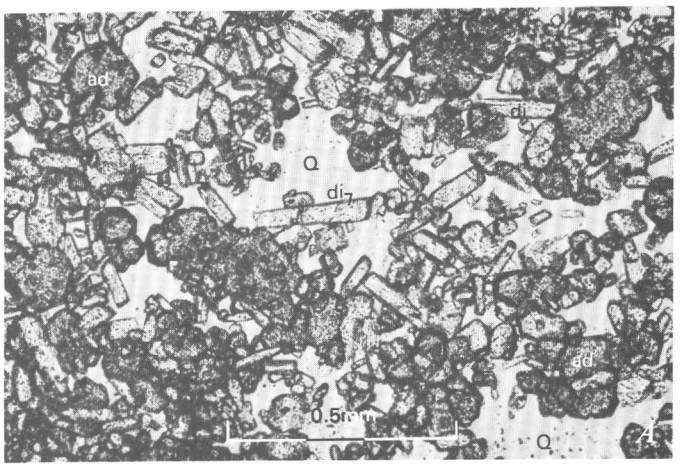

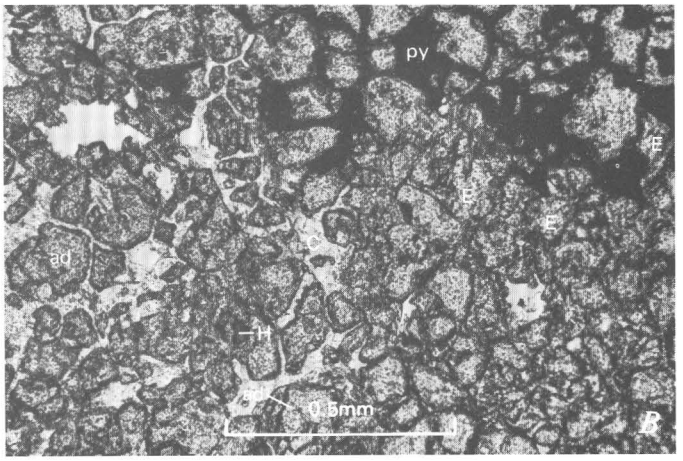

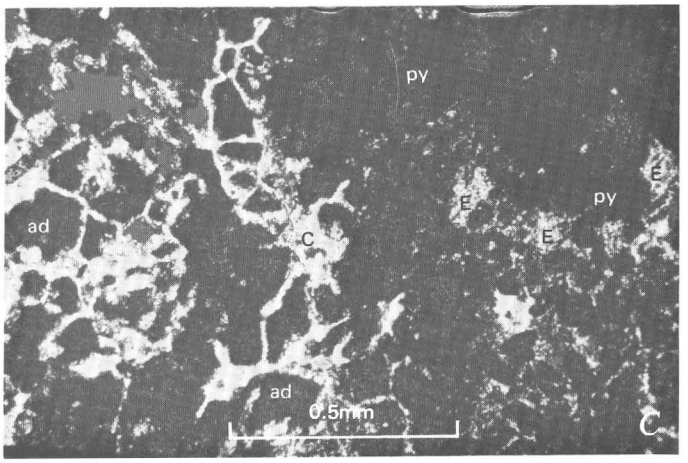

FIGURE 14.—Photomicrographs showing garnetite. *A*, Andradite (ad), diopside (di), and quartz (Q) from DDH–4, depth 54 m. Plane-polarized light. *B*, Andradite (ad) with primary hematite (H) set in matrix of calcite (C) which has been partially replaced by pyrite (py) and epidote (E). From DDH–4, depth 54 m. Plane-polarized light. *C*, Same as *B*. Partially crossed nicols.

anomalously high amounts of fluorine (Theodore and others, 1973), which relation may be fairly typical in porphyry-type environments (Jacobs and Parry, 1974). Hydrothermal biotite at the Ray, Ariz., porphyry copper deposit contains about 1.4–1.7 percent fluorine as opposed to 0.1–0.86 percent fluorine in primary biotite of spatially associated Laramide igneous rocks (Banks, 1976).

GARNETITE

The petrogenetic development of the garnetite at Copper Canyon is still somewhat enigmatic. No probable unaltered equivalent of these rocks at Copper Canyon is exposed, nor has one been penetrated in holes drilled by 1975. Thus, we could not determine the complete suite of petrochemical changes that the rocks underwent from unaltered sedimentary rock, through coarse-grained metasilicate rock, to sulfidized silicate rock. Systematic zoning of the garnetite with its surrounding rocks, the relatively coarse- to medium-grained garnets themselves (fig. 14), their occurrence in a high-temperature hydrothermal environment (Theodore and Blake, 1975), and their overall petrologic similarity to many other similar rocks in or near porphyry copper deposits that replace carbonate (Ransome, 1904; Lindgren, 1905; Knopf, 1918; Spencer, 1917; Gale, 1965; Moolick and Durek, 1966; Eastlick, 1968; James, 1971; Himes, 1972; and many others) all suggest to us these rocks grew in part at the expense of some carbonate. Certainly there is some textural evidence that garnet and pyroxene at Copper Canyon may have grown from a carbonate-rich host. We interpret some rare 1- to 2-cm² domains of garnet with interstitial calcite to reflect possibly relict calcite incompletely converted to calc-silicate minerals. Thus, the garnetite and its closely allied calc-silicate assemblages most likely replace calcareous argillite, siltstone, and limy shale. Limestone or dolomitic limestone does not crop out anywhere in the Pumpernickel Formation (Roberts, 1964; Theodore and Blake, 1975).

The mineralogy of 20 samples collected from across 29 m of garnetite (zone 3) is shown in table 10, and the mineralogy of 25 other samples of garnetite obtained from other drill holes is shown in table 11. Even in single hand samples, garnets have highly varied colors; amber to reddish-tan hues are typical. Most garnetite samples are composed of a massive, closely packed array of subhedral to euhedral dodecahedrons. Although garnets compose close to 95 volume percent of some small domains, modal compositions of garnetite vary highly throughout the garnetite zone. Some 4- to 5-m clots of almost pure garnet grade into roughly equal proportions of garnet and diopside across about a 3-m interval. Throughout the garnetite, garnets range

TABLE 10.—*Mineralogy of garnetite (zone 3) in DDH–4, collared 155 m north of the altered granodiorite of Copper Canyon*

[X, mineral present; Tr, mineral present in trace amounts; ?, questionably present; ----, not found]

	1	2	3	4	5	6	7	8	9	10	11	12	13	14	15	16	17	18	19	20
Depth (in meters)	29.3	35.8	39.4	39.7	41.5	42.5	44.3	45.3	47.3	47.9	49.5	50.6	50.7	52.0	53.1	54.4	58.0	58.5	59.6	69.0
Field No.	6-96	6-117	6-129	6-130	6-136	6-139	6-145	6-148	6-155	6-157	6-162	6-166	6-167	6-170	6-174	6-178	6-190	6-193	6-195	6-226
Andradite	X	X	X	X	X	X	X	X	X	X	X	X	X	X	X	X	X	Tr	X	X
Isotropic	---	X	X	X	X	X	X	Tr	Tr	Tr	X	X	Tr	Tr	X	X	Tr	---	Tr	X
Anisotropic	X	X	X	X	Tr	X	Tr	X	X	Tr	X	X	X	X	X	X	X	Tr	X	X
Diopside	X	X	X	X	Tr	Tr	X	X	X	X	X	X	X	X	Tr	Tr	X	Tr	X	X
Quartz	X	---	---	X	Tr	---	Tr	Tr	---	---	X	X	X	X	Tr	Tr	---	---	---	X
Potassium feldspar	---	---	---	---	---	---	---	---	---	---	---	---	---	---	---	---	---	---	---	---
Sphene	X	---	---	Tr	---	---	---	---	---	Tr	X	Tr	---	---	---	Tr	X	---	Tr	---
Epidote	---	Tr	---	Tr	---	---	---	---	---	---	---	---	---	---	---	---	---	---	---	---
Tremolite-actinolite	---	---	---	---	Tr	---	---	---	---	X	X	---	---	---	---	---	---	---	---	---
Apatite	---	Tr	---	---	---	---	---	---	Tr	Tr	---	---	---	Tr	---	---	---	---	---	Tr
Chlorite	X	X	X	X	Tr	X	Tr	Tr	Tr	Tr	X	Tr	Tr	Tr	---	---	Tr	---	Tr	---
Carbonate	X	Tr	Tr	X	Tr	X	Tr	---	Tr	Tr	X	X	---	X	---	---	X	X	X	X
White mica	---	---	---	Tr	Tr	---	---	---	---	---	Tr	X	Tr	X	---	---	---	---	---	Tr
Pyrrhotite	---	X	---	X	X	X	X	X	Tr	X	X	X	---	X	X	X	X	X	X	X
Pyrite	X	X	---	X	X	X	---	X	X	X	X	X	X	X	X	X	X	X	X	X
Chalcopyrite	Tr	---	---	X	---	X	---	X	---	X	X	Tr	Tr	Tr	X	X	Tr	X	X	Tr
Marcasite	X	---	---	X	---	X	---	X	---	X	X	Tr	X	X	---	X	X	---	Tr	---
Covellite	---	---	---	Tr	---	---	---	---	---	---	---	---	---	---	---	---	---	Tr	---	---
Chalcocite	?	---	?	X	Tr	---	Tr	---	---	Tr	---	---	---	---	---	---	?	---	---	---
Hematite	X	X	X	Tr	X	X	Tr	X	X	X	X	Tr	X	X	Tr	X	X	X	Tr	X

TABLE 11.—*Mineralogy of garnetite (zone 3) in six drill holes put down into the Pumpernickel Formation*

[X, mineral present; Tr, mineral present in trace amounts; ?, questionably present; ____, not found]

	1	2	3	4	5	6	7	8	9	10	11	12	13	14	15	16	17	18	19	20	21	22	23
	Garnets and pyroxenes analyzed by microprobe[1]																						
Loc. pl. 1, fig. 3	DDH–12	DDH–4	DDH–2	DDH–1		DDH–2			DDH–1				DDH–3			DDH–1	DDH–12	DDH–20					
Field No.	2–232	936	8–212	0–347	0–394	8–215	8–223	8–266	1–361	1–364	1–371	1–428	02–132	02–164	02–173	0–261	2–233	45–121	45–144	45–153	45–164	5–167	5–182
Andradite[2]																							
Isotropic	93-99	99	99	99	____	X	Tr	X	X	X	X	____	X	X	X	X	X	X	X	X	X	X	X
Anisotropic	57-61	93	88	39-77	78-80	X	X	X	X	X	X	X	Tr	Tr	Tr	Tr	____	X	X	X	X	X	X
Diopside[3]	X	90	91-93	95	85-90	X	X	X	X	Tr	X	X	X	X	X	X	X	X	X	X	____	X	X
Quartz	____	X	X	X	Tr	X	X	X	X	X	X	X	Tr	Tr	X	X	X	X	X	X	X	X	X
Potassium feldspar	____	____	Tr	____	____	X	____	____	Tr	____	____	X	____	____	Tr	X	____	Tr	X	Tr	____	____	____
Sphene	____	____	Tr	____	Tr	Tr	Tr	____	____	____	____	X	____	____	____	Tr	____	____	Tr	X	____	Tr	____
Epidote	____	____	X	X	X	X	X	Tr	X	X	X	____	____	____	____	Tr	____	X	X	X	X	X	X
Tremolite-actinolite	____	____	____	____	____	____	____	X	____	X	____	____	____	____	____	____	____	____	X	X	____	X	____
Apatite	____	____	____	____	____	Tr	____	____	____	____	____	Tr	____	____	____	Tr	____	X	Tr	Tr	____	X	____
Chlorite	____	____	____	____	____	____	X	X	Tr	____	Tr	____	____	____	____	____	Tr	Tr	Tr	Tr	Tr	Tr	Tr
Carbonate	____	Tr	Tr	Tr	____	Tr	X	X	X	Tr	X	____	____	____	____	____	Tr	____	____	X	____	____	____
White mica	____	____	____	____	____	____	____	____	Tr	____	____	____	____	____	____	____	____	____	Tr	____	____	____	____
Pyrrhotite	X	X	X	X	X	X	X	____	____	X	X	X	X	X	X	X	X	____	____	____	____	X	X
Pyrite	____	X	X	X	X	X	X	X	X	X	Tr	X	X	____	X	____	X	X	X	X	X	X	X
Chalcopyrite	X	X	X	X	X	Tr	____	____	____	Tr	X	X	Tr	X	Tr	X	Tr	____	____	Tr	Tr	X	X
Marcasite	____	____	____	____	____	Tr	X	____	____	Tr	Tr	____	____	____	Tr	____	____	____	____	____	____	X	Tr
Chalcocite	____	____	____	____	____	____	____	____	____	____	____	____	____	____	____	____	____	____	X	____	____	____	____
Hematite	Tr	X	X	X	X	X	X	Tr	Tr	Tr	Tr	Tr	Tr	Tr	X	Tr	Tr	X	Tr	Tr	X	X	X

[1]From tables 12 and 13.

[2]Numerical values indicate molecular percent andradite in selected grains of garnet.

[3]Numerical values indicate molecular percent diopside in selected grains of pyroxene.

from 0.5 mm to 1.5 cm in size, although the size distribution in single samples is more restricted than this. Textural relations observed in the garnetite yield a fairly consistent crystallization history; isotropic garnet forms the cores of individual crystals (fig. 15); diopside and hematite occur as minor included accessories during these earliest stages of garnet growth. Typically the isotropic cores of the garnet crystals are yellow to yellowish green in thin section, whereas they are mantled by colorless rim areas. Some cores are anhedral, as opposed to the euhedral overgrowths of the rim areas, and crystallization of these cores may reflect some early, nonadditive stages of garnet growth. The rim areas of garnets usually are sectorially twinned, oscillatory anisotropic-isotropic growth zones. Contacts between the zones are planar and sharp; up to 20 such zones across a millimeter-sized rim area of a crystal are common. Such garnets are fairly common in contact deposits (see Deer and others, 1962; Gale, 1965, James, 1971). Most of the diopside in the garnetite recrystallized along with or later than the crystallization of these optically oscillatory zones. This tightly spaced oscillation between isotropic and anisotropic garnet suggests significant, probably rapid, fluctuations in the physical and (or) chemical environment of the rocks. In summary, after early crystallization of isotropic garnet during isochemical processes in the garnetite, anisotropic garnet-diopside assemblages then followed; quartz-potassium feldspar-sulfide assemblages then filled open spaces. All of these assemblages were in turn cut by mineral assemblages dominated by hydrous silicates and additional sulfides. Compositions of garnet and pyroxenes in the garnetite were studied by the electron microprobe to document fully their small-scale, yet striking and important, chemical variations.

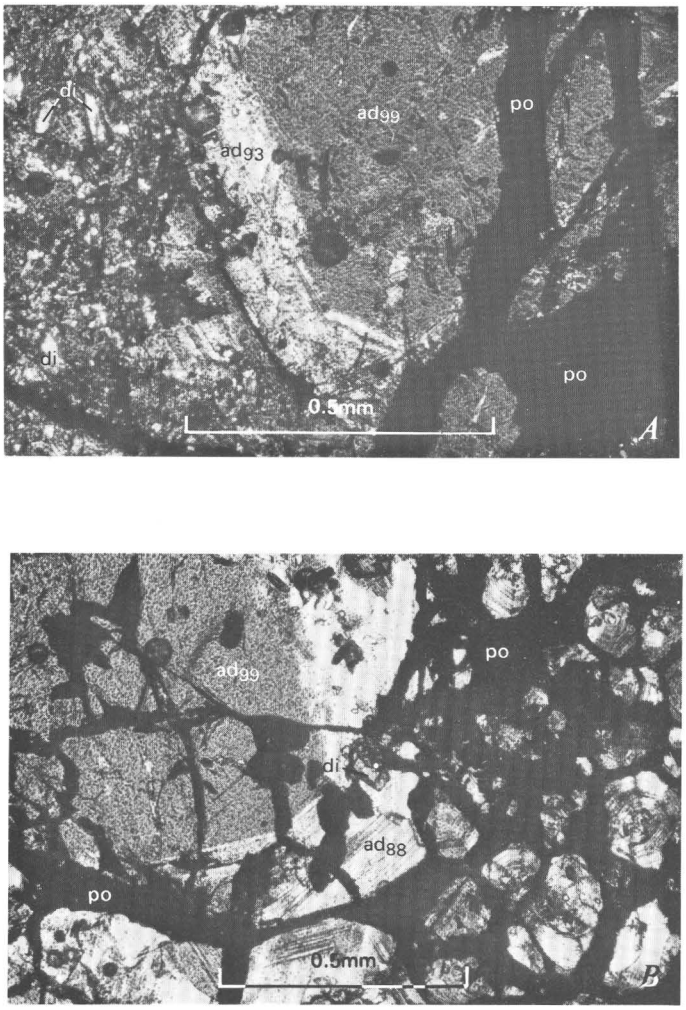

FIGURE 15.—Photomicrographs showing garnets and pyroxenes analyzed with electron microprobe. Plane-polarized light, partially crossed nicols. *A*, Anisotropic andradite, consisting of 93 molecular percent of andradite end member (ad_{93}) in andradite-grossularite series, together with diopside (di) mantles isotropic andradite (ad_{99}) from DDH–4 (fig. 3). Andradite cut by pyrrhotite (po). *B*, Anisotropic rim of andradite (ad_{88}) around isotropic core of andradite (ad_{99}) with a few grains of diopside (di) in rim region; pyrrhotite (po) occurs as a fracture filling.

ELECTRON MICROPROBE ANALYSES OF ANDRADITE AND DIOPSIDE

By NORMAN G. BANKS

Twenty-one garnet (10 grains) and six pyroxene (6 grains) analyses were obtained with an A.R.L. model EMX–SM electron microprobe using an ADP crystal for silicon, aluminum, calcium, and potassium, an LIF crystal for iron and manganese, and a RAP crystal for sodium and magnesium. The mineralogy of the five specimens studied with the electron microprobe is listed in table 11 (nos. 1–5). Labradorite, andradite, grossularite, rhodonite, and biotite of known composition were used as standards. Run conditions included an excitation voltage of 15 kV, a sample current of 3×10^{-8} amperes on brass, and a fully focused electron beam. Carbon contamination and volatilization of components were avoided either by moving the beam with magnetic deflectors to sweep areas 10 by 8 micrometers or by slightly shifting the sample's position under a focused beam once every 20 seconds. X-ray intensity data (counts) were obtained by averaging 5 to 10 observations per analyzed area. The X-ray intensity data were corrected by computer for drift, background, and matrix effects (mass absorption, secondary fluorescence, and atomic number; Beeson, 1967; Beaman and Isasi, 1970). Detection levels are established at three times the square root of the average background counts (Boyd, 1969).

Chemical analyses, structural formulas, and molecular compositions for the garnets are listed in table 12,

TABLE 12.—*Electron microprobe analyses and*
[N.d.=not detected; Analytical detection level

Loc. pl. 1, fig. 3	DDH–12								DDH–4
Grain No.	Isotropic 1						Anisotropic 2	3	Isotropic 4
Analysis No.	1	2	3	4	5	6	7	8	9
Major oxides[1] (weight percent)									
SiO_2	33.8 ±0.3	33.4 ±0.2	34.1 ±0.4	34.1 ±0.2	34.3 ±0.3	34.2 ±0.3	37.1 ±0.1	35.4 ±0.3	34.0 ±0.4
Al_2O_3	.03± .02	.09± .01	.06± .03	.06± .01	.04± .02	.82± .04	9.9 ± .1	8.0 ± .1	.03± .02
Fe_2O_3[2]	31.9 ± .2	31.7 ± .2	32.0 ± .1	31.9 ± .2	31.8 ± .1	29.6 ± .2	19.1 ± .3	20.5 ± .3	31.4 ± .2
MgO	.17± .01	.25± .01	.15± .01	.14± .003	.13± .01	.17± .01	.08± .001	.07± .002	.02± .001
CaO	33.0 ± .1	32.8 ± .1	33.1 ± .1	32.9 ± .1	33.0 ± .1	33.3 ± .1	35.2 ± .2	35.3 ± .1	32.8 ± .2
Na_2O	N.d.	N.d.	N.d.	N.d.	N.d.	N.d.	N.d.	N.d.	N.d.
K_2O	N.d.	N.d.	N.d.	N.d.	N.d.	N.d.	N.d.	N.d.	N.d.
TiO_2	N.d.	N.d.	N.d.	N.d.	N.d.	N.d.	.12± .01	.16± .02	N.d.
MnO	.02± .001	.03± .001	.03± .001	N.d.	N.d.	N.d.	.03± .002	.01± .001	.20± .01
Total	98.9 ± .4	98.3 ± .3	99.4 ± .4	99.1 ± .3	99.3 ± .3	98.1 ± .4	101.5 ± .4	99.4 ± .5	98.5 ± .5
Structural formulas[3]									
Si	5.82	5.80	5.84	5.86	5.87	5.90	5.89	5.81	5.88
Fe^{+3} Z	.17 → 6.00	.18 → 6.00	.15 → 6.00	.13 → 6.00	.12 → 6.00	.10 → 6.00	.11 → 6.00	.19 → 6.00	.11 → 6.00
Al^{iv}	.01	.02	.01	.01	.01				.01
Al^{vi}	N.d.	N.d.	N.d.	N.d.	N.d.	.07	1.73	1.35	N.d.
Fe^{+3} Y	3.97 → 3.97	3.96 → 3.96	3.97 → 3.97	3.99 → 3.99	3.98 → 3.98	3.83 → 3.90	2.28 → 4.02	2.53 → 3.90	3.97 → 3.97
Ti	N.d.	N.d.	N.d.	N.d.	N.d.	N.d.	.01	.02	N.d.
Mg	.04	.07	.04	.04	.03	.04	.02	.02	.01
Fe^{+2}	N.d.	N.d.	N.d.	N.d.	N.d.	N.d.	N.d.	N.d.	N.d.
Mn X	N.d. → 6.13	N.d. → 6.17	N.d. → 6.11	N.d. → 6.09	N.d. → 6.09	N.d. → 6.20	.01 → 6.02	N.d. → 6.24	.03 → 6.12
Ca	6.09	6.10	6.07	6.05	6.06	6.16	5.99	6.22	6.08
Na	N.d.	N.d.	N.d.	N.d.	N.d.	N.d.	N.d.	N.d.	N.d.
K	N.d.	N.d.	N.d.	N.d.	N.d.	N.d.	N.d.	N.d.	N.d.
Molecular percent[4]									
Andradite	99.2	98.9	99.4	99.4	99.5	93.0	57.0	60.7	99.3
Grossularite	N.d.	N.d.	N.d.	N.d.	N.d.	6.3	42.7	38.5	N.d.
Spessartine	.1	.1	.1	N.d.	N.d.	N.d.	N.d.	N.d.	.5
Pyrope	.7	1.	.5	.6	.5	.7	.3	.8	.2

[1]Analyst: N. G. Banks.
[2]Total iron expressed as Fe_2O_3.
[3]Calculated on the basis of 24 oxygen atoms per formula unit using the computer program of Jackson, Stevens, and Bowen (1967).
[4]Stoichiometry assumed.

roughly in order of decreasing intensity of copper metallization in the surrounding garnetite. Table 13 contains the analytical determinations for pyroxenes. The uncertainty limits after the reported oxide weight percents in tables 12 and 13 are measures of the homogeneity of the standard and sample. These limits do not imply accuracy of measurement with respect to the absolute amount of the oxide present. However, when, as in this case, analyses are made using the same instrument, standards, and computer program, the limits are useful and meaningful in comparing or evaluating differences in the amount of oxide present in each analyzed area or grain.

Garnets from the garnetite show about a 60-molecular-percent variation in the grandite isomorphous series (Winchell and Winchell, 1951), between grossularite ($Ca_3Al_2Si_3O_{12}$) and andradite ($Ca_3Fe_2^{+3}Si_3O_{12}$) (fig. 16*A*). About half of these analyses indicate garnet compositions of nearly pure andradite. Although garnet with a composition of one of the end members of either the pyralspite or grandite series were once considered to be rare (Deer and others, 1962), end-member garnets may be, in fact, quite common in geologic environments similar to that of Copper Canyon (see James, 1971). Although figure 16*A* suggests a continuous variation in composition for garnets at Copper Canyon, from six analyses of one grain (analyses 1–6, table 12) we infer that individual garnet grains of the optically isotropic variety in the garnetite chemically may not be zoned significantly (fig. 17). Garnet near the rim of this grain, however, shows about a 2-weight-percent decrease in its iron content, shown as Fe_2O_3 on figure 17. The grain is sharply bounded by a growth zone of garnet with even less iron (analyses 7–8, table 12), which is anisotropic. Furthermore, as shown in table 12, the optically isotropic garnet grains are extremely rich in andradite (Ad_{93-99}), whereas the anisotropic ones contain less andra-

structural formulas of garnets from the garnetite
for Na_2O=0.01%, TiO_2=0.04%, and K_2O=0.03%]

DDH-4		DDH-2		DDH-1							
Isotropic 5	Anisotropic	Isotropic 6	Anisotropic	Anisotropic 7		Anisotropic 8		Isotropic		Anisotropic 9	10
10	11	12	13	14	15	16	17	18	19	20	21
Major oxides[1] (weight percent)											
32.8 ±0.4	33.5 ±0.1	34.5 ±0.2	35.0 ±0.3	35.6 ±0.4	36.1 ±0.3	35.9 ±0.4	35.1 ±0.2	34.3 ±0.3	34.1 ±0.2	36.8 ±0.3	37.6 ±0.3
.46± .1	1.6 ± .5	.47± .03	3.4 ± .06	5.4 ± .01	6.4 ± .1	6.1 ± .6	5.5 ± .1	1.8 ± .03	.73± .01	12.9 ± .2	13.3 ± .7
31.9 ± .2	28.9 ± .5	32.1 ± .3	28.1 ± .5	24.1 ± .1	24.9 ± .2	23.3 ±2.1	24.5 ± .4	31.3 ± .1	31.2 ± .1	13.7 ± .2	13.2 ± .1
.03± .001	.06± .004	.15± .003	.08± .01	.06± .002	.05± .003	.06± .003	.06± .003	.05± .002	.04± .002	.18± .01	.11± .01
31.6 ± .1	32.5 ± .1	32.7 ± .1	33.3 ± .1	32.4 ± .1	32.6 ± .1	34.3 ± .1	33.6 ± .2	32.9 ± .1	32.8 ± .1	36.0 ± .2	35.6 ± .2
N.d.	N.d.	N.d.	N.d.	N.d.	N.d.	N.d.	N.d.	N.d.	N.d.	N.d.	N.d.
N.d.	N.d.	N.d.	N.d.	N.d.	N.d.	N.d.	N.d.	N.d.	N.d.	N.d.	N.d.
N.d.	.33± .03	N.d.	.09± .01	N.d.	N.d.	N.d.	N.d.	N.d.	N.d.	.44± .04	.15± .02
.20± .01	.17± .01	.14± .01	.14± .01	.23± .01	.22± .01	.21± .01	.22± .01	.09± .003	.08± .01	.44± .02	.53± .02
97.0 ± .5	97.1 ± .7	100.1 ± .4	100.1 ± .6	97.8 ± .4	100.3 ± .4	99.9 ±2.2	99.0 ± .5	100.4 ± .3	99.0 ± .2	100.0 ± .5	100.5 ± .8
Structural formulas[3]											
5.77	5.83	5.85	5.84	5.97	5.90	5.90	5.85	5.78	5.85	5.82	5.92
.13 } 6.00	.17 } 6.00	.06 } 6.00	.16 } 6.00	.03 } 6.00	.10 } 6.00	.10 } 6.00	.15 } 6.00	.22 } 6.00	.15 } 6.00	.18 } 6.00	.08 } 6.00
.10	.02	.09	.51	1.04	1.14	1.09	.94	.13	N.d.	2.23	2.37
N.d.	.16	N.d.	.51	3.05 } 4.09	3.06 } 4.20	2.89 } 3.98	3.08 } 4.02	3.97 } 4.10	4.03 } 4.03	1.63 } 3.91	1.57 } 3.96
4.09 } 4.09	3.78 } 3.98	4.04 } 4.04	3.53 } 4.05	N.d.	N.d.	N.d.	N.d.	N.d.	N.d.	.05	.02
N.d.	.04	N.d.	.01	.02	.01	.02	.02	.02	.01	.04	.03
.01	.02	.04	.02	N.d.	N.d.	.02	N.d.	N.d.	N.d.	N.d.	N.d.
N.d.	N.d.	N.d.	N.d.	.03 } 5.89	.03 } 5.74	N.d.	.03 } 6.06	.01 } 5.97	.01 } 6.04	.06 } 6.21	.07 } 6.10
.03 } 5.99	.03 } 6.10	.02 } 6.01	.02 } 6.00	5.84	5.70	.03 } 6.09	6.01	5.94	6.02	6.11	6.00
5.95	6.05	5.95	5.96	N.d.	N.d.	6.04	N.d.	N.d.	N.d.	N.d.	N.d.
N.d.	N.d.	N.d.	N.d.	N.d.	N.d.	N.d.	N.d.	N.d.	N.d.	N.d.	N.d.
N.d.	N.d.	N.d.	N.d.	N.d.	N.d.	N.d.	N.d.	N.d.	N.d.	N.d.	N.d.
Molecular percent[4]											
99.5	93.1	99.1	88.2	77.7	79.9	71.0	76.2	99.6	99.6	39.4	38.5
N.d.	6.3	N.d.	11.	21.5	19.4	28.2	23.0	N.d.	N.d.	58.9	60.0
.4	.4	.3	.4	.6	.5	.5	.5	.2	.2	1.	1.2
.1	.2	.6	.4	.3	.2	.3	.3	.2	.2	.7	.3

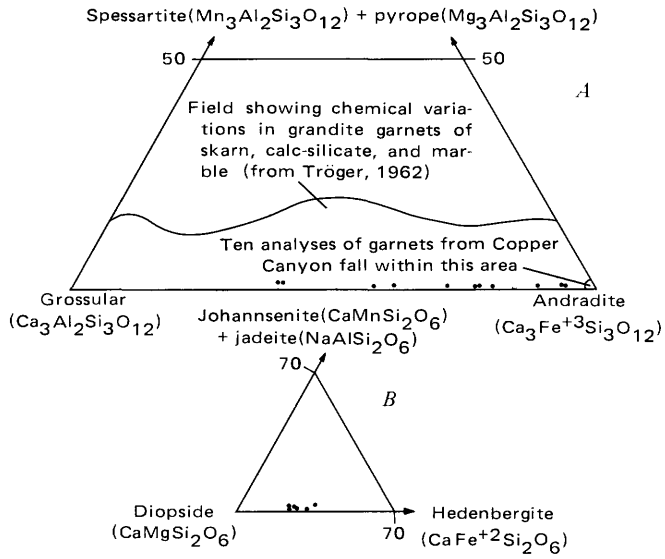

FIGURE 16.—Composition of garnets and pyroxenes. *A*, 21 garnet analyses of table 12 in terms of grossular, andradite, and spessartite plus pyrope molecular end members. *B*, Six pyroxene analyses of table 13 in terms of diopside, hedenbergite, and johannsenite plus jadeite molecular end members.

dite, from 39 to 93 molecular percent. Thus, end-member garnets in the grandite series appear to be isotropic (see also Lessing and Standish, 1973). Laboratory experiments seem to corroborate these chemical-optical data, because Kalinin (1967) synthesized under hydrothermal conditions both anisotropic and isotropic garnets in the grossular-andradite series. He found that isotropic garnets grew from mixtures with compositions of the end members, whereas anisotropic garnets grew from starting mixtures chemically intermediate to the end-member ones. Although we have shown that compositional differences in the garnets at Copper Canyon correlate with birefringence and isotropy, we have not established relations between composition and polysynthetic twinning as Morgan (1975) showed in the Mount Morrison pendant, Sierra Nevada, Calif. In one of the skarns he studied there, Morgan found that birefringence in garnet is a structural effect independent of chemical zonation.

Garnet has the general half-cell formula unit X_3 Y_2 Z_3 O_{12}, where Z is tetrahedral Si, Al, and minor Fe^{+3}, and Y and X or octahedral Al, Fe^{+3}, Ti, Mg, Fe^{+2}, Mn,

TABLE 13.—*Electron microprobe analyses and structural formulas of pyroxenes from the garnetite*
[N.d., not detected; Analytical detection levels for Na_2O=0.01%, TiO_2=0.04%, K_2O=0.03%]

Loc. pl. 1	DDH-4	DDH-2		DDH-1		
Grain No.	1–2	3	4	5	6	
Analysis No.	1	2	3	4	5	6
Major oxides[1] (weight percent)						
SiO_2	54.5 ±0.4	53.8 ±0.3	54.0 ±0.4	49.2 ±0.2	53.5 ±0.2	54.4 ±0.3
Al_2O_3	.13± .05	.08± .04	.09± .02	.61± .02	.59± .02	.59± .01
FeO[2]	3.7 ± .5	3.8 ± .6	3.7 ± .6	4.4 ± .06	4.7 ± .04	3.2 ± .02
MgO	16.6 ± .3	16.7 ± .4	17.0 ± .4	16.3 ± .1	15.9 ± .04	17.0 ± .03
CaO	26.5 ± .2	26.3 ± .2	26.6 ± .1	27.6 ± .1	24.1 ± .03	24.5 ± .2
Na_2O	N.d.	N.d.	N.d.	N.d.	.13± .001	.13± .001
K_2O	N.d.	N.d.	N.d.	N.d.	N.d.	N.d.
TiO_2	N.d.	N.d.	N.d.	N.d.	N.d.	N.d.
MnO	.16± .02	.11± .01	.08± .004	.15± .01	.23± .01	.09± .004
Total	101.6 ± .7	100.8 ± .8	101.8 ± .8	98.3 ± .2	99.2 ± .2	99.9 ± .4
Structural formulas[3]						
Si	1.98	1.97	1.96	1.88	1.98	1.99
Al^{iv}	N.d.	N.d.	N.d.	.02	.02	.01
Z Fe^{+3}	.02 → 2.00	.03 → 2.00	.04 → 2.00	.10 → 2.00	N.d. → 2.00	N.d. → 2.00
Al^{vi}	N.d.	N.d.	N.d.	N.d.	.01	.01
Ti	N.d.	N.d.	N.d.	N.d.	N.d.	N.d.
Mg	.90	.91	.92	.93	.88	.93
Y Fe^{+2}	.09 → 2.03	.09 → 2.03	.07 → 2.03	.04 → 2.11	.15 → 2.02	.10 → 2.01
Mn	.01	N.d.	N.d.	.01	.01	N.d.
Ca	1.03	1.03	1.04	1.13	.96	.96
Na	N.d.	N.d.	N.d.	N.d.	.01	.01
K	N.d.	N.d.	N.d.	N.d.	N.d.	N.d.
Molecular percent[4]						
Diopside	90.2	90.9	92.6	95.3	84.8	89.8
Hedenbergite	9.2	8.7	7.2	4.1	14.1	9.5
Johannsonite	0.6	.4	.2	.6	.7	.3
Jadeite	N.d.	N.d.	N.d.	N.d.	.4	.4

[1]Analyst: N. G. Banks.
[2]Total iron expressed as FeO.
[3]Calculated on the basis of 6 oxygen atoms per formula unit using the computer program of Jackson, Stevens, and Bowen (1967).
[4]Stoichiometry assumed.

Ca, Na, and K. The unit cell of garnet contains eight formula units (Deer and others, 1962). In our calculations of the structural formulas (table 12), we calculated the analyses on the basis of 24 oxygen anions. In the calculations, we also assumed a minimum of six Z cations in tetrahedral coordination and that iron is ferric (Deer and others, 1962). Tetrahedral cations of silicon occupy from 5.77 to 5.97 of the available Z-group sites. To fill the remainder of these sites, we presume them to be filled first by aluminum then by ferric iron. However, analyses of these garnets (table 12) do not suggest a correspondence between an entry of titanium into the andradite structure and a move of ferric iron into the tetrahedral site as found by Dowty (1971). From our data, we infer sparse amounts of ferric iron in the Z site in many of the garnets richest in iron. The Y octahedral sites are occupied by 3.83 to 4.09 ferric iron atoms in the isotropic garnets, and from 1.57 to 3.78 ferric iron atoms in the anisotropic ones. Titanium was detected in six of the ten anisotropic garnets analyzed, and it presumably fills only 0.01 to 0.05 of the four available sites there. In all but four of the 21 garnet analyses, combined magnesium, manganese, and calcium cations total more than the six X-group positions allowable in the ideal formula. This probably reflects erroneously high analytical determinations of calcium because manganese and magnesium together fill at most 0.07 sites.

Pyroxenes from the garnetite show about a 10-molecular-percent variation in their composition mostly in the diopside (Di) to hedenbergite (Hd) series (table 13; fig. 16*B*). This variation is from about $Di_{95}Hd_4$ to $Di_{85}Hd_{14}$. All of the pyroxene grains analyzed are associated at the millimeter scale with anisotropic garnet, and they appear to be coexisting stably with it. Johannsenite, the manganese end member of this pyroxene group, makes up from 0.2 to 0.7 molecular percent. Minor jadeite molecule, $NaAlSi_2O_6$, is present in two grains at concentrations of about 0.4 molecular percent. Our calculations from

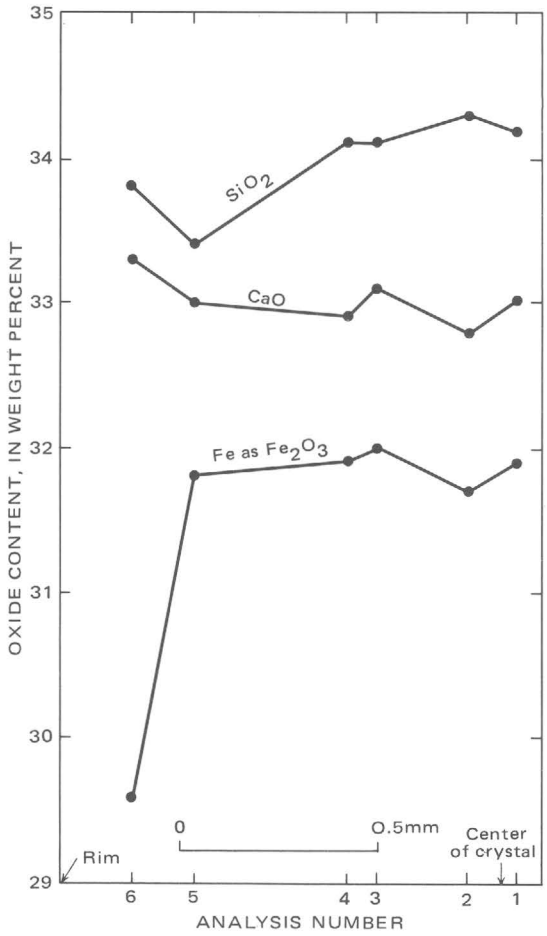

FIGURE 17.—Distribution of Fe_2O_3, SiO_2, and CaO across garnet crystal from DDH–12. Numbers correspond to analyses 1–6 of table 12.

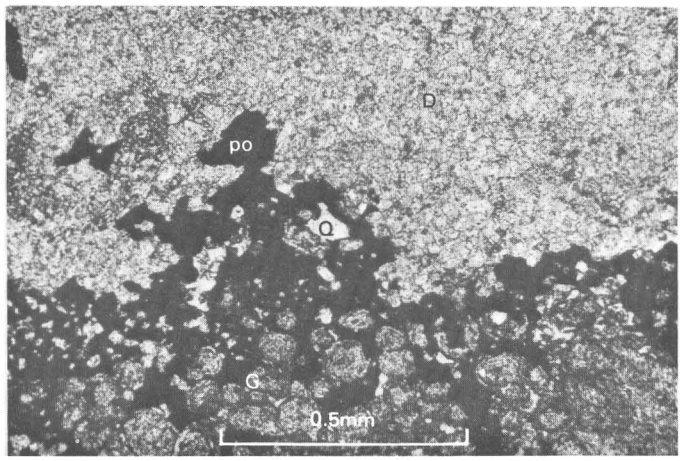

FIGURE 18.—Photomicrograph showing contact between garnetite (G) and diopside rock (D). Pyrrhotite (po) is concentrated, typically on garnetite side, close to the contact in many places, and quartz (Q) is a typical accessory mineral. Plane-polarized light.

the microprobe analyses of the pyroxenes suggest that the tetrahedrally coordinated Z-group sites are not fully occupied by silicon and aluminum in most of the grains, and we presume that ferric iron fills the remaining positions. In addition, there is some excess of Y cations. Magnesium cations compose about 45 percent of the latter sites.

TEXTURAL RELATIONS AMONG SILICATES AND SULFIDES

Critical to the overall paragenetic history of the Copper Canyon area is the time of crystallization of the garnetite relative to the surrounding diopside rock. Observations with the microscope of the contact between them, however, are not everywhere particularly diagnostic. Some contacts are typically knife-edge sharp in sinuous planes that show low-amplitude crenulations along their traces (fig. 18). Garnetite several centimeters away from the contact generally composes tightly packed aggregates of an andradite-diopside assemblage, with about 15 volume percent diopside. Minor accessory minerals may include quartz, pyrrhotite, and chalcopyrite with secondary siderite, hematite, and chlorite mostly in microveinlets. Within about 4–5 mm of the actual contact, the andradite and diopside do not form such a tight mosaic fabric but are instead filled interstitially with quartz and pyrrhotite. Diopside makes up about 75–80 percent of the diopside rock with accessory sphene, apatite, potassium feldspar, and quartz. In other places, the contact between diopside rock and garnetite is a 4- to 5-mm-wide zone that is heavily silicated and sulfidized and includes angular fragments of relict andradite and diopside. Most important, we have found approximately 1-mm-wide veins of diopside in several places that cut the contact between garnetite and diopside rock. These diopside veins have reaction rims, about as wide as the veins, of very finely recrystallized diopside. We thus infer crystallization of some diopside rock, at least, continued after most of the garnetite had formed. Quartz-pyrrhotite veins and pyrite-quartz veins also cut contacts between garnetite and diopside rock, suggesting repeated opening and closing of the rocks during sulfidization.

We previously described our textural evidence from the garnetite that nearly pure andradite ($Ad_{93–99}$), including traces of diopside and possibly primary hematite, probably was among the very first minerals to crystallize. It was followed closely by deposition or growth of less pure andradite rapidly fluctuating with the very pure varieties, and by an increase in the amount of diopside deposited. We cannot conclusively demonstrate the deposition of sulfides during the earliest stages of garnet growth. Nonetheless, garnetite forms the locus for most sulfides in the Pumpernickel

Formation, especially pyrrhotite (fig. 3). Yet, close examination of many polished and thin sections of garnetite shows that chalcopyrite, the main ore mineral in the deposit, is associated with several different textures in the rocks. It may occur along 0.1- to 0.5-mm-wide, highly irregular microfractures through andradite. These generally monomineralic veins of chalcopyrite are typically removed by less than a centimeter from concentrations of pyrrhotite, although some chalcopyrite and pyrrhotite are apparently compatible elsewhere in the samples. Some filiform veinlets of chalcopyrite and pyrrhotite commonly cut both isotropic and anisotropic andradite without any optical effect notable in either variety of andradite. In addition, chalcopyrite is concentrated with diopside, quartz, pyrrhotite, or pyrite as fillings of convex polygonal cavities lined by andradite. Finally some replacement of nearly pure andradite by pyrrhotite apparently occurred in some of the most heavily sulfidized rocks (fig. 19). Such massive replacement of andradite was very selective, because diopside inclusions in andradite seem to have been unaffected during the andradite's breakdown. Thus, diopside-pyrrhotite domains adjoin andradite-diopside ones, which contain sparse vein fillings of earlier chalcopyrite and pyrrhotite that preceded most of the pyrrhotite introduced into the rocks during the andradite-replacement stage.

Pyrite makes up about one-third of the total sulfide in the garnetite (fig. 3). We have established several parageneses for pyrite, despite the tendency for pyrite to crystallize euhedrally, obscuring age relations in many polished sections. (1) Pyrite replaced calcite interstitial to andradite (fig. 14*B* and *C*); the amount of pyrite in this association is minor. Near the reaction front between calcite and pyrite, some andradite has been converted to epidote. These reactions probably occurred during the early stage of sulfide deposition before crystallization of pyrrhotite and chalcopyrite. (2) Most pyrite in the garnetite, however, probably recrystallized on a volume-for-volume basis from a pyrrhotite-bearing host. Pyrite idioblasts hosted by pyrrhotite are fairly common throughout the pyrrhotite-bearing areas of the garnetite. In fact, we judge most of this pyrite in the garnetite to have recrystallized after the conversion of some pyrrhotite to marcasite. Figure 20 shows pyrrhotite that is cut by a gray marcasite vein that has in turn been cut by pyrite. As we previously described for the east ore body (Theodore and Blake, 1975), conversion of some pyrrhotite to marcasite in the garnetite apparently was a hypogene event that produced associated siderite as one of the breakdown products of the pyrrhotite. Furthermore, X-ray study of marcasite-bearing veinlets and clots from the garnetite shows them invariably to contain pyrite. (3) Textural relations between andradite and paragenetically later calcite and pyrite suggest recrystallization of some garnets during the introduction of sparse late calcite and pyrite. In garnetite around the general area of DDH–1 (fig. 3), where combined copper, gold, and silver total less than 0.15 weight percent copper equivalent, isotropic andradite (Ad_{99}) generally makes up less than 2 volume percent of the rocks. However, it typically forms irregular reaction rims about 0.1 mm wide along the edges of medium-grained (1.0 mm) subhedral crystals of anisotropic garnet. These anisotropic garnets make up from 80 to 85 percent of the rock in this part of the garnetite, and they commonly have well-developed sector twinning. Some reaction rims of Ad_{99} mantle anisotropic andradite with composition $Ad_{71\text{-}76}$ (fig. 21). We emphasize that

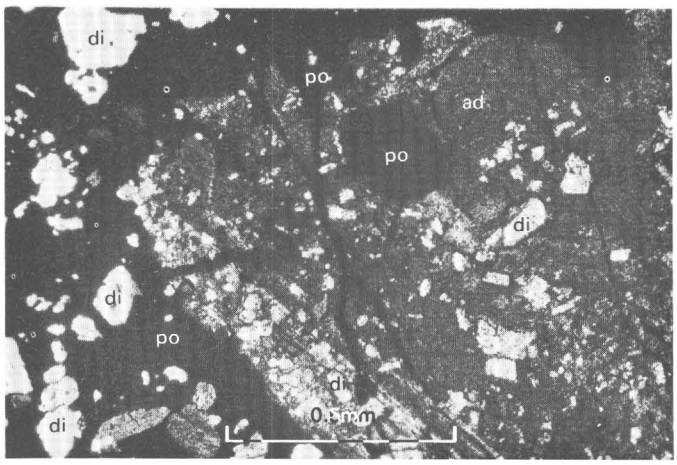

FIGURE 19.—Photomicrograph showing isotropic and anisotropic andradite (ad) with inclusions of diopside (di). Andradite is partly replaced by pyrrhotite (po). From DDH–4, depth 52.5 m; partially crossed nicols.

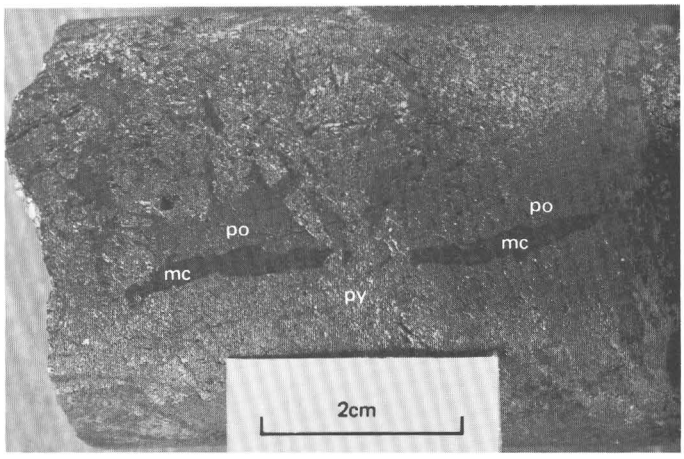

FIGURE 20.—Photograph showing sulfide rock from the garnetite with pyrrhotite (po) cut by marcasite (mc) veinlet that has in turn been cut by pyrite (py).

the textural relation shown in figure 21 between anisotropic and isotropic garnet must reflect a different paragenesis from that shown in figures 15 and 19. We infer the former texture (fig. 21) to reflect changes of that garnet's composition and structure very late in the sulfidization stage of the garnetite, and we infer the latter textures (figs. 15 and 19) to reflect growth transitions of garnet during the predominantly silication stage of calc-silicate growth. At the Mission, Ariz. porphyry copper deposit there apparently is a sharp spatial separation between isotropic and anisotropic garnet (Gale, 1965).

MINERALOGY OF POSTGARNET VEINS

The mineralogy of veins that cut the garnetite suggests significant changes in the chemistry of fluids circulating after widespread crystallization of andradite-diopside. Throughout the garnetite, however, veins are sparse, undoubtedly reflecting only minor penetration of postgarnetite fluids because of the tightness of the rocks. Tremolite-actinolite veins cut about 20 percent of the garnetite samples examined (tables 10 and 11); they also include quartz, epidote, and pyrite with potassium feldspar, chalcopyrite, or carbonate. The veins generally are 0.25–1.0 cm wide, and typically there are no alteration halos in the enclosing andradite-diopside wallrock. Sparse potassium feldspar in the veins may be altered to white mica, and some epidote in the veins replaces andradite fragments torn from the wallrocks. From the apparent compatibility of tremolite-actinolite and epidote in some of these veins, we infer a probable overlap in time of growth of the tremolite-actinolite and epidote rock to be described below. Some other veins that cut the garnetite show the following mineralogy (abbreviations are the same as in tables 8 and 9):

1. Q-kf-po
2. P-kf-py
3. C-py-hem-chl
4. Q-epi-chl-po-c
5. Hem-chl-c
6. Q-hem-c
7. Q-po
8. C-hem-ms

Tremolite-actinolite veins generally were followed by hematite-chlorite-carbonate ± (quartz-marcasite)-bearing veins. The hematitic veins occur along hairline microfractures and probably developed very late during the garnetite's paragenesis.

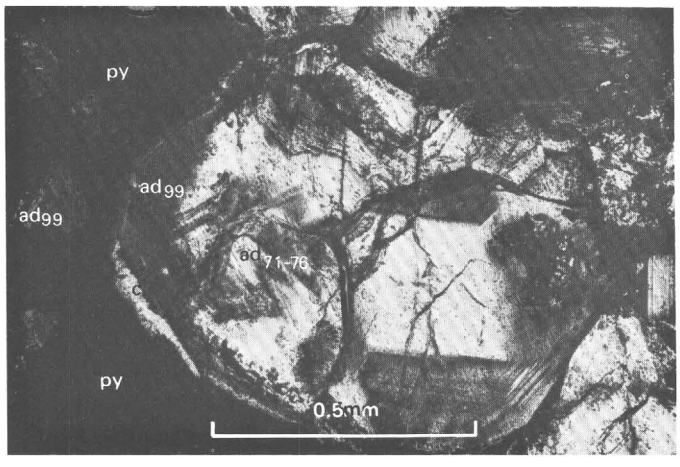

FIGURE 21.—Photomicrograph showing garnetite from DDH–1. Anisotropic andradite (ad_{71-76}) grain with isotropic andradite (ad_{99}) along its rim adjacent to pyrite (py) and secondary calcite (C). Partially crossed nicols.

EPIDOTE ROCK

Gray-green epidote rock (zone 4), formed by nearly complete replacement of andradite, is concentrated in an irregularly shaped mass that extends up to 225 m north of the altered granodiorite (fig. 4). This major concentration of epidote includes only traces of andradite in all drill holes from the area. Probably much of the minor pale-amber isotropic andradite we found in these rocks is recrystallized postepidote garnet. This sparse andradite, which includes some quartz and pyrite in veins, locally cuts a mineral assemblage dominated by epidote pseudomorphs after earlier andradite. The projection of epidote rock coincides with about one-third of the outlined ore body. In addition, a few zones of epidote rock were found locally replacing garnet in DDH–4 and DDH–12. In all, the mineralogy of five samples of epidote rock was determined systematically (table 14).

Typically, epidote, quartz, and pyrite, form a granoblastic fabric whose average grain size is generally 0.3 to 1.0 mm. Some small volumes of rock are composed almost entirely of epidote, cut by additional epidote in monomineralic veins. From sparse but clear textural relations, we infer that most of the epidote in these rocks, especially the coarser varieties, formed from andradite. Relict diopside in some rocks seems to have been unaffected during the conversion of andradite to epidote. Minor accesory minerals that are apparently compatible with epidote include tremolite-actinolite, potassium feldspar, sphene, apatite, and chalcopyrite in varying proportions throughout these rocks. Epidote rock is almost completely devoid of pyrrhotite; only traces were found either as finely dispersed grains among silicates adjacent to some pyrite veins, or as thin blades sparsely intergrown with quartz in some other veins. Most of the pyrite in epidote rock probably replaced earlier pyrrhotite and must reflect chemical changes with time in the environment of the skarn.

TABLE 14.—*Mineralogy of epidote rocks (zone 4) formed by alteration of garnetite in the Pumpernickel Formation*

[X, mineral present; Tr, present in trace amounts; ?, questionably present; ----, not found]

	1	2	3	4	5
	Pumpernickel Formation				
Locs. Nos., pl. 1	DDH–4		DDH–19		DDH–12
Field No.	6–233	[1]6–235	5–163	5–184	2–239
Epidote	X	X	X	X	X
Tremolite-actinolite	----	X	----	X	X
Quartz	X	X	X	X	X
Sphene	X	Tr	Tr	----	X
Potassium feldspar	Tr	X	X	X	----
Diopside	X	X	X	----	----
Andradite	Tr	----	----	?	----
Plagioclase	----	----	----	----	X
Biotite	----	----	----	X	
Chlorite	X	Tr	----	X	Tr
White mica	----	----	----	X	----
Apatite	X	X	Tr	----	X
Pyrite	X	X	X	X	X
Pyrrhotite	----	Tr	----	----	----
Chalcopyrite	Tr	X	Tr	Tr	----
Hematite	Tr	Tr	Tr	X	Tr
Carbonate	----	Tr	Tr	----	----
Marcasite	----	X	----	----	----

[1]Includes trace amounts of detrital zircon.

Many veins that contain highly varied mineral assemblages cut epidote rock, and they indicate repeated and complex circulation of chemically diverse fluids. Although these veins generally are less than 1 cm wide, they nonetheless make up a significant fraction of the epidote rock near some of the major structures in the area, such as the Golconda thrust. We briefly described the andradite-bearing veins above. The mineralogy of some other veins and some reaction textures that cut epidote reflect the late, second major stage of potassic alteration, which is confined to areas fairly close to the altered granodiorite (BIO II, fig. 4). In a later section of the report, we will expand our hypothesis that this postepidote potassic alteration in the west ore body was almost contemporaneous with potassic alteration in the east ore body.

Several mineral assemblages that contain hydrothermal biotite and potassium feldspar characterize the postepidote potassic alteration; they are found in quartz-biotite veins and a felted intergrowth of fine-grained biotite, tremolite-actinolite, apatite, and pyrite that cuts epidote (fig. 22). The felted intergrowths locally flood the rocks, and at places they are cut in turn by veins with the following mineralogies:

1. Q-wm-chl-py-cp
2. Ta-py
3. Q-kf-py±hem±chl

The alteration adjacent to these veins is minimal and consists of a slight recrystallization of epidote and introduction of some quartz. Along some 0.5-cm-wide fractures, very late fluids reacted with pyrite to yield marcasite tightly intergrown with chlorite, hematite, and a carbonate (probably siderite).

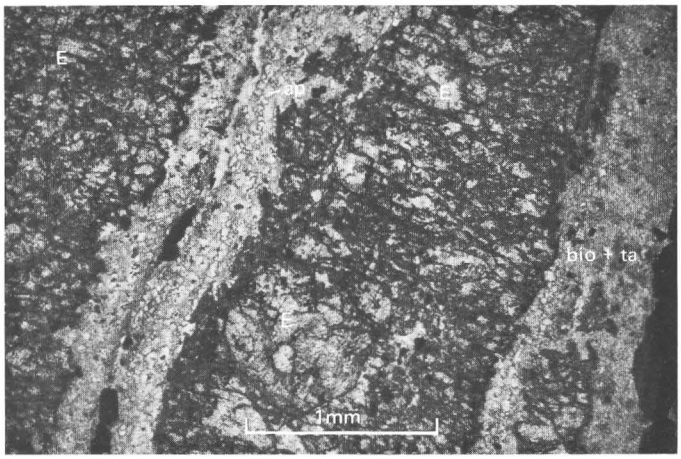

FIGURE 22.—Photomicrograph showing epidote rock with epidote (E) veined by intergrown tremolite-actinolite (ta), biotite (bio), and apatite (ap). Plane-polarized light.

BATTLE FORMATION

The mineralogy of 23 drill core samples of the Battle Formation is shown in table 15. These samples are a fairly representative suite of alteration assemblages from the formation, and all of these samples, with the exception of three (12–14), were obtained from an unexposed block of rock of the Battle Formation below the Golconda thrust and between the West Ridge and Virgin faults (pl. 1). Samples 12–14 are from DDH–17, which was collared east of the Virgin fault in an area where the Battle Formation crops out. In general, the fabric of metamorphosed conglomerate, quartzite, and shale of the Battle Formation shows relict sedimentary rock fragments and quartz, all at various stages of recrystallization, set in a felted matrix of fine- to medium-grained metamorphic minerals. The matrix typically is made up of well-crystallized silicate minerals that show the classic alteration stages associated with porphyry copper deposits, and varying amounts of intergrown sulfides. Away from the very intense metasomatism and metamorphism centered on the skarn, the Battle Formation has an outermost metamorphic fringe typified by secondary biotite that locally is heavily inundated by increasing amounts of tremolite-actinolite and diopside toward the skarn. Pyrite, pyrrhotite, chalcopyrite, and sparse bornite and late marcasite generally make up about 2–3 volume percent of the rocks; sparse bornite was found in only one sample, and traces of molybdenite occur in holes close to the altered granodiorite. The low sulfide content of the Battle Formation in this tectonic block be-

TABLE 15.—*Mineralogy of the Battle Formation in the general area of the west ore body*

[X, mineral present; Tr, present in trace amounts; ?, questionably present; ____, not found]

	1	2	3	4	5	6	7	8	9	10	11	12	13	14	15	16	17	18	19	20	21	22	23
Locs. Nos., pl. 1	DDH–2											DDH–17			DDH–1	DDH–12	DDH–19	DDH–20					
Field Nos.	8–326	8–351	8–397	8–438	8–459	8–472	8–537	8–562	8–578	8–664	8–809	3–248	3–290	3–377	[1]1–480	2–287	15–201	5–349	5–426	5–487	5–707	[2]5–806	[3]5–831
Hypogene Constituents																							
Quartz	X	X	X	X	X	X	X	X	X	X	X	X	X	X	X	X	X	X	X	X	X	X	X
Diopside	____	____	____	X	X	X	X	____	____	____	____	____	____	____	X	____	X	____	X	____	____	____	____
Tremolite-actinolite	____	X	X	X	X	X	X	X	X	____	____	____	____	____	X	____	X	?	X	X	X	____	____
Potassium feldspar	____	X	X	X	X	X	Tr	X	X	?	____	X	____	____	X	X	X	X	Tr	?	____	X	X
Biotite	X	____	____	____	____	____	X	X	Tr	X	X	____	____	?	____	X	____	X	____	____	X	Tr	____
White mica	X	____	Tr	____	____	X	____	____	X	X	X	X	____	____	____	Tr	____	____	____	X	____	X	X
Epidote	____	____	____	____	____	X	____	____	____	Tr	____	____	____	____	____	____	X	____	X	____	Tr	____	____
Chlorite	X	____	Tr	____	____	____	X	____	X	Tr	X	X	X	X	____	____	____	Tr	X	?	X	____	____
Sphene	____	X	____	____	____	X	____	X	X	Tr	____	Tr	X	____	X	X	X	X	____	____	____	____	X
Apatite	____	Tr	____	____	____	____	____	X	____	____	Tr	____	____	____	X	X	X	X	Tr	____	X	X	X
Pyrite	X	X	Tr	____	Tr	X	X	X	X	X	X	X	X	____	Tr	X	X	X	X	X	X	X	____
Pyrrhotite	____	____	X	Tr	Tr	Tr	____	X	____	____	____	____	X	X	X	____	____	____	X	____	____	X	X
Chalcopyrite	____	____	Tr	Tr	____	Tr	X	Tr	Tr	____	X	Tr	X	Tr	____	____	____	Tr	X	____	X	X	X
Marcasite	X	____	____	____	____	____	____	____	____	____	____	____	____	X	X	____	____	____	X	____	____	____	X
Carbonate	X	____	____	____	X	X	____	Tr	Tr	____	X	X	X	X[4]	X	Tr	____	Tr	____	Tr	Tr	X	X
Supergene Constituent																							
Iron oxide	X	X	Tr	____	X	Tr	X	Tr	Tr	Tr	____	X	____	Tr	X	X	Tr	____	____	Tr	Tr	X	X
Detrital Constituents																							
Rock fragments	X	____	X	____	____	____	____	____	X	____	X	X	X	X	X	X	X	X	____	X	____	X	X
Quartz	X	X	X	X	X	X	____	____	X	X	X	X	X	X	X	X	X	X	X	X	____	X	X
Zircon	____	Tr	____	____	____	____	Tr	Tr	Tr	Tr	____	____	Tr	____	____	Tr	____	Tr	____	____	Tr	____	X
Apatite	____	____	____	____	____	____	____	____	?	Tr	____	X	____	Tr	____	____	____	____	____	____	____	____	____
Plagioclase	____	____	X	X	____	Tr	____	____	____	X	____	____	____	____	____	____	____	____	____	____	____	____	____
Potassium feldspar	____	____	X	____	____	____	____	____	____	Tr	____	____	____	____	____	____	____	____	____	____	____	____	____

[1]Includes moderate amount of Mg-vermiculite.

[2]Includes sparse bornite intergrown with chalcopyrite and pyrrhotite.

[3]Includes sparse rutile.

[4]Includes some siderite, verified by X-ray.

neath the thrust strongly contrasts with the Battle Formation in the east ore body. There, some of these rocks contain as much as 50 percent hypogene sulfides (Theodore and Blake, 1975). Furthermore, there are other differences in mineralogy between the Battle Formation in the east ore body and that below the Golconda thrust under the west ore body. However, before we detail these petrochemical and paragenetic differences, we will present a systematic examination of the silicate and sulfide alteration assemblages derived from surface and subsurface samples in the Battle Formation around the west ore body.

Our microscopic and hand specimen studies reveal an apparent local contrast in alteration facies at the surface across the trace of the Virgin fault in the general area of DDH–17. East of the Virgin fault, the middle and upper members of the Battle Formation primarily show minerals typical of propylitic alteration (fig. 4). West of the Virgin fault, exposed rocks of the Pumpernickel Formation contain potassic alteration assemblages, typified principally by secondary biotite. We believe that this difference in alteration assemblages between the two tectonic blocks cannot be accounted for simply by movements along the Virgin fault. The downdropped block west of the Virgin fault should contain propylitic, rather than potassic, mineral assemblages if postmineralization movements alone are to account for the observed contrast in alteration across the fault trace. At the surface, the Battle Formation contains chlorite and pyrite with epidote, tremolite, rutile, or potassium feldspar. Throughout these rocks, however, patchy small domains of relict secondary biotite, variably altered to chlorite, strongly suggest that the propylitic alteration here occurred sometime after potassic alteration, the dominant type of alteration in the district. Near the southeast corner of the area (pl. 1), the lower member of the Battle Formation primarily shows potassic assemblages that may be the second-generation potassic alteration recognized in the Pumpernickel Formation and in part of the west ore body.

The Battle Formation west of the Virgin fault and at depth beneath the Pumpernickel Formation consists of a highly varied suite of hypogene minerals that may be grouped into three assemblages:

1. Diop-ta-kf±bio±chl±sph±ep±py±po±cp
2. Ta-py±kf±bio±wm±sph±ep±chl±cp
3. Bio-py±kf±wm±ep±chl±cp

The first two of these alteration assemblages are predominantly calc-silicate, whereas the third is potassic, modified somewhat by subsequent propylitic alteration. Although the diopside-tremolite-actinolite-potassium feldspar assemblage is best developed in the middle unit of the Battle Formation, it occurs throughout the formation, even as far north of the granodiorite as DDH–1. From such a broad spatial distribution, we infer that fluids temporally associated with the development of the copper-skarn bodies in the overlying rocks of the Pumpernickel also circulated widely through, and strongly metamorphosed, the Battle Formation. Additional support for this conclusion comes from our studies of fluid inclusion, presented below.

The wide distribution of a diopside-bearing metamorphic assemblage in the Battle Formation, north of the granodiorite and below the Golconda thrust, strongly contrasts with its apparent absence from any of the Battle Formation in the east ore body. We cannot ascribe such mineralogical differences to variations in distance from the exposed granodiorite, the apparent heat source. In fact, our petrologic data from the two ore bodies show an inverse relation between distance from the granodiorite and the presence of the apparently early, and thus presumably hot, diopside-bearing rocks. Within the east ore body, our detailed petrochemical investigations were concentrated along the 6450 bench, as much as 150 m from the granodiorite contact (Theodore and Blake, 1975). Yet nowhere, after intensive investigations in the east ore body, have we found either diopside or andradite in the Battle Formation. Certainly their prealteration mineral composition must have been receptive to the crystallization of diopside and andradite, because, where unmetamorphosed, these rocks contain both magnesium carbonates and various iron oxides. Furthermore, we have not found any textural evidence to suggest that diopside or andradite recrystallized during some earlier stage in the overall alteration of the east ore body. In some of the magnesium-rich horizons, tremolite±epidote assemblages that reflect recrystallization during an early or prograde stage occur in place of diopside. On the other hand, andradite- and diopside-bearing rocks extend to at least 410 m from the granodiorite in the skarn hosted by the Pumpernickel Formation. In fact, even at this distance from the granodiorite, we see no indication of any lessening of the diopside-bearing skarn's presence. Presumably, the argillite and chert of the Pumpernickel Formation were less permeable than the conglomerate and quartzite of the Battle Formation, which suggests that the penetration of metamorphosing fluids must have been significantly enhanced by premineralization channels. The Copper Canyon fault must have been one of these channels. We propose, therefore, that the bulk of the early metamorphic and metasomatic crystallization in the area focused on a block of rocks west of the Virgin fault. We will discuss in detail the evolution of the skarn in the section entitled, "Paragenesis and Model of Skarn Development."

ALTERED GRANODIORITE OF COPPER CANYON

In several previous reports (Nash and Theodore, 1971; Theodore and others, 1973; Batchelder, 1973; Theodore and Blake, 1975), the altered granodiorite was discussed at some length because the intrusive body is spatially associated with the nearby ore deposits, although the relations between the intrusion and ore deposits are complex. In this report, we stress the petrology of the granodiorite immediately adjacent to the skarn; in all, we studied about 20 representative rocks for this part of the report. We especially were concerned with the sequential development of alteration assemblages within the main mass of the granodiorite and the sill of altered granodiorite emplaced along the Golconda thrust below the skarn. Furthermore, we relate alteration and metallization in the intrusive rocks to the various stages of crystallization of skarn in the wallrocks of the intrusion. We found neither skarn formed from the granodiorite (endoskarn of Korszhinskiy, 1964) nor veins with anhydrous calc-silicate minerals that cut the granodiorite. When we consider this relation together with (1) the orientation of the mineral zonation in the skarn at right angles to the granodiorite contact rather than parallel to it and (2) the absence of skarn from the east ore body, we infer that crystallization of most of the anhydrous minerals in the skarn must have preceded emplacement, final crystallization, and consolidation of the adjacent granodiorite. If the skarn had formed as fluids emanated from a penecontemporaneously crystallizing adjacent intrusion, the mineral zones should parallel roughly the intrusion's contact, and a skarn type of metamorphic assemblage would have formed largely at the present site of the east ore body. We emphasize that there is no skarn in the east ore body. We will first describe the granodiorite in DDH–7, which is in the granodiorite just south of the ore (pl. 1).

The granodiorite of Copper Canyon is porphyritic and contains medium- to coarse-grained phenocrysts of plagioclase, quartz, biotite, hornblende, and potassium feldspar set in a fine-grained groundmass that has been altered (Theodore and Blake, 1975). The metamorphic petrology of the altered granodiorite in DDH–7 shows typical assemblages of the potassic facies. Quartz-potassium feldspar veins are common. Some 0.01- to 0.02-mm-sized shreds of hydrothermal biotite have recrystallized both from primary phenocrystic biotite and as replacements of hornblende throughout the granodiorite (fig. 23). Some crystals of hornblende are replaced by mixtures of biotite, chlorite, quartz, and apatite—all crude pseudomorphs after the original crystals. These secondary, presumably magnesian biotites are pale tan, and less pleochroic than relict primary biotite. G. K. Czamanske (written commun., 1974) found by electron microprobe studies of optically similar hydrothermal biotite from the east ore body that the biotite has a mean Mg/Mg+Fe ratio of about 0.78. Primary biotites from three unaltered Tertiary plutons in the mining district have Mg/Mg+Fe ratios in the 0.49–0.56 range; primary biotite from the altered granodiorite of Copper Canyon has a 0.65–0.69 ratio (Theodore and others, 1973). In addition, Czamanske determined that TiO_2 is depleted significantly in the hydrothermal biotite compared to the primary biotite of the granodiorite. Newly crystallized quartz and potassium feldspar, including small amounts of white mica, are concentrated in some of the granodiorite dominated by abundant hydrothermal biotite and hydrothermal apatite and sphene. Plagioclase laths, about 4–5 mm long, range from calcic oligoclase to andesine. Some are strongly zoned and euhedral and have more calcic cores than rims, whereas others show oscillatory zoning. Most plagioclase crystals in domains where hydrothermal biotite is extensively developed seem to have remained fairly fresh; they have sharp lamella traces and extinction positions. Sparse white mica has recrystallized preferentially along margins and some crystallographic directions of the plagioclase.

Throughout the entire depth of DDH–7, sulfides make up about 2 volume percent of the rocks. Pyrite and chalcopyrite are ubiquitous; pyrrhotite, arsenopyrite, sphalerite, molybdenite, and marcasite occur in various associations along veinlets and as disseminations in domains rich in hydrothermal biotite. Pyrrhotite and molybdenite occur more frequently at depth,

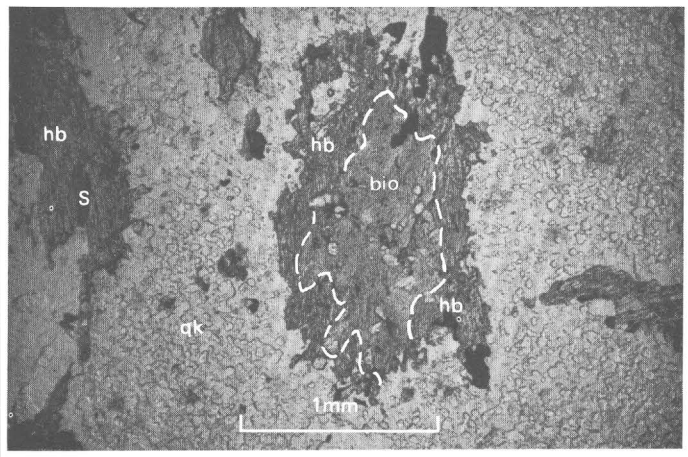

FIGURE 23.—Photomicrograph showing primary hornblende (hb) grain almost completely replaced by felted secondary biotite (bio). Other hornblende phenocrysts in field of view are optically unaffected, one has inclusion of sphene (S). All are set in quartz-potassium feldspar groundmass (qk). From altered granodiorite of Copper Canyon. Plane-polarized light.

while paragenetically late chalcocite and covellite are sprinkled throughout.

The granodiorite adjacent to the skarn at Copper Canyon appears neither to be desilicated nor to reflect assimilation of calcium from carbonate-rich wallrock. We recognize no zones in the granodiorite suggestive of calcium-magnesium assimilation. In fact, our chemical data from many plutons across the district show a decrease in calcium and strontium concomitant with increasing intensity of potassic alteration (Theodore and others, 1973). However, some postmagmatic mobilization of magnesium probably occurred within the pluton along with sulfidization and alteration. Moore and Czamanske (1973) have shown that secondary hydrothermal biotite associated with ore in the Bingham porphyry copper deposit is more magnesian than the primary biotite.

In the granodiorite a plagioclase-destructive type of alteration locally postdates the widespread potassic alteration. This type of alteration occurs in highly irregular zones that generally are structurally controlled and are near the Virgin fault. Some zones measure about 60 to 90 m in extent and depth. In these zones, plagioclase is replaced by white mica and minor kaolinite to the extent that only euhedral shadows of fine-grained white mica indicate the former presence of plagioclase. In addition, relict primary potassium feldspar phenocrysts locally have been heavily altered to white mica, whereas secondary potassium feldspar in the groundmass remains unaltered.

Some parts of the thin granodiorite sill along the Golconda thrust below the west ore body show an alteration mineralogy somewhat different from that of the main mass of the granodiorite. White mica heavily replaces plagioclase. Locally the sill also contains two conspicuous generations of amphibole; one is apparently primary and is very pale bluish gray in thin section and shows ragged crystal outlines. The other is much finer, almost colorless, and probably is a secondary tremolite-actinolite. In addition, crystallization of secondary sphene and possibly some apatite occurred within optically continuous grains of primary amphibole. Some secondary amphibole is replaced by quartz. Epidote is scattered throughout the sill as replacements of the calcic cores of plagioclase phenocrysts. Other plagioclase phenocrysts show fairly good volume-for-volume replacement by potassium feldspar that occurs in reaction zones adjacent to chlorite-tremolite-pyrite veins that are roughly several millimeters wide. The chlorite in these veins shows a good colloform texture, suggesting it was not derived from previously crystallized biotite. Some tremolite-pyrite-chalcopyrite veins that measure several centimeters across also cut the sill.

GEOCHEMISTRY OF BEDROCK EXPOSED AROUND THE SKARN

In this part of the report, we evaluate the exploration potential of various metals as pathfinders to ore by comparing geochemical data from bedrock exposed at the surface around the skarn with geochemical data gathered from the skarn. Abundant geochemical data are available for the Copper Canyon area (Theodore, 1969, 1970; Theodore and Blake, 1975). The material analyzed for those studies consisted of composite 1-kg rock-chip samples that generally were collected over an outcrop area of 10 m^2. These geochemical data consist of analytical determinations in the U.S. Geological Survey laboratories in the field and at Denver. They include analyses for 29 elements by a six-step spectrographic method (Grimes and Marranzino, 1968) and analyses by atomic-absorption methods for mercury and gold (Vaughn and McCarthy, 1964; Thompson and others, 1968).

AREAL ZONATION OF MINOR ELEMENTS

The Pumpernickel Formation exposed above the skarn reflects best the primary areal zonation of 11 minor elements (Ag, Au, Bi, Co, Cu, Hg, Fe, Mo, Pb, Sr, and Zn) in the hypogene system at Copper Canyon (Theodore and Nash, 1973). The Pumpernickel Formation probably shows limited hypogene migration of these elements away from ore because of the rocks' relative impermeability. The relatively unfractured and apparently impervious chert and argillite of the Pumpernickel Formation effectively restricted the numbers of channels available to the hypogene fluids, in contrast to the more intensely fractured and faulted Battle Formation, where abundant hydrothermal veins extend along numerous preexisting structures far beyond the ore bodies known in this formation. Ground water must also have circulated much more freely through the porous conglomerate of the Battle Formation than the relatively impermeable rocks of the Pumpernickel Formation, possibly modifying the hypogene geochemistry.

The distribution of 11 elements in the Pumpernickel Formation along a section northward from the granodiorite into unpyritized rock is shown in figure 24; the location of the west ore body is also shown on the cross section. The relative strengths of individual element zones in figure 24 were determined by comparing the concentration of each element dispersed around the granodiorite and ore bodies with its concentration in unmetallized rocks from northern parts of the area sampled for the geochemical study. We were concerned chiefly with detecting changes in concentrations of elements in rock not conspicuously fractured. As a re-

sult, this profile does not reflect concentrations of elements related to the fracture-controlled vein deposits of base metals peripheral to the granodiorite. Furthermore, the profile is somewhat simplified and includes geochemical data projected to it from many tens of meters away. Additional geochemical details are discussed in Theodore and Blake (1975); Theodore and Nash (1973) compare these zonations of minor elements with the distribution of high-salinity fluids at Copper Canyon.

The primary dispersion of copper in the Pumpernickel Formation differs from north to south in the area studied geochemically (see Theodore and Blake, 1975, pl. 2*A* for the distribution of copper in outcrops at Copper Canyon). Copper concentrations in rocks of the Pumpernickel near the edge of the pyritized zone (fig. 2) are about 20 ppm, not significantly greater than those in unmetallized rocks. Concentrations of copper in exposures of Pumpernickel Formation commonly exceed 50 ppm about 300 m north of the granodiorite in an area where several drill holes penetrated skarn metallized at subeconomic grades. The median copper value determined for 211 surficial samples of bedrock from an area of about 0.6 km^2 of pyritized rocks of the Pumpernickel Formation above the skarn is 150 ppm.

The median concentration of copper in 190 surface rock samples of the granodiorite at Copper Canyon is 1,500 ppm. Copper is most abundant in green, altered plagioclase phenocrysts (Clement, 1968), and lesser concentrations of copper occur in chalcopyrite inclu-

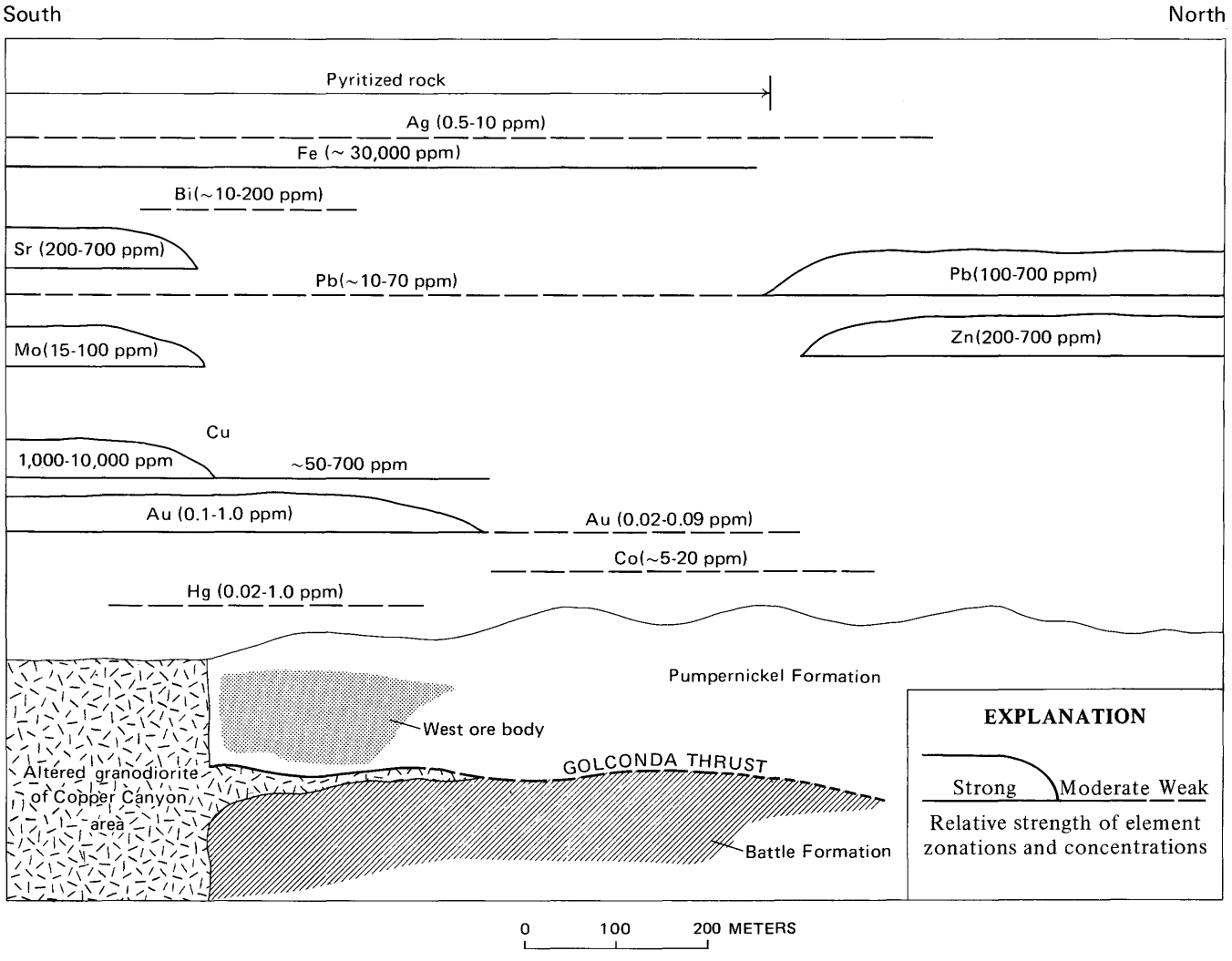

FIGURE 24.—Relative positions and strengths of element zones in outcrops of the Pumpernickel Formation near granodiorite of Copper Canyon. Analytical ranges given for individual elements are from Theodore (1969, 1970). Structure section is stylized to show general geologic relations and location of west ore body. Location of profile is shown in figure 2.

sions in biotite (Theodore and others, 1973), in chalcopyrite-bearing veins, and as sparse chalcopyrite dispersed in the intrusion's matrix. In addition, cuprite veins mantled by chrysocolla, and fracture coatings of amorphous black copper oxides are common throughout the surface exposures of the granodiorite. Much of the secondary copper in the granodiorite is restricted to thin enrichment zones that closely follow the present erosion surface. Most of this secondary copper is probably derived principally from the east ore body, which is topographically higher than the granodiorite. We suggest that copper was leached by rainwater from exposed sulfides in the east ore body and then deposited as secondary copper in the granodiorite.

Ten other metals are also differentially dispersed about the granodiorite as follows (fig. 24): (1) Iron is generally enriched to concentrations of about 3 weight percent in the pyritized rocks of the Pumpernickel Formation surrounding the granodiorite. The median value for iron in the unpyritized rocks of the formation farther away from the granodiorite is typically less than 1 percent. (2) Silver occurs throughout the pyritized rocks, generally at concentrations from 0.5 to 10 ppm. (3) A localized enrichment of bismuth (10–200 ppm) occurs above ore in the skarn. Concentrations of (4) lead and (5) zinc increase in many samples just outside the area of pyritized rock, and spotty anomalous concentrations of lead extend farther to the south into the intrusion. The distribution of these metals may reflect the strong introduction of lead and zinc along veins just to the north, in the area around the townsite of Galena (see Roberts and Arnold, 1965). The southern extent of anomalous zinc concentration is obscured because of the low sensitivity (200 ppm) of the spectrographic method employed. (6) Molybdenum (from quartz-molybdenite veinlets) and (7) strontium are more abundant in the granodiorite than in the surrounding wallrocks. Comparison of strontium concentrations in the granodiorite at Copper Canyon to that in unaltered granodiorites elsewhere in the mining district, however, demonstrates that strontium actually has been depleted in this body during hydrothermal alteration (Theodore and others, 1973). (8) Although anomalous concentrations of gold were found in some samples near the edge of the pyrite envelope, gold concentrations (0.1–1.0 ppm) are most common over the west ore body and in the granodiorite. Much of the gold anomaly along the profile (fig. 24) is over skarn that includes significant copper-gold ore zones (fig. 3). (9) Anomalous 5–20 ppm concentrations of cobalt exhibit a weak zonation along the outer 450 m of pyritized rock in the general area of the profile. (10) The distribution of mercury is anomalous (0.02–1.0 ppm) across the northern part of the granodiorite and part of the skarn.

Chemical sampling for copper and many other metals around the deposits at Copper Canyon points to the granodiorite as the most likely host for ore rather than the metasedimentary wallrocks where the ore occurs (Theodore and Nash, 1973). The zonation of minor elements is dominated by a strong concentration of copper and gold at the surface of the granodiorite; most copper there is supergene as we described previously. Copper is enriched by a factor of about 100 relative to concentrations of copper in unaltered granitic rocks; gold is enriched possibly by a factor of about 1,000. However, it is important that at Copper Canyon the abundance of metal dispersed through rocks rather than occurrences of metals as fracture fillings or coatings is a more specific geochemical indicator of ore. Although mercury and potassium abundances, or increase in the rubidium : strontium ratio might be suitable guides to the ore zones (Theodore and others, 1973; Theodore and Blake, 1975), it is unlikely that these, together with the moderate concentrations of dispersed copper in the metasedimentary rocks, would have directed a geologist to focus initially on the intruded wallrocks as the most likely ore hosts. Anomalous concentrations of mercury in rock exposed directly above the skarn are difficult to evaluate because mercury is not particularly abundant in the ore body. Fifteen drill-core samples of skarn rich in sulfide do not show high concentrations of mercury (table 3). The highest concentration of mercury in these samples (0.086 ppm) is in the sample with the most zinc (1,140 ppm). This suggests that some mercury may have been introduced together with sphalerite, possibly during some of the late stages of metallization in the ore body.

MINOR-ELEMENT FREQUENCY DISTRIBUTIONS

The geochemical data obtained from the surface at Copper Canyon were divided into two groups for this part of the report (fig. 25). Sample group 1 consists of analyses of 185 samples from a 1.5-km^2 area of unpyritized and very sparsely mineralized rock belonging to the upper chert unit of the Pumpernickel Formation northwest of the ore body (see Theodore and Blake, 1975, fig. 46, Area 1 for the area sampled for group 1). The area from which the group 1 samples were collected is about 0.9 km west of a locus of lead-silver metallization at the White and Shiloh mine near the abandoned townsite of Galena. In the area from which the group 2 samples were collected, altered silty argillite and chert, and biotite hornfels of the lower unit of the Pumpernickel Formation crop out (Theodore and Blake, 1975, fig. 46, Area 6). Fairly large areas of unmineralized rock belonging to the lower unit of this formation were not available for study. Thus, for com-

parative purposes, the best we could do was to consider group 1 data to represent local geochemical background, although this assumption is not justified geologically because the upper unit is largely chert and the lower unit is largely argillite.

Histograms for the samples from the unmineralized area (group 1, fig. 25) indicate widely varying shapes in their log-frequency distributions; these geochemical data were transformed by common logarithms before construction of the frequency distribution. Group 1 distributions for 15 elements (Ag, As, Be, Bi, Cd, Co, La, Mo, Nb, Sb, Sc, Sn, Sr, W, and Zn) are strongly censored, with 45 (La) to 100 (W) percent of the analyses for these elements falling below their respective lower detection limits. The lower detection limits range from 0.5 ppm (Ag) to 200 ppm (As and Zn) for the spectrographic method used in these analyses. The distributions of many elements are unimodal in the group 1 data set, with the notable exceptions of iron and titanium, which show more than one peak. None of the histograms for these 15 elements for which we have more than 50 percent of the analyses above the detection threshold reflects perfect normal or lognormal shapes. However, the histograms for magnesium, calcium, barium, and zirconium are fairly symmetrical. On the other hand, the histograms for silver, copper, iron (?), manganese, and lead are positively skewed. Of these five elements, lead has probably the strongest positive skewness. This probably reflects sparse occurences of galena-bearing vein material in the group 1 samples. The histogram for boron constructed from the group 1 data set has a slight negative skewness.

Comparison of histograms prepared from analyses of mineralized rocks with those of unmineralized rocks reveals that metallization significantly changed concentrations of many of the elements. However, distributions of 13 elements in the mineralized rocks (As, Be, Bi, Cd, Co, La, Mo, Nb, Sb, Sn, Sr, W, and Zn) are strongly censored, with from 37 (La) to 94 (W) percent of the samples having concentrations below the lower detection limits (group 2, fig. 25). Group 2 distributions for seven elements (Ag, B, Ca, Ni, Pb, Sc, and Hg) are moderately censored. Compared with group 1, group 2 data show substantial decreases in the numbers of analyses for many elements that fall below their lower detection limits. We judge such changes for seven elements (Ag, As, Bi, Co, Mo, Pb, and Sn) to reflect metallization. Histograms for silver, boron, copper, lead, and mercury are positively skewed, whereas those for manganese, titanium, and vanadium suggest negative skewness. Six elements (Ag, B, Fe, Mg, Mn(?), and Ni) seem to have multimodal distributions. We will now consider in detail the apparent chemical changes these rocks have undergone during metallization.

TABLE 16.—*Comparison of medians for 12 elements in analyses of samples of the Pumpernickel Formation from a sparsely mineralized area (group 1) and from around the skarn (group 2)*

Element	Median (in parts per million)	
	Group 1	Group 2
Fe	7,000	30,000
Ca	3,000	1,500
Ti	700	3,000
Ag	.5	20
B	70	20
Ba	500	1,500
Cr	50	100
Cu	20	100
Pb	10	30
V	30	100
Zr	50	300
Au	<.02	.07

Table 16 lists those 11 elements whose medians we judge to show significant differences between the groups 1 and 2 data sets. From these median values we initially might infer gains of ten elements (Fe, Ti, Ag, Ba, Cr, Cu, Pb, V, Zr, and Au) and losses of calcium and boron during metallization of the Pumpernickel Formation at Copper Canyon. Certainly additions of gold, iron, silver, copper, and lead and losses of calcium are compatible with overall chemical changes for rocks in a porphyry copper environment. Such changes occurred in the east ore body, and they are reflected also in the primary zonation of elements in the Copper Canyon area (fig. 24; see also Theodore and Blake, 1975; Theodore and Nash, 1973). However, the apparent gains for barium, chromium, titanium, vanadium, and zirconium and the apparent loss of boron implied by shifts in the medians for these elements must be evaluated critically; such changes apparently due to metallization might in fact reflect inherent differences of premetallization chemistry between the two localities. In an attempt to resolve these problems, we quantified the statistical associations of barium, chromium, titanium, vanadium, and zirconium for other elements.

STATISTICAL ASSOCIATIONS OF BARIUM, CHROMIUM, TITANIUM, VANADIUM, AND ZIRCONIUM

Calculations of Spearman rank correlation coefficients for the group 1 data show that barium, chromium, titanium, vanadium, and zirconium are all very strongly associated with one another; that is, their concentrations commonly vary directly (table 17). The mutual strong associations among these five elements are consistent with their belonging to the same major geochemical class of lithophile elements, or elements that tend to be bound to oxygen in silicate min-

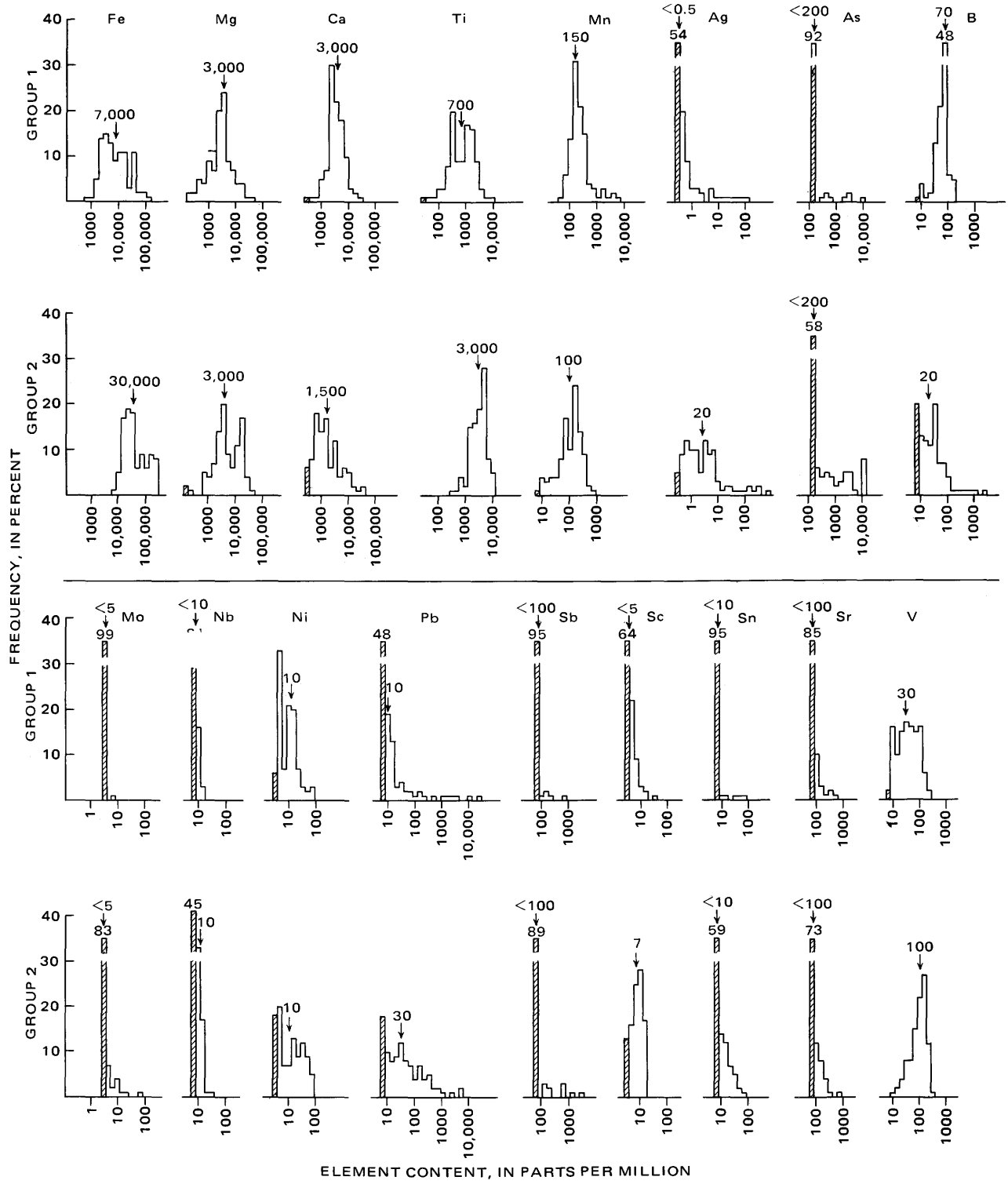

FIGURE 25.—Log-frequency distribution of elements from analyses of 185 samples from an area of unpyritized and very sparsely
Formation around

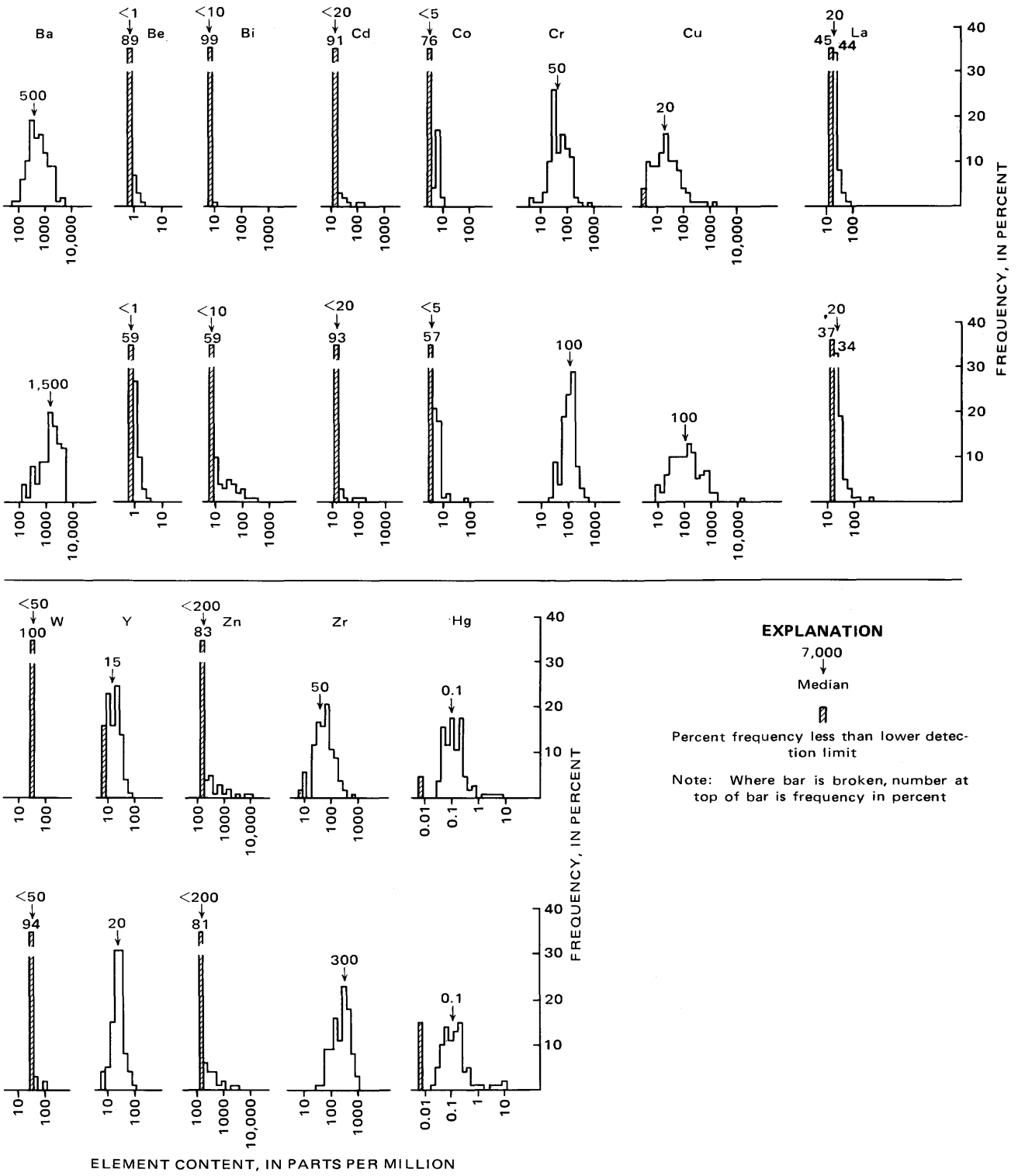

mineralized rock of the Pumpernickel Formation (group 1), and analyses of 211 samples of pyritized rock of the Pumpernickel the skarn (group 2).

erals (Goldschmidt, 1954). In addition each of these five elements is strongly associated with several other elements in this data set:

Ba	Cr	Ti	V	Zr
Mg	Cu	Cu	Cu	Fe
Ni	Fe	Fe	Fe	Mg
	Mg	Ni	Mg	Ni
	Ni			

All of these associations for group 1 are consistent with those reported by Vine and Tourtelot (1969) for geosynclinal chert and claystone that contain minor organic material or carbonate minerals.

Correlation calculations for group 2 data, which come from the mineralized area around the skarn, demonstrate similar element associations (table 18). The strongest associations of these five elements are:

Ba	Cr	Ti	V	Zr
Mg	V	Ba	Ba	Ti
Ti		V	Cr	

Although many direct variations in the group 2 data set are the same as in group 1 (compare tables 17 and 18), the strengths of the associations significant for group 1 are diminished for the group 2 data. This relation must reflect in part local mobilization of many elements in the rocks during alteration and metallization.

Negative correlation coefficients of barium, chromium, titanium, vanadium, and zirconium for other metals in the group 2 correlation matrix also bear on their geochemistry (table 18). Previous studies of minor-element distributions established the zonation of 11 elements (Ag, Au, Bi, Co, Cu, Fe, Hg, Mo, Pb, Sr, and Zn) near the granodiorite of Copper Canyon, in the area sampled for the group 2 rocks (Theodore and Nash, 1973; Theodore and Blake, 1975). The overwhelming bulk of these metals was introduced during epigenetic metallization. Yet, in the group 2 correlation matrix, barium, chromium, titanium, vanadium, and zirconium have moderate negative correlation coefficients with seven elements (Ag, As, Au, Bi, Fe, Hg, and Mo). Copper shows either no correlation or a slight negative correlation with barium, chromium, and vanadium (table 18). These relations strongly suggest that barium, chromium, titanium, vanadium, and zirconium were not metasomatically introduced into the group 2 rocks during metallization. We infer, thus, from an evaluation of these geochemical data by correlation techniques, and from a comparison with typical abundances of elements in marine geosynclinal rocks elsewhere, that the differences detected between sample groups 1 and 2 in these elements most likely result from premetallization chemical differences.

TABLE 17.—*Array of numbers of paired-element analyses and Spearman correlation coefficients calculated from analytical determinations on 185 samples of sparsely mineralized rock of the Pumpernickel Formation (group 1, see text)*

[N.d., not determined, less than three paired analyses; *, coefficients numerically greater than ±0.50 and based on at least 50 paired-element analyses]

	Ag	As	Au	B	Ba	Bi	Co	Cr	Cu	Fe	Hg	Mg	Mo	Ni	Pb	Ti	V	Zr
Ag		0.65	0.85	−0.34	−0.19	N.d.	0.17	0.27	0.52*	0.52*	0.51*	0.14	N.d.	0.07	0.51*	0.11	0.26	0.06
As	14		.79	−.57	−.59	N.d.	N.d.	.28	.66	.81	.89	−.04	N.d.	−.33	.86	.13	.49	.21
Au	35	12		−.57*	−.38	N.d.	.32	.33	.57*	.67*	.68*	.06	N.d.	.00	.83	.11	.34	−.06
B	85	14	57		−.05	N.d.	.06	−.32	−.30	−.42	−.24	−.28	N.d.	−.25	−.38	−.34	−.37	−.27
Ba	85	14	57	183		N.d.	−.01	.51*	.29	.46	−.14	.57*	N.d.	.62*	−.36	.70*	.60	.64*
Bi	2		2	2	2		N.d.	N.d.	N.d.	N.d.	N.d.	N.d.	N.d.	N.d.	N.d.	N.d.	N.d.	N.d.
Co	22	1	13	44	44	0	0	.00	.22	−.12	.16	.10	N.d.	.12	−.12	−.22	.88	−.13
Cr	85	14	57	183	185	2	44		.61*	.67*	.32	.62*	N.d.	.70*	−.01	.71*	.77*	.59*
Cu	85	14	56	177	178	2	44	178		.57*	.29	.48	N.d.	.41	.23	.53*	.58*	.43
Fe	85	14	57	183	185	2	44	185	178		.35	.74*	N.d.	.63*	.40	.81*	.83*	.69*
Hg	83	14	57	173	175	2	43	175	169	175		.27	N.d.	.22	.30	.12	.20	.09
Mg	85	14	57	183	185	2	44	185	178	185	175		N.d.	.71*	.09	.09	.73*	.67*
Mo	2	1	1	2	2	0	0	2	2	2	2	2		N.d.	N.d.	N.d.	N.d.	N.d.
Ni	83	14	53	172	174	2	44	174	98	174	164	174	2		−.13	.67*	.70*	.54*
Pb	64	13	40	94	96	1	35	96	95	96	93	96	2	93		.01	.13	−.01
Ti	85	14	57	182	184	2	44	184	178	184	174	184	2	173	96		.88*	.90*
V	83	14	56	177	181	2	44	180	175	181	171	181	2	171	93	180		.78*
Zr	85	14	56	180	182	2	43	182	177	182	173	182	2	171	95	182	178	

Correlation coefficients

Numbers of pairs of elements

TABLE 18.—*Array of numbers of paired-element analyses and Spearman correlation coefficients calculated from analytical determinations on 211 rocks of the Pumpernickel Formation from around the west ore body (group 2, see text)*

[*, coefficients numerically greater than ±0.50 a nd based on at least 50 paired element analyses]

	Ag	As	Au	B	Ba	Bi	Co	Cr	Cu	Fe	Hg	Mg	Mo	Ni	Pb	Ti	V	Zr
Ag		0.64*	0.67*	−0.04	−0.32	0.66*	−0.03	−0.26	0.49	0.49	0.46	−0.50*	0.46	−0.30	0.50*	−0.29	−0.28	−0.24
As	88		.70*	−.04	−.11	.62*	.06	−.27	.31	.59*	.43	−.52*	.07	.05	.39	−.40	−.31	−.35
Au	168	86		−.03	−.34	.70*	.04	−.14	.50	.53*	.43	−.45	.21	−.12	.35	−.38	−.25	−.24
B	159	71	139		.01	−.06	.01	.19	−.03	.13	.01	−.02	.04	−.19	−.03	.13	.23	.03
Ba	200	88	173	169		−.26	.03	.26	−.14	−.20	−.37	.54*	−.23	.45	−.01	.59*	.51*	.39
Bi	87	63	84	68	87		.15	−.30	.38	.54*	.48	−.47	.07	−.10	.30	−.48	−.35	−.36
Co	83	35	62	67	90	34		.00	−.04	−.06	.26	.27	−.46	.18	−.17	.01	−.07	−.20
Cr	200	88	173	169	211	87	90		.02	−.02	−.15	.32	−.12	.19	−.03	.30	.60*	.09
Cu	199	88	173	169	210	87	89	210		.58*	.25	−.18	.09	−.06	.27	−.11	.07	−.07
Fe	200	88	173	169	211	87	90	211	210		.34	−.30	.14	−.06	.44	−.23	.00	−.19
Hg	172	74	150	141	180	75	79	180	179	180		−.39	.03	−.22	.19	−.27	−.28	−.23
Mg	196	84	169	167	207	83	86	207	206	207	176		−.28	.62*	−.10	.48	.46	.34
Mo	35	19	35	30	36	21	11	36	36	36	32	36		−.20	−.05	−.16	.04	.20
Ni	164	68	140	138	174	68	78	174	174	174	149	172	29		.05	−.33	.35	−.21
Pb	168	84	144	139	174	81	69	174	173	174	148	170	33	140		−.10	−.01	−.10
Ti	200	88	173	169	211	87	90	211	210	211	180	207	36	174	174		.61*	.73*
V	198	86	171	169	209	85	88	209	208	209	178	207	36	173	172	209		.31
Zr	200	88	173	169	211	87	90	211	210	211	180	207	36	173	209	211	209	

Numbers of pairs of elements

Correlation coefficients

BEHAVIOR OF BORON DURING METALLIZATION

The loss of boron during metallization suggested by figure 25 and table 16 merits detailed consideration. Figure 25 indicates marked differences in the boron content in the two data groups. In group 1, boron has a fairly symmetrical unimodal distribution with a slight negative skewness; its mode and median are in the 70-ppm class interval. In group 2, from the metallized rocks around the skarn, boron possibly has a multimodal distribution and a seeming positive skewness; one mode in this group is in the 30-ppm class interval, and the median is in the 20-ppm class interval.

Correlation studies suggest alternate interpretations of boron behavior during metallization at Copper Canyon. They show that boron varies independently of fluctuations in eight elements in the group 2 data set (Ag, As, Au, Bi, Cu, Hg, Mo, and Pb) as indicated by correlation coefficients close to zero (table 18). Further, in group 1, boron has a relatively high negative correlation coefficient (-0.57) for gold, and intermediate negative coefficients (-0.1 to -0.4) for most other metals associated typically with copper mineralization (table 17). The negative associations suggest depletion of boron, possibly accompanying some of the lead-zinc-silver vein mineralization dominant in areas near the group 1 samples.

On the other hand, there appears to be fairly good evidence for the introduction of boron locally into some rocks during pyritization and alteration. Boron concentrations greater than 70 ppm occur chiefly in pyritized rock belonging to the upper chert member of the Pumpernickel Formation (Theodore, 1969, fig. 6), and many of these rocks contain more than 2,000 ppm boron. This domain of high boron is restricted to about a 2-km^2 area just west of the granodiorite of Copper Canyon and west of the main Copper Canyon drainage. By way of comparison, most samples from the upper chert member of this formation that are unpyritized and very sparsely mineralized by a few veins contain 10–70 ppm boron. However, correlation studies for the domain of high boron showed boron (1) to be moderately correlated with bismuth, cobalt, and chromium, (2) to have negative associations for copper and arsenic, and (3) to vary independently of iron and gold concentrations. These data suggest that the behavior of boron is different in this 2-km^2 area from that of many other metals at Copper Canyon.

The correlation tests and abundance comparisons for boron do not provide an unequivocal answer regarding gains or losses of boron during mineralization. The abundance data could suggest that some boron was removed from the lower member of the Pumpernickel Formation, then redeposited in the upper member during hydrothermal alteration. However, this does not

correspond to any previously documented parageneses and occurrences (see Watanabe, 1967). Elsewhere, boron seems to be depleted during shallow- and deep-seated metamorphism of marine sediments (Ernst and others, 1958; Ernst and Lodeman, 1965). Near a pluton 120 km northwest of Copper Canyon, Wodzicki (1971) found sharp decreases of boron toward the pluton in its contact aureole. At Iron Canyon, about 3 km northeast of Copper Canyon, systematic geochemical studies of deep drill core through the Lower or Middle Cambrian Scott Canyon Formation yielded inconclusive data on changes in boron contents during pyritization there (Theodore and Roberts, 1971). Those studies did show, however, fairly direct variations of boron, generally ranging between 10 to 100 ppm, with barium, chromium, nickel and vanadium in unpyritized carbonaceous black shale.

GEOCHEMISTRY OF SOIL AROUND THE SKARN

Cursory studies were undertaken around the skarn to evaluate the usefulness of soil as a sampling medium in the geochemical prospecting for mineralized skarn. Along three traverses across the surface projection of the skarn (*X–X'*, *Y–Y'*, *Z–Z'*; pl. 1), 140 residual soil samples were collected about 6 m apart from the B soil horizon and analyzed for their minor metal content (tables 19–21). Chemical and spectrographic analyses were made either in mobile field laboratories or in the permanent analytical laboratories of the U.S. Geological Survey at Denver. Bulk soil samples approximately 3 kg in weight were collected from about 15 cm below the ground surface. They were sieved at the mobile field laboratory and the minus-80 mesh (Tyler standard sieve, 0.175-mm opening) fraction retained for analysis. These required no further treatment, and the coarse material was discarded. All element concentrations except those for arsenic, gold mercury, antimony, and zinc were determined by a spectrographic method (Grimes and Marranzino, 1968); those for the five elements were determined by atomic absorption methods (Ward and others, 1963; Vaughn and McCarthy, 1964; Thompson and others, 1968). Although the three sample traverses roughly parallel topographic contours (pl. 1), the surface geometry in the general area of the west ore body necessarily complicates the evaluation of these geochemical data. Topographic relief around the skarn is dominated by a westward-facing steep slope east of the south-flowing drainage through Copper Canyon. It is probable that material bearing some metals was eroded and leached from exposed metallized strands of the Virgin fault system and migrated westward across the buried west ore body. We do not believe, however, that downslope movement of surface soils has affected the soil profile to any great depth, because study of five samples collected at one locality from 15 to 150 cm below ground surface revealed no significant differences in element concentrations across the entire soil profile.

COLOR, MINERALOGY, AND pH OF FINE FRACTIONS

Color, mineralogy, and pH of the minus-80-mesh fractions of the residual soil samples are strikingly uniform. The pH is typically 9.0–9.6. Further, there is no color contrast between soil above ore in skarn and that on unmetallized parts of the Pumpernickel Formation 1,500 m north of the outer limit of pyrite introduction. Soil colors are derived principally from their fine fractions. Over the skarn, the minus-80-mesh soil fractions are drab shades of gray, orange, and brown. About 70 percent of them are yellowish gray (5Y7/2) (Goddard and others, 1948), 15 percent moderate yellowish brown (10YR5/4), 10 percent grayish orange (10YR7/4), and 5 percent light olive gray (5Y6/1). In addition, there is no systematic geographic variation of these colors along the three traverses. The dominant mineralogy of the fine soil fractions, as determined in 29 samples by X-ray, is quartz, plagioclase, chlorite, and white mica. Calcite was found in about one-third of the samples studied. No mineralogical difference was detected between soils developed above skarn and that developed on unmetallized parts of the Pumpernickel Formation.

VARIATION OF MINOR ELEMENTS IN SOIL ABOVE THE SKARN

From our data we infer that concentrations of most metals in soil above the skarn show little, if any, specific relation to underlying ore, perhaps reflecting the very restricted area we sampled and the depth to ore (tables 19–21; figs. 26–28). The low sensitivity of the spectrographic method for some metals and their low concentrations in the soil yielded few analyses above detection thresholds. Percentages of samples with detectable cadmium, molybdenum, niobium, tin, and tungsten range from 29 to 0 percent. Geochemical highs for six elements (Au, Bi, Cu, As, Sb, and Pb) near the west end of profile *Y–Y'* (fig. 27) most likely reflect the concentration of these metals in veins along north-striking faults there (pl. 1). In the general area of profile *Z–Z'*, our geochemical sampling did not extend far enough away from ore for us to establish changes in the minor-element content of soil.

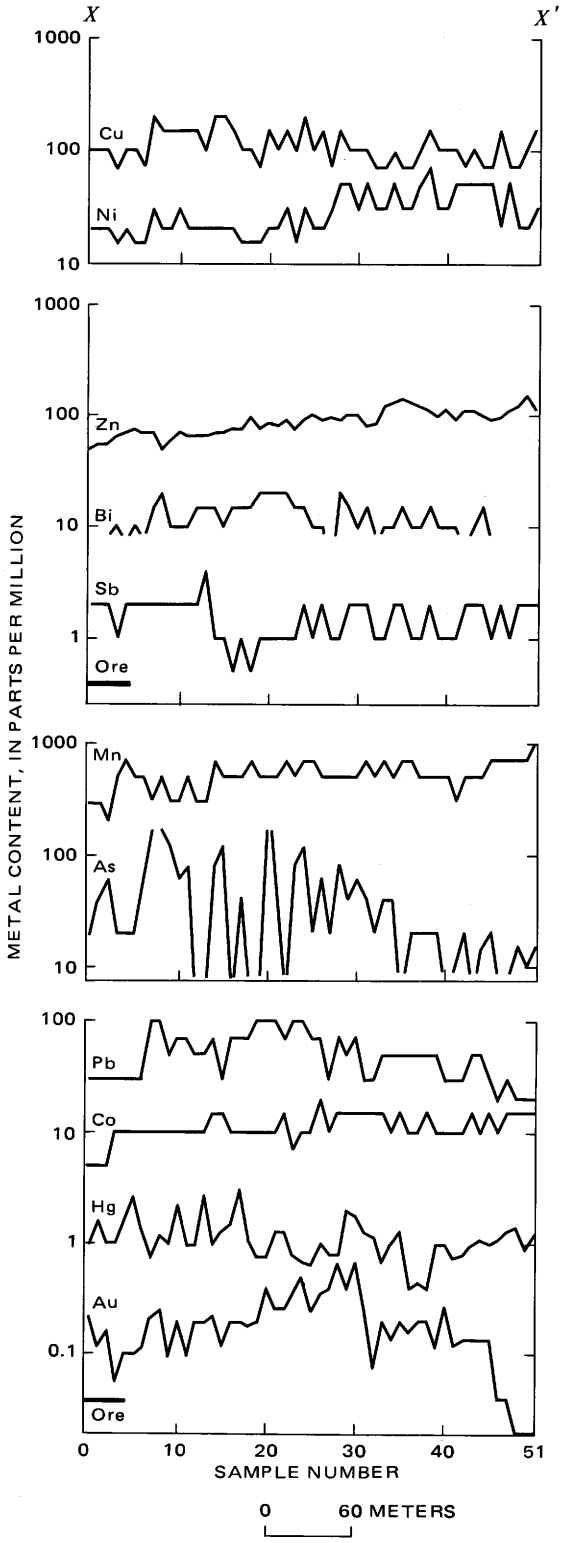

FIGURE 26.—Concentrations of 11 elements in soil along traverse X–X' (pl. 1). Lateral extent of horizontal projection of ore in underlying skarn is shown. Sample numbers taken from table 19.

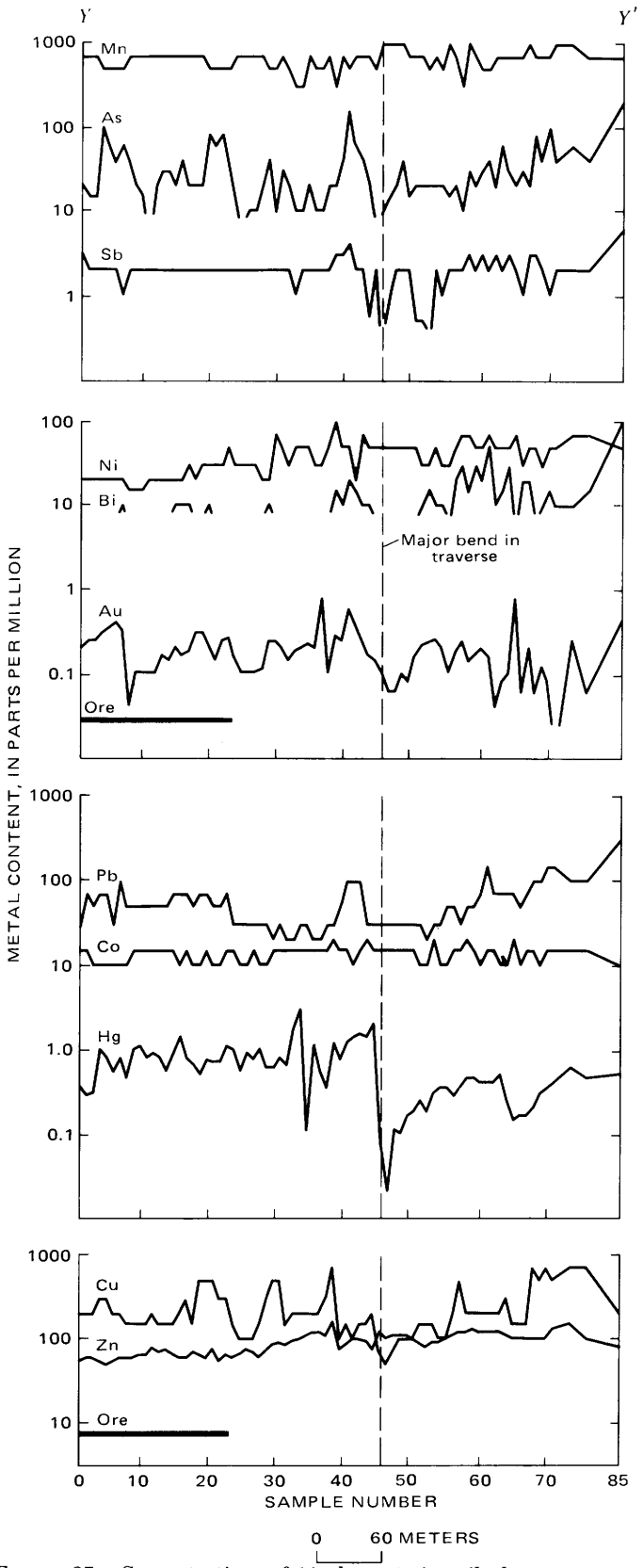

FIGURE 27.—Concentrations of 11 elements in soil along traverse Y–Y' (pl. 1). Lateral extent of horizontal projection of ore in underlying skarn is shown. Sample numbers taken from table 20.

TABLE 19.—*Analyses for minor metals in*

[—, not

	1	2	3	4	5	6	7	8	9	10	11	12
Lab. No.	BBK–001	BBK–002	BBK–003	BBK–004	BBK–005	BBK–006	BBK–007	BBK–008	BBK–009	BBK–010	BBK–011	BBK–012
Field No.	70–9	70–10	70–11	70–12	70–13	70–14	70–15	70–16	70–17	70–18	70–19	70–20
Semiquantitative spectrographic analyses (weight percent)[1]												
Ag	0.0001	0.00015	0.0002	0.0001	0.0003	0.0002	0.00015	0.0005	0.001	0.0002	0.0005	0.0003
As	—	—	—	—	—	—	—	—	.02	—	—	—
B	.005	.005	.005	.005	.003	.005	.003	.005	.007	.005	.005	.005
Ba	.05	.05	.05	.05	.05	.05	.03	.07	.07	.07	.07	.07
Be	.0001	.0001	.0001	.00015	.0001	.0001	.0001	.0001	.0001	.0001	.0001	.0001
Bi	<.001	<.001	<.001	.001	<.001	.001	<.001	.0015	.002	.001	.001	.001
Ca	1	.7	1.5	.7	.7	.7	.7	1	1.5	2	.7	.7
Co	.0005	.0005	.0005	.001	.001	.001	.001	.001	.001	.001	.001	.001
Cr	.007	.01	.01	.005	.007	.007	.007	.015	.01	.01	.01	.007
Cu	.01	.01	.01	.007	.01	.01	.007	.02	.015	.015	.015	.015
Fe	3	3	3	3	3	3	3	5	3	5	5	3
La	.002	.002	.002	<.002	.002	.002	<.002	.003	.003	.003	.002	.003
Mg	1	1	1	1	1	1.5	1	1	1	1	1	1
Mn	.03	.03	.02	.05	.07	.05	.05	.03	.05	.03	.03	.05
Nb	—	—	—	—	—	—	—	—	—	—	—	—
Ni	.002	.002	.002	.0015	.002	.0015	.0015	.003	.002	.002	.003	.002
Pb	.003	.003	.003	.003	.003	.003	.003	.01	.01	.005	.007	.007
Sc	.001	.001	.001	.001	.0015	.0015	.001	.0015	.001	.0015	.0015	.001
Sn	—	—	—	—	—	—	—	.001	.001	—	—	—
Sr	.02	.02	.03	.02	.02	.02	.015	.02	.03	.03	.02	.02
Ti	.3	.3	.5	.3	.3	.3	.3	.5	.5	.3	.3	.3
V	.01	.01	.01	.01	.01	.01	.01	.01	.01	.01	.01	.01
Y	.0015	.0015	.002	.0015	.002	.0015	.0015	.0015	.002	.002	.0015	.002
Zn	—	—	—	—	—	—	—	—	—	—	—	—
Zr	.015	.02	.02	.02	.02	.02	.02	.02	.03	.02	.015	.02
Chemical analyses (parts per million)[2]												
As	20	40	60	20	20	20	60	>160	>160	120	60	80
Au	.22	.12	.16	.06	.10	.10	.12	.22	.26	.10	.20	.10
Hg	1.0	1.6	1.0	1.0	1.6	2.6	1.3	.75	1.2	1.0	2.2	1.0
Sb	2	2	2	1	2	2	2	2	2	2	2	2
Zn	50	55	55	65	70	75	70	70	50	60	70	65

	27	28	29	30	31	32	33	34	35	36	37	38
Lab. No.	BBK–027	BBK–028	BBK–029	BBK–030	BBK–031	BBK–032	BBK–033	BBK–034	BBK–035	BBK–036	BBK–037	BBK–038
Field No.	70–35	70–36	70–37	70–38	70–39	70–40	70–41	70–42	70–43	70–44	70–45	70–46
Semiquantitative spectrographic analyses (weight percent)												
Ag	0.0003	0.0001	0.0007	0.0003	0.0005	0.0003	0.0002	0.0003	0.0005	0.0005	0.0005	0.0007
As	—	—	—	—	—	—	—	—	—	—	—	—
B	.005	.005	.005	.007	.005	.003	.003	.005	.005	.005	.003	.005
Ba	.05	.05	.07	.07	.07	.07	.07	.07	.07	.07	.07	.07
Be	.0001	.00015	.00015	.0001	.0001	.0001	.0001	.0001	.0001	.0001	.0001	.0001
Bi	.001	—	.002	.0015	.001	.0015	<.001	.001	.001	.0015	.001	.001
Ca	.7	.7	1.5	1.5	.7	.7	.7	.7	.7	1	1.5	.7
Co	.002	.001	.0015	.0015	.0015	.0015	.0015	.0015	.001	.0015	.001	.001
Cr	.01	.007	.015	.01	.01	.01	.007	.007	.007	.01	.007	.01
Cu	.015	.007	.015	.01	.01	.01	.007	.007	.01	.007	.007	.01
Fe	3	3	5	3	3	3	3	5	3	3	3	3
La	.002	.002	.003	.002	.002	.002	.002	.002	.003	.003	.003	.003
Mg	1	1	1.5	1	1	1	1	1	1	1	1	1
Mn	.05	.05	.05	.05	.05	.07	.05	.07	.05	.07	.07	.05
Nb	—	—	—	—	—	—	—	—	.001	—	—	—
Ni	.002	.003	.005	.005	.003	.005	.003	.003	.005	.003	.003	.005
Pb	.007	.003	.007	.005	.007	.003	.003	.005	.005	.005	.005	.005
Sc	.001	.001	.0015	.001	.001	.001	.001	.001	.001	.001	.001	.0015
Sn	—	—	—	—	—	—	—	—	—	—	—	—
Sr	.02	.02	.02	.03	.015	.02	.02	.03	.03	.03	.03	.03
Ti	.3	.3	.5	.3	.3	.3	.3	.5	.3	.3	.3	.3
V	.01	.01	.015	.01	.01	.01	.01	.015	.01	.01	.01	.01
Y	.002	.002	.003	.002	.0015	.002	.0015	.0015	.002	.0015	.0015	.0015
Zn	—	—	—	—	—	—	—	—	—	—	—	—
Zr	.02	.02	.02	.015	.015	.015	.015	.02	.02	.015	.015	.015
Chemical analyses (parts per million)												
As	60	20	80	40	60	40	20	40	40	<10	20	20
Au	.36	.40	.66	.40	.66	.26	.08	.20	.14	.20	.16	.20
Hg	1.0	.80	.80	2.0	1.8	1.3	1.2	.7	1.0	1.3	.4	.45
Sb	2	1	1	2	2	2	1	1	2	2	1	1
Zn	90	95	90	100	100	80	85	120	130	140	130	120

[1]Spectrographic analyses by D. Siems. Results are reported to the nearest number in the series 1, 0.7, 0.5, 0.3, 0.2, 0.15, 0.1, 0.07, and so on, which represent approximate midpoints of interval data on a geometric scale. The precision of a reported value is approximately plus or minus one series interval at 68 percent confidence, or two intervals at 95 percent confidence.

[2]Chemical analyses by J.G. Frisken, J.D. Hoffman, R.M. O'Leary, and L.A. Vinnola.

samples of soil from traverse X–X' of plate 1
detected]

13	14	15	16	17	18	19	20	21	22	23	24	25	26
BBK–013 70–21	BBK–014 70–22	BBK–015 70–23	BBK–016 70–24	BBK–017 70–25	BBK–018 70–26	BBK–019 70–27	BBK–020 70–28	BBK–021 70–29	BBK–022 70–30	BBK–023 70–31	BBK–024 70–32	BBK–025 70–33	BBK–026 70–34
Semiquantitative spectrographic analyses (weight percent)[1]													
0.0003	0.0002	0.0003	0.00015	0.0005	0.0005	0.0003	0.0007	0.001	0.0005	0.001	0.0005	0.0005	0.0002
—	—	—	—	—	—	—	—	—	—	—	—	—	—
.005	.005	.005	.005	.003	.007	.005	.005	.007	.005	.005	.005	.007	.007
.07	.07	.07	.05	.05	.07	.07	.07	.07	.07	.07	.07	.07	.05
.0001	.0001	.00015	.0001	.0001	.0001	.0001	.0001	.0001	.0001	.0001	.0001	.00015	.00015
.0015	.0015	.0015	.001	.0015	.0015	.0015	.002	.002	.002	.002	.0015	.0015	.001
1	1	.7	.5	1	1	.7	.7	.7	.7	2	1	1	1
.001	.001	.0015	.0015	.001	.001	.001	.001	.001	.001	.0015	.0007	.001	.001
.01	.01	.007	.015	.01	.005	.005	.01	.015	.01	.007	.01	.015	.007
.015	.01	.02	.02	.015	.01	.01	.007	.015	.01	.015	.01	.02	.01
3	3	3	5	5	3	3	3	5	3	3	2	5	3
.003	.002	.002	.005	.003	.002	<.002	.002	.003	.003	.003	.002	.003	.002
.7	.7	1	1	1	1	1	1	1	1	1	1	1.5	1.5
.03	.03	.07	.05	.05	.05	.07	.05	.05	.05	.07	.05	.07	.07
—	—	—	—	—	—	—	—	—	—	—	—	—	—
.002	.002	.002	.002	.002	.0015	.0015	.0015	.002	.002	.003	.0015	.003	.002
.005	.005	.007	.003	.007	.007	.007	.01	.01	.01	.007	.01	.01	.007
.001	.001	.001	.0015	.001	.001	.001	.001	.0015	.001	.001	.001	.0015	.001
—	—	—	—	—	<.001	—	.001	<.001	<.001	.001	—	<.001	—
.02	.03	.03	.015	.03	.03	.02	.02	.03	.03	.03	.03	.03	.03
.3	.3	.3	.3	.3	.3	.3	.3	.3	.3	.3	.5	.5	.5
.01	.01	.01	.01	.01	.01	.01	.01	.01	.01	.01	.01	.015	.01
.002	.0015	.002	.002	.002	.0015	.0015	.0015	.002	.002	.002	.0015	.003	.002
—	—	—	—	—	—	—	—	—	—	—	—	—	—
.02	.02	.02	.02	.03	.015	.015	.015	.02	.015	.015	.02	.02	.015
Chemical analyses (parts per million)[2]													
<10	<10	80	120	<10	40	<10	<10	>160	60	<10	80	120	20
.20	.20	.22	.12	.20	.20	.18	.20	.40	.26	.26	.36	.50	.26
1.0	2.8	1.0	1.3	1.5	3.0	1.1	.75	.75	1.3	1.3	.80	.70	.65
2	4	1	1	0.5	1	0.5	1	1	1	1	1	2	1
65	65	70	70	75	75	95	75	85	80	90	75	90	100

39	40	41	42	43	44	45	46	47	48	49	50	51
BBK–039 70–47	BBK–040 70–48	BBK–041 70–49	BBK–042 70–50	BBK–043 70–51	BBK–044 70–52	BBK–045 70–53	BBK–046 70–54	BBK–047 70–55	BBK–048 70–56	BBK–049 70–57	BBK–050 70–58	BBK–051 70–59
Semiquantitative spectrographic analyses (weight percent)												
0.0005	0.0003	0.0005	0.0003	0.0003	0.0003	0.00015	0.00005	—	<0.00005	—	<0.00005	—
—	—	—	—	—	—	—	—	—	—	—	—	—
.005	.003	.003	.003	.003	.005	.005	.005	.005	.007	.007	.005	.007
.07	.07	.07	.07	.07	.07	.07	.07	.07	.05	.05	.07	.07
.00015	.0001	.0001	.0001	.0001	.00015	.0001	.00015	.0001	.0001	.0001	.0001	.0001
.0015	.001	.001	.001	<.001	.001	.0015	<.001	—	—	—	—	—
.7	.7	.7	.7	.7	.7	.7	1	2	1.5	1.5	1.5	2
.0015	.001	.001	.001	.001	.0015	.001	.0015	.001	.0015	.0015	.0015	.0015
.01	.007	.01	.015	.01	.01	.01	.015	.007	.01	.007	.015	.015
.015	.01	.01	.01	.007	.01	.007	.007	.015	.007	.007	.01	.015
3	3	3	3	3	3	3	5	3	3	3	3	5
.003	.003	.003	.003	.003	.005	.003	.005	.003	.003	.002	.002	.003
1	1	1	1	1	1	1	1	2	2	2	2	2
.05	.05	.05	.03	.05	.05	.05	.07	.07	.07	.07	.07	.1
—	—	—	—	—	—	—	—	.001	—	.001	.001	.001
.007	.003	.003	.005	.005	.005	.005	.005	.002	.005	.002	.002	.003
.005	.005	.003	.003	.003	.005	.005	.003	.002	.003	.002	.002	.002
.0015	.001	.001	.0015	.001	.001	.001	.0015	.001	.001	.001	.001	.0015
—	—	—	—	—	—	—	—	—	—	—	—	—
.03	.03	.02	.03	.015	.02	.02	.03	.02	.03	.03	.02	.05
.5	.3	.3	.5	.3	.3	.5	.5	.5	.5	.3	.5	.5
.015	.01	.01	.015	.01	.015	.01	.015	.01	.01	.01	.01	.01
.002	.002	.002	.003	.002	.002	.002	.003	.002	.002	.002	.002	.003
—	—	—	—	—	—	—	—	—	<.02	<.02	<.02	—
.02	.02	.015	.015	.015	.015	.02	.02	.03	.03	.015	.02	.03
Chemical analyses (parts per million)												
20	20	<10	10	20	<10	15	20	<10	<10	15	10	15
.20	.12	.28	.12	.14	.14	.14	.14	.04	.04	.02	.02	.02
.40	1.0	1.0	.75	.8	1.0	1.1	1.0	1.1	1.3	1.4	.9	1.2
2	1	1	1	2	2	2	1	2	1	2	2	2
110	95	110	90	110	110	100	90	95	110	120	150	110

TABLE 20.—*Analyses for minor metals in*

[—, not

	1	2	3	4	5	6	7	8	9	10	11	12
Lab. No.	BBK–074	BBK–073	BBK–072	BBK–071	BBK–070	BBK–069	BBK–068	BBK–067	BBK–066	BBK–065	BBK–064	BBK–063
Field No.	70–82	70–81	70–80	70–79	70–78	70–77	70–76	70–75	70–74	70–73	70–72	70–71
Semiquantitative spectrographic analyses (weight percent)[1]												
Ag	0.0003	0.0003	0.0003	0.0003	0.0003	0.00015	0.0002	0.0002	0.0001	0.0001	0.0001	0.0001
As	—	—	—	—	—	—	—	—	—	—	—	—
B	.005	.005	.005	.005	.005	.005	.007	.005	.005	.005	.007	.007
Ba	.07	.07	.07	.07	.07	.07	.07	.07	.07	.05	.05	.05
Be	.00015	.00015	.0001	.00015	.00015	.0001	.0001	.0001	.0001	.0001	.0001	.00015
Bi	<.001	<.001	<.001	.001	<.001	<.001	.001	.001	.001	—	—	—
Ca	1	1	1	1.5	1.5	.7	1	1	.7	.7	1	1
Co	.0015	.001	.001	.0015	.001	.001	.0015	.001	.0015	.0015	.0015	.0015
Cr	.015	.015	.015	.015	.015	.01	.015	.01	.01	.01	.01	.01
Cu	.03	.03	.05	.05	.05	.015	.03	.02	.015	.015	.015	.02
Fe	5	5	5	5	5	5	7	5	5	5	5	7
La	.003	.003	.002	.003	.003	.003	.003	.003	.002	.003	.003	.003
Mg	1.5	1.5	1.5	1.5	2	1	1.5	1.5	1	1	1.5	1.5
Mn	.05	.05	.05	.05	.07	.07	.07	.07	.07	.07	.07	.07
Nb	.001	—	—	—	—	—	.001	—	—	—	.001	—
Ni	.005	.003	.003	.003	.003	.002	.003	.002	.002	.002	.002	.002
Pb	.007	.005	.005	.007	.007	.005	.007	.007	.007	.005	.005	.005
Sc	.0015	.0015	.0015	.0015	.0015	.0015	.0015	.0015	.0015	.0015	.0015	.0015
Sn	<.001	<.001	<.001	<.001	<.001	<.001	<.001	—	—	—	—	—
Sr	.03	.03	.03	.03	.03	.03	.03	.03	.03	.03	.03	.05
Ti	.5	.5	.5	.5	.7	.3	.5	.3	.3	.3	.3	.3
V	.015	.01	.01	.015	.015	.01	.015	.015	.01	.01	.01	.01
Y	.002	.0015	.002	.002	.002	.002	.003	.002	.0015	.002	.002	.002
Zn	—	—	—	—	—	—	—	—	—	—	—	—
Zr	.02	.02	.02	.03	.03	.02	.02	.02	.02	.02	.02	.02
Chemical analyses (parts per million)[2]												
As	30	80	60	80	20	20	20	40	20	30	30	20
Au	.26	.24	.14	.2	.3	.3	.18	.16	.2	.14	.16	0.1
Hg	1.1	.7	.7	.75	.5	.65	.75	1.4	.9	.55	.8	.9
Sb	2	2	2	2	2	2	2	2	2	2	2	2
Zn	65	55	75	60	65	70	60	60	65	75	70	80

	26	27	28	29	30	31	32	33	34	35	36	37
Lab No.	BBK–077	BBK–078	BBK–079	BBK–080	BBK–081	BBK–082	BBK–083	BBK–084	BBK–085	BBK–086	BBK–087	BBK–088
Field No.	70–85	70–86	70–87	70–88	70–89	70–90	70–91	70–92	70–93	70–94	70–95	70–96
Semiquantitative spectrographic analyses (weight percent)												
Ag	0.0002	0.0001	0.0001	0.0002	0.0002	0.0002	0.0001	0.0002	0.0002	0.00007	0.0001	0.0001
As	—	—	—	—	—	—	—	—	—	—	—	—
B	.005	.005	.005	.007	.005	.005	.005	.003	.005	.005	.005	.005
Ba	.05	.07	.07	.07	.1	.07	.05	.07	.07	.07	.07	.07
Be	.00015	.0001	.00015	.00015	.00015	.00015	.0001	.0001	.00015	.00015	.00015	.0001
Bi	—	—	—	.001	—	<.001	—	—	—	—	—	—
Ca	1	1	1.5	.7	1	.7	.7	.7	1	1	1	.7
Co	.001	.0015	.001	.001	.0015	.0015	.0015	.0015	.0015	.0015	.0015	.0015
Cr	.007	.01	.01	.015	.015	.015	.01	.01	.01	.015	.007	.015
Cu	.01	.01	.015	.03	.05	.05	.015	.02	.02	.02	.02	.02
Fe	5	5	5	7	7	7	5	3	5	5	5	5
La	.003	.002	.003	.005	.005	.005	.002	.002	.003	.003	.003	.003
Mg	1	1	1	1.5	1.5	1.5	1	1	1	1.5	1.5	1.5
Mn	.07	.07	.07	.05	.05	.07	.05	.03	.03	.07	.05	.05
Nb	.001	.001	<.001	.001	.001	.0015	—	—	—	—	—	—
Ni	.003	.003	.002	.002	.007	.005	.003	.005	.005	.005	.003	.003
Pb	.003	.003	.003	.003	.002	.003	.002	.002	.003	.003	.002	.002
Sc	.0015	.001	.001	.0015	.0015	.0015	.001	.001	.001	.001	.001	.001
Sn	—	—	—	—	—	—	—	—	—	—	—	—
Sr	.03	.03	.03	.02	.02	.02	.02	.015	.02	.03	.02	.015
Ti	.3	.5	.3	.5	.5	.5	.3	.3	.3	.5	.3	.3
V	.015	.01	.01	.015	.015	.015	.01	.01	.01	.01	.01	.01
Y	.0015	.0015	.0015	.003	.003	.003	.0015	.002	.002	.002	.002	.002
Zn	—	—	—	—	—	—	—	—	<.02	<.02	<.02	<.02
Zr	.02	.015	.02	.015	.02	.03	.02	.02	.02	.02	.02	.02
Chemical analyses (parts per million)												
As	10	10	20	40	10	30	20	10	10	20	10	10
Au	.1	.1	.11	.24	.24	.2	.14	.18	.2	.22	.2	.78
Hg	.9	.75	1.0	.6	.6	.8	.65	1.8	3.0	.11	1.1	.55
Sb	2	2	2	2	2	2	2	1	2	2	2	2
Zn	75	70	60	70	85	90	85	95	100	110	120	120

samples of soil from traverse Y–Y′ of plate 1

detected]

13	14	15	16	17	18	19	20	21	22	23	24	25
BBK–062 70–70	BBK–061 70–69	BBK–060 70–68	BBK–059 70–67	BBK–058 70–66	BBK–057 70–65	BBK–056 70–64	BBK–055 70–63	BBK–054 70–62	BBK–053 70–61	BBK–052 70–60	BBK–075 70–83	BBK–076 70–84
Semiquantitative spectrographic analyses (weight percent)												
0.0001	0.0001	0.00015	0.0001	0.0002	0.00015	0.0007	0.0005	0.0005	0.0005	0.0002	0.00015	0.0002
—	—	—	—	—	—	—	—	—	—	—	—	—
.007	.007	.005	.007	.005	.005	.005	.005	.005	.007	.005	.005	.005
.07	.05	.05	.05	.07	.07	.07	.07	.07	.05	.07	.05	.07
.0001	.0001	.0001	.0001	.0001	.0001	.0001	.00015	.0001	.0001	.0001	.00015	.00015
—	—	<.001	<.001	.001	<.001	—	—	—	—	—	—	—
.7	.7	.7	.7	.7	.7	2	.7	1	1.5	3	.7	1
.0015	.0015	.0015	.001	.001	.001	.001	.001	.001	.0015	.0015	.0015	.001
.01	.007	.01	.007	.015	.015	.015	.015	.015	.015	.01	.01	.007
.015	.015	.015	.015	.02	.02	.03	.03	.02	.02	.02	.015	.01
5	5	5	5	5	7	5	5	5	5	5	5	5
.003	.003	.003	.003	.003	.005	.003	.005	.003	.005	.003	.002	.003
1.5	1.5	1	1	1	1.5	1	1	1	1	1.5	1	1
.07	.07	.07	.07	.05	.05	.05	.05	.07	.07	.07	.07	.07
.001	—	—	.001	.001	—	—	—	.001	.001	—	.001	.001
.002	.0015	.0015	.0015	.002	.002	.002	.002	.002	.002	.002	.003	.003
.005	.005	.005	.005	.01	.003	.007	.007	.005	.007	.003	.003	.003
.0015	.0015	.0015	.0015	.0015	.0015	.0015	.0015	.0015	.0015	.0015	.0015	.001
—	—	—	<.001	<.001	—	—	—	—	—	—	—	—
.05	.05	.03	.03	.03	.03	.05	.03	.03	.03	.05	.03	.03
.5	.3	.3	.3	.3	.5	.3	.3	.3	.3	.5	.5	.5
.015	.01	.01	.01	.01	.01	.01	.01	.01	.01	.01	.01	.01
.002	.002	.002	.002	.002	.002	.003	.002	.002	.002	.002	.0015	.0015
—	—	—	—	—	—	—	—	—	—	—	—	—
.02	.02	.02	.02	.03	.02	.03	.015	.03	.02	.03	.02	.02
Chemical analyses (parts per million)												
—	15	20	40	60	40	60	100	15	15	20	10	<10
0.1	0.1	0.1	.04	.32	.4	.34	.3	.24	.24	.2	.14	.1
.8	1.1	1.0	.45	.8	.55	.8	1.0	.3	.28	.35	1.0	.55
2	2	2	2	1	2	2	2	2	2	3	2	2
65	65	60	60	60	55	50	55	60	60	55	60	65

38	39	40	41	42	43	44	45	46	47	48	49	50
BBK–089 70–97	BBK–090 70–98	BBK–091 70–99	BBK–092 70–100	BBK–093 70–101	BBK–094 70–102	BBK–095 70–103	BBK–096 70–104	BBK–097 70–105	BBK–098 70–106	BBK–099 70–107	BBK–100 70–108	BBK–101 70–109
Semiquantitative spectrogrphic analyses (weight percent)												
0.0001	0.0003	0.0002	0.0007	0.0005	0.0007	0.0005	0.0003	0.0003	0.0002	0.0002	0.0003	0.0002
—	—	—	—	—	—	—	—	—	—	—	—	—
.005	.005	.005	.005	.007	.007	.007	.007	.005	.005	.005	.005	.005
.07	.07	.07	.07	.07	.07	.07	.07	.05	.05	.05	.07	.05
.0001	.0002	.0001	.0001	.0001	.00015	.00015	.00015	.00015	.00015	.0001	.00015	.00015
—	.0015	.001	.002	.0015	.001	.001	—	—	—	—	—	—
.7	.7	1	1.5	1	1	1.5	.7	1.5	2	2	2	1
.0015	.002	.0015	.0015	.001	.0015	.002	.0015	.0015	.0015	.0015	.0015	.0015
.01	.02	.015	.015	.01	.015	.007	.01	.01	.01	.015	.015	.015
.03	.07	.01	.015	.01	.015	.015	.02	.007	.005	.007	.01	.01
5	7	7	7	5	7	5	5	3	5	5	5	5
.002	.005	.005	.005	.002	.003	.002	.003	.002	.003	.003	.003	.003
1.5	1.5	1	1	1.5	1.5	1.5	1.5	1.5	1.5	1.5	1.5	1
.07	.03	.07	.05	.07	.07	.07	.05	.1	.1	.1	.1	.07
—	—	.001	.001	—	<.001	—	—	—	—	—	—	.001
.005	.01	.005	.005	.002	.007	.005	.005	.005	.005	.005	.005	.005
.003	.003	.005	.01	.01	.01	.003	.003	.003	.003	.003	.003	.003
.001	.0015	.0015	.0015	.0015	.002	.0015	.0015	.001	.001	.001	.001	.001
—	—	—	<.001	<.001	—	—	—	—	—	—	—	—
.02	.02	.03	.03	.03	.03	.03	.03	.05	.05	.05	.05	.03
.5	.3	.5	.5	.5	.5	.3	.3	.5	.5	.5	.5	.5
.01	.015	.015	.015	.01	.015	.01	.01	.01	.015	.01	.015	.015
.002	.003	.002	.002	.002	.005	.002	.002	.002	.002	.002	.003	.002
—	—	—	—	<.02	—	—	—	—	—	—	—	—
.03	.015	.03	.02	.02	.03	.02	.02	.02	.02	.015	.02	.015
Chemical analyses (parts per million)												
20	20	40	160	60	40	20	<10	10	15	20	40	15
.1	.28	.24	.56	.36	.24	.16	.14	0.1	.06	.06	0.1	.08
.35	1.2	.75	1.2	1.4	1.5	1.4	2.0	.08	.02	.11	.10	.16
2	3	3	4	2	2	0.5	2	<.5	1	2	2	2
110	160	75	85	100	100	95	75	120	100	110	110	110

TABLE 20.—*Analyses for minor metals in samples*

	51	52	53	54	55	56	57	58	59	60	61	62
Lab No.	BBK–102	BBK–103	BBK–104	BBK–105	BBK–106	BBK–107	BBK–108	BBK–109	BBK–110	BBK–111	BBK–112	BBK–113
Field No.	70–110	70–111	70–112	70–113	70–114	70–115	70–116	70–117	70–118	70–119	70–120	70–121
Semiquantitative spectrographic analyses (weight percent)												
Ag	0.0002	0.0005	0.0005	0.0002	0.00015	0.0002	0.0005	0.001	0.0005	0.0007	0.0007	0.001
As	—	—	—	—	—	—	—	—	—	—	—	—
B	.005	.003	.005	.005	.005	.005	.005	.007	.005	.005	.005	.007
Ba	.05	.03	.03	.03	.03	.05	.05	.05	.03	.05	.05	.07
Be	.0001	.0001	.0001	.00015	.0001	.00015	.00015	.00015	.0001	.0001	.00015	.0001
Bi	—	.001	.0015	.001	.001	<.001	.002	.003	.0015	.003	.002	.005
Ca	1	1.5	.7	1	.7	.7	1	.7	.7	.7	1	.7
Co	.0015	.001	.001	.002	.001	.001	.0015	.0015	.002	.0015	.001	.0015
Cr	.015	.01	.015	.015	.01	.01	.01	.015	.015	.01	.015	.015
Cu	.01	.015	.015	.015	.01	.01	.02	.05	.02	.02	.02	.02
Fe	5	3	5	5	3	5	5	5	7	7	5	5
La	.003	.002	.002	.003	.002	.003	.003	.003	.002	.002	.002	.005
Mg	1	1.5	1	1	1	1	1	1.5	1	1	1	1
Mn	.07	.07	.05	.07	.05	.1	.07	.03	.1	.07	.05	.05
Nb	<.001	.001	.001	.001	—	—	—	—	—	—	—	—
Ni	.005	.003	.003	.005	.003	.003	.005	.007	.007	.005	.005	.007
Pb	.003	.003	.002	.003	.003	.005	.005	.003	.005	.005	.007	.015
Sc	.001	.001	.001	.001	.001	.001	.001	.0015	.0015	.0015	.0015	.002
Sn	—	<.001	—	<.001	—	<.001	.001	.001	.001	.001	.001	.001
Sr	.03	.03	.03	.03	.02	.03	.03	.015	.02	.02	.02	.03
Ti	.5	.3	.3	.5	.3	.3	.3	.5	.3	.3	.5	.5
V	.015	.01	.01	.015	.01	.01	.01	.015	.015	.015	.01	.015
Y	.002	.002	.002	.002	.002	.0015	.002	.003	.002	.002	.002	.003
Zn	—	—	—	—	—	—	—	—	—	—	—	—
Zr	.02	.015	.02	.02	.02	.015	.02	.02	.02	.02	.02	.03
Chemical analyses (parts per million)												
As	20	20	20	20	20	15	20	10	30	20	30	40
Au	.16	.22	.24	.26	0.2	0.1	.18	.24	.14	.16	.2	.16
Hg	.18	.24	.18	.3	.35	.35	.28	.35	.45	.45	.4	.4
Sb	.5	.5	<.5	2	1	2	2	2	3	2	3	2
Zn	100	90	80	90	90	100	110	120	120	130	120	120

TABLE 21.—*Analyses for minor metals in samples of soil from traverse Z–Z′ of plate 1*

[—, not detected]

	1	2	3	4	5	6	7	8	9	10
Lab No.	BBK–136	BBK–135	BBK–134	BBK–133	BBK–132	BBK–131	BBK–127	BBK–128	BBK–129	BBK–130
Field No.	70–144	70–143	70–142	70–141	70–140	70–139	70–135	70–136	70–137	70–138
Semiquantitative spectrographic analyses (weight percent)[1]										
Ag	0.0001	0.0001	0.0003	0.00005	0.00015	0.0001	0.0003	0.0002	0.0002	0.0002
As	—	—	—	—	—	—	—	—	—	—
B	.005	.005	.007	.007	.007	.007	.007	.007	.007	.007
Ba	.07	.07	.07	.07	.05	.07	.07	.07	.07	.07
Be	.00015	.00015	.00015	.00015	.00015	.00015	.00015	.00015	.00015	.00015
Bi	<.001	.001	.001	—	—	—	—	.001	—	—
Ca	1	1.5	1.5	1	1	1	.7	1	1	1.5
Co	.0015	.0015	.0015	.0015	.0015	.0015	.0015	.0015	.0015	.0015
Cr	.015	.015	.015	.015	.015	.015	.02	.02	.015	.02
Cu	.015	.015	.02	.015	.015	.015	.02	.02	.015	.02
Fe	5	5	5	5	5	5	7	7	5	7
La	.003	.005	.003	.003	.003	.003	.002	.003	.005	.005
Mg	1	1.5	1.5	1.5	1	1	1.5	2	1.5	2
Mn	.1	.1	.1	.1	.1	.1	.05	.1	.1	.1
Nb	<.001	<.001	.001	.0015	.001	.001	<.001	.001	.001	.001
Ni	.003	.003	.005	.005	.005	.005	.005	.005	.005	.007
Pb	.007	.01	.01	.005	.005	.005	.003	.01	.007	.005
Sc	.0015	.0015	.002	.002	.002	.002	.002	.002	.002	.003
Sn	—	—	—	—	—	—	—	—	—	—
Sr	.03	.05	.05	.03	.03	.03	.02	.03	.03	.03
Ti	.5	.5	.7	.5	.5	.5	.5	.7	.7	.7
V	.015	.015	.02	.015	.015	.02	.02	.015	.015	.02
Y	.002	.002	.002	.002	.002	.002	.003	.002	.002	.003
Zn	—	—	—	—	—	—	—	—	—	—
Zr	.02	.02	.02	.02	.03	.02	.02	.02	.03	.02
Atomic absorption analyses (parts per million)[2]										
As	40	10	20	10	15	10	20	60	10	10
Au	.04	.04	.1	.04	.04	.16	.1	.22	.06	.1
Hg	.08	.1	.16	.3	.35	.3	.45	.40	.40	.40
Sb	1	1	3	2	3	3	3	3	3	2
Zn	80	80	80	80	80	80	90	80	80	80

[1]Spectrographic analyses by D. Siems. Results are reported to the nearest number in the series 1, 0.7, 0.5, 0.3, 0.2, 0.15, 0.1, 0.07, and so on, which represent approximate midpoints of interval data on a geometric scale. The precision of a reported value is approximately plus or minus one series interval at 68 percent confidence, or two intervals at 95 percent confidence.

[2]Chemical analyses by J.G. Frisken, J.D. Hoffman, R.M. O'Leary, and L.A. Vinnola.

of soil from traverseY–Y′ of plate 1—Continued

63	64	65	66	67	68	69	70	71	72	73	74	75
BBK–114 70–122	BBK–115 70–123	BBK–116 70–124	BBK–117 70–125	BBK–118 70–126	BBK–119 70–127	BBK–120 70–128	BBK–121 70–129	BBK–122 70–130	BBK–123 70–131	BBK–124 70–132	BBK–125 70–133	BBK–126 70–134
Semiquantitative spectrographic analyses (weight percent)—												
0.0005	0.0005	0.0005	0.0005	0.0003	0.0007	0.0007	0.0007	0.0007	0.0003	0.0002	0.0005	0.0007
—	—	—	—	—	—	—	—	—	—	—	—	.05
.007	.005	.007	.005	.005	.01	.007	.01	.007	.005	.01	.01	.01
.05	.05	.05	.07	.05	.05	.07	.07	.07	.1	.1	.1	.1
.0001	.00015	.00015	.0001	.0001	.0001	.00015	.0002	.00015	.0002	.00015	.00015	.00015
.001	.0015	.003	<.001	.002	.002	<.001	.001	.0015	.001	.001	.0015	.01
.7	1	.7	2	2	2	2	3	.7	1	1	1	1
.0015	.001	.001	.002	.001	.0015	.0015	.001	.0015	.0015	.0015	.0015	.001
.015	.01	.015	.02	.01	.02	.03	.03	.05	.02	.03	.05	.15
.02	.02	.03	.015	.015	.015	.07	.05	.07	.05	.07	.07	.02
7	5	5	7	3	5	7	5	7	5	7	7	7
.005	.002	.005	.003	.002	.003	.005	.003	.003	.005	.005	.003	.005
1	1	1	1.5	1	1.5	2	2	2	2	2	1.5	2
.07	.07	.07	.07	.07	.1	.07	.07	.07	.1	.1	.07	.07
—	—	—	.001	—	<.001	.001	.001	.001	—	<.001	.001	<.001
.005	.005	.005	.007	.003	.005	.005	.003	.005	.005	.007	.007	.005
.007	.007	.007	.007	.005	.007	.01	.01	.015	.015	.01	.01	.03
.0015	.0015	.0015	.002	.0015	.0015	.002	.002	.002	.0015	.002	.002	.003
<.001	<.001	<.001	.001	<.001	.001	<.001	—	.001	—	—	.001	.002
.03	.03	.03	.05	.05	.05	.05	.05	.03	.03	.03	.03	.03
.5	.3	.5	.5	.5	.5	.7	.5	.5	.5	.5	.5	.5
.015	.015	.015	.015	.015	.01	.02	.02	.02	.015	.02	.02	.03
.003	.002	.003	.003	.0015	.002	.003	.003	.005	.003	.003	.003	.005
—	—	—	—	—	—	—	—	—	—	—	—	—
.02	.02	.02	.02	.02	.02	.02	.02	.015	.015	.02	.015	.015
Chemical analyses (parts per million)—												
20	60	30	20	30	20	80	40	100	40	60	40	>160
.04	.08	0.1	.8	.06	.2	.06	.12	.08	<.02	.26	.06	.4
.4	.5	.24	.14	.16	.16	.2	.3	.35	.4	.6	.45	.5
3	2	3	2	1	3	3	2	1	2	2	2	6
120	120	110	100	100	100	100	100	100	130	150	100	80

[1]Spectrographic analyses by D. Siems. Results are reported to the nearest number in the series 1, 0.7, 0.5, 0.3, 0.2, 0.15, 0.1, 0.07, and so on, which represent approximate midpoints of interval data on a geometric scale. The precision of a reported value is approximately plus or minus one series interval at 68 percent confidence, or two intervals at 95 percent confidence.

[2]Chemical analyses by J.G. Frisken, J.D. Hoffman, R.M. O'Leary, and L.A. Vinnola.

and *Y–Y′*. Concentrations of arsenic, gold, copper, mercury, and lead tend to decrease slightly with distance from the underlying ore, as does the ratio Cu:Pb+Zn. The content of arsenic, a relatively mobile element in the supergene environment (Andrews-Jones, 1968), fluctuates strongly from sample to sample, even at the tight spacing of our sample locations. Some arsenic in the soil, however, may reflect downslope contamination from arsenopyrite-bearing veins along the Virgin fault system. The concentrations of bismuth seem to follow those for lead. Cobalt, manganese, and antimony concentrations are uniform across both underlying ore and subeconomic sulfide-rich skarn. In contrast, zinc and nickel concentrations increase gradually with distance from ore.

The frequency distributions for some elements (Ag, As, Au, Cu, Ni, Pb, and Hg) differ somewhat from those of other elements and may reflect hypogene introduction of these metals into the underlying bedrock (fig. 29). Data for all seven elements show greater dispersion than for other elements in the data set. The greater dispersion is shown by greater ranges of values, and, if standard deviations were computed assuming the frequency distributions are reasonably close to lognormal, it would also be shown by larger logarithmic standard deviations. Mercury has a negatively skewed distribution. The histograms of the soil analyses emphasize that concentrations of most of the remaining metals vary across narrow ranges, probably because most of these metals are indigenous to the bedrock and were not introduced during copper metallization (fig. 29).

Concentrations of eight elements (Ag, As, Au, Bi, Cu, Ni(?), Pb, and Hg) in soil above the skarn are generally anomalous compared to their concentrations in soil from unmineralized parts of the Pumpernickel Formation; gold, mercury, silver, and copper are perhaps the most anomalous above the skarn (fig. 30): median values for gold, mercury, silver, and copper, show respectively a fifteenfold, sevenfold, sixfold, and

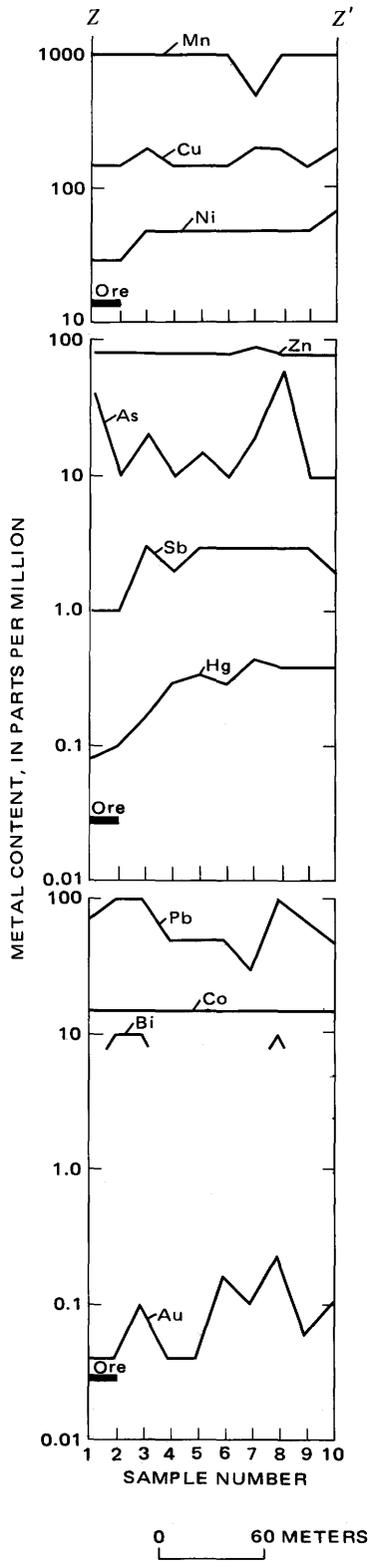

FIGURE 28.—Concentrations of 10 elements in soil along traverse Z–Z′ (pl. 1). Lateral extent of horizontal projection of ore in underlying skarn is shown. Sample numbers taken from table 21.

twofold enrichment in the residual soil above the skarn. The data shown in figure 30 also indicate some general relations between the geochemistry of bedrock and the overlying soil around the skarn. Median values of analyses for seven metals (Cu, Pb, Ni, Bi, Ag, Hg, and Au) are slightly higher than bedrock values. Ranges of analytical determinations are greater in bedrock than in soil.

Log-probability plots of geochemical data are another graphical method by which their frequency distributions may be evaluated. From such plots, we infer that copper and mercury concentrations in the soil may reflect two populations, perhaps a metallized one and a more metallized one or a local background one and a metallized one (fig. 31; see Tennant and White, 1959; Lepeltier, 1969). In addition log-probability plots that show straight lines like those for silver, gold and lead in figure 31 likely reflect a single population, possibly a background one. We believe, however, that all of the data of figure 31 are derived from one or more sources more metallized than our established background (*B*, fig. 30). Stated another way, the plots for silver, gold and lead shown on figure 31, although they represent data that are very close to being lognormally distributed, are derived from a population of samples that are weakly but uniformly metallized with respect to these elements. Furthermore, although the log-probability plots suggest that copper and mercury concentrations are the result of more complex processes, high values (>300.0 ppm Cu, and >0.2 ppm Hg on fig. 31) do not seem to be related to underlying ore in the skarn.

STATISTICAL CORRELATIONS AMONG 19 ELEMENTS

Spearman correlation coefficients calculated for 19 minor elements (Ag, As, Au, B, Ba, Bi, Co, Cr, Cu, Fe, Hg, Mg, Ni, Pb, Ti, V, Zn, Zr, and Sb) from the 140 analyses of soil above the skarn reveal many similarities to elemental associations in the underlying bedrock. However, the percentage of determinations below detection thresholds for these elements is less than for the bedrock samples (table 22). This is primarily due to the higher sensitivity of analytical techniques used for arsenic, antimony, and zinc in the soils. Some changes in elemental associations may have occurred during and after development of the soil (compare tables 18 and 22).

FLUID-INCLUSION STUDIES

Fluid-inclusion studies initiated by Nash (in Nash and Theodore, 1971; Theodore and Nash, 1973) and Batchelder (1973; Batchelder and others, 1976) were enlarged by Theodore to include detailed investiga-

TABLE 22.—*Array of numbers of paired-element analyses and Spearman correlation coefficients calculated from analytical determinations on 140 samples of soil on the Pumper-nickel Formation above skarn*

[*, coefficients statistically significant at 99.5 percent confidence level]

	Ag	As	Au	B	Ba	Bi	Co	Cr	Cu	Fe	Hg	Mg	Ni	Pb	Ti	V	Zn	Zr	Sb
Ag		0.40*	0.35*	0.07	0.14	0.61*	−0.13	0.20	0.19	−0.05	0.03	−0.05	0.19	0.47*	0.00	0.07	0.29*	−0.15	−0.03
As	118		.32*	−.01	.17	.06	−.26*	.10	.22	.03	.24*	−.08	−.20	.50*	−.05	.01	−.20	−.03	−.05
Au	133	119		−.10	.25*	.21	−.13	.14	.19	.00	.17	−.13	−.04	.25*	−.13	−.11	−.13	−.07	−.06
B	135	121	138		.12	.19	.23*	.36*	.32*	.44*	−.21	.48*	.19	.38*	.41*	.39	.02	.17	.35
Ba	135	121	138	138		−.07	.03	.27*	.26*	.17	.10	.26*	.20	.33*	.27*	.26*	−.03	−.03	.06
Bi	73	60	72	73	73		−.05	.13	.13	.04	−.08	−.17	.15	.23	.08	.01	.16	.01	.15
Co	135	121	138	140	140	73		.30*	.19	.41*	−.18	.30*	.52*	−.08	.22*	.34*	.35*	.09	.20
Cr	135	121	138	140	140	73	140		.59*	.65*	−.49*	.41*	.52*	.29*	.58*	.60*	.10	.15	.37*
Cu	135	121	138	140	140	73	140	140		.62*	−.22*	.38*	.23*	.29*	.25*	.37*	−.11	.27*	.34*
Fe	135	121	138	140	140	73	140	140	140	140	−.38*	.42*	.41*	.20	.41*	.58*	−.01	.26*	.45*
Hg	135	121	138	140	140	73	140	140	140	140	140	−.24*	−.40*	−.11	−.51*	−.46*	−.21	−.12	−.17
Mg	135	121	138	140	140	73	140	140	140	140	140	140	.27*	.04	.54*	.37*	.17	.15	.18
Ni	135	121	138	140	140	73	140	140	140	140	140	140	140	.01	.47*	.59*	.58*	.03	.27*
Pb	135	121	138	140	140	73	140	140	140	140	140	140	140	140	.21	.31*	−.10	.03	.09
Ti	135	121	138	140	140	73	140	140	140	140	140	140	140	140	140	.60*	.09	.31*	.29*
V	135	121	138	140	140	73	140	140	140	140	140	140	140	140	140	140	.19*	.11	.29*
Zn	135	121	138	140	140	73	140	140	140	140	140	140	140	140	140	140	140	−.23*	−.04
Zr	135	121	138	140	140	73	140	140	140	140	140	140	140	140	140	140	138	138	.22*
Sb	133	119	136	138	138	72	138	138	138	138	138	138	138	138	138	138	138	138	

Correlation coefficients

Numbers of pairs of elements

tions of inclusions in the skarn and in the altered granodiorite of Copper Canyon. Although published fluid-inclusion studies of minerals from the geologic environment of skarn are relatively sparse, studies of primary and pseudosecondary fluid inclusions in andradite, one of the first silicates to crystallize near the onset of metallization at Copper Canyon, provided data on the origins and evolution of the fluid-rock system at Copper Canyon. Primary fluid inclusions are those that were trapped mostly along growth imperfections on a crystal's rim during its formation, and primary pseudosecondary ones are those that are trapped by healing fractures formed in a crystal during its growth (Roedder, 1972).

Preparation of samples and investigation of their fluid inclusions followed generally the techniques of Roedder (1967), Nash and Theodore (1971), and J. T. Nash (unpub. data). Of the several hundred rocks examined in thin section at Copper Canyon, those from about 50 locations were selected. From these selected samples doubly polished plates were prepared. However, the typically small inclusion size in most samples, and the tendency for many inclusions from the district to form notably clear ice in the freezing stage (J. T. Nash, oral commun., 1974) precluded successful tests with the freezing stage. However, tests were possible on the heating stage. Some approximate measures of the salinity of fluid inclusions with prominent halide daughter minerals were obtained from the temperatures at which the crystals dissolved and reference to the system $NaCl–H_2O$ (see Roedder, 1971). Replicate heating tests suggest a precision of better than ±5°C for the reported homogenization temperatures, and calibration tests of the heating stage using pure metals and prepared metal mixtures with known melting points in evacuated glass capillaries suggest an accuracy of about ±5°C at temperatures of about 300°C (see Roedder, 1971, for a discussion of calibration methods). Higher temperatures than this have somewhat larger uncertainties, probably about ±15°C at 500°C.

TEXTURES AND AGES OF FLUID INCLUSIONS

In both the altered granodiorite and the skarn, we found significant concentrations of three of the five types of fluid inclusions and very sparse occurrences of one of the others previously recognized by Nash and Theodore (1971) in and near the east ore body at Copper Canyon. We summarize briefly in table 23 data from the four types of inclusions found in our study of rocks in and near the west ore body.

Textural relations suggest liquid-rich inclusions reflect both primary and pseudosecondary, and definitely secondary origin relative to their host minerals. The

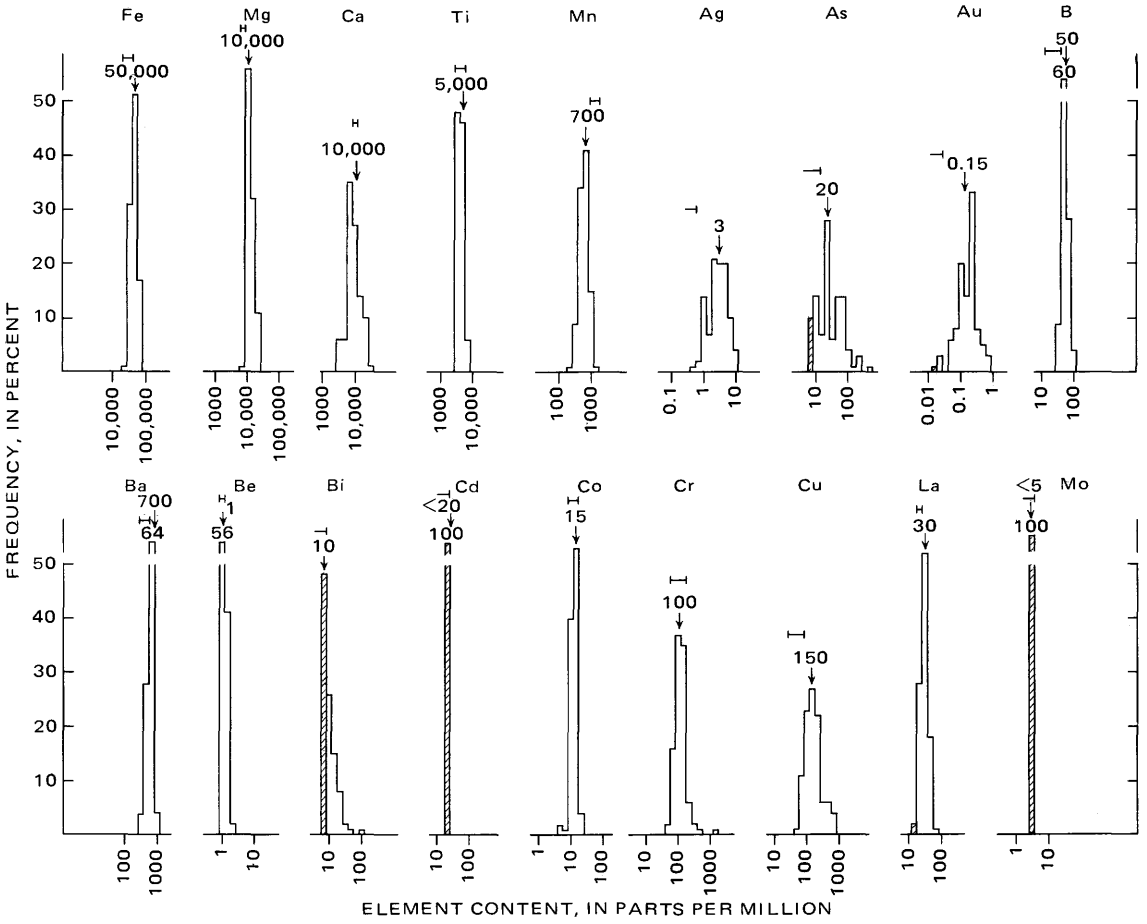

FIGURE 29.—Log-frequency distributions of elements from analyses of soil above the skarn. Data from tables 19–21.

TABLE 23.—*Summary table showing ranges of homogenization temperatures measured for the different types of inclusions*

[Gar, garnetite; Di, diopside rock; Ta, tremolite-actinolite rock; Mic, secondary-mica-rich rock; Gd, altered granodiorite]

Fluid-inclusion type[1]	Relative abundance	Host rock	Age relative to host mineral[2]	Range of filling temp. (°C)
I	Common	Gar	S;PPS	161–565
		Di	PPS	337–510
		Ta	PPS	202–412
		Mic	S;PPS	202–515
		Gd	S;PPS	249–490
II	do.	Ta	PPS	332–503
		Mic	S;PPS	317–530
		Gd	S;PPS	337–590
III	do.	Gar	PPS	219–337
		Di	S;PPS	215–425
		Ta	PPS	205–400
		Mic	S;PPS	208–396
		Gd	S;PPS	186–317
IV	Rare	Gd	S	345

[1]I, liquid-rich; II, gas-rich; III, halide-bearing with low gas volumes; IV, same as type III but also with optically recognizable liquid CO_2 at 25°C.

[2]S, secondary; PPS, primary-pseudosecondary.

repeated opening and rehealing of the rocks on a microscopic scale in a high temperature hydrothermal environment yields exceedingly complex and overlapping parageneses among populations of inclusions. This is especially true in quartz, less so in andradite (see Roedder, 1971 and Moore and Nash, 1974 for additional descriptions of fluid inclusions in other porphyry districts). At Copper Canyon, many liquid-rich inclusions occur in andradite in three textural associations: (1) isolated, relatively large (15–40 μm) angular inclusions in the core areas of crystals without visible traces of any related planar features (fig. 32); (2) local concentrations of angular inclusions generally oriented with their long dimensions at right angles to the traces of the andradites' growth lines; and (3) swarms of small (<10 μm) ovoid to ellipsoid inclusions with their long axes parallel to the traces of growth lines. We suggest each of these three types of associations reflects trapping of fluid very close in time to the primary growth

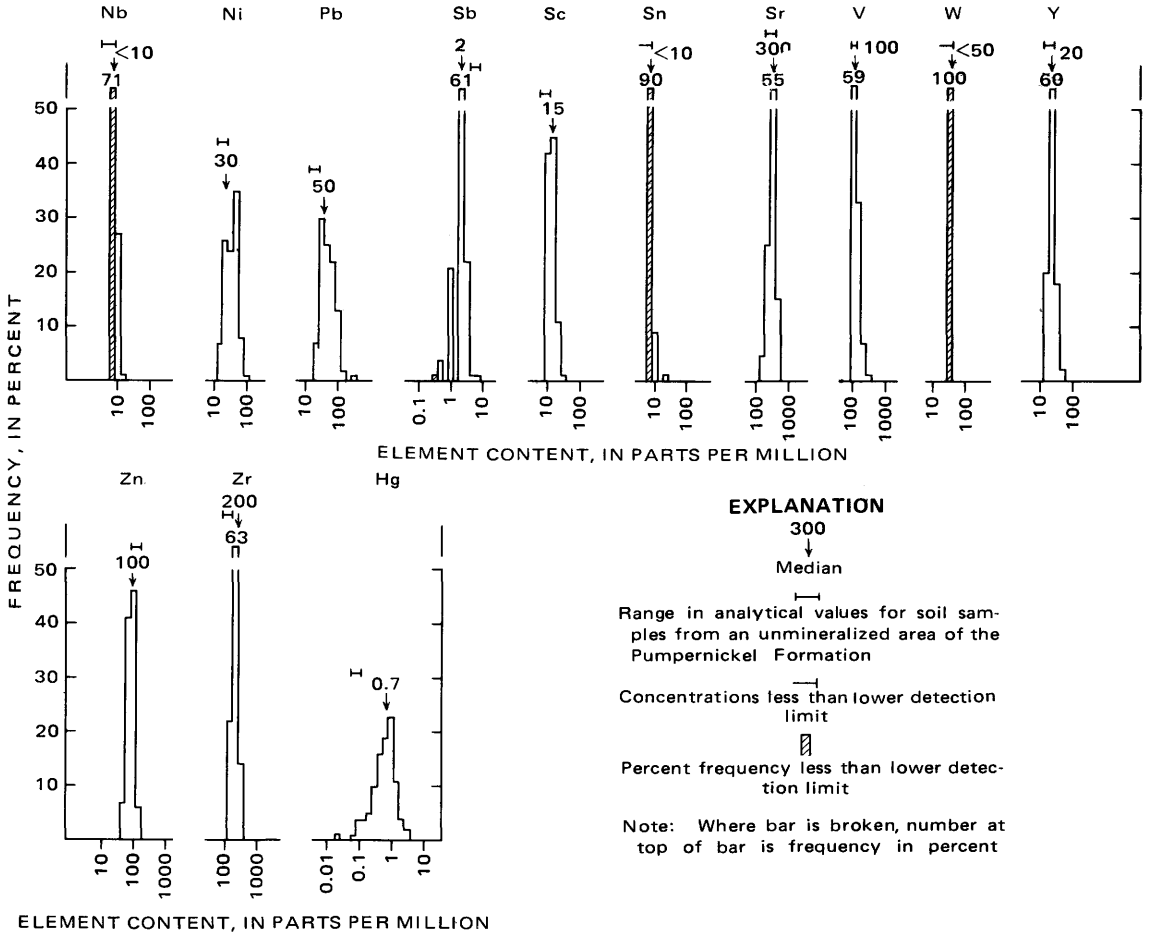

FIGURE 29.—Continued.

of the andradites. Elsewhere, Tugarinov and Naumov (1969) also describe some inclusions they judge to be primary that have their long dimensions oriented at right angles to growth lines in garnet. Textural relations at high magnification in andradite also suggest some superposed generations of inclusions and sulfides. Some microfractures have been partially filled by anastomosing fingers of postandradite sulfides, chiefly pyrrhotite.

The mechanism of trapping of primary fluid inclusions during the growth of replacement minerals in skarn deposits is poorly understood (J. T. Nash, written commun., 1975). This uncertainty may reflect the fact that the actual mechanisms of growth of the replacement minerals are themselves enigmatic. Such growth can result from either diffusion or infiltration (see Korszhinskiy, 1964). Crystallization of most replacement minerals, andradite for example, probably does not occur in an open-cavity environment. The best evidence for such an environment would be the preservation of vugs or cavities at, or along, the interface between skarn and unreplaced carbonate. Although the skarn–carbonate interface cannot be studied at Copper Canyon, at many other deposits where it has been observed and studied intensely, vugs have not been described. However, the late fluids in such rocks would tend to concentrate in any available open space, to precipitate late minerals, and to obscure initial relations between early skarn minerals and carbonate. Nonetheless, at Copper Canyon the extreme fluctuations in andradite compositions across millimeter-size and smaller domains strongly suggests that crystallization of andradite occurred in the presence of a fluid phase. We cannot determine whether or not some dissolution of carbonate led to open cavities and preceded the initial crystallization of andradite and diopside.

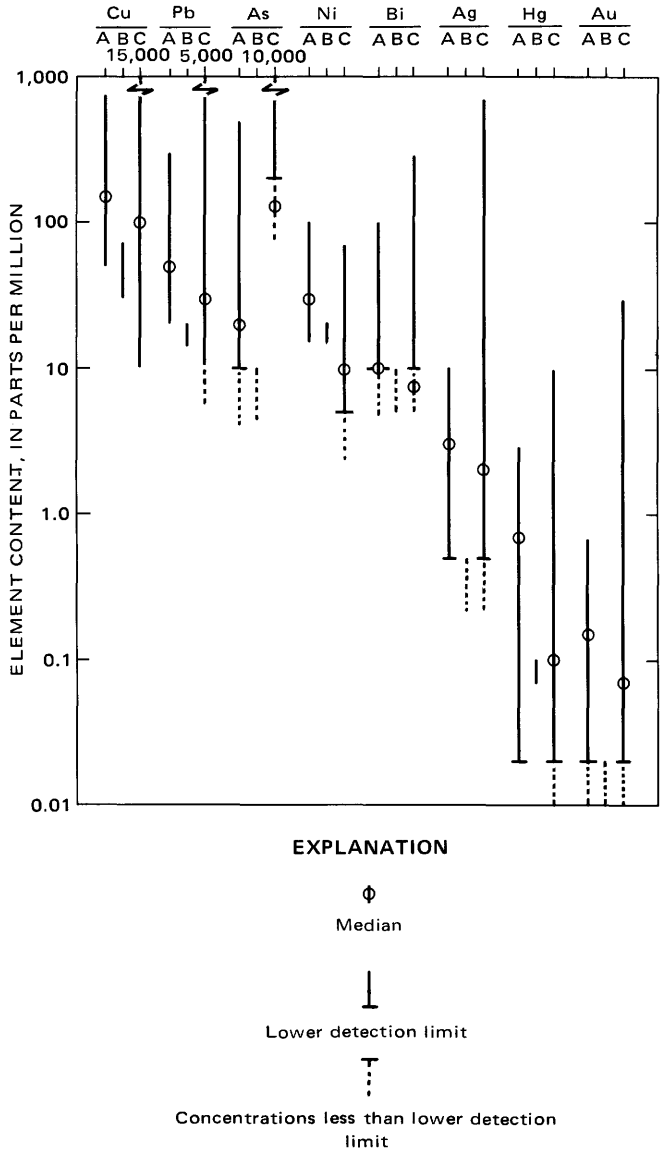

FIGURE 30.—Ranges and medians from analyses for eight elements in (A) soil in general area of skarn (tables 19–21); (B) soil from unmineralized area of the Pumpernickel Formation, 1,500 m north of ore deposits at Copper Canyon (six samples); and (C) exposed bedrock in general area of skarn (sample group 2, fig. 25).

TYPES OF FLUID INCLUSIONS

TYPE I. LIQUID PLUS SMALL VAPOR BUBBLE

The volume of vapor in the two-phase (liquid-plus-vapor) fluid inclusions ranges from about 10 to 40 percent at room temperature. Most of the inclusions contain about 15 volume percent vapor (fig. 33). All of the type I inclusions in Copper Canyon samples homogenize to a liquid when heated. The absence of cubic salt daughter minerals in these inclusions at room temperature suggests the fluids can have a maximum salinity of 26 weight percent NaCl equivalent; high concentrations of calcium and potassium could go undetected, however. Some of these inclusions also contain a very small opaque mineral that we judge to be hematite. Freezing-stage determinations by Nash indicate salinites of 2–15 weight percent NaCl equivalent for type I inclusions in late-stage veins in the east ore body (Nash and Theodore, 1971). Salinities of some of the type I inclusions in nearby rocks outside the skarn are probably relatively low because of the low-salinity chemical compositions of inclusion waters, which were studied in mixed-inclusion population made up of various proportions of type I, gas-rich (type II), and halide-bearing (type III) inclusions (table 24). Some of these samples contain halide-bearing inclusions; dissolution temperatures of their daughter minerals suggest salinities of 32–36 weight percent NaCl equivalent for individual inclusions.

TYPE II. LIQUID PLUS A LARGE BUBBLE

Type II fluid inclusions that contain more than 50 percent vapor by volume at room temperature are most common in quartz phenocrysts in the granodiorite (fig. 34). These gas-rich fluid inclusions generally are larger (typically 30–40 μm) than the type I inclusions. They are less common but still prominent in some of the vein quartz and generally seem to be restricted to the immediate area of the granodiorite (Nash and Theodore, 1971). In samples from the granodiorite, our visual estimates in some quartz phenocrysts suggest that this type of inclusion makes up about 60 volume percent of the total inclusion population. A few type II inclusions contain a very small opaque daughter mineral, possibly hematite, that persists beyond the filling temperatures of the inclusions during prolonged heating tests. Although liquid CO_2 is not optically resolvable in these inclusions at room temperature, from which we infer less than roughly 2 or 3 molecular percent CO_2 (Ypma, 1963), crushing tests by Batchelder (1973) revealed the presence of some CO_2 in them. Some rare inclusions consisting of almost all vapor are in andradite. They are probably inclusions that have leaked during the preparation of the samples. Some "inclusions of dry gases" found by Lesnyak (1965) in grossularite-andradite from the Tyrny-Auz skarn, U.S.S.R., are thought by him to be primary. Type II inclusions previously studied by Nash and Batchelder in the east ore body and in the peripheral vein deposits suggest varied salinities for the entrapped liquids; minimum salinities determined by the freezing stage for individual type II inclusions are 0.4 weight percent NaCl equivalent, whereas some other samples, which contain about 70 volume percent of the type II inclusions, yielded total salinities of about 11.0 percent by leaching methods (Batchelder, 1973).

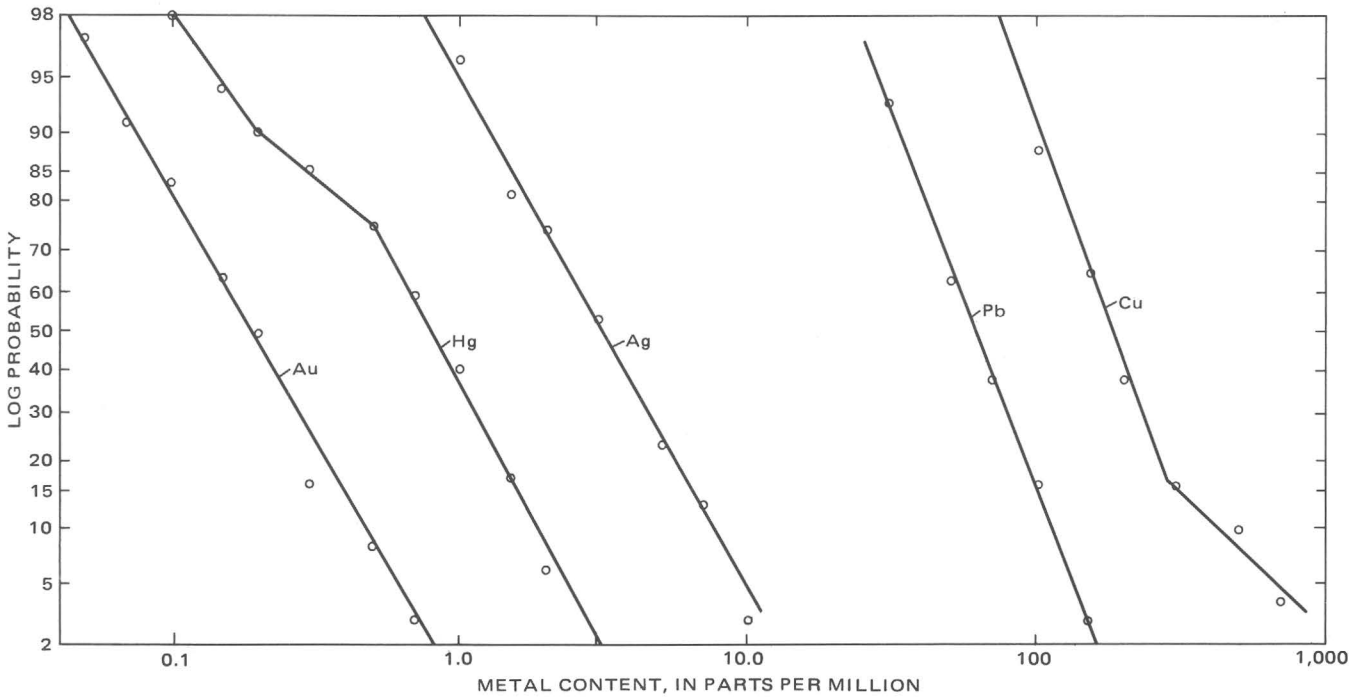

FIGURE 31.—Log-probability plots for five metals from analyses of soil above the skarn.

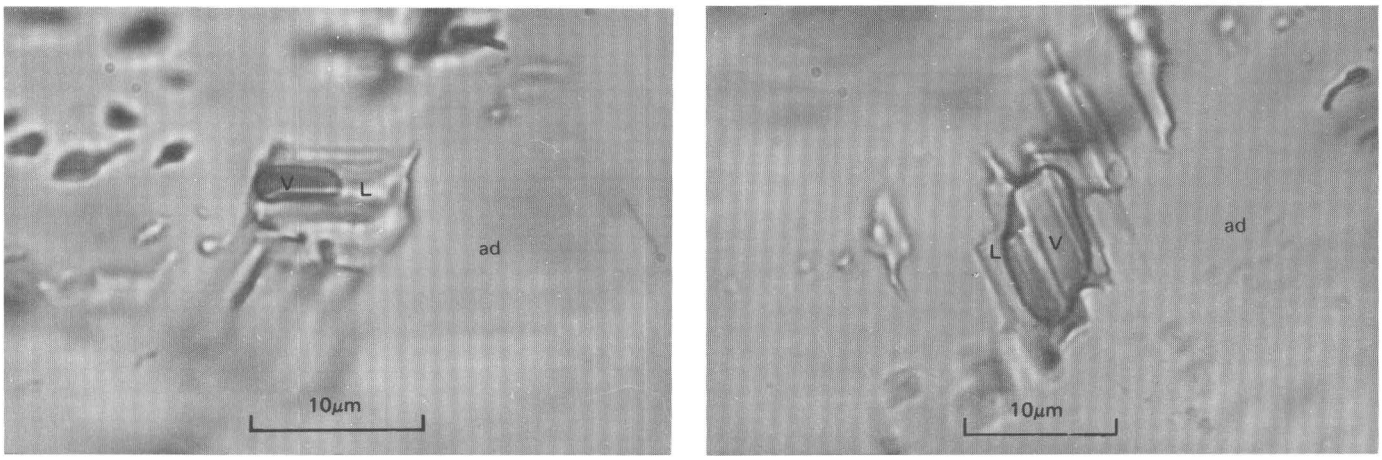

FIGURE 32.—Photomicrographs showing type I, liquid-rich inclusions in andradite. ad, andradite; L, liquid, mostly water; V, vapor bubble. Plane-polarized light.

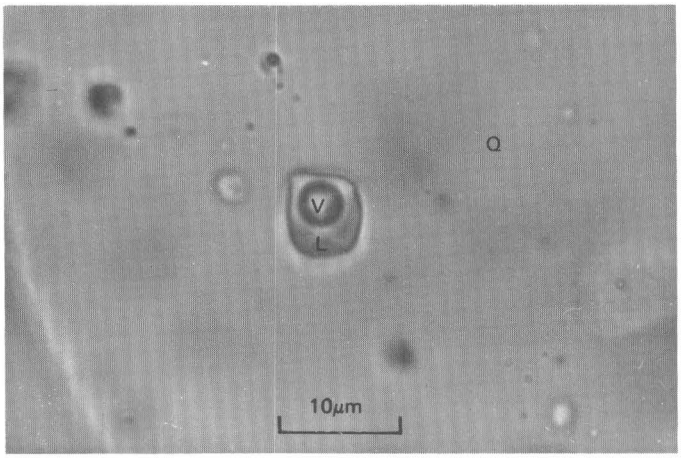

FIGURE 33.—Photomicrograph showing type I fluid inclusion in quartz phenocryst (Q) from altered granodiorite of Copper Canyon. V, vapor bubble; L, liquid, mostly water. Plane-polarized light.

TYPE III. HALIDE-BEARING INCLUSIONS WITH LOW GAS VOLUME

Around the skarn the most typical of the type III inclusions at 25°C is about 10–15 volume percent vapor, commonly with daughter minerals including a cube of halite and less commonly an associated very small opaque mineral. The liquid is probably mostly water (fig. 35*A*). The opaque, very small grains are probably hematite in type III inclusions. In addition, the type III inclusions from the skarn generally seem to include much less anhydrite and sylvite than type III inclusions in the east ore body. Our studies of samples from the granodiorite, however, suggest that sylvite daughter minerals are more common in type III

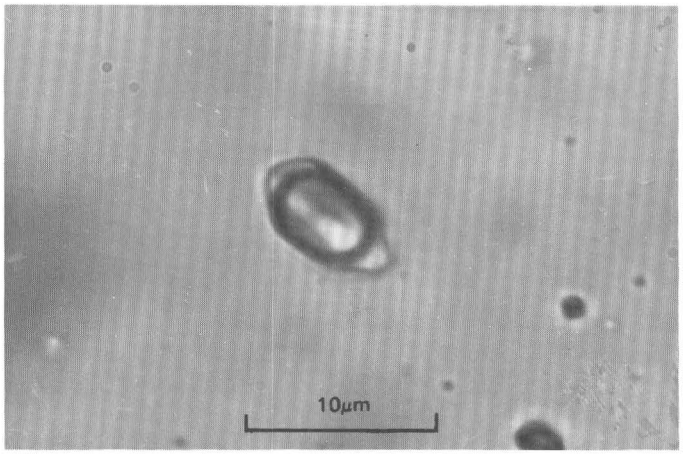

FIGURE 34.—Photomicrograph showing type II fluid inclusion in quartz phenocryst from altered granodiorite of Copper Canyon. Plane-polarized light.

TABLE 24.—*Chemical and filling temperature data of fluid inclusions*

[Analysts: Joseph Haffty, Na, K, Ca, Mg, Cu, and Zn by atomic absorption spectroscopy; J. H. Christie and L. Schlocker, Cl by a spectrophotometric method. From Batchelder, 1977]

Sample No.	Filling temperature[1] (°C)	Na (ppm)	K (ppm)	Ca (ppm)	Mg (ppm)	Cl (ppm)	Cu (ppm)	Zn (ppm)	Na-K-Ca temperature[2] (°C)	Sample locality
BM–25	270–300	11,000	1,700	4,600	800	24,700	2,200	700	230	East ore body.
BM–53	350	8,800	1,200	3,100	400	10,700	900	1,900	225	Do.
TN4–69–1	270	3,800	700	1,100	200	5,100	400	100	360	Do.
TN4–69–2	270	3,800	700	1,500	300	5,700	200	200	230	Do.
BM–3	305–400	9,600	1,800	4,600	1,000	24,400	100	700	245	Vein in altered granodiorite of Copper Canyon.
BM–60	385	7,500	2,800	7,500	1,500	18,500	200	400	285	Vein at contact between altered granodiorite of Copper Canyon and Pumpernickel Formation.
BM–48	300	6,200	700	3,600	800	6,600	200	1,000	210	Modoc mine, 4.8 km west-southwest of Copper Canyon.
BM–32	300–385	3,300	800	1,000	200	4,900	200	100	250	Tomboy mine, 2.0 km south of east ore body.

[1]From Nash and Theodore (1971) and Batchelder (1973).
[2]Based on the Na-K-Ca geothermometer of Fournier and Truesdell (1973).

inclusions there (fig. 35*B*) than in the skarn. Where type II (gas-rich) inclusions and type III inclusions occur in the same samples, the type III inclusions average about 10–12 μm across and are generally much smaller than the type II inclusions. The shapes and optical properties of the daughter minerals in the Copper Canyon area, their behavior during heating tests, and their overall distribution in rocks have been described previously (Nash and Theodore, 1971; Theodore and Nash, 1973). Dissolution temperatures of halite suggest salinities of 31–44 weight percent NaCl equivalent for brines trapped in type III inclusions in skarn. These salinities are about the same as those determined for type III inclusions in the east ore body (Nash and Theodore, 1971).

Rocks with relatively large and abundant fluid inclusions that include halide daughter minerals are characteristic of 32 of 34 porphyry copper districts studies by J. T. Nash (unpub. data). Copper Canyon is one of these 32 districts.

TYPE IV. TWO LIQUIDS PLUS VAPOR AND SOLIDS

Fluid inclusions that contain two liquids plus vapor and solids are very rare in the northern parts of the granodiorite. Most liquid in these inclusions is water, but another liquid phase in these inclusions is most likely liquid CO_2, as it occurs only at temperatures less than about 30°C. We find the type IV fluid inclusions only rarely in the samples of altered granodiorite studied.

FLUIDS IN GARNETITE

Liquid-rich inclusions with small gas volumes (type I) are the dominant type of inclusion in andradite within the garnetite. Tests with the heating stage on type I inclusions in garnet yield a bimodal distribution of filling temperatures (table 25). One group of type I inclusions fills with liquid when heated to 300°±25°C, and the other when heated to 500°±50°C. The first temperature may reflect the postandradite crystallization of pyrrhotite-chalcopyrite-quartz in the garnetite, and the second may reflect temperatures dating from the earlier crystallization of the andradites themselves. One group of coplanar type I inclusions spatially associated with iron oxide-filled microfractures in andradite yielded filling temperatures of 161°–216°C sample 0–347, table 25). The highest temperature recorded in andradite is 565°C, which is estimated from the rate of filling of an inclusion up to the time of its decrepitation. Thus, the garnetite seems to have been affected by hypogene fluids over a temperature interval of about 400°C. Our best estimate of the average temperature for the earliest fluids to circulate during the growth of andradite is about 500°±50°C.

Some generalizations about the composition of the early fluids associated with the crystallization of the bulk of the andradite may be made from the thermometry of the fluid inclusions. Although these early fluids apparently are unsaturated with respect to NaCl at 25°C, they may be highly saline and may contain significant amounts of calcium and possibly magnesium, which do not generally precipitate as daughter minerals. Inclusions made up of pure water (liquid plus vapor) cannot homogenize to liquid at temperatures above the critical point at 374°C (Roedder, 1972). Furthermore, the liquid-rich inclusions that homogenize at high temperatures (roughly 500°±50°C, table 25) have fairly constant proportions of liquid and vapor

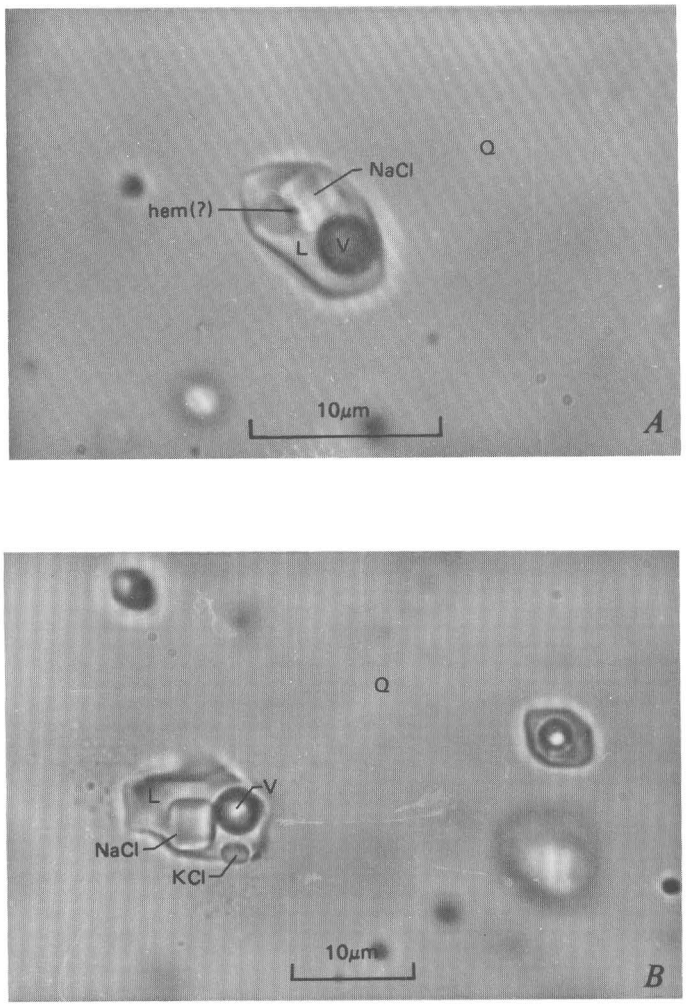

FIGURE 35.—Photomicrographs showing type III fluid inclusions with halide daughter minerals and small gas volumes. *A*, In quartz vein that cuts skarn. *B*, In quartz phenocryst from the granodiorite. Right-hand inclusion shown in *B* also has an opaque grain in it obscured by vapor–liquid interface. KCl, sylvite daughter mineral; NaCl, salt daughter mineral; hem (?), probable hematite; L, liquid, mostly water; V, vapor bubble; Q, quartz host mineral. Plane-polarized light.

TABLE 25.—*Temperature and salinity data from fluid-inclusion studies around the west ore body*

[At 25°C; I, low gas volume + liquid; II, high gas volume + liquid; III, low gas volume + polyphase daughter minerals; S, secondary; PPS, primary-pseudosecondary]

Sample No.	DDH (pl. 1, fig. 3)	Depth (m)	Mineral	Type of inclusion	Age of inclusion	Homogenization temperature: Number measured	Homogenization temperature: Range (°C)	Homogenization temperature: Mean (°C)	Salinity (equiv. wt % NaCl)	Comments
Garnetite										
6–150	4	45.8	G[1]	I	PPS	3	394–426	412.		Pumpernickel Formation.
8–170	2	52.	HQ	I	PPS	9	[2]327–470e	407.		Do.
8–170	2	52.	HQ	II	PPS	10	300–500e	387.		Do.
8–170	2	52.	HQ	III	PPS	8	263–308	280.	[3]32–38(6)	Do.
6–167	4	51.	G	I	S	8	279–305	289.		Do.
8–233	2	71.	HQ	I	PPS	10	221–315	284.		Do.
8–233	2	71.	HQ	III	PPS	6	219–314	267.	32–38(2)	Do.
8–146	2	44.6	G	I	PPS	5	420–479	455.		Do.
2–233	12	71.	G	I	S	10	249–321	291.		Do.
8–201	2	61.4	G	I	PPS	3	385–500e	435.		Do.
8–201	2	61.4	G	I	S	6	266–327	294.		Do.
6–162	4	49.4	G	I	S	5	255–293	278.		Do.
2–232	12	71.	G	I	S	7	244–305	269.		Do.
2–232A	12	71.	G	I	S	12	265–377	317.		Do.
2–232A	12	71.	G	I	PPS(?)	1	----	465.		Do.
8–212	2	64.9	G	I	S	4	267–363	302.		Do.
8–212	2	64.9	G	I	PPS	12	414–540e	500.		Do.
8–212	2	64.9	HQ	I	PPS	3	292–308	301.		Do.
8–212	2	64.9	HQ	III	PPS	6	227–337	280.	36–43(5)	Do.
0–347	1	105.8	G	I	S	7	161–216	191.		Do.
0–347	1	105.8	G	I	S	2	260–296	279.		Do.
0–347	1	105.8	G	I	PPS	3	499–510	506.		Do.
0–398	1	121.	G	I	S	4	230–295	259.		Do.
0–398	1	121.	G	I	PPS	4	518–565e	543.		Do.
Diopside rock										
6–207	4	63.2	D	I	PPS	6	362–404	391		Pumpernickel Formation.
6–207	4	63.2	D	III	PPS	1	----	425	40	Do.
6–210	4	64.2	HQ	I	S	4	240–311	263		Do.
6–227Y	4	69.4	HQ	I	PPS	7	337–510e	414		Do.
6–227V	4	69.4	HQ	II	PPS	1	----	510e		Do.
6–227V	4	69.4	HQ	III	S(?)	4	215–261	240	32(3)	Do.
6–227V	4	69.4	HQ	I	S	6	196–297			Do.
Tremolite-actinolite rock										
6–243	4	74.1	HQ	I	PPS	8	221–369	312		Pumpernickel Formation.
6–243	4	74.1	HQ	III	PPS	6	219–240	228	33–41(5)	Do.
6–257	4	78.5	HQ	I	PPS	6	277–400	333		Do.
6–264	4	80.8	HQ	I	PPS	13	216–390	294		Do.
6–264	4	80.8	HQ	II	PPS	7	345–375	360		Do.
6–265	4	81.	HQ	I	PPS	7	227–412	334		Do.
6–265	4	81.	HQ	II	PPS	12	332–503	427		Do.
6–265	4	81.	HQ	III	PPS	13	216–400	301	38–40(5)	Do.
5–201	19	61.4	HQ	I	PPS	13	212–365	297		Battle Formation.
5–201	19	61.4	HQ	II	PPS	11	332–400	390		Do.
5–201	19	61.4	HQ	III	PPS	2	320–327	324	32	Do.
1–480	1	146.5	HQ	III	PPS	5	205–220	212		Do.
8–578	2	176.	HQ	I	PPS	7	202–300	239		Do.
8–578	2	176.	HQ	III	PPS	2	236–250	243		Do.
Mica-bearing rock										
3–248	17	75.9	DQ	III	S	6	221–240	228		Battle Formation.
3–377	17	115.	DQ	I	S	16	212–440	299		Do.
3–377	17	115.	DQ	II	S	2	337–480	409		Do.
3–377	17	115.	DQ	III	S	2	208–229	219	31–39(2)	Do.
5–707	20	216.	HQ	I	PPS	13	265–371	315		Do.
5–707	20	216.	HQ	II	PPS	24	317–450	398		Do.
5–707	20	216.	HQ	III	PPS	9	219–382	272	36–42(4)	Do.
8–809	2	247.	DQ	I	S	26	290–409	348		Do.[4]
8–809	2	247.	DQ	III	S	24	246–364	298		Do.[4]
5–831	20	254.	DQ	I	S	17	202–515e	336		Do.[5]
5–831	20	254.	DQ	II	S	5	451–530e	495		Do.[5]
5–831	20	254.	DQ	III	S	2	317–346	331	33–39(2)	Do.[5]
8–832	2	254.	HQ	I	PPS	7	270–396	337		Harmony Formation.

[1]G, garnet; HQ, hydrothermal quartz; D, diopside; DQ, detrital quartz.

[2]e, estimated temperature of homogenization from temperature of decrepitation, or rate of filling.

[3]In parentheses, number of determinations of the solution temperature of NaCl daughter minerals. The reported range of salinity of the fluid is estimated from the solution temperatures by referring to experimentally determined stabilities in the system $NaCl-H_2O$.

[4]Some secondary chlorite and carbonate that partially replace hydrothermal biotite.

[5]Sample of the lower member of the Battle Formation with a well-developed quartz-white mica-potassium feldspar-pyrrhotite-chalcopyrite-carbonate hypogene alteration assemblage.

phases. They fill to liquid when heated. At several skarn deposits elsewhere, Sazonov (1962) and Sivoronov (1968) also determined that primary or pseudosecondary inclusions in garnets there are of a liquid-plus-vapor variety (our type I) that fills to liquid in the temperature interval 450°–560°C. All such fluids, including those at Copper Canyon, must be highly saline, at lease 20 weight percent NaCl equivalent. Other experiments also suggest that fluids associated with skarn development may be highly saline (Kiseleva, 1968; Vidale, 1969).

Moderate amounts of carbon dioxide in solution with the early fluids would produce significant effects. At a given temperature carbon dioxide would cause effervescence or boiling to begin at a depth greater than if it were not present, because its presence would increase the coefficient of thermal expansion of the trapped fluid (see Roedder, 1972, for a discussion of this phenomenon). We infer, however, that partial pressures of carbon dioxide in the early fluids at Copper Canyon were low because of the absence of liquid carbon dioxide from the early inclusions in andradite. Thus, the effects of carbon dioxide are probably not very large.

Deposition of quartz in the skarn was wide ranging both in time and space after early andradite and diopside had crystallized. Fluids circulated through the garnetite during the deposition of two generations of quartz, one a disseminated variety and the other vein quartz. The fluids in these two types of quartz seem to differ from each other both in chemistry and in the prevailing temperatures at which their inclusions homogenize. Textural relations suggest that crystallization of disseminated quartz followed closely crystallization of the andradite and much of the diopside. This quartz typically occurs in minor amounts sprinkled throughout the garnetite as anhedral grains, locally intergrown with mats of potassium feldspar and some diopside and sulfides, mostly pyrrhotite. The quartz fills open spaces among previously crystallized euhedral crystals of andradite and diopside. Heating tests of the fluid inclusions in disseminated quartz (samples 8–233 and 8–212, table 25) yield homogenization temperatures in the range 221°–315°C for both liquid-rich type I and halite-bearing type III inclusions, the predominant varieties. Thus, deposition of disseminated quartz and some of the first sulfides to precipitate there occurred at temperatures roughly 200°C less than the temperatures associated with the onset of the crystallization of andradite. In addition, the chemistry of the fluids changed; it appears to show higher concentrations of sodium during the disseminated quartz stage, and possibly higher overall salinities, than during the andradite stage. Approximate salinities of the type III inclusions in disseminated quartz, measured from the solution temperatures of halite daughter minerals, are 32–43 weight percent NaCl equivalent (table 25). A major unknown, however, is the concentration of calcium in the fluids during crystallization of andradite in the skarn.

Some of the continued changes in the physical and chemical environment of the skarn are reflected by fluids associated with quartz-pyrrhotite-epidote veins, which contain minor potassium feldspar and tremolite (sample 8–170, table 25). A vein of this type cuts garnetite near the northern fringe of the west ore body, and it also contains minor amounts of secondary carbonate and hematite. Abundant swarms of type I, II, and III inclusions with extremely complex and overlapping relations among planar alinements of inclusions typify the quartz of this vein. These inclusions appear remarkably similar to those in the granodiorite. Very wide ranging homogenization temperatures and phase proportions for type I and II inclusions, from 327° to 470°C and from 300° to 500°C, respectively, typify these inclusions. Type II inclusions, the gas-rich ones, homogenize in most cases to vapor, but some homogenize to liquid. The halide-bearing type III inclusions homogenize to liquid at somewhat lower temperatures, 263°–308°C. The liquid-rich type I inclusions, whose liquid-vapor proportions are fairly constant in small volumes of the polished chips, homogenize to liquid at temperatures of about 400°–420°C. From this we infer that the fluids associated with the deposition of some postandradite quartz in veins were boiling at approximately these temperatures. These homogenization temperature data also suggest a local influx of hot, low-density fluids circulated through the skarn as some veins opened after part of the disseminated quartz had already crystallized in the skarn.

Heating experiments on many type III inclusions in quartz from the skarn repeatedly yielded filling temperatures less than the dissolution temperatures of the included halite daughter minerals. Although Roedder (1972) notes that such behavior may reflect nonequilibrium during the experiment because of differences in the rates of solubilities between inclusion walls and daughter minerals, the long duration (4–5 hours) of many of our tests suggests to us that equilibrium was maintained. Perhaps as Roedder further suggests, the dissolution temperature of the daughter mineral may be a better approximation of these inclusions' trapping temperatures. For example, in sample 8–212 (table 25) six type III inclusions filled with liquid (the vapor bubble disappeared) in the range 227°–337°C, whereas the dissolution temperatures of their included halite daughter minerals were 280°–360°C. Alternatively, as pointed out by J. T. Nash (written

commun., 1975), a large part of the difference between the measured filling temperatures and the measured dissolution temperatures may reflect a pressure effect. However, not all of the difference between these two temperature measurements can be accounted for by elevated pressure at the time the inclusions formed. For example, one inclusion yields a 66°C temperature difference between the dissolution temperature of a halite daughter mineral and its homogenization temperature to a liquid. A pressure of about 700 bars would be required for such a difference if the fluid had a salinity of about 30 weight percent NaCl equivalent (Lemmlein and Klevtsov, 1961). This large a pressure during metallization was not likely at Copper Canyon (Nash and Theodore, 1971).

FLUIDS IN DIOPSIDE ROCK

Fluids that circulated through diopside rock during early crystallization of the skarn could not be sampled adequately. The generally small size of inclusions in diopside restricted significantly the number of inclusions available to us for heating tests. As a result, only a few tests were made with the heating stage on three samples from this metamorphic zone (samples 6–207, 6–210, and 6–227V, table 25); only one represents primary-pseudosecondary inclusions in diopside. The most common inclusion in diopside is of the liquid-rich type I variety; the six inclusions tested homogenized to liquid over the range 362°–404°C. One determination of a halide-bearing inclusion in diopside yielded a filling temperature of 425°C, the highest such temperature recorded for a type III inclusion during our study. Salinity, measured as before, was about 40 weight percent NaCl equivalent. These data again suggest that highly saline hot fluids were involved in the crystallization of early minerals in the skarn.

Fluids representing several different stages of the skarn's mineralization history were entrapped by primary-pseudosecondary and secondary inclusions in quartz-pyrite veins, which also contain minor tremolite and epidote and which cut diopside-pyrrhotite rock. Millimeter-wide alteration rinds around the quartz-pyrite veins are made up of epidote and pyrite. Liquid-rich type I inclusions that we judge to show primary-pseudosecondary relations with the host vein quartz yield homogenization temperatures from 337° to 510°C (sample 6–227V, table 25). In addition, these inclusions typically contain wide-ranging proportions of vapor at 25°C. Type II inclusions homogenize to vapor at approximately 500°C. The fluids associated with these quartz-pyrite-tremolite-epidote veins probably were boiling at temperatures of about 350°C, based on the homogenization temperatures of type I inclusions, which have roughly uniform vapor proportions in very small volumes of vein material. Some presumably late fluids that homogenize in the temperature range 196°–297°C also circulated through these rocks. Although the early fluids associated with the quartz-pyrite-tremolite-epidote veins seem to reflect deposition temperatures slightly lower than those of the quartz-epidote-pyrrhotite veins that cut garnetite, the fluids associated with both veins seem to have been boiling.

FLUIDS IN TREMOLITE-ACTINOLITE ROCK

Our attempts to assess the physical and chemical conditions of the fluids circulating through the tremolite-actinolite zone during its crystallization are based primarily on tests with the heating stage on rocks from seven localities (table 25). They include rocks from both the Pumpernickel and Battle Formations. Those from the Battle Formation include some beneath the ore body (sample 5–201, loc. DDH–19, table 25), and some 380 m north of the ore body (sample 1–480, loc. DDH–1). In contrast with the tremolite-actinolite rocks of the Pumpernickel Formation, in which the sedimentary fabric has been obliterated, the tremolite-actinolite-bearing rocks of the Battle Formation still retain some relict detrital clasts.

Tests with the heating stage yield very wide ranging filling temperatures for inclusions from this metamorphic zone. Inclusion types I and III fill in the 200°–400°C range; type II inclusions fill at somewhat higher temperatures, about 330°–500°C (table 25). These data suggest probably repeated trapping of fluids at any given locality within the zone as the rocks opened and closed to fluid circulation. There also may have been some necking and thermal resetting of the earliest inclusions to be trapped there. The highly variable vapor fractions in inclusions throughout these rocks suggest that the fluids there were boiling during much of their recrystallization. The fluids associated with these tremolite-actinolite-bearing rocks peripheral to the garnetite seem to be similar to those in the quartz-pyrrhotite-epidote veins that cut garnetite.

FLUIDS IN MICA-BEARING ROCK

The fluid inclusions from six mica-bearing rocks peripheral to the tremolite-actinolite zone were studied (table 25). Three samples are from the Battle Formation below the Golconda thrust west of the Virgin fault, one is from the Harmony Formation below the Golconda and west of the Virgin fault, and two are from the Battle Formation just east of the Virgin fault. Hydrothermal biotite is the dominant mica in five of these six rocks, although it is slightly altered to chlorite and carbonate in two (table 25). The sixth sample (5–831) has abundant hydrothermal white mica and associated

potassium feldspar, pyrrhotite, chalcopyrite, and some carbonate. We will discuss first the rocks with relatively abundant hydrothermal biotite.

Our microscopic examinations of rocks from the biotite zone, the lowest prograde metamorphic rocks around the skarn, suggest that the fluids present when this zone developed were boiling and at times saline. Tests with the heating stage on secondary inclusions in detrital quartz clasts and primary-pseudosecondary inclusions in hydrothermal quartz yield the following ranges in filling temperatures: type I, 265°–440°C; type II, 317°–480°C; and type III, 219°–382°C. Salinities of type III inclusions are inferred to have been in the range 31- to 39-weight-percent NaCl equivalent, determined from the dissolution temperatures of NaCl daughter minerals and referral to the system NaCl–H_2O (Sourirajan and Kennedy, 1962). As we pointed out above, however, some of these samples tested include some chlorite and carbonate that seem to be younger than the biotite. Nonetheless, we see no notable difference in the overall filling temperatures measured in chlorite-free versus chlorite-bearing biotitic rocks this suggests to us that the bulk of our data, even in the chlorite-bearing rocks, probably reflects the biotitic or potassic alteration that surrounds the skarn. For example, sample 8–809 (table 25) is probably representative of thermal conditions in the rocks during potassic alteration; its type I inclusions fill when heated to between 290° and 409°C (348°C mean), and its type III inclusions fill at lower temperatures, 246°–364°C (298°C mean). A reasonable estimate is that the fluids were boiling largely in the 350°–360°C interval, or roughly at the same temperatures indicated in the east ore body (Nash and Theodore, 1971).

Some of the highest filling temperatures measured at Copper Canyon are from a sample from the lower member of the Battle Formation (sample 5–831, table 25). The rock contains a quartz-white mica-potassium feldspar-pyrrhotite-chalcopyrite-carbonate alteration assemblage. As in the other mica- and tremolite-bearing rocks that enclose the skarn the fluids in this rock apparently were boiling. Maximum filling temperatures, although problematical, are estimated at 515°C and 530°C for type I and type II inclusions, respectively. The mean temperatures of filling measured for type I and type III inclusions are lower, 336°C for type I and 331°C for type III. Type II inclusions, however, fill on the average at temperatures of about 495°C, significantly higher than the other types. We are not sure why the gas-rich inclusions tend to have very high filling temperatures, but it may involve trapping of some low-density fluid above the boiling curve (see Roedder, 1967, fig. 12.2). In fact, most of the gas-rich inclusions around the skarn have filling temperatures significantly higher than those recorded in coexisting liquid-rich inclusions of the halide-bearing variety (type III, fig. 36). Most of these gas-rich inclusions were observed and their filling temperatures measured in samples from the altered granodiorite.

FLUIDS IN THE ALTERED GRANODIORITE

Studies with the heating stage were conducted on six rocks obtained from three drill holes into the granodiorite; two of the rocks studied include prominent veins that cut the granodiorite (BM–71, BM–224V; table 26). Secondary type I inclusions are fairly common in quartz phenocrysts in the altered granodiorite, as are primary-pseudosecondary type I inclusions in the quartz-sulfide veins of many different sizes and orientations that cut the granodiorite. Filling temperatures on a few secondary type I inclusions in plagioclase phenocrysts were also determined (sample BM–220, table 26). The type I inclusions in the granodiorite have an exceptionally wide range of filling temperatures, 249°–490°C; their filling tempera-

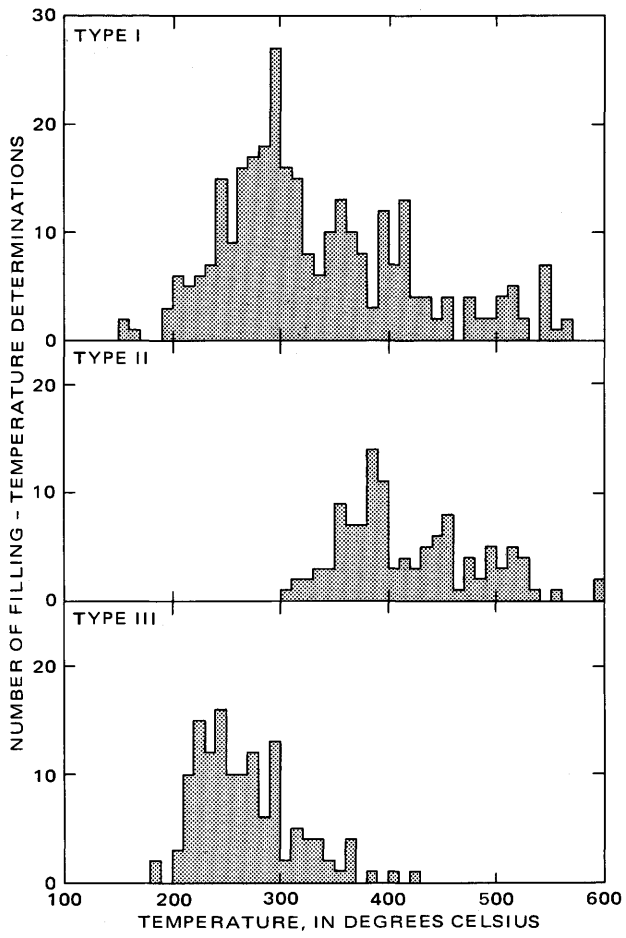

FIGURE 36.—Distributions of filling temperatures of type I, II, and III fluid inclusions.

tures, however, generally are between those of type II and type III inclusions in the same samples.

Gas-rich type II inclusions are very common in igneous and vein quartz in the granodiorite. Within small volumes of rock they dominate the inclusion population. Tests of type II inclusions with the heating stage yielded filling temperatures of 342° to 590°C in quartz phenocrysts from the granodiorite. Heating tests conducted on similar inclusions in quartz veins that cut the granodiorite (BM–71 and 224V) yielded about the same results (337°–550°C, table 26). Although there is some overlap in the temperatures of filling of type I and II inclusions in the granodiorite, on the whole, the two types have significantly different filling temperatures. The filling temperatures for type II inclusions in the granodiorite are close to the primary type I inclusions in andradite described above (table 25). These gas-rich inclusions in the granodiorite yield the highest filling temperatures measured in the Copper Canyon area. Moreover, these filling temperatures probably represent minimums because of the difficulty of resolving optically the precise merger of an expanding vapor bubble with an inclusion's wall. Calculated temperatures of 510°–550°C were obtained by Batchelder (1977) from $\delta^{18}O$ compositions of primary quartz and biotite from the granodiorite.

Type III inclusions from the granodiorite, the halide-bearing ones with relatively low gas volumes, have filling temperatures from 186° to 317°C (table 26). This temperature interval was typical of this type of inclusion throughout the study area (fig. 37). Most striking, however, is the fact that all of the filling temperatures of type III inclusions in the granodiorite are less than those of type II inclusions. It thus is critical to establish the time of the generation of gas-rich, type II inclusions relative to other events in the granodiorite, and to keep in mind that final emplacement of the granodiorite probably occurred after the bulk of the anhydrous andradite and diopside had crystallized in the skarn, as described above.

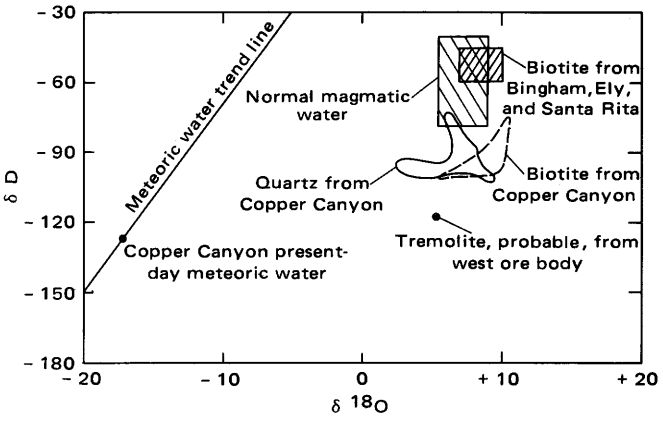

FIGURE 37.—Calculated isotopic compositions of water in isotopic equilibrium with quartz, biotite, and tremolite at inferred temperatures of crystallization at Copper Canyon. Range of calculated isotopic compositions of water in isotopic equilibrium with hydrothermal biotite at Bingham, Utah; Ely, Nev.; and Santa Rita, N. Mex.; determined by Sheppard, Nielsen, and Taylor (1971); and range of composition of water in isotopic equilibrium with normal magmas (H. P. Taylor, Jr., 1974).

TABLE 26.—*Temperature and salinity data from fluid inclusions in the altered granodiorite of Copper Canyon*

[At 25°C; I, low gas volume + liquid; II, high gas volume + liquid; III, low gas volume + halide daughter minerals; IV, liquid CO_2 bearing; S, secondary; PPS, primary-pseudosecondary]

Sample No.	DDH (pl. 1, fig. 3)	Depth (meters)	Mineral[1]	Type of inclusion	Age of inclusion	Homogenization temperature: Number measured	Homogenization temperature: Range (°C)	Homogenization temperature: Mean (°C)	Salinity (equiv. wt % NaCl)	Comments
BM 224	7	43.6	PQ	I	S	7	[2]249–490e	338		Granodiorite.
				II	S	9	367–510e	435		Do.
				III	S	5	186–238	212		Do.
BM 217	7	62.1	PQ	I	S	3	263–277	271		Do.
				II	S	7	350–479	427		Do.
				III	S	6	210–275	238		Do.
BM 231	7	97.6	PQ	II	S	6	389–500e	411		Do.
				III	S	7	227–289	260		Do.
BM 71	[3]981	216.	HQ	I	PPS	2	354–362	358		Vein.
				II	PPS	7	337–550e	376		Do.
				III	PPS	10	205–290	246	[4]36–44(5)	Do.
BM 60	981	116.	PQ	I	S	8	337–452	383		Granodiorite.
				II	S	7	342–510	411		Do.
				III	S	5	249–317	272		Do.
				IV	S	1	----	345		Do.
BM 220	21	83.	Pg	I	S	5	266–352	297		Do.
			PQ	I	S	5	275–414	328		Do.
				II	S	5	393–590e	516		Do.
BM 224V	7	43.6	HQ	I	PPS	2	288–370	329		Vein.
				II	PPS	2	450–485	468		Do.
				III	PPS	5	230–272	242	31–42(2)	Do.

[1]PQ, phenocrystic quartz; HQ, hydrothermal quartz; Pg, plagioclase.

[2]e, estimated temperature of homogenization from temperature at decrepitation, or rate of filling.

[3]DDH 981 collared about 100 m south of area of plate 1.

[4]In parentheses, number of determinations of the solution temperature of NaCl daughter minerals to yield the reported range of salinity of the fluid as estimated from the solution temperature by referring to experimentally determined stabilities in the system NaCl-H_2O.

Relations between silicate alteration, fluid inclusions, and deposition of sulfides in the veins are helpful in delineating the sequence of events in the granodiorite. One of the samples of porphyritic granodiorite cut by veins (BM–71, table 26) is particularly useful in this regard. This rock, from 216 m below the surface, is intricately cut by many quartz-biotite-potassium feldspar-pyrrhotite-chalcopyrite veins that typically measure 0.5–1.0 cm in width. In addition, the veins show a very slight alteration of some of their biotite to chlorite; there are also sparse grains of carbonate of probably the same general age as the chlorite. Away from the veins, the groundmass of the granodiorite contains intergrown quartz and potassium feldspar and interspersed wisps of hydrothermal biotite. Fluid inclusions are very abundant in these veins, roughly in the following proportions: type I, 45 percent; type II, 20 percent; and type III, 35 percent. The type II inclusions fill between 337° and 550°C, whereas the type III inclusions fill between 205° and 290°C. Within the veins themselves, it is virtually impossible to establish convincing age relations among the different types of inclusions. Nevertheless, some of the high-temperature type II inclusions in these veins seem to establish that they were trapped either penecontemporaneous with, or subsequent to, vein emplacement. Furthermore, the veins must have been emplaced after the surrounding granodiorite magma had solidified to the point where it could sustain brittle fracture. In addition, if these veins are the same age as the potassic alteration that cuts epidote rock in the nearby skarn, the gas-rich inclusions in the granodiorite must also postdate the andradite stages of the skarn's growth.

When we consider these filling-temperature data in light of geologic evidence that relatively low pressures prevailed at Copper Canyon during alteration and metallization (Nash and Theodore, 1971; see below), the type II inclusions in the granodiorite must reflect a low-density hot fluid trapped generally under conditions above the boiling curve (see Roedder, 1967, fig. 12.2). Such a low-density fluid, seemingly late relative to skarn development, may have evolved either because of a gradually decreasing rate of water recharge into the system (White and others, 1971), or because of a violent blowout of water as the system opened to the late Eocene or early Oligocene ground surface, sometime after the granodiorite's emplacement. Batchelder (1977) demonstrated, from the δD and $\delta^{18}O$ ratios of water calculated to be in equilibrium with biotites (primary and hydrothermal) and by similar ratios of water in fluid inclusions from hydrothermal quartz, the mixed magmatic-meteoric character of the fluids involved in the final crystallization of the granodiorite and in the development of the east ore body (fig. 37). His data suggest strongly that the fluid system at the sites of the ore bodies was open to the surface. Thus, the occurrence of high filling temperatures in a deposit and the overall thermal decline with time for many sulfide silicate systems (Sawkins, 1964; Lesnyak, 1965; Rye, 1966; Kelly and Turneaure, 1970) alone are not sufficient evidence to fix the inclusions' times of trapping, mainly because the volume of water available to transfer heat from the intrusion and rapid pressure variations produced by opening and closing of channels to the surface are important additional variables.

DISCUSSION

BAROMETRY

Fluid pressures during mineralization must reflect some combination of the stratigraphic cover at the time of mineralization and the degree of openness of the site to the ground surface. From geologic reconstruction of the stratigraphic section at Copper Canyon during late Eocene or early Oligocene time, we previously estimated a maximum cover of about 2.5 km and a more likely one of about 1.5 km (Theodore and Blake, 1975). Thus, the maximum pressures likely at the sites of mineralization in both the west and east ore bodies, reflecting purely lithostatic conditions, would then have been about 380 bars (assuming a 2.6-g/cm^3 density); whereas, if conditions were entirely hydrostatic, pressures would have been approximately 150 bars. Experimental studies to date have not yielded sufficiently sensitive geobarometers for the complex silicate-sulfide-fluid systems undergoing low-pressure metamorphism at Copper Canyon. We can under certain conditions, however, obtain information on the pressure during mineralization in such an environment from fluid inclusions by making appropriate assumptions and by referring to some experimentally studied fluid systems.

As described, there is abundant textural evidence for boiling in the primary fluid-inclusion populations of the mica (largely biotite), the tremolite-actinolite, and the diopside rocks around the garnetite. Phase proportions in the fluid inclusions of these rocks vary widely; liquid- and gas-rich inclusions are abundant. We found that, if we consider the type I inclusions with the most uniform vapor-liquid proportions in very small volumes of quartzose rock, these inclusions typically fill to liquid somewhere in the 360°–400°C interval (see above). This relation was found both in the widespread mineral zones that surround the garnetite and in narrow veins that cut the garnetite. However, the pressure and temperature of the boiling or two-phase (gas-plus-liquid) curve for the system NaCl-H_2O vary significantly with composition (Haas, 1971). We suggest an overall salinity for these fluids at Copper Canyon of

about 20-weight-percent NaCl equivalent (see also Nash and Theodore, 1971); we have no direct measurements of their salinities with the freezing stage. In a hydrostatic system open to the surface, a fluid of such a composition will boil at 360°C anywhere from the surface to a depth of about 1.9 km (153 bars); at 400°C, to a depth of about 3.3 km (182 bars). These depths are based on the calculations of Haas (1971), and in part on an extrapolation of his data. However, his calculations assume neither throttling points along a vertical column of brine, nor suspended vapor bubbles along the column. Nonetheless, the shallow depths of formation for the ore bodies inferred from these data are consistent with our geologic reconstruction of the cover rocks at the time of mineralization.

These barometric considerations for rocks around the west ore body, exclusive of the garnetite which we will discuss spearately below, are consistent with the calculations and interpretations made from the primary fluid inclusions by Nash (Nash and Theodore, 1971) that suggest boiling in the east ore body. Nash also considered the barometric implications of liquid carbon dioxide-bearing fluid inclusions with halide daughter minerals, and concluded that they were trapped at somewhat greater pressures of about 320 bars (Nash and Theodore, 1971). These higher pressures may reflect some periodic fluctuations of pressure in the east ore body because of the clogging of the channels by silica at some intermediate depths.

The primary-pseudosecondary type I inclusions in andradite from the garnetite clearly contrast with inclusions in all other rocks at Copper Canyon. The fluids associated with the crystallization of andradite apparently were not boiling; many have nearly uniform proportions of liquid and gas, and they fill to liquid when heated to about 500°±50°C (table 18). Such supercritical fluids must have been highly saline (Roedder, 1972). However, there must have been sufficient pressure on the fluid to retard physical separation of a vapor phase during the andradite's growth. If these fluids can be referred properly to the system NaCl–H_2O, a vapor pressure of about 380 bars, close to lithostatic for Copper Canyon (Nash and Theodore, 1971), could be maintained at 500°C (Sourirajan and Kennedy, 1962). From the same experimental work, we would also infer that such a fluid must have had a salinity of about 20-weight-percent NaCl equivalent. Most important, however, the fluid-inclusion data suggest that pressure in the skarn may have been near lithostatic during the early period of crystallization.

Although lithostatic pressures probably prevailed in the environment of the skarn during its early crystallization, in the east ore body, which formed after skarn development, fluid-inclusion relations are compatible with a boiling hydrostatic environment from the very onset of mineralization (Nash and Theodore, 1971). The high permeability of the intensely shattered rocks in the east ore body between the Hayden and Virgin faults (Theodore and Blake, 1975), and of the conglomerate of the Battle Formation, may have enhanced development of a hydrostatic environment. The pressures at both mineralization sites, however, may have been at some time between hydrostatic and lithostatic, depending upon the time and depth of sealing by silica. If we assume that the two geologically distinct sites finally sealed themselves at some intermediate depth (possibly 600 m as suggested previously (Nash and Theodore, 1971)), pressures may have approached about 270 bars in both ore bodies during their final stages of development. Moore and Nash (1974) likewise postulated an early lithostatic and a later hydrostatic pressure environment for the Bingham Canyon, Utah, porphyry copper deposit.

Any inclusion not trapped on the gas-liquid boundary (not boiling) requires a correction of its measured filling temperature. This correction is a function of the pressure on the fluid at the time of its trapping. At pressures of 380 bars and less during the skarn's development, conversion of filling temperatures (tables 25 and 26) to actual trapping temperatures for all inclusions not trapped on the boiling curve is accomplished by adding about 25°C, at most 50°C, to the observed filling temperatures (Lemmlein and Klevtsov, 1961).

THERMOMETRY IN OTHER SKARNS

Skarns as a group compose one of the most intensely studied rock types because of their commonly associated economic concentrations of metals and their well-preserved silicate and sulfide minerals that formed complexly in a magmatic-hydrothermal environment. In table 27 we present a short compilation of the temperatures of formation for different skarns related to ore deposits. Certainly some of the methods used previously to infer many of these skarns' thermal histories would now be in question (for example, the sphalerite geothermometer). Furthermore, we would have liked to compare our results to other fluid-inclusion studies of the skarn facies in porphyry copper districts elsewhere, but such studies are not known to us. Intensive study of the fluid inclusions in skarn deposits largely has been neglected; some exceptions are those by Lesnyak (1961, 1965), Kissling and Pomîrleanu (1970), Elinson and Alidodov (1973), and Sigurdson and Lawrence (1975). Nonetheless, several relations seem to emerge from the tabulation. Many skarns apparently had a very broad thermal range dur-

TABLE 27.—*Inferred formation temperatures and measured filling temperatures of early and late stages of mineralization in various skarn deposits*

[----, not determined; po, pyrrhotite; magn, magnetite; sl, sphalerite; gn, galena; hed, hedenbergite]

Fluid-inclusion studies

Deposit	Metals	Temperature (°C)		Minerals hosting inclusions	Reference
		Early	Late		
Tyrny-Auz, U.S.S.R.	Mo, W	350–400	50–80	Early garnet, late calcite	Lesnyak (1961).
Do.	do.	510–575	----	Fluorite and quartz	Lesnyak (1965).
Do.	do.	240–650	----	Garnet, decrepitation methods	Rodzyanko (1969).
Concepción del Oro, Mexico	Cu, Au	490–500	315–330	Late quartz	Buseck (1966).
Ocna-de Fier, Dognecea, Romania	W	483–504	232	Early andradite, late calcite	Kissling and Pomîrleanu (1970).
Chorulch-Dayron, U.S.S.R.	W	270	150–115	Early scheelite and garnet	Elinson and Alidodov (1973).
Maikhura, U.S.S.R.	W	550–600	160–300	Early hed, late quartz	Rakhmanov (1963).
Lebedinoye, U.S.S.R.	Au, U	430–590	----	Early calcite	Tugarinov and Naumov (1969).
Lespromkhozny, U.S.S.R.	----	890	>480	Early monticellite	Sinyakov (1967, 1968).
----, U.S.S.R.	F, Be	400–420	180–230	Early vesuvianite, late quartz	Kosals and others (1973).
South Yangitan, U.S.S.R.	Cu, Mo, Fe as magn	450–500	225	Early garnet and pyroxene; decrepitation methods	Mamontov (1968).
Tungsten Jim, Idaho	W	400–420	----	Early garnet, scheelite and diopside	Sigurdson and Lawrence (1975).
Kuga, Japan	W, Cu	308	140	Early hed, late fluorite; decrepitation methods	Imai and Ito (1959).

Other studies

Deposit	Metals	Temperature (°C)		Method of thermometry	Reference
		Early	Late		
Puyvalador, France	Fe as po	630	----	Wollastonite stability	Watters (1958).
Darwin, California	Pb, Ag, Zn	550	300	Sl geothermometer	Hall and MacKevett (1962).
Do.	do.	416,377	----	Fractionation of Cd and Mn in sl-gn	Hall and others (1971).
Mission, Arizona	Cu, Ag, Pb, Zn	800	250	Garnet isotropy	Gale (1965).
Meme, Haiti	Cu, Mo	550	250	Heat flow plus sulfide exsolution	Kesler (1968).
Keban, Turkey	Pb, Zn, W	700	225	do.	Kines (1969).
Christmas, Arizona	Cu, Zn	600–650	400	Referral to garnet syntheses	Perry (1969).
Sasca Montana, Romania	Cu, Mo	525–600	----	Orthoclase-microcline inversion	Constantinescu (1971).
Mt. Hope, Nevada	Zn, Pb, Cu	600	200	Referral to garnet syntheses	Missallati (1973).
Laurium, Greece	Fe as magn, Zn, Pb, Cu	500–600	----	----	Leleu and others (1973).
Pine Creek, California	W	>374	----	Critical temperature of water	Bateman (1965).
Kiangsu, China	Cu, Mo	>500	----	----	Ying-tsuen (1966).
Hope Valley, California	Sparse Fe as po	450–550	----	Referral to silicate equilibria	Kerrick and others (1973).
Linchburg, New Mexico	Zn, Pb, Cu	>450	----	Sl geothermometer	Titley (1961).

ing their hypogene stages, as did the skarn at Copper Canyon. Our heating tests in andradite have documented a minimum hypogene temperature interval of about 300°C, from 500°±50°C (primary type I inclusions in andradite) to 161°–216°C (late secondary type I inclusions in andradite associated with iron-oxide-filled microfractures). Second, there does not appear to be any significant thermal distinction of the copper-gold skarn in the porphyry copper environment at Copper Canyon from some of the lead-zinc skarns (Darwin, Linchburg) and the tungsten skarns (Pine Creek, Ocna de Fier, Maikhura). Zharikov (1968), in a compilation of the inferred formation temperatures of garnet in skarn, shows a 375°–550°C range by homogenization techniques, and a 380°–675°C range by decrepitation. However, contrary to our observations at Copper Canyon, he suggests that copper-gold skarn develops principally through the imposition of chalcopyrite (with sericitic or propylitic alteration) on early formed skarn. Thus, our filling temperatures of primary and pseudosecondary inclusions from the andradites at Copper Canyon seem consistent with the temperatures that many others have inferred for recrystallization of such pyroxene hornfels-facies skarns; they certainly are less than the temperatures of formation (over 750°C) inferred for the sanidinite-facies magnesian skarns (Winkler, 1965; Sinyakov, 1967, 1968; Pertsev, 1973).

PARAGENESIS AND MODEL OF SKARN DEVELOPMENT

From our mineralogic studies of rocks around the west ore body, the paragenesis of principal ore and gangue minerals is summarized diagrammatically in figure 38. The petrologic data detailed above from the zoned skarn allow us to develop a comprehensive petrogenetic model that includes relations among the granodiorite, the east ore body, and magmatic and meteoric fluids. One of the most important relations diagrammatically shown on figure 38 is the paragenetic position of an apparent second generation of hydrothermal biotite in the Copper Canyon area. Mineral textures in epidote rock (fig. 22) show that veins of this biotite cut epidote that is largely derived from andradite. This second-generation biotite, also partly shown as biotite halos around quartz-potassium-feldspar-sulfide veins that cut disseminated biotite, seems to have crystallized chiefly in the metasedimentary wallrock close to the granodiorite (fig. 4). Furthermore, second-generation biotite, or potassic alteration minerals, in the west ore body probably recrystallized along with the bulk of similar potassic assemblages in the granodiorite and in the east ore body. Thus, because potassic assemblages in the granodiorite seem to be largely postmagmatic (Roberts and Arnold, 1965; Nash and Theodore, 1971; Theodore and others, 1973; Theodore and Blake, 1975), emplacement of the granodiorite at its present level and final consolidation from a magma may have occurred sometime after the crystallization of andradite and before the bulk of the ore was deposited in the east ore body. Allcock (1974) also suggested that skarn crystallization was followed by the intrusion of salic porphyries at the Gaspé Copper deposit, Quebec. Accordingly, a highly simplified

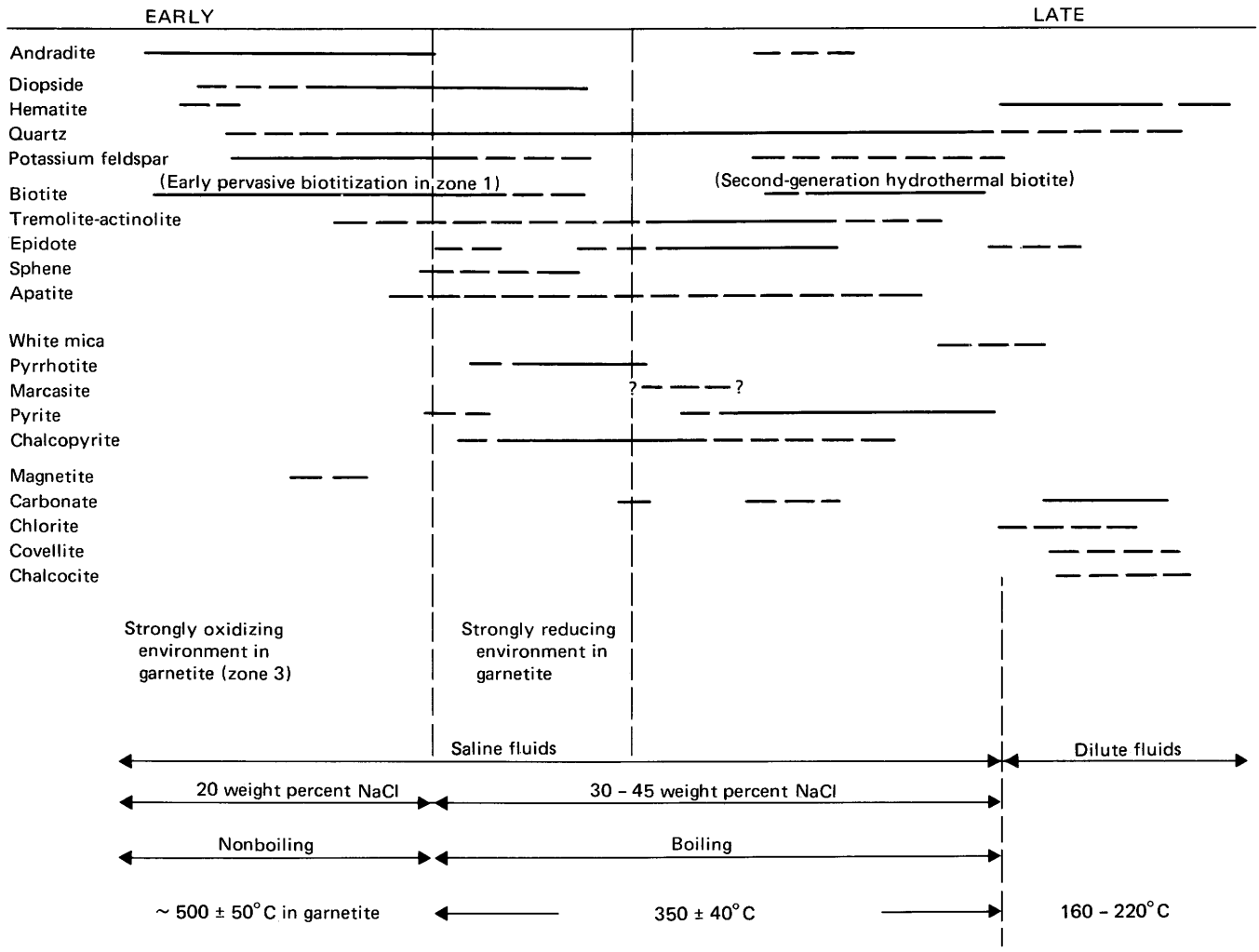

FIGURE 38.—Paragenesis of principal ore and gangue minerals. Minerals commonly present indicated by solid line; minerals rarely or sparsely present by a dashed line.

sequence of geologic events at Copper Canyon might have been:(1) recrystallization of andradite-diopside in the skarn and a widespread halo of early potassic assemblages, (2) rise of the granodiorite magma to where it is now exposed, and (3) growth of a second generation of potassic mineral assemblages partly in the west ore body, but especially concentrated in the east ore body and in the granodiorite (fig. 39). The largest tonnage of

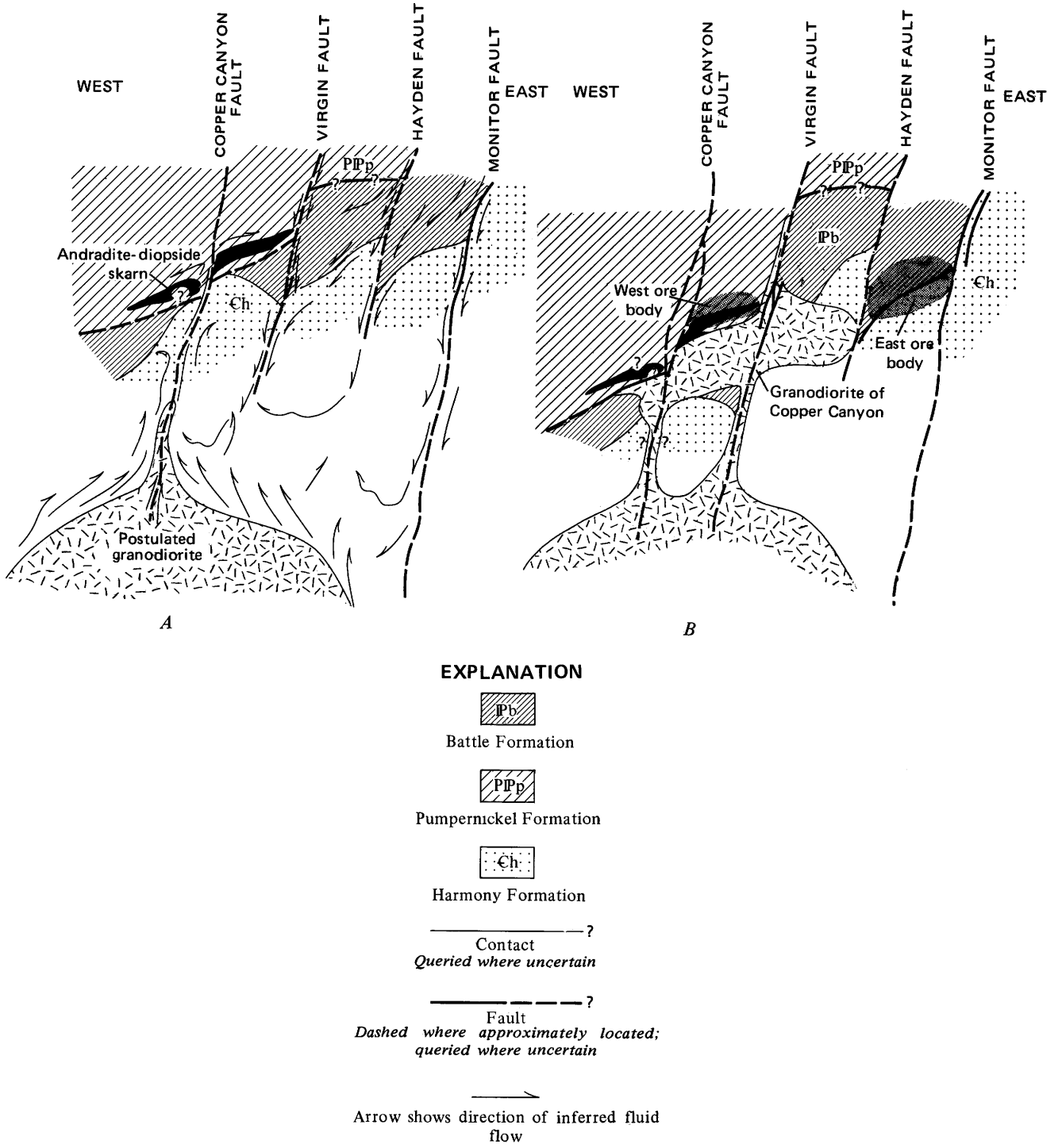

FIGURE 39.—Cross section of model proposed for sequential formation of ore bodies at Copper Canyon. *A*, Development of andradite-diopside skarn early in history of porphyry copper system with heat supplied from deeply buried intrusion. *B*, Subsequent development of east ore body mostly after final emplacement of granodiorite of Copper Canyon.

ore at Copper Canyon formed in the east ore body during this second period of potassic alteration; it may reflect a disruption of established fluid flow in the rocks by the magma. We will now attempt to relate more fully the sequential development of sulfide-silicate relations within the framework of a working model of skarn development.

A review of the two-end-member processes of contact metasomatic zonation, the infiltration and diffusion models as described by Korzhinskiy (1964), suggests that the skarn at Copper Canyon shows characteristics of both models. An infiltration model of skarn formation proposes that physical transport of the chemical components needed in a skarn deposit takes place by a low-viscosity aqueous fluid that is moving through the available pore spaces. The driving force for infiltration would be a pressure gradient in the aqueous fluid (Hofmann, 1972). In a diffusion model, the chemical components themselves diffuse through a static medium along a chemical potential gradient. The medium presumably is also an aqueous fluid as in the infiltration case. The chief criterion to distinguish zoned infiltration from diffusion skarns is the presence in the diffusion skarn of solid solution minerals showing gradual changes in composition through the zones. In addition, Korzhinskiy (1964) points out that contact metasomatic reaction zones that are attributed primarily to diffusive processes are quite narrow and are generally restricted to zones measured in millimeters even in high-pressure and -temperature geologic environments. The persistence of extreme sharp variation and oscillation in chemical compositions and optical properties across micrometer-sized domains of individual andradite crystals at Copper Canyon (fig. 15) strongly suggests infiltration phenomena were dominant in the garnetite during the andradite's growth. Notwithstanding the occurrence of some infiltration phenomena, there are still several models possible to explain the present geometry of the metamorphic zones in the skarn at Copper Canyon. The zones might reflect passage of fluids during several separate stages of skarn growth; an early fluid may have metamorphosed calcite-rich beds to andradite assemblages and dolomite-rich ones to diopside assemblages. In this model, there would be no genetic tie by metasomatic zoning between garnetite and diopside rocks, and after the andradite and diopside zones had already crystallized, a separate pulse of fluids must be invoked to yield the tremolite-actinolite and epidote zones. Fluids related to this pulse would have been emplaced initially along the outer margins of the diopside rock and subsequently have migrated outward from there. However, we cannot completely rule out the possibility that some diffusion phenomena contributed to the growth of the skarn.

The parageneses and symmetric zonation of mineral assemblages about the flat-lying skarn at Copper Canyon suggest that some growth may have involved diffusion metasomatic zonation. The mineral zonation in the skarn is symmetrical about a roughly horizontal plane that bisects the main mass of garnetite (fig. 3). Our consideration of diffusion as a skarn-producing process is based on the experimental data of Vidale (1969). Vidale produced zoned mineral assemblages typical of skarns in the system $K_2O-CaO-MgO-SiO_2-KCl-(\pm CO_2)$ at elevated temperatures and pressures (table 28). Each of her experimental capsules contained calcite in contact with a synthetic pelite, a mixture of muscovite, phlogopite, and quartz; she demonstrated differential movement of potassium, calcium, magnesium, and probably aluminum through chloride-rich fluids during the heating of the capsules. Magnesium moved toward the calcite, and calcium moved toward the pelite. The final configuration of diopside in some of these experimental runs, where it appears in the former calcite zone and where large amounts of diopside and tremolite grew in the adjacent pelite, have some bearing on the geometry of mineral zonation at Copper Canyon. From these experimental results, we infer that the outer margins of diopside-bearing rock in the Pumpernickel Formation mark the outermost former presence of magnesian and possibly iron-bearing carbonate-rich sedimentary beds at Copper

TABLE 28.—*Diffusion of minerals in zoned capsules*

[Capsules treated with 0.4N KCl, kept at 600°C and 2,000 bars for 28 days by Rosemary Vidale. Modified from Vidale (1969)]

Initial configuration:

Calcite	Muscovite Phlogopite Quartz	Quartz

Final configuration:

———	Calcite
—	Calcite-wollastonite
—	Calcite-wollastonite-diopside
—	Diopside-tremolite-quartz-(anorthite)
—	Tremolite-quartz-(anorthite)
—	Tremolite-phlogopite-quartz-(anorthite)
—	Phlogopite-quartz-(anorthite)
———	Phlogopite-quartz-sanidine-(anorthite)

Displacement:

K	→	No K-bearing minerals remain in the left half of the former "pelite" zone, and a high concentration of sanidine appears in the right end.
Ca	→	Ca-bearing minerals appear throughout the former "pelite" zone.
Mg	←	Diopside appears in the former calcite zone and a high concentration of diopside and tremolite in the left end of the former "pelite" zone.
Si	←	Diopside and wollastonite appear in the former calcite zone.
Al	←	Anorthite may be present in the former calcite zone.
H	←	H may have moved to balance the large shift of K and Ca.

Canyon. The first-heated fluids to arrive at the general level of the relatively impervious argillite of the Pumpernickel Formation also may have promoted some chemical reaction between the argillite and carbonate-rich beds. The presence of sphene throughout the diopside rock and much of the garnetite suggests that rather impure carbonate rocks may have been their unmetamorphosed equivalents (Korzhinskiy, 1964).

Paragenetic relations at Copper Canyon suggest also that some diffusion, especially of magnesium may have occurred. A simplified schematic model of the zonation at Copper Canyon shows the sequence of replacement and veining we observed (fig. 40). Diopside rock of zone

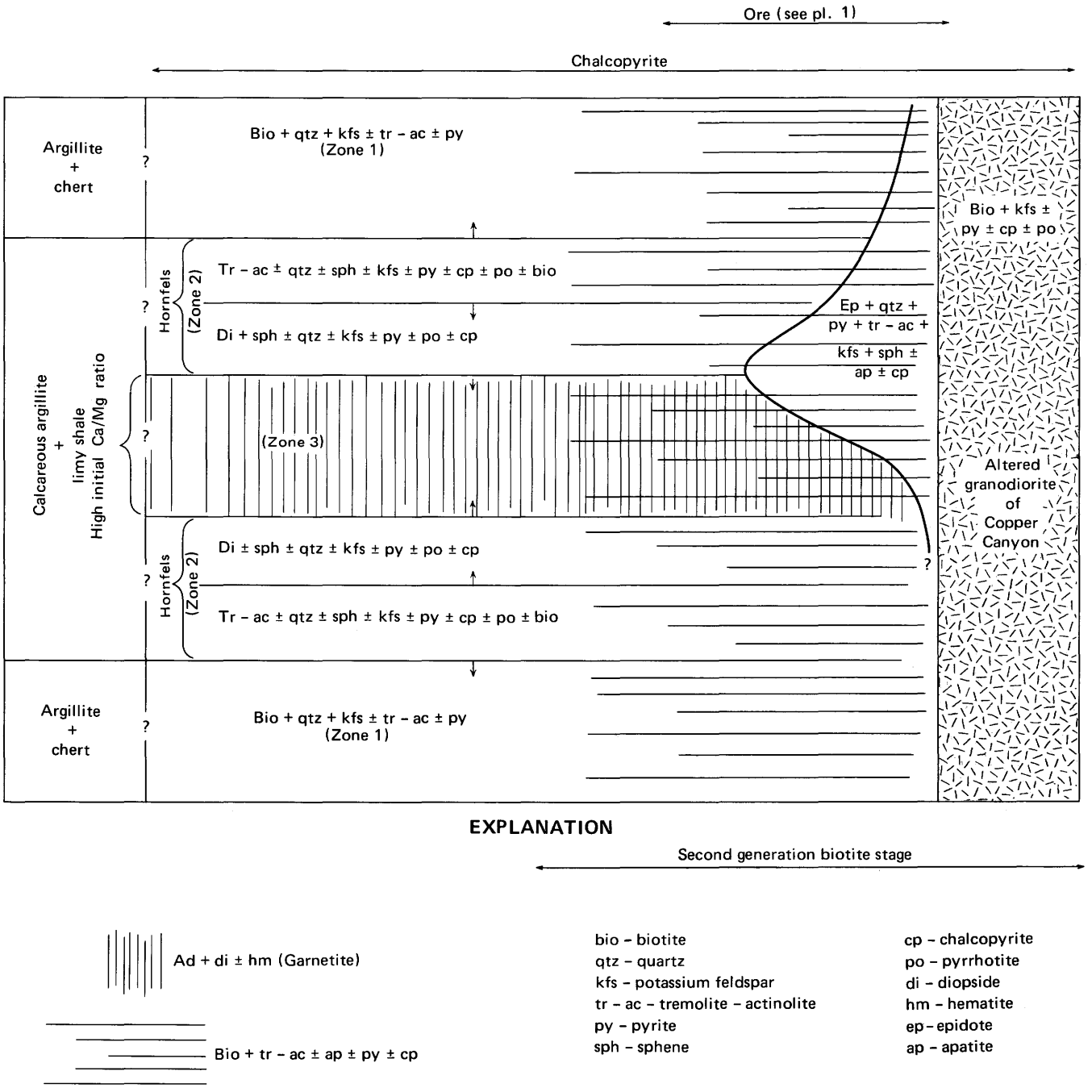

FIGURE 40.—Schematic model of metasomatic zonation at Copper Canyon. Arrows show direction of growth of major zonal indicator minerals.

2 has grown or continued to grow at the expense of zone 3, the garnetite (at least locally). In addition, there is textural evidence in the rocks that the other major part of zone 2, tremolite-actinolite rock, grew largely at the expense of diopside rock, but also at the expense of biotite-potassium feldspar assemblages locally in zone 1. Unequivocal temporal relations between the garnetite and diopside rock are difficult to establish, but the few observations we have suggest some diopside rock must have grown at the expense of garnetite. Further,

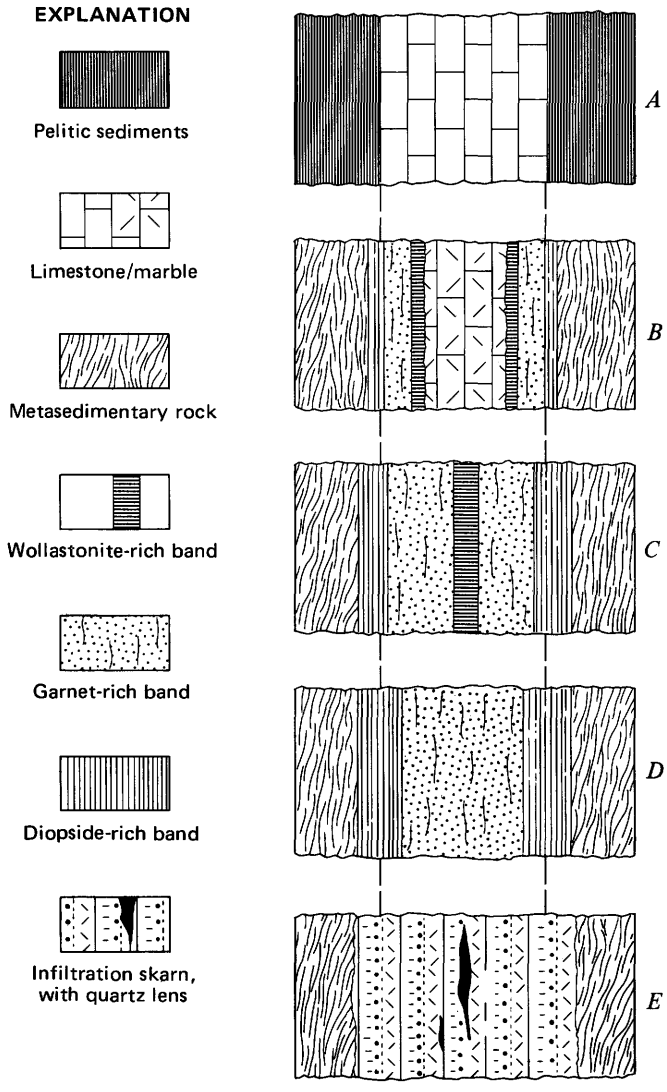

FIGURE 41.—Progressive development of diffusion skarn at Garnet Hill, Calif., by reaction of limestone with pelitic sedimentary rocks. *A*, Original sediments. *B*, Partial metamorphism, revealing development of sequential mineralogic bands. *C*, Carbonate entirely consumed, mineralogic bands continue to migrate inward. *D*, Disappearance of early formed wollastonite bands. *E*, Conversion of original diffusion skarn to coarse infiltration skarn through interaction with magamatically derived aqueous solutions. From Brock (1972).

these temporal relations are supported by the sequence of crystallization within the garnetite: first, andradite (Ad_{99}) and some diopside crystallized; second, slightly more grossularitic andradite and larger amounts of diopside; and third, diopside, quartz, and sulfides, possibly as open cavity fillings. The variable sequences of zonation and paragenesis alert us that all these rocks did not develop by simple unidirectional infiltration. In infiltration skarns, outer mineralogic zones are replaced successively by inner ones because the infiltration fronts must all travel in the same direction (Hofmann, 1972). Nokleberg (1970) illustrated such a uniform sequence of replacement in an infiltration skarn in the central Sierra Nevada, Calif.

Geologic relations described by Brock (1972) at the Garnet Hill skarn, also in the central Sierra Nevada, are relevant to the genetic model we propose for the skarn at Copper Canyon. At Garnet Hill, some diffusion skarn apparently developed where limestone beds reacted with adjacent pelitic sedimentary rocks. Some aspects of the geometry, mineralogy, and stages of paragenetic evolution of this skarn body (fig. 41) are remarkably similar to the skarn at Copper Canyon. Two salient points must be stressed. First, comparison of Brock's mineral stages *C* and *D* (fig. 41) shows continued growth of the diopside-rich band after the garnet-rich band had ceased to migrate outward. We found a similar temporal relation between the garnetite and diopside rock at Copper Canyon. Second, consumption of wollastonite-rich zones early in the diffusion process as Brock suggests (stages *B–D*, fig. 41) may explain the absence of wollastonite at Copper Canyon, if we further assume that the environment of the skarn at some time reached the wollastonite stability field. Among the notable differences between the skarns at Garnet Hill and Copper Canyon is the apparent growth of the garnetite at Copper Canyon almost exclusively by infiltration. We envision that this occurred when diffusion predominated in the surrounding rocks nearby.

IMPLICATIONS OF EXPERIMENTAL STUDIES

Many experimental and theoretical investigations bear on the petrogenesis of the skarn at Copper Canyon. The stability of andradite-quartz fluid relative to fugacity of oxygen and temperature suggests that a strongly oxidizing environment (fig. 38) may have prevailed during the growth of andradite-quartz assemblages (Gustafson, 1970; Liou, 1974). From the calculations of Kerrick (1970) and the experimental data of Gordon and Greenwood (1971), we might also infer that the andradite assemblages at Copper Canyon crystallized initially with very restricted molecular

fractions of carbon dioxide in the coexisting fluid phase. Their study in the system $CaO-Al_2O_3-SiO_2-H_2O-CO_2$ carried out between 400° and 900°C at 2 kilobars suggests that at temperatures below 600°C grossularite is restricted to fluids containing less than 15 molecular percent CO_2. The primary-pseudosecondary fluid inclusions in andradite fill at 500°±50°C, and they apparently do not contain any liquid carbon dioxide as a separate phase at 25°C, suggesting a very low carbon dioxide content of these fluids. In addition, these fluids, rich in iron, must have had a high Ca+Mg/K ratio that rapidly diminished with the deposition of calcium and iron in andradite, and calcium and magnesium in diopside. Nonetheless, carbon dioxide may have been very important in the generation of the skarn. Nokleberg (1973) suggests that carbon dioxide from the breakdown of carbonate may provide a source for some of the oxygen needed to yield andradite with its high Fe^{+3}:Fe^{+2} ratio. Possibly an early dissociation of mixed magmatic and meteoric H_2O and removal of molecular hydrogen from the site of the developing andradite-diopside skarn also may have maintained the oxidizing environment that yielded the andradite (Czamanske and Wones, 1973). During crystallizations of andradite and diopside, any magmatic component of these mixed waters most probably would have been derived from our postulated deep granodiorite (fig. 39*A*).

Physical and chemical conditions must have changed dramatically in the skarn as it evolved. We inferred previously that the overall fugacities of oxygen of the ore-forming fluids during the ore-forming stages at Copper Canyon generally must have been low relative to those at most other porphyry copper districts. This is primarily because of the abundance of pyrrhotite-chalcopyrite assemblages at Copper Canyon, and because this assemblage is known to crystallize generally under reducing conditions (see Barnes and Czamanske, 1967). Nokleberg's (1973) studies show also that at low initial fugacities of oxygen a carbon-hydrogen-oxygen fluid will be dominated by methane and molecular hydrogen, both of which have been detected elsewhere in gaseous inclusions in andradite (Elinson and Polykovskiy, 1967). In the skarn at Copper Canyon, pyrrhotite-chalcopyrite assemblages and low oxygen fugacities became dominant only during deposition of sulfides that generally followed the crystallization of most of the andradite. Certainly the pH of the fluids in the general area of the skarn was also changing continuously as the skarn evolved, possibly from an early slightly alkaline environment to a late slightly acidic one. Magnetite, common in many other skarn deposits, is exceptionally rare in and around the east and west ore bodies at Copper Canyon; it most likely forms under alkaline conditions (Barnes and Czamanske, 1967). The low fugacity of oxygen in the fluids associated with the crystallization of pyrrhotite-chalcopyrite in the skarn may reflect a continued recharge of reduced fluids into the environment of the skarn concomitant with a decrease in the oxygen content of any fluids remaining from the prior crystallization of andradite (see Helgeson, 1970). Temperatures were probably lower by then, probably about 320°±40°C from our filling temperature measurements. Chalcopyrite has a 557°C upper stability limit (Pankratz and King, 1970), but the mineral assemblage chalcopyrite-pyrrhotite is generally thought to reflect formation at temperatures less than this. We suggested previously (Theodore and Blake, 1975) that this sulfide assemblage may have crystallized in the east ore body at temperatures less than 334°C from the experimental studies of Yund and Kullerud (1966). More recent data, however suggest that chalcopyrite-pyrrhotite may form stably at temperatures greater than 334°C. The assemblage chalcopyrite-pyrrhotite is stable to slightly less than 500°C on the CuFe-S join in the system Cu-Fe-S according to Barton (1973). At these temperatures, pyrrhotite would contain about 48.5 atomic percent sulfur. Although we have not determined compositions of pyrrhotite from the west ore body, no pyrrhotite found after intensive study of them from the east ore body contained more than 47.3 atomic percent sulfur (Theodore and Blake, 1975). Such a pyrrhotite would have formed stably at some temperature less than 350°C, if the rock system under question can be referred properly to the CuFe-S join in the Cu-Fe-S system.

The fluids were certainly much more saline during deposition of the sulfides than they were prior to sulfide deposition, possibly reaching 30 to 45 weight percent NaCl equivalent locally (fig. 38). Although much of the pyrrhotite and chalcopyrite in the skarn occurs as fracture- and open-cavity fillings, most of the abundant pyrrhotite near the granodiorite and peripheral to the epidote-pyrite rock reflects a replacement of andradite by pyrrhotite with diopside still apparently stable. Lindner and Gruner (1939) showed experimentally that garnet can break down under reducing conditions, and Burt (1972b) further suggested that early formed silicates in skarn could exert a chemical control on later deposition of sulfides.

Final consumption of sedimentary calcite, conceivably together with the cessation of escape of hydrogen as the ore sites were sealed to the surface by silicate deposition, is an attractive hypothesis to explain the transition from a largely oxidizing environment (andradite) to a reducing one (pyrrhotite-chalcopyrite). Timing of geologic events around the skarn, however,

seems to argue against the importance of hydrogen build-up in such a decrease in the oxygen fugacity there. From our fluid-inclusion relations detailed above, we postulated that a lithostatic regime (closed to the surface) at the time of the growth of andradite was followed by hydrostatic conditions during subsequent mineralization stages in the skarn. Thus, a significant build-up of hydrogen around the skarn by a sealing of channels does not seem likely because the channels to the surface were most likely open when most of the pyrrhotite and chalcopyrite was being deposited.

The experimental studies of Barnes and Czamanske (1967) suggest that the strongly reducing environment during the chalcopyrite-pyrrhotite stage (fig. 38) was followed by an increase, perhaps gradual, in the fugacities of both sulfur and oxygen during the epidote-pyrite stage. Chalcopyrite was still stable, but it was deposited in diminishing amounts.

SOURCES OF THE FLUIDS

The overall extent of the garnetite and diopside rock places constraints on any inferred source of the fluids associated with their crystallization, and also on the direction of the fluid transport. The absence of andradite and diopside from the east ore body (Nash and Theodore, 1971; Theodore and Blake, 1975; see above) effectively rules out the adjacent granodiorite, or some other geologic agent at the present position of the granodiorite, as the source of the skarn-forming fluids. If these fluids were derived from the adjacent granodiorite, then the Battle Formation in the east ore body and far beyond would have been converted to mineral assemblages typical of skarn. Andradite and diopside would have formed in this tectonic block east of the Virgin fault much farther than their known extent in the Pumpernickel Formation, probably in the porous calcareous conglomerate of the Battle Formation there.

Our genetic model for the skarn must also account for some widespread very high filling temperatures (500°±50°C) centered on a tabular block of rock of the Pumpernickel Formation in contrast with temperatures of about 310°–400°C (Nash and Theodore, 1971) in the east ore body. We suggest much of the highly fractured Battle Formation between the Hayden and Monitor faults (see Theodore and Blake, 1975, pl. 1), including intensely broken rock near the Virgin fault, acted as a conduit for descending, relatively cool meteoric fluids. We further suggest that these fluids were than heated somewhere below the present position of the skarn near a crystallizing and rising magma, and that they mixed with fluids partly equilibrated with magmatic silicates (fig. 39*A*). These mixed fluids then migrated upward largely along the Copper Canyon–West Ridge fault system (pl. 1). Initial contact of the fluids with carbonate to form skarn may have taken place just west of the main mass of the west ore body. It is probable that fluid flow eventually established a roughly east-west convecting system (fig. 39*A*), somewhat similar to the models proposed by White (1968), by filtration mainly through the rocks where the garnetite was crystallizing. Initial studies of the stable isotopes ^{18}O and D in tremolite and quartz from the skarn seem to confirm the isotopically light nature of the fluids involved in their crystallization.

The $\delta^{18}O$ and δD values from one sample of tremolite from the west ore body are +9.4 and −150, respectively. This tremolite is colorless in thin section, with a Mg/Mg+Fe ratio of 0.90 (N. G. Banks, written commun., 1975), and it occurs in a 2-cm-wide reaction rim about a 0.5-cm vein of quartz, blue-green tremolite-actinolite (Mg/Mg+Fe = 0.54 to 0.58), pyrite, sphene, and some potassium feldspar near the wall of the vein. The wallrock is a buff-colored diopside rock made up of diopside, sphene, quartz, and sparse pyrite. Fluid inclusions are very abundant in the vein quartz, and their vapor proportions are extremely variable, a relation that suggests that fluids were boiling during emplacement of the vein. Heating tests of the inclusions yield filling temperatures of 220° to 370°C, from which we suggest that temperatures of about 350° to 400°C most likely approximated initial thermal conditions during the vein's emplacement. A δD value of −117 for water in equilibrium with tremolite was calculated from these data, using the hydrogen isotope fractionation data of Suzuoki and Epstein (1976). This is undoubtedly a minimum value because the actual δD value of these calculated waters would probably be somewhat greater owing to the presence of fluorine in the system (J. R. O'Neil, oral commun., 1975). Oxygen isotope fractionation factors between tremolite and water have not yet been determined experimentally. Nonetheless, we infer the oxygen isotopic composition of the fluids associated with the crystallization of tremolite from the $\delta^{18}O$ composition of the coexisting vein quartz that is paragenetically the same age as the tremolite. Quartz from the tremolite-actinolite-bearing vein has a $\delta^{18}O$ value of +12.2. The calculated value of $\delta^{18}O$ for water in isotopic equilibrium with this quartz is +5.3. We suggest that this value closely approximates the oxygen isotopic composition of fluids during the vein's emplacement and penecontemporaneous crystallization of its tremolite-bearing reaction zone. At some time, then, isotopically light fluids or fluids probably with a meteoric component must have been involved in the generation of the skarn.

The participation of meteoric fluids in the develop-

ment of skarn is not a new idea. Ransome (1904, p. 153) concluded that some fluids other than purely magmatic ones must have been involved in the formation of the copper-bearing skarn in the Bisbee, Ariz. porphyry copper deposit:

*** Water moving along the lower beds, say at the base of the Abrigo limestone, would reach the Dividend fault and the porphyry at a depth of over 1,000 feet below the deepest ore bodies now known. It would then tend either to rise, by hydrostatic pressure along the Dividend fault and the contact with the porphyry, or it would tend to sink deeper into the earth along these structures. Whether it would follow either or both of these courses would depend upon the adjustment of a number of factors, such as hydrostatic head, volume of flow, relative size of channels, and difference in temperature. If the porphyry mass still retained a part of its original heat of intrusion, the waters would have some of this heat imparted to them and tend to rise. If in addition, solutions, presumably heated, were rising from depths below the bottom of the Paleozoic syncline through the Dividend fault and along the contact of the porphyry and limestone, then there would be a mingling of solutions and localized chemical activity in the vicinity of the fault and the porphyry.

It is accordingly advanced as a tentative hypothesis that the deposition of the cupriferous pyrite and the metamorphism of the limestone, schist, and porphyry was affected by the mingling of solutions from different sources in the vicinity of the Dividend fault and of the Sacramento Hill porphyry. The principal function of the porphyry is believed to have consisted in supplying heat to such solutions as rose from great depth and in thus determining the locus of the chemical activity that resulted in the deposition of the ore.

The source of the ore materials is not known. They may have risen through the Dividend fault from depths far below the bottom of the syncline of Paleozoic rocks. They may have been collected by solutions moving through one or more of the Paleozoic limestones on their way down to the locus of depositon. Lastly, they may have been derived from both sources.***

Bartholome (1970) also discusses the diverse origins of fluids in the formation of skarn deposits. Recently, B. E. Taylor (1974) inferred from the hydrogen isotope ratios in amphibole and in water of fluid inclusions in quartz that meteoric fluids may have been involved significantly during the recrystallization of skarn in the Osgood Mountains 70 km northwest of Copper Canyon.

SUGGESTIONS FOR EXPLORATORY PROGRAMS

The occurence of copper-gold-silver ore as widespread replacement deposits in skarn belonging to the Pumpernickel Formation suggests the possibility that other such deposits may occur in the district primarily in four other areas where the geology is favorable and carbonates are likely to occur. Areas that might be considered include the contact aureoles around (1) the granodiorite of Trenton Canyon, 10 km northwest of Copper Canyon (see Roberts, 1964; Theodore and others, 1973) and (2) the granodiorite of the Modoc mine area, 5 km west of Copper Canyon. This granodiorite intrudes rocks, locally carbonate-rich, belonging to the Trenton Canyon Member of the Middle Pennsylvanian and Lower Permian Havallah Formation (Roberts, 1964). The Havallah Formation lies disconformably above the Pumpernickel Formation. Commercial skarn deposits may also have developed anywhere in (3) rocks within an approximately 3-km-wide east-west-trending belt between the granodiorite of the Modoc mine area and the altered granodiorite of Copper Canyon. Gravel-covered areas along this belt should be tested carefully by geophysical methods. Other possibilites for small but possibly high-grade mineralized limestone bodies are in the Scott Canyon Formation, east and northeast of Copper Canyon.

Exploration programs for a skarn ore body in the district should expand beyond the recognition of direct spatial relations at the surface between intrusions and carbonate-rich wallrock, on the basis of our studies at Copper Canyon. Indeed, Umpleby (1916) pointed out many years ago that in many skarn deposits the ore develops preferentially on the carbonate side of garnet-rich rock rather than on the side of the intrusive body. However, if our hypotheses of the evolution of the porphyry system at Copper Canyon are generally correct, then a potential target is a porphyry system that evolved through the development of mineralized skarn without subsequent emplacement of an intrusion to present erosion levels. These targets conceivably might make up a fairly large tonnage although at low grade, because they most likely would not have had many postanhydrous stages of alteration. For example, although the known ore in the west ore body composes only about 4 million tonnes, a minimum of about 66 million tonnes at 0.15-weight-percent copper equivalent can be reasonably inferred in mineralized skarn between the Virgin and Copper Canyon fault systems. Geophysical methods might be the best method to search for such concealed skarn deposits in the district. In addition, the presence of the upper chert unit of the Pumpernickel Formation, which acted as an apparent barrier to the migration of ore-forming fluids at Copper Canyon, should also be considered in exploration programs.

Analyses of minor metals in soil around the west ore body indicate that gold, silver, copper, lead, arsenic, and possibly mercury are potential indicator elements for underlying copper ore in skarn, and that soil samples may actually have greater concentrations than bedrock. However, at Copper Canyon there is only a very small contrast between areas over economic skarn and adjacent areas over noneconomic skarn. These areas over noneconomic skarn are of substantial size compared to the ore-bearing area. However, the contrast in soils between these areas in the vicinity of the skarn (both economic and noneconomic) and areas

some distance away known to be barren is large; presumably geochemical sampling of large areas should show anomalies in the vicinity of metallized skarn. However, considering the high-background halo of minor metals in soil around the west ore body (inferred to extend at least 0.5 km out from ore according to our geochemical sampling of rock, fig. 25), the massive sampling of soils needed most likely would not produce targets in addition to those resulting from detailed field mapping and interpretation. Geochemical sampling of soil and rock probably would not have directed an exploration geologist's attention to either of the known ore bodies at Copper Canyon.

REFERENCES CITED

Ageton, R. W. and Greenspoon, G. N., 1970, Copper, *in* Mineral facts and problems: U.S. Bur. Mines Bull. 650, p. 535–553.

Allcock, J. B., 1974, Gaspe Copper—A Devonian skarn/porphyry copper complex (abs.): Geol. Soc. America Abs. with Programs, v. 6, no. 7, p. 632.

Andrews-Jones, D. A., 1968, The application of geochemical techniques to mineral exploration: Colorado School Mines Mineral Industries Bull., v. 11, no. 6, p. 1–31.

Banks, N. G., 1976, Halogen contents of igneous minerals as indicators of magmatic evolution of rocks associated with the Ray porphyry copper deposit, Arizona: U.S. Geol. Survey Jour. Research, v. 4, no. 1, p. 91–118.

Barnes, H. L., and Czamanske, G. K., 1967, Solubilities and transport of ore minerals, *in* Barnes, H. L., ed., Geochemistry of hydrothermal ore deposits: New York, Holt, Rinehart, and Winston, Inc., p. 334–381.

Bartholome, Paul, 1970, Minerais et skarns dans les auréoles de métamorphisme: Mineralium Deposita, v. 5, no. 4, p. 345–353.

Barton, P. B., Jr., 1973, Solid solutions in the system Cu-Fe-S. Part I; The Cu-S and CuFe-S joins: Econ. Geology, v. 68, no. 4, p. 455–465.

Batchelder, J. N., 1973, A study of stable isotopes and fluid inclusions at Copper Canyon, Lander County, Nevada: California State Univ., San Jose, M.S. thesis, 92 p.

———1977, Light-stable-isotope and fluid-inclusion study of the porphyry copper deposit at Copper Canyon, Nevada: Econ. Geology, v. 72, no. 1, p. 60–70.

Batchelder, J.N., Theodore, T. G., and Blake, D. W., 1976, Stable isotopes and geology of the Copper Canyon porphyry copper deposit, Lander County, Nevada: New York, Am. Inst. Mining Metall. Petroleum Engineers Ann. Mtg., 1976, Las Vegas, Nevada, 17 p.

Bateman, P. C., 1965, Geology and tungsten mineralization of the Bishop district, California, *with a section on* Gravity study of Owens Valley *by* Pakiser, L. C., and Kane, M. F., *and a section on* Seismic profile *by* Pakiser, L. C.: U.S. Geol. Survey Prof. Paper 470, 208 p.

Beall, J. V., 1973, Copper in the United States—A position survey: Mining Eng., v. 25, p. 35–47.

Beaman, D. R., and Isasi, J. A., 1970, A critical examination of computer programs used in quantitative electron microprobe analysis: Anal. Chemistry, v. 42, no. 13, p. 1540–1568.

Beeson, M. H., 1967, A computer program for processing electron microprobe data: U.S. Geol. Survey open-file report, 40 p.

Blake, D. W., 1971, Exploration aspects of the Copper Canyon porphyry copper deposit, Lander County, Nevada—Pt. I, Geology and geometry: Am. Inst. Mining Metall. Petroleum Engineers, Pacific Southwest Mineral Industry Conf., Reno, Nev., 1971, Program, p. 9.

Blake, D. W., Theodore, T. G., and Kretchmer, E. L., 1977, Alteration and distribution of sulfide mineralization at Copper Canyon, Lander County, Nevada (abs.), *in* Porphyry Copper Symposium, 1976: Tucson, Ariz. (cosponsored by Arizona Geol. Soc. and Univ. Arizona), p. 15.

Borg, I. Y., and Smith, D. K., 1969, Calculated X-ray powder patterns for silicate minerals: Geol. Soc. America Mem. 122, 896 p.

Boyd, F. R., 1969, Electron-probe study of diopside inclusions from kimberlite: Am. Jour. Sci., v. 267–A (Schairer Volume), p. 50–69.

Brock, K. J., 1972, Genesis of garnet skarn, Calaveras County, California: Geol. Soc. America Bull., v. 83, no. 11, p. 3391–3404.

Burt, D. M., 1972a, The facies of some Ca-Fe-Si skarns in Japan: Internat. Geol. Cong., 24th, Montreal, Canada, 1972, Proc., Sec. 2, p. 284–288.

———1972b, Silicate-sulfide equilibria in Ca-Fe-Si skarn deposits, in Geophysical Laboratory (rept.): Carnegie Inst. Washington Year Book 71, 1971–72, p. 450–457.

Buseck, P. R., 1966, Contact metamorphism and ore deposition—Concepción del Oro, Mexico: Econ. Geology, v. 61, no.1, p. 97–136.

Carson, D. J. T., and Jambor, J. L., 1974, Mineralogy, zonal relationships and economic significance of hydrothermal alteration at porphyry copper deposits, Babine Lake area, British Columbia: Canadian Mining Metall. Bull., February 1974, p. 110–133.

Clement, S. C., 1968, Supergene copper concentration in altered plagioclase feldspar, Copper Canyon, Nevada: Econ. Geology, v. 63, no. 4, p. 401–408.

Coats, R. R., and Stephens, E. C., 1968, Mountain City copper mine, Elko County, Nevada, *in* Ridge, J. D., ed., Ore deposits of the United States, 1933-1967 (Graton-Sales Volume), v. 2: New York, Am. Inst. Mining, Metall., and Petroleum Engineers, p. 1074–1101.

Constantinescu, E. I., 1971, Observatii asupra skarnelor şi mineralizatiei cuprifere laramice de la Sasca Montana (in Romanian): Bucureşti Univ. Analele, Ser. Ştiinţ. Nat., Geologie-Geografie, v. 20, p. 65–74.

Cooper, J. R., 1957, Metamorphism and volume losses in carbonate rocks near Johnson Camp, Cochise County, Arizona: Geol. Soc. America Bull., v. 68, no. 5, p. 577–610.

Cox, D.P., Schmidt, R. G., Vine, J. D., Kirkemo, H., Tourtelot, E. B., and Fleischer, M., 1973, Copper, *in* Brobst, D. A., and Pratt, W. P., eds., United States mineral resources: U.S. Geol. Survey Prof. Paper 820, p. 163–190.

Creasey, S. C., 1966, Hydrothermal alteration, *in* Titley, S. R., and Hicks, C. L., eds., Geology of the porphyry copper deposits, southwestern North America: Tucson, Ariz., Univ. Arizona Press, p. 51–74.

Czamanske, G. K., and Wones, D. R., 1973, Oxidation during magmatic differentiation, Finnmarka Complex, Oslo area, Norway —Part 2, The mafic silicates: Jour. Petrology, v. 14, no. 3, p. 349–380.

Deer, W. A., Howie, R. A., and Zussman, J., 1962, Rock-forming minerals—v. 1, Ortho- and ring silicates: London, Longmans, Green and Co., 333 p.

———1963, Rock-forming minerals—v. 2, Chain silicates: London, Longmans, Green and Co., 379 p.

Dowty, E., 1971, Crystal chemistry of titanian and zirconian garnet—I. Review and spectral studies: Am. Mineralogist, v. 56, p. 1983–2009.

Eastlick, J. T., 1968, Geology of the Christmas mine and vicinity,

Banner mining district, Arizona, *in* Ridge, J. D., ed., Ore deposits of the United States, 1933–1967 (Graton-Sales Volume), v. 2: New York, Am. Inst. Mining, Metall., and Petroleum Engineers, p. 1191–1210.

Elinson, M. M., and Alidodov, B. A., 1973, Gas composition of inclusions in minerals and physicochemical conditions of mineral formation in Chorukh-Dayron ore field: Internat. Geology Rev., v. 16, no. 5, p. 557–564.

Elinson, M. M., and Polykovskiy, V. S., 1967, On the gaseous composition of solutions which participated in the formation of rock crystal-bearing veins in skarns: Geochemistry Internat., no. 1, p. 108–114.

Engineering and Mining Journal, 1971, In the United States—Nevada: Eng. and Mining Jour., v. 172, no. 6, p. 253.

Erickson, R. L., and Marsh, S. P., 1974, Geologic map of the Iron Point quadrangle, Humboldt County, Nevada: U.S. Geol. Survey Geol. Quad. Map GQ–1175, scale 1:24,000.

Ernst, W., and Lodemann, W., 1965, Die Verteilung des Bors im Kristallin der SE- Saualpe/Ostkärnten: Neues Jahrb. Geologie u. Paläontologie Monatsh., v. 11, p. 641–647.

Ernst, W., Krejci-Graf, K., and Werner, H., 1958, Parallelisierung von Leithorizonten im Ruhrkarbon mit Hilfe des Bor-Gehaltes: Geochim. et Cosmochim. Acta, v. 14, p. 211–222.

Fournier, R. O., and Truesdell, A. H., 1973, An empirical Na-K-Ca geothermometer for natural waters: Geochim. et Cosmochim. Acta, v. 37, p. 1255–1275.

Gale, R. E., 1965, The geology of the Mission Copper mine, Pima mining district, Arizona: Arizona Univ., Tucson, Ariz., Ph. D. thesis, 162 p.

Gary, Margaret, McAfee, Robert, Jr., and Wolf, C. L., eds., 1972, Glossary of geology: Washington, D.C., American Geological Institute, 805 p.

Goddard, E. N., chairman, and others, 1948, Rock color chart: Washington, D. C., Natl. Research Council; repr. by Geol. Soc. America, 1963.

Goldschmidt, V. M., 1954, Geochemistry: London, Oxford Univ. Press, 730 p.

Gordon, T. M., and Greenwood, H. J., 1971, The stability of grossularite in H_2O-CO_2 mixtures: Am. Mineralogist, v. 56, p. 1674–1688.

Gott, G. B., McCarthy, J. H., Jr., Oda, Uteana, Lakin, H. W., and Thompson, C. E., 1966, Preliminary report comparing geochemical halos around an exposed and a concealed copper deposit, *in* Seminar on field techniques for mineral exploration, Iran, 1965: Ankara, Turkey, Central Treaty Organization, p. 133–144.

Grimes, D. J., and Marranzino, A. P., 1968, Direct-current arc and alternating-current spark emission spectrographic field methods for the semiquantitative analysis of geologic materials: U.S. Geol. Survey Circ. 591, 6 p.

Gustafson, W. I., 1970, Stability relations of andradite, hedenbergite, and related minerals in the system Ca-Fe-Si-O-H: California Univ., Los Angeles, Ph. D. thesis, 224 p.

Haas, J. L., Jr., 1971, The effect of salinity on the maximum thermal gradient of a hydrothermal system at hydrostatic pressure: Econ. Geology, v. 66, no. 6, p. 940–946.

Hall, W. E., and MacKevett, E. M., Jr., 1962, Geology and ore deposits of the Darwin quadrangle, Inyo County, California: U.S. Geol. Survey Prof. Paper 368, 87 p.

Hall, W. E., Rose, H. J., Jr., and Simon, Frederick, 1971, Fractionation of minor elements between galena and sphalerite, Darwin lead-zinc-silver mine, Inyo County, California, and its significance in geothermometry: Econ. Geology, v. 66, no. 4, p. 602–606.

Helgeson, H. C., 1970, A chemical and thermodynamic model of ore deposition in hydrothermal systems, *in* Morgan, B. A., ed., Symposium on sulfides—Fiftieth anniversary symposia: Mineralog. Soc. America Spec. Paper 3, p. 155–186.

Hernon, R. M., and Jones, W. R., 1968, Ore deposits of the Central mining district, Grant County, New Mexico, *in* Ore deposits of the United States, 1933–1967 (Graton-Sales volume), v. 2: New York, Am. Inst. Mining, Metall., and Petroleum Engineers, p. 1211–1237.

Hess, F. L., 1918, Tactite, the product of contact metamorphism: Am. Jour. Sci., 4th ser., v. 48, p. 377–378.

Himes, M. D., 1972, Mineralization and alteration at the Pima mine, a complex porphyry copper deposit, Pima County, Arizona: Soc. Mining Engineers, Ann. Mtg., San Francisco, Preprint 72–I–57.

Hofmann, A., 1972, Chromatographic theory of infiltration metasomatism and its application to feldspars: Am. Jour. Sci., v. 272, p. 69–90.

Imai, H., and Ito, K., 1959, Geologic structure and tungsten-copper mineralization of the Kuga mine, Yamaguchi prefecture: Mining Geology, v. 9, no. 34, p. 95 –100 (in Japanese).

Jackson, E. D., Stevens, R. E., and Bowen, R. W., 1967, A computer-based procedure for deriving mineral formulas from mineral analyses, *in* Geological Survey research 1967: U.S. Geol. Survey Prof. Paper 575–C, p. C23–C31.

Jacobs, D. C., and Parry, W. T., 1974, Geochemistry of biotite from the Santa Rita stock and its associated potassic and phyllic alteration zones, Central mining district, Grant County, New Mexico [abs.]: Geol. Soc. America, Abs. with Programs, v. 6, no. 7, p. 809.

James, L. P., 1971 (1972), Zoned hydrothermal alteration and ore deposits in sedimentary rocks near mineralized intrusions, Ely area, Nevada: Pennsylvania State Univ., University Park, Ph.D. thesis, 241 p.

Johnson, M. G., 1977, Geology and mineral deposits of Pershing County, Nevada: Nevada Bur. Mines Bull. (in press).

Kalinin, D. V., 1967, Anisotropism in garnets in relation to composition and chemical background of their synthesis: Akad. Nauk SSSR Doklady, v. 172, nos. 1–6, p. 128–130.

Keith, T. E. C., Muffler, L. J. P., and Cremer, Marcelyn, 1968, Hydrothermal epidote formed in the Salton Sea geothermal system, California: Am. Mineralogist, v. 53, nos. 9–10, p. 1635–1644.

Kelly, W. C., and Turneaure, F. S., 1970, Mineralogy, paragenesis, and geothermometry of the tin and tungsten deposits of the eastern Andes, Bolivia: Econ. Geology, v. 65, no. 6, p. 609–680.

Kerrick, D. M., 1970, Contact metamorphism in some areas of the Sierra Nevada, California: Geol. Soc. America Bull., v. 81, no. 10 p. 2913–2937.

Kerrick, D. M., Crawford, K. E., and Randazzo, A. F., 1973, Metamorphism of calcareous rocks in three roof pendants in the Sierra Nevada, California: Jour. Petrology, v. 14, pt. 2, p. 303–325.

Kesler, S. E., 1968, Contact-localized ore formation at the Memé mine, Haiti: Econ. Geology, v. 63, no. 5, p. 541–552.

Kines, Tuncay, 1969, Geothermometry of the Keban mine area, Eastern Turkey: Bull. Miner. Res. Explor. Inst. Turkey 1969, no. 73, p. 28–33.

Kiseleva, I. A., 1968, Hydrothermal synthesis of skarn minerals: Internat. Geology Rev., v. 12, no. 4, p. 401–405.

Kissling, A., and Pomîrleanu, V., 1970, On the formation temperature of minerals from the Ocna de Fier-Dognecea skarn, Romania (abs.), *in* Collected abstracts, IMA–IAGOD meetings 1970: Tokyo, Science Council of Japan abstract reprinted in Fluid Inclusion Research, Proc. COFFI [Commission on ore-forming fluids in inclusions], v. 3, 1970, p. 34.

Knopf, Adolph, 1918, Geology and ore deposits of the Yerington district, Nevada: U.S. Geol. Survey Prof. Paper 114, 68 p.

Korzhinskiy, D. S., 1964, An outline of metasomatic processes:

Internat. Geol. Rev., v. 6, p. 1713–1734, 1920–1952, 2169–2198.
Kosals, Y. A., Dmitriyera, A. N., Arkhipchuk, R. Z., and Gal'chenko, V. I., 1973, Temperature conditions and formation sequence in deposition of fluorite-phenacite-bertrandite ores: Internat. Geology Rev., v. 16, no. 9, p. 1027–1036.
Leleu, M., Morikis, A., and Picot, P., 1973, Sur des mineralisations de type skarn au Laurium (Grèce): Mineralium Deposita, v. 8, p. 259–263.
Lemmlein, G. G., and Klevtsov, P. V., 1961, Relations among the principal thermodynamic parameters in a part of the system H_2O-NaCl: Geochemistry, 1961, no. 2, p. 148–158.
Lepeltier, Claude, 1969, A simplified statistical treatment of geochemical data by graphical representation: Econ. Geology, v. 64, no. 5, p. 538–550.
Lesnyak, V. F., 1961, Some characteristic features of the formation of skarn-ore complexes: L'vov. Geol. Obshch. Mineralog. Sbornik, v. 15, p. 129–137 (in Russian).
———1965, Mineralothermometric research at the Tyrny-Auz skarn-ore complex, north Caucasus, *in* Yermakov, N. P., Research on the nature of mineral-forming solutions, with special reference to data on fluid inclusions, Volume 22 *of* International Series of Monographs in Earth Sciences: Oxford, Pergamon Press, p. 458–503.
Lessing, P., and Standish, R. P., 1973, Zoned garnet from Crested Butte, Colorado: Am. Mineralogist, v. 58, p. 840–842.
Lindgren, W., 1905, Copper deposits of the Clifton-Morenci district, Arizona: U.S. Geol. Survey Prof. Paper 43, 375 p.
Lindner, J. L., and Gruner, J. W., 1939, Action of alkali sulphide solutions on minerals at elevated temperatures: Econ. Geology, v. 34, no. 5, p. 537–560.
Liou, J. G., 1974, Stability relations of andradite-quartz in the system Ca-Fe-Si-O-H: Am. Mineralogist, v. 59, p. 1016–1025.
Lovering, T. G., 1963, Use of nonparametric statistical tests in the interpretation of geological data: Soc. Mining Engineers Trans., v. 226, no. 2, p. 137–140.
Lovering, T. G., Lakin, H. W., and Hubert, A. E., 1968, Concentration and minor element association of gold in ore-related jasperoid samples, *in* Geological Survey research 1968: U.S. Geol. Survey Prof. Paper 600–B, p. B112–B114.
Lowell, J. D., and Guilbert, J. M., 1970, Lateral and vertical alteration-mineralization zoning in porphyry ore deposits: Econ. Geology, v. 65, no. 4, p. 373–408.
Mamontov, B. V., 1968, Temperature conditions of formation of the South-Yangikan copper-molybdenum deposits (abs.): Fluid inclusion research, Proc. COFFI [Commission on ore-forming fluids in inclusions], v. 1, p. 57.
Miesch, A. T., 1967, Methods of computation for estimating geochemical abundance: U.S. Geol. Survey Prof. Paper 574–B, p. B1–B15.
Missallati, A. A., 1973, Geology and ore deposits of Mount Hope mining district: Stanford Univ., Stanford, Calif. Ph.D. thesis, 160 p.
Moolick, R. T., and Durek, J. J., 1966, The Morenci district, *in* Titley, S. R., and Hicks, C. L., eds., Geology of the porphyry copper deposits, southwestern North America: Tucson, Ariz., Univ. Arizona Press, p. 221–231.
Moore, W. J., and Czamanske, G. K., 1973, Compositions of biotites from unaltered and altered monzonitic rocks in the Bingham mining district, Utah: Econ. Geology, v. 68, no. 2, p. 269–274.
Moore, W. J., and Nash, J. T., 1974, Alteration and fluid inclusion studies of the porphyry copper ore body at Bingham, Utah: Econ. Geology, v. 69, p. 631–645.
Morgan, B. A., 1975, Mineralogy and origin of skarns in the Mount Morrison pendant, Sierra Nevada, California: Am. Jour. Sci., v. 275, no. 2, p. 119–142.
Nash, J. T., and Theodore, T. G., 1971, Ore fluids in the porphyry copper deposit at Copper Canyon, Nevada: Econ. Geology, v. 66, p. 385–399.
Noble, J. A., 1970, Metal provinces of the western United States: Geol. Soc. America Bull., v. 81, no. 6, p. 1607–1624.
Nokleberg, W. J., 1970, Geology of the Strawberry mine roof pendant, central Sierra Nevada: California Univ., Santa Barbara, Ph. D. thesis, 157 p.
———1973, CO_2 as a source of oxygen in the metasomatism of carbonates: Am. Jour. Sci., v. 273, p. 498–514.
Pankratz, L. B., and King, E. G., 1970, High-temperature enthalpies and entropies of chalcopyrite and bornite: U.S. Bur. Mines Rept. Inv. 7435, 10 p.
Perry, C. V., 1969, Skarn genesis at the Christmas mine, Gila County, Arizona: Econ. Geology, v. 64, no. 3, p. 255–270.
Pertsev, N. N., 1973, Skarns as magmatic and postmagmatic formations: Internat. Geology Rev., v. 16, no. 5, p. 572–582.
Phan, K. D., 1969, Skarn et mineralisations associées: Chronique Mines et Recherche Minière, v. 37, p. 292–311 and 339–362.
Rakhmanov, A. M., 1963, Mineralo-thermometric study of some minerals from Maikhura skarn deposit (southern Giesars), *in* Baskakov, M. P., ed., Vopzosy geologii Sredneilegii 1 Kazakhatana: Tashkent, Akad. Nauk Uzbek. SSR, Otdel. Geol. Nauk, p. 67–74 (in Russian).
Ramberg, Hans, 1952, The origin of metamorphic and metasomatic rocks: Chicago, Ill., Univ. Chicago Press, 317 p.
Ransome, F. L., 1904, Geology and ore deposits of the Bisbee quadrangle, Arizona: U.S. Geol. Survey Prof. Paper 21, 168 p.
Roberts, R. J., 1964, Stratigraphy and structure of the Antler Peak quadrangle, Humboldt and Lander Counties, Nevada: U.S. Geol. Survey Prof. Paper 459–A, p. A1–A93.
Roberts, R. J., and Arnold, D.C., 1965, Ore deposits of the Antler Peak quadrangle, Humboldt and Lander Counties, Nevada: U.S. Geol. Survey Prof. Paper 459–B, p. B1–B94.
Rodzyanko, N. G., 1969, Mineralogical-thermometric study of skarn formation conditions in the Tyrny-Auz ore field: Problemy Metasomatizima, 1969, p. 401–410 (in Russian).
Roedder, Edwin, 1967, Fluid inclusions as samples of ore fluids (Chap.) 12, *in* Barnes, H. L., ed., Geochemistry of hydrothermal ore deposits: New York, Holt, Rinehart and Winston, p. 515–574.
———1971, Fluid inclusion studies on the porphyry-type ore deposits at Bingham, Utah, Butte, Montana, and Climax, Colorado: Econ. Geology, v. 66, no. 1, p. 98–120.
———1972, Composition of fluid inclusions: U.S. Geol. Survey Prof. Paper 440–JJ, 164 p.
Rye, R. O., 1966, The carbon, hydrogen, and oxygen isotopic composition of the hydrothermal fluids responsible for the lead-zinc deposits at Providencia, Zacatecas, Mexico: Econ. Geology, v. 61, no. 8, p. 1399–1427.
Sawkins, F. J., 1964, Lead-zinc ore deposition in the light of fluid inclusion studies, Providence mine, Zacatecas, Mexico: Econ. Geology, v. 59, no. 5, p. 883–919.
Sayers, R. W., Tippett, M. C., and Fields, E. D., 1968, Duval's new copper mines shown complex geologic history: Mining Eng., v. 20, no. 3, p. 55–63.
Sazonov, V. D., 1962, Geochemical and physiochemical characteristics of the process of hypogene mineralization of the Kurusaisk ore field: Akad. Nauk Tadzhik. SSR Inst. Geol. Trudy, v. 6, p. 137–164 (in Russian).
Sheppard, S. M. F., Nielsen, R. L., and Taylor, H. P., Jr., 1971, Hydrogen and oxygen isotope ratios in minerals from porphyry copper deposits: Econ. Geology, v. 66, no. 1, p. 515–542.
Siegel, Sidney, 1956, Nonparametric statistics—For the behavioral sciences: New York, McGraw-Hill Book Co., 312 p.
Sigurdson, D. R., and Lawrence, E. F., 1975, Paragenesis and fluid inclusion thermometry of a ferberite-bearing contact metasomatic deposit: Tungsten Jim mine, Custer County, Idaho (abs.): Geol. Soc. America, Abs. with Programs, v. 7, no. 3, p. 374–375.

Sillitoe, R. H., 1973, The tops and bottoms of porphyry copper deposits: Econ. Geology, v. 68, p. 799–815.

Silverman, S. R., Fuyat, R. K., and Weiser, J. D., 1952, Quantitative determination of calcite associated with carbonate-bearing apatites: Am. Mineralogist, v. 37, nos. 3–4, p. 211–222.

Sinyakov, V. I., 1967, The temperature of formation of magnesian skarns of the hypabyssal depth facies: Akad. Nauk SSSR Doklady, v. 175, p. 193–195.

———1968, Formation temperatures of magnesian skarns of a hypabyssal depth facies, *in* Ermakov, N. O., ed., Mineralogical thermometry and barometry, v. 2, New methods and results of investigations of the conditions of ore formation: Moscow, "Nauka" Press, p. 149–151 (in Russian).

Sivoronov, A. A., 1968, Use of liquid inclusions during study of metamorphic rocks of iron-ore deposits, *in* Ermakov, N. O., ed., Mineralogical thermometry and barometry, v. 1, Geochemistry of deep mineral-forming solutions: Moscow, "Nauka" Press, p. 181–184 (in Russian).

Sourirajan, S., and Kennedy, G. C., 1962, The system H_2O-NaCl at elevated temperatures and pressures: Am. Jour. Sci., v. 260, no. 2, p. 115–141.

Spencer, A. C., 1917, The geology and ore deposits of Ely, Nevada: U.S. Geol. Survey Prof. Paper 96, 189 p.

Sutulov, A., 1974, Copper porphyries: Univ. Utah Printing Services, Salt Lake City, Utah, 200 p.

Suzuoki, Tetsuro, and Epstein, Samuel, 1976, Hydrogen isotope fractionation between OH-bearing minerals and water: Geochim. et Cosmochim. Acta., v. 40, p. 1229–1240.

Taylor, B. E., 1974, Communication between magmatic and meteoric fluids during formation of Fe-rich skarns in north-central Nevada (abs.): Am. Geophys. Union Geophys. Trans., v. 55, no. 4, p. 478.

Taylor, H. P., Jr., 1974, The application of oxygen and hydrogen isotope studies to problems of hydrothermal alteration and ore deposition. Econ. Geology, v. 69, no. 6, p. 843–883.

Tennant, C. B., and White, M. L., 1959, Study of the distribution of some geochemical data: Econ. Geology, v. 54, no. 7, p. 1281–1290.

Theodore, T. G., 1969, Surface distribution of selected elements around the Copper Canyon copper-gold-silver open pit mine, Lander County, Nevada: U.S. Geol. Survey open-file report, 21 p.

———1970, Rock analyses around the Copper Canyon open pit mine, Lander County, Nevada: U.S. Geol. Survey open-file report, 238 p.

Theodore, T. G., and Blake, D. W., 1975, Geology and geochemistry of the Copper Canyon porphyry copper deposit and surrounding area, Lander County, Nevada: U.S. Geol. Survey Prof. Paper 798–B, 86 p.

Theodore, T. G., and Nash, J. T., 1973, Geochemical and fluid zonation Copper Canyon, Lander County, Nevada: Econ. Geology, v. 68, p. 565–570.

Theodore, T. G., and Roberts, R. J., 1971, Geochemistry and geology of deep drill holes at Iron Canyon, Lander County, Nevada, *with a section on* Geophysical logs of drill hole DDH–2 *by* C. J. Zablocki: U.S. Geol. Survey Bull. 1318, 32 p.

Theodore, T. G., Silberman, M. L., and Blake, D. W., 1973, Geochemistry and K-Ar ages of plutonic rocks in the Battle Mountain mining district, Lander County, Nevada: U.S. Geol. Survey Prof. Paper 798–A, 24 p.

Thompson, C. E., Nakagawa, H. M., and Vansickle, G. H., 1968, Rapid analysis for gold in geologic materials, *in* Geological Survey research 1968: U.S. Geol. Survey Prof. Paper 600–B, p. B130–B132.

Titley, S. R., 1961, Genesis and control of the Linchburg orebody, Socorro County, New Mexico: Econ. Geology, v. 56, no. 4, p. 695–722.

———1972, Copper mining and Arizona land use planning, a geologist speaks: Fieldnotes, Arizona Bur. Mines, v. 2, no. 4, p. 1–3, 5, 8, 10.

———1973, "Pyrometasomatic"—An alteration type: Econ. Geology, v. 68, no. 8, p. 1326–1329.

Tröger, E., 1962, The garnet group—Relation between mineral chemistry and rock type: Internat. Geology Rev., v. 4, no. 6, p. 663–693.

Tugarinov, A. I., and Naumov, V. B., 1969, Thermobaric conditions of formation of hydrothermal uranium deposits: Geochemistry Internat., v. 6, no. 1, p. 89–103.

Umpleby, J. B., 1916, The occurrence of ore on the limestone side of garnet zones: California Univ. Pubs. Geology, v. 10, no. 3, p. 25–37.

U.S. Bureau of Mines, 1974, Copper in 1974, U.S. Bur. Mines, Mineral Industry Surveys, 2 p.

Vaughn, W. W., and McCarthy, J. H., Jr., 1964, An instrumental technique for the determination of submicrogram concentrations of mercury in soils, rocks, and gas, *in* Geological Survey research 1964: U.S. Geol. Survey Prof. Paper 501–D, p. D123–D127.

Vidale, Rosemary, 1969, Metasomatism in a chemical gradient and the formation of calc-silicate bands: Am. Jour. Sci., v. 267, no. 8, p. 857–874.

Vine, J. D., and Tourtelot, E. B., 1969, Geochemical investigations of some black shales and associated rocks: U.S. Geol. Survey Bull. 1314–A, 43 p.

Ward, F. N., Lakin, H. W., Canney, F. C., and others, 1963, Analytical methods used in geochemical exploration by the U.S. Geological Survey: U.S. Geol. Survey Bull. 1152, 100 p.

Watanabe, T., 1967, Geochemical cycle and concentration of boron in the earth's crust, *in* Vinogradov, A. P., ed., Chemistry of the earth's crust, v. II: Israel Program Sci., p. 167–178.

Watters, W. A., 1958, Some zoned skarns from granite-marble contacts near Puyvalador, in the Querigut area, eastern Pyrenees, and their petrogenesis: Mineralog. Mag., v. 31, p. 703–725.

White, D. E., 1968, Environments of generation of some base-metal ore deposits: Econ. Geology, v. 63, no. 4, p. 301–335.

White, D. E., Muffler, L. J. P., and Truesdell, A. H., 1971, Vapor-dominated hydrothermal systems compared with hot-water systems: Econ. Geology, v. 66, no. 1, p. 75–97.

Winchell, A. N., and Winchell, Horace, 1951, Description of minerals, Pt. 2 *of* Elements of optical mineralogy—An introduction to microscopic petrography: New York, John Wiley and Sons, 4th ed., 551 p.

Winkler, H. G. F., 1965, Petrogenesis of metamorphic rocks: New York, Springer-Verlag, 220p. (transl. from German).

Wodzicki, A., 1971, Migration of trace elements during contact metamorphism in the Santa Rosa range, Nevada, and its bearing on the origin of ore deposits associated with granitic intrusions: Mineralium Deposita, v. 6, p. 49–64.

World Mining, 1971, United States, Duval Corporation, Battle Mountain production and costs, *in* What's going on in world mining: World Mining, July 1971, p. 41.

Ying-tsuen, Lui, 1966, Geochemical characteristics of a certain skarn occurrence in Koangsu: Internat. Geology Rev., v. 11, no. 9, p. 1005–1015.

Ypma, P. J. M., 1963, Rejuvenation of ore deposits as exemplified by the Belledonne metalliferous province: Univ. Leiden, Netherlands, Ph. D. thesis, 212 p.

Yund, R. A., and Kullerud, Gunnar, 1966, Thermal stability of assemblages in the Cu-Fe-S system: Jour. Petrology, v. 7, no. 3, p. 454–488.

Zharikov, V. A., 1968, Skarn source fields of ore, p. 280–302, *in* Genesis of endogenic ore deposits: Nedra Press, Moscow, 719 p. (in Russian); Internat. Geology Rev., v. 12, no. 7, p. 760–775 (transl.).

Geochemistry of the Porphyry Copper Environment in the Battle Mountain Mining District, Nevada

GEOLOGICAL SURVEY PROFESSIONAL PAPER 798

This volume was published as separate chapters A–C

UNITED STATES DEPARTMENT OF THE INTERIOR

CECIL D. ANDRUS, *Secretary*

GEOLOGICAL SURVEY

V. E. McKelvey, *Director*

CONTENTS

[Letters designate the chapters]

789-107/60